NATIONAAL LUCHT- EN RUIMTEVAARTLABORATORIUM

NATIONAL AEROSPACE LABORATORY NLR

THE NETHERLANDS

NLR MP 85023 U

COMPARISON OF THREE–DIMENSIONAL TURBULENT BOUNDARY LAYER CALCULATIONS WITH EXPERIMENT

THE EUROVISC 1982 BERLIN WORKSHOP

BY

B. VAN DEN BERG, NLR, THE NETHERLANDS
D.A. HUMPHREYS, FFA, SWEDEN
E. KRAUSE, RWTH AACHEN, GERMANY
J.P.F. LINDHOUT, NLR, THE NETHERLANDS

NLR MP 85023 U

COMPARISON OF THREE-DIMENSIONAL TURBULENT BOUNDARY
LAYER CALCULATIONS WITH EXPERIMENT
The Eurovisc 1982 Berlin Workshop

by

B. van den Berg, NLR, The Netherlands
D.A. Humphreys, FFA, Sweden
E. Krause, RWTH Aachen, Germany
J.P.F. Lindhout, NLR, The Netherlands

SUMMARY

The results of several three-dimensional turbulent boundary layer
calculations have been compared with each other and with experiment for
a number of test cases. The calculation methods applied range from integral
methods to field methods using a turbulence model based upon the Reynolds
stress transport equations. The test cases comprise various pressure-driven
flows and one shear-driven flow. Agreement between theory and experiment was
often not very satisfactory. This holds particularly for the quantities
directly related to the empiricism employed in the calculation methods, the
Reynolds shear stresses.

CONTENTS

(166 pages in total)

LIST OF SYMBOLS

(symbols used locally only are not included)

$C_f = \dfrac{\tau_w}{q_e}$ Skin friction coefficient

$C_p = \dfrac{p - p_\infty}{q_\infty}$ Static pressure coefficient

$H = \dfrac{\delta^*}{\Theta}$ Boundary layer shape factor

L   Reference length scale for test case

p   Static pressure

$q = \tfrac{1}{2} \rho Q^2$ Dynamic pressure

Q   Magnitude of velocity vector

r   Radius of curvature

R   Radius of curvature of the wall

Ri   Richardson number

$R_\delta{}^* = \dfrac{Q_e \delta^*}{\nu}$ Reynolds number based upon displacement thickness

$R_\Theta = \dfrac{Q_e \Theta}{\nu}$ Reynolds number based upon momentum thickness

U,W   Mean velocity components parallel to the surface in and normal to the external streamline direction

u_τ Skin friction velocity

$-\overline{uv}, \; -\overline{wv}$ Reynolds shear stress components parallel to the surface in and normal to the external streamline direction

x,z   Surface coordinates in and normal to the external streamline direction

y   Normal coordinate, measured from the wall

$$y^+ = \frac{y\, u_\tau}{\nu}$$ Dimensionless wall distance

β Angle between local and external streamline direction, measured parallel to the surface

$$\delta^* = \int_0^\delta \frac{U_e - U}{Q_e}\, J\, dy$$ Boundary layer displacement thickness

Δ Reference boundary layer thickness, length scale for plots

$$\Theta = \int_0^\delta \frac{(U_e - U)U}{Q_e^2}\, J\, dy$$ Boundary layer momentum thickness

ν Kinematic viscosity

ν_t Eddy viscosity

ρ Density

$\tau_x = \rho(-\overline{uv} + \nu\, \partial U/\partial y)$ Shear stress components parallel to the surface in

$\tau_z = \rho(-\overline{wv} + \nu\, \partial W/\partial y)$ and normal to the external streamline direction

$\Omega_n, \Omega_s, \Omega_x, \Omega_z$ Residuals of momentum integral equations

Subscripts

e Outer edge of the boundary layer

w Wall

x,z Components parallel to the surface in and normal to the external streamline direction

∞ Free-stream

1   INTRODUCTION

In many flows about three-dimensional bodies at high Reynolds
number, viscous effects are restricted principally to a thin layer
near the surface. The flow in this thin boundary layer is approximately
parallel to the surface, but is usually three-dimensional in the sense
that its direction varies through the boundary layer. The ability to
predict the three-dimensional boundary layer development by calculation
is important for many fields, as for example in the design of aircraft,
ships and turbomachinery. It was very difficult to meet the need
before access to modern computing aids became widespread. However,
since 1970 progress has been made and today a variety of three-
dimensional turbulent boundary layer calculation methods is available.

It soon became obvious that a controlled comparison of results
obtained with various calculation methods would be useful. The first
such comparison was made in 1975 as a part of Euromech Colloquium No.
60 held at Trondheim - the "Trondheim Trials" (East 1975). The comparison
showed that the numerical difficulties associated with solving the
equations were in many cases by no means mastered. Inflexible coordinate
systems were the norm and calculations tended to fail well upstream of
separation. Serious shortcomings became apparent also in the empirical
closure assumptions made in the calculation methods.

In order to gain more insight into these problems an Eurovisc
Working Party on "Three-dimensional Shear Layers" was established. The
Working Party has organized a number of Workshops with further comparisons
of calculated results. Workshops were held in Stockholm (Humphreys
1979) and in Amsterdam (Lindhout, van den Berg & Elsenaar 1981).

The Stockholm Workshop revealed unacceptably large differences between
calculated results even for a simple wing with only mild three-
dimensionality. The Amsterdam Workshop uncovered a wide variation in
computing efficiency, but there was clear improvement over the Trondheim
Trials in predicting the flow up to near separation.

While much valuable information can be gleaned from comparisons
of calculation results with each other, a validation of closure as-
sumptions and solutions of the boundary layer equations can only be
obtained by comparing with reliable measurements. An opportunity to
evaluate the nearly one hundred existing three-dimensional turbulent
boundary layer experiments arose within the framework of the 1980/81
Stanford Conferences on "Complex Turbulent Flows" (Humphreys & van den
Berg 1981). A major evaluation criterion was the availability of
measured Reynolds stresses, in order to enable direct comparisons with
calculated stresses. Further criteria were defined which a set of
measured data should satisfy in order to qualify as a reliable test
case. It turned out that none of the existing experiments satisfied
fully all the criteria laid down. Nevertheless four potentially useful
test cases were identified and three more were regarded as acceptable
even though appearing to be deficient in some way.

The evaluation was the basis of the test case selection for the
Eurovisc Berlin Workshop, with which this report is concerned. A dist-
inction is made between recommended test cases and optional test cases.
Since two of the most satisfactory data sets are very similar, three
cases were recommended for the Workshop. Of the three other experiments
which were considered probably acceptable, one was only marginally
three-dimensional. The remaining two were added as optional test cases.

Two of the recommended test cases are quasi-two-dimensional flows. The test case termed "BEEL72" simulates swept infinite wing flow on a flat plate, and the test case termed "LOHM73" is an axi-symmetric flow at nominally constant pressure on a long cylinder with rotating afterbody. The third recommended test case, termed "DEFE77", concerns fully three-dimensional boundary layer flow generated on a flat plate by a cylindrical body on the plate. The optional test case "MUKR79" concerns also a fully three-dimensional boundary layer on a flat plate generated by guide walls. In test case "FEVA78" such a flow is produced on a cylinder with its axis parallel to the free stream direction. The test cases are defined for calculation purposes in Appendix A, but some relevant features are repeated in the chapters dealing specifically with each case. For full description of the experiments reference is made to the original publications. Some data on measurement errors are collected in Appendix B.

Fourteen calculation methods were engaged in the Berlin Workshop. None of the methods has been applied to all test cases. However, enough calculation results were obtained, except for test case "FEVA78", to allow a fruitful comparison. Three of the calculation methods engaged in the comparison are integral methods, with no explicit turbulence model, and eleven are field (or differential) methods. Seven of the field methods used an algebraic eddy viscosity. Only two of the calculation methods employed transport equations. Table 1.1 lists the names of scientists who contributed to the Workshop and the test cases which were calculated.

The objective of the Berlin Workshop was to examine the validity of the closure assumptions made in the various calculation methods for three-dimensional turbulent boundary layers. Chapter 2 describes briefly the most important features of the calculation methods.

Following this the test cases for which results were obtained are discussed in alphabetical order. The final chapter is devoted to a general discussion of the outcome of the Workshop.

Table 1.1 <u>Summary of calculations performed for the various test cases</u>

computational methods		test cases				
		BEEL72	DEFE77	LOHM73	MUKR79	FEVA78
denomination	class [1]					
CEBECI/HUANG	F, A	X	X	X	-	-
COUSTEIX/BERRUE	I	X	X	X	-	-
CROSS	I	X	X	-	X	-
GIBSON/YOUNIS	F, T	-	-	X	-	-
HOEKSTRA	F, A	X	X	X	-	-
HUMPHREYS	F, A	X	-	-	-	-
GALMES/LAKSHMINARAYANA	F, T	-	-	X	-	-
LINDHOUT/DE BRUIN	F, A	X	X	X	-	-
MULLER	F, A	X	X	-	X	-
NAKKASYAN	F, A	X	-	-	-	-
PATEL/KROGSTAD/BAEK	F, A	X	X	X	X	-
PIERCE/AGUILAR/TREVENTI	F, A	-	-	X	-	-
SCHNEIDER	F, A	X	-	-	-	-
SMITH	I	X	-	-	-	-

(1) Key: F,A - Field method, algebraic eddy viscosity model

       F,T - Field method, transport equation model

       I   - Integral method

2   COMPUTATIONAL METHODS

A thorough discussion of the various calculation methods used at
the Workshop is given in Humphreys & Lindhout 1987. Here only short
descriptions of the various calculation methods will be given. These
descriptions are largely as supplied to the organisers by the
contributors of results themselves.

Method descriptions appear below in an order intended to emphasize
features they have in common.

The COUSTEIX/BERRUE, CROSS and SMITH methods

These three integral methods are described together. Two of the
three (Smith 1972 and Cousteix 1974) are well established. The CROSS
method has not been published yet but details are given in two internal
British Aerospace reports (Cross 1979, 1980).

The boundary layer equations are written in general wall-normal
coordinates for all three methods. Forward integration is carried out
with explicit Runge/Kutta schemes. The COUSTEIX/BERRUE solution rests
on a fourth order and the other two on a second order integration.
Crosswise derivatives are dealt with in the same way in all three
solutions. Two point, one-sided differences or three point, centred
differences are used, respectively, to satisfy the domain of dependence
condition.

The methods differ mainly in their auxiliary formulae. All three
solve the integral continuity equation but supply the entrainment
velocity in different ways. The CROSS method has an algebraic
formulation whereas the SMITH method integrates a differential equation,

taking into account changes in the turbulence structure produced by divergence and convergence of the external streamlines. Various integral thicknesses are related on assuming families of mean velocity profiles. SMITH uses power law streamwise profiles and Mager crossflow profiles. CROSS uses Coles profiles in both directions. This is not the three-dimensional proposal of Coles (1956), but an alternative generalization of the two-dimensional form, in which the direction of the wake component is assumed to vary through the boundary layer. In addition, the shape of the wake component in the Cross variant depends on the local pressure gradient. Finally, SMITH uses the skin friction formula proposed by Green, Weeks and Brooman (1973) to give the streamwise component of C_f. The CROSS C_f-law follows from the profile family assumed.

The COUSTEIX/BERRUE method depends on functions obtained by solving the full differential equations assuming local similarity. The turbulence model is a simple mixing length formulation (Michel et al 1968), with the modification suggested by Rotta (1977) to account for eddy viscosity anisotropy. The similarity solutions provide relations between the integral thicknesses, a skin friction law and the entrainment velocity.

The CEBECI/HUANG method

The CEBECI/HUANG method is described in detail in Cebeci & Smith (1974). The coordinate systems used are cartesians or cylindrical polars. The method solves the boundary layer equations transformed with a similarity transformation. The equations are discretized with the box scheme suggested by Keller (1970). All derivatives are approximated by two point centred differences. Finally, the discretized equations are solved by the Newton/Raphson procedure. Calculations can be started by reading in initial profiles.

The Reynolds stresses are modelled with an isotropic two-layer eddy viscosity. Van Driest's damping factor for the inner layer mixing length depends on the streamwise pressure gradient and the outer layer eddy viscosity incorporates a low Reynolds number correction. Transverse curvature effects on the inner layer mixing length are approximated by writing in the relevant formula Y for y, where $\partial y/\partial Y = 1 + y/R$ (Rao 1967). For the LOHM73 calculations a term vw/r was dropped from the crosswise momentum equations and the pressure gradient caused by swirl was neglected.

The SCHNEIDER method

A description of this differential method is given in Schneider (1977). The solution is restricted to infinite swept wing flows. The equations are transformed with similarity formulae. The coordinate normal to the wall is scaled to counteract growth in the computational space. The difference equations are solved with the Keller box scheme and the Newton/Raphson procedure. Skin friction components emerge as part of the main solution rather than by differentiating the velocity profiles.

Starting profiles are generated by expressing the crossflow velocity component as a polynomial but taking the streamwise component from a series of two-dimensional flat plate calculations, if necessary adjusting the turbulence model to match any experimental starting values. The turbulence model is algebraic. The mixing length is as given by Michel et al (1968) and the eddy viscosity is made non-isotropic following Rotta (1977).

Four sets of calculations were submitted to the Workshop for the NLR experiment (case BEEL72). The runs differed in the external flow conditions assumed.

The HUMPHREYS method

This is a differential procedure. A detailed description of the original method is given by Fanneløp & Humphreys (1975). The present version can be used only for quasi-two-dimensional flow (infinite swept wing). The boundary layer equations are written in streamline coordinates and a similarity transformation is introduced. The finite difference method is fully implicit. The usual starting procedure for this program is to assume a self-preserving boundary layer upstream of the initial point. Upstream conditions are then adjusted until the desired initial data are matched.

For two-dimensional flow the turbulence model is identical to the Cebeci/Smith eddy viscosity formulation but without corrections for low Reynolds number or strong pressure gradient. Correction terms have been added, however, which allow for the effects of streamline curvature and divergence (Humphreys 1982). These terms lead to an eddy viscosity non-isotropy. In the Workshop calculations it was assumed that the eddy viscosity non-isotropy, in streamline coordinates, is independent of y and equal to the value given by the full model at the edge of the inner layer.

The NAKKASYAN method

This differential procedure is very similar to the one just described, but does allow direct input of initial profiles. The analysis and numerical method are taken from the same source (Fanneløp & Humphreys 1975). The eddy viscosity is almost identical in two-dimensional flow, but the specific allowance for three-dimensionality is essentially different. The NAKKASYAN method follows the theory recently presented by Ryhming & Fanneløp (1982). Guided by experimental data on eddy viscosity non-isotropy Ryhming & Fanneløp have deduced

corrections tending to give the observed behaviour. The correction applied is a function of the amount of skewing of the mean velocity vector in the boundary layer.

The MÜLLER method

The calculations were carried out with a differential method. The boundary layer is taken to be on a developable surface and is oriented in a cartesian frame. No coordinate transformation is used to offset growth. The program has options to calculate quasi-two-dimensional flows, both spanwise invariant and plane of symmetry types, and has access to four different semi-implicit schemes. The Hall scheme is used when tracing free boundaries.

Smoothed experimental starting profiles can be used as input. For the Workshop calculations Müller matched the prescribed data by simulating the flow upstream of the initial line. Outer boundary conditions are calculated from a given pressure field by solving the Euler equations. Bicubic splines are used for interpolating experimental pressure coefficients. In order to avoid oscillations (Müller 1982 b) least squares bicubic smoothing is applied first and then fifth degree polynomial interpolation within the smoothed data.

An isotropic eddy viscosity was chosen for all runs submitted to the Workshop. It is a single layer model obtained by using Michel's mixing length (Michel et al 1968) and the van Driest damping factor with Cebeci's modification for (streamwise) pressure gradient.

The HOEKSTRA method

This method solves the differential equations in general wall-normal coordinates. Boundary layer growth is accommodated by adding more points. The discretized equations are solved with an alternating direction implicit scheme.

The isotropic eddy viscosity turbulence model used is that
described in Cebeci & Smith (1974), including corrections for low
Reynolds number and pressure gradient. In the presence of transverse
curvature, the inner layer formulae have y replaced by Y, where
$\partial y/\partial Y = 1 + y/R$ (Rao 1967).

This turbulence model has been used for the computations of test
case DEFE77 and LOHM73. For test case BEEL72 the turbulence model has
been changed by Hoekstra as follows. In the inner layer, the eddy
viscosity formula is multiplied by the ratio of the local shear stress
magnitude to its wall value. In the outer layer the eddy viscosity is
multiplied by a function expressing the departure from self-preserving
flow.

The PATEL/KROGSTAD/BAEK method

This is the original differential method from which the HOEKSTRA
program was developed. The equations are written in a system which is
composed of two orthogonal surface coordinates and the perpendicular
distance from the surface. The calculation method is explained in
detail by Chang & Patel (1975). The algorithm reduces to an implicit
Crank/Nicolson scheme with a stability condition limiting the forward
step and preventing marching into regions with negative crossflow.
Growth is allowed for partly by introducing a transformation and
partly by redistribution.

The turbulence model is the isotropic eddy viscosity of Cebeci/
Smith and includes the modifications to the van Driest damping factor
suggested for strong pressure gradients and to the outer region eddy
viscosity for low Reynolds numbers. For the LOHM73 case, Version 2
calculations have the eddy viscosity factored in both directions with
$(1-4.5 \text{ Ri})^2$, where Ri is a Richardson number, formed from the cross-
flow velocity and the transverse curvature of the cylinder.

The LINDHOUT/DE BRUIN method

This is a differential method for solving the laminar or turbulent boundary layer equations in arbitrary wall-normal coordinates. The program can trace free boundaries and step around "forbidden" zones (characterized in practice by small C_f or large β_w), keeping within the region determined by the initial data. To counteract growth a transformation depending on boundary layer thickness and Reynolds number is applied explicitly to the wall normal coordinate before discretization. In the computational space stepsize is constant along the wall normal and also in the cross stream direction, except at side boundaries. The method is described in detail in Lindhout et al (1981).

Off the surface, second order central differences are used for the wall normal derivatives whereas in-plane derivatives are given by Hermitian-type formulae connecting the function value and its first derivative at both points. The Newton/ Raphson procedure is employed in the solution. Four finite difference molecules are used. The program can accept pressure data as well as external velocities. In the former case the magnitude of the external velocity is given by the pressure but its direction is taken from an integration of the Euler equations.

The Reynolds stresses are represented with an isotropic eddy viscosity model based on the mixing length of Michel et al (1968) with the constant in the van Driest damping factor modified for pressure gradient (in the skin friction direction) following Cebeci.

The PIERCE/AGUILAR/TREVENTI method

The differential method was developed for calculating the axi-symmetric turbulent boundary layer on a body of revolution with swirl

(Aguilar & Pierce 1979). Pressure variation normal to the wall, caused
by the swirl, is allowed for and obtained from the lowest order normal
momentum equation.

The fully implicit numerical scheme uses: first order, two point
formulae for the axial derivatives, three-point centred differences
for the radial derivatives. The step size is held constant along the
body. In the perpendicular direction the computational domain is di-
vided into up to five regions and the step size is constant in each.
Extensive experimentation has been carried out to determine optimum
grid spacings.

The Reynolds stresses are represented by the isotropic eddy
viscosity model of Cebeci/Smith. For thick axi-symmetric boundary
layers the near wall formulation of Rao (1967) is incorporated.
Cebeci's proposal for the variation of the outer region eddy viscosity
with Reynolds number is adopted.

The GALMES/LAKSHMINARAYANA method

This method is constructed for axi-symmetric flow over bodies of
revolution. The boundary layer equations are solved in cylindrical
polar coordinates. The independent variable in the wall normal direction
is taken as the non-dimensional stream function, which serves to
offset boundary layer growth to a large extent. The pressure field
induced by the swirl is not allowed for.

The implicit method of Patankar & Spalding (1970) is used to
solve the difference equations. The linearization scheme consists
simply in representing coefficients using values from the adjacent
upstream station. For the Workshop calculations (LOHM73 only) forward
steps were taken as small as one percent of the boundary layer thickness

(as compared with a typical forward step of the order of the boundary layer thickness in most methods discussed earlier). At the start of the calculation, where the experimental initial profiles were specified, and at the start of the rotating afterbody, the step length taken was ten times smaller than this, for 50 steps.

The effects of turbulence are simulated with an isotropic eddy viscosity model based on the (k,ε) equations of Jones & Launder (1972). The corrections for low turbulence Reynolds number are incorporated, obviating the need for wall functions. At the initial station profiles of turbulence kinematic energy k and dissipation rate ε were taken from standard flat plate data.

The GIBSON/YOUNIS method

The boundary layer equations for axi-symmetric turbulent flow on a body of revolution are solved. The equations are written in cylindrical polar coordinates. Normal pressure gradient caused by swirl is included (but has quite negligible effect in the LOHM73 case, Gibson, private communication, 1982). The first off-body point y_1 must lie within the logarithmic layer ($50 < y_1^+ < 150$) where wall functions are applied as inner boundary conditions. The logarithmic law is applied assuming collateral flow relative to the wall (with or without surface rotation) in $y < y_1$.

The integration of the equations is carried out using the numerical method given by Patankar & Spalding (1970). Distance normal to the wall is replaced in the calculations by the stream function, so that the width of the computational domain is automatically expanded as the boundary layer grows. No iterations are performed to correct for non-linearity, coefficients being taken from known upstream values.

The forward step is of the order of one percent of local boundary layer thickness, which is relatively small. For the LOHM73 runs submitted, even smaller steps were taken (10 times smaller) within 5% δ either side of the start of the rotating section.

The turbulence model in this program is by far the most sophistic-ated of those represented at the Workshop. The stresses are calculated using a full Reynolds stress transport model: six Reynolds stress equations and one for the energy dissipation rate. In essence the model is as described by Launder, Reece & Rodi (1975) but incorporates improvements for the wall region. A comprehensive summary of the model is given by Gibson, Jones & Younis (1981).

3   TEST CASE BEEL72

This incompressible three-dimensional turbulent boundary layer
experiment was performed at NLR in 1972. The experiment provides data
for testing the details of closure assumptions in a swept infinite
wing flow. Since in a quasi-two-dimensional flow the pressure field
does not change in the spanwise direction, the momentum equations can
be greatly simplified and their integration is less cumbersome than
for fully three-dimensional conditions. The closure problem, however,
is of equal difficulty and approximations must be constructed for both
of the tangential stresses appearing in the momentum equations.

In order to provide appropriate initial conditions for calculations,
the forward portion of the experimental model (Figure 3.1) was designed
such that the pressure remained nearly constant near the leading edge.
By suspending a body over the flat test surface the pressure was made
to increase gradually in the direction of the main stream and separation
was enforced in the vicinity of the trailing edge by adjusting down-
stream blockage.

The boundary layer could be maintained very nearly quasi- two-
dimensional with the help of guide vanes on either side of the region
investigated, ensuring correct inviscid streamline shape. The stations
at which velocity profiles, Reynolds stresses and skin friction were
measured are shown in figure 3.2. Details of the measurements and the
experimental techniques may be found in van den Berg & Elsenaar
(1972), Elsenaar & Boelsma (1974) and van den Berg (1976).

The test case BEEL72 has been used before for comparison, at the
Trondheim Trials in 1975. All nine solution methods which participated
failed to simulate the flow in the vicinity of separation. Figure 3.3
shows some of the results of the Trondheim Trials (East 1975).
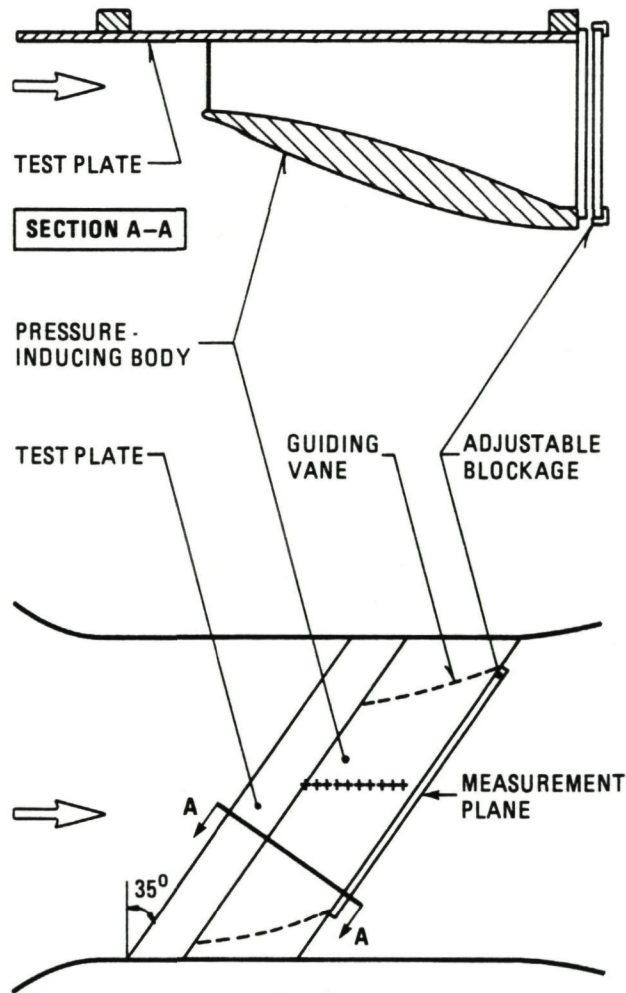
Fig. 3.1   BEEL72 test set-up
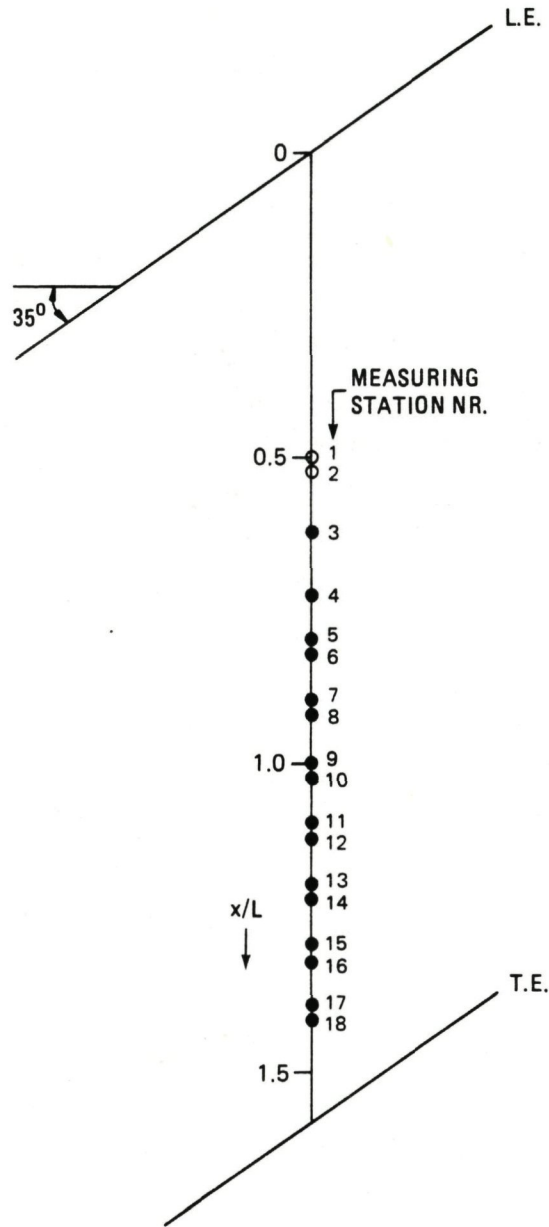
Fig. 3.2 Position of measuring
stations

Here the crossflow angle at the wall β_w is plotted versus the stream-
wise coordinate x/L. The comparison clearly demonstrates that the
computed crossflow behaviour is in error well upstream of separation
(x/L ≅ 1.3). The ten years since the Trondheim Trials has been an
active period in three-dimensional turbulent boundary layer calculation
methods, and it was considered worthwhile to employ this test case
again for the Berlin Workshop.

Eleven calculation methods were applied to the test case in the
Berlin Workshop. Three of them are integral methods: SMITH, COUSTEIX/
BERRUE and CROSS. The first two took part in the Trondheim Trials, but
the empirical assumptions have been altered since then. All three
methods differ in the assumptions made about the streamwise and
crossflow velocity profiles, the skin friction and the entrainment
rate.

The field methods CEBECI/HUANG, LINDHOUT/DE BRUIN, MÜLLER and
PATEL/KROGSTAD/BAEK employ simple algebraic eddy viscosity or mixing
length models, similar to the ones applied earlier at the Trondheim
Trials. A modified algebraic eddy viscosity model is used in the
method HOEKSTRA. The calculation methods HUMPHREYS, NAKKASYAN and
SCHNEIDER employ algebraic non-isotropic eddy viscosity models. Note
that calculation methods with more advanced turbulence models, such as
those based upon the turbulence transport equations, have not been
applied to this test case.

In a comparison of calculations and measurements the accuracy of
the calculated and measured data should be considered. The estimated
experimental accuracies are given in Appendix B. To obtain information
on the numerical accuracy of the calculations some tests were required
to be carried out (see Appendix A), comprising repeat calculations
with different step sizes and a measure of the accuracy with which
the momentum integral equations hold. The results of the numerical
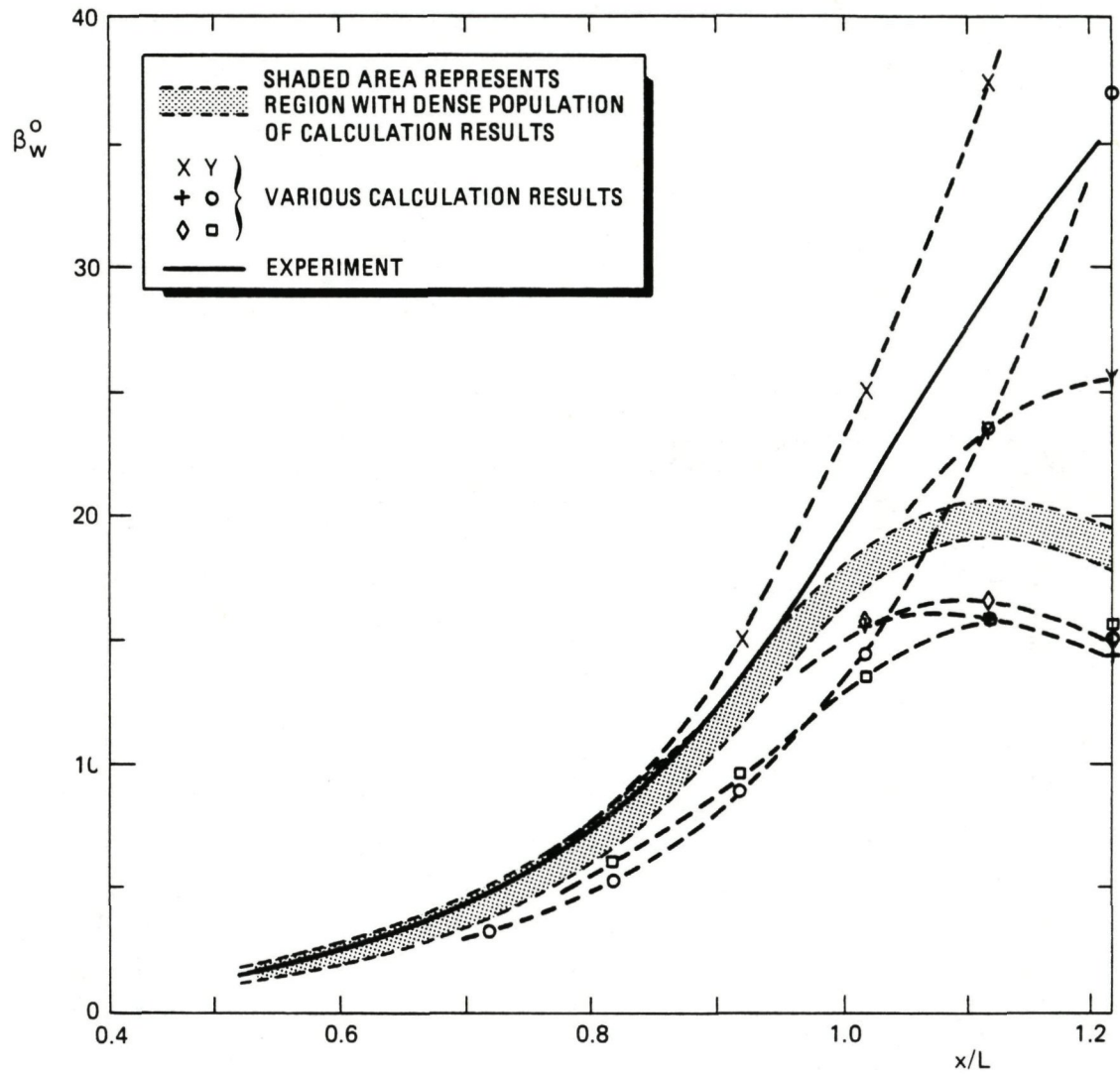
Fig. 3.3 Wall flow angle as given by nine methods of the Trondheim
          Trials in 1975

accuracy tests, as far as they were performed by the participants, are contained in Table 3.1. The uncertainty in the integral momentum balance was determined only in two cases, but most participants carried out repeat calculations with reduced step sizes. The data in Table 3.1 suggest that the numerical errors in the computations are in most cases not large and should not hamper the comparisons significantly.

Table 3.1   Results of numerical accuracy studies for BEEL72 test case

(a) Stepsize variation

results submitted	stepsize factor	coordinate direction	station number	effect on calculations
CEBECI/HUANG	2	x,y	10	$\Delta C_f \cong 1\%$
COUSTEIX/BERRUE	2	x		$\Delta \beta_w < .35°$
CROSS	2	x	10	$\Delta \beta_w = .05°$
HUMPHREYS	2	x,y	10	$\Delta C_f = 3.1\%$
LINDHOUT/DE BRUIN	8	x	10	$\Delta \beta_w = .4°$ $\Delta C_f^w = .5\%$
MÜLLER	2	x,y		$\Delta \beta_w < 1°$ $\Delta C_f^w = 1\%$
NAKKASYAN	2	x,y	18	$\Delta \beta_w = .2°$
PATEL/KROGSTAD/BAEK	2	x	10	$\Delta C_f = .2\%$
SCHNEIDER	2	x,y		$\Delta C_f < 1\%$

(b) Integral momentum balance

results submitted	station number	local error	
HOEKSTRA		$\Omega_s \cong 0.03\%$	$\Omega_n \cong 0.04\%$
MÜLLER	10	$\Omega_x \cong 0.30\%$	$\Omega_z \cong 1.30\%$

The participants were asked to submit amongst others results for the integral quantities R_Θ, C_f and β_w. The comparison between calculations and measurements begins in figure 3.4 with the local Reynolds number based on the momentum thickness, R_Θ. Uncertainty in the measured values is estimated to be no more than a few percent for the whole range shown. Agreement with the experimental data is thus obtained up to $x/L \cong 1.0$. The only exception to this is the NAKKASYAN calculation which fails considerably earlier. All results then deviate markedly from the experimental data, the computed and experimentally determined variations showing quite different behaviour.

The calculated and measured wall flow angles β_w are plotted in figure 3.5. The measurements are accurate to $\pm 1°$. It is seen that all methods agree with the experimental data up to $x/L \cong 0.9$ (where β_w is only about 12°), except for the SCHNEIDER and SMITH values, which are slightly high and low respectively. For stations further downstream, only the integral methods CROSS and COUSTEIX/BERRUE and the HOEKSTRA field method are able to follow the experimental data up to $x/L \cong 1.1$. Beyond this station the flow angle at the wall cannot be reproduced by any of the participating methods (separation occurs near $x/L \cong 1.3$). The reason for this deviation from the experimental data will become clear when the shear stress profiles are discussed.

Large deviations are encountered also in the calculation of the skin friction C_f (figure 3.6). General agreement with measured values (considered accurate to $\pm 1.5 \times 10^{-4}$) is again obtained up to $x/L \cong 1.0$, but the HUMPHREYS, LINDHOUT/DE BRUIN and SCHNEIDER results are somewhat low in the upstream part. Downstream of $x/L \cong 1.0$ only the HOEKSTRA and CROSS results can follow the experimental data to separation. The other methods compute the skin friction here thirty or forty percent too high, well outside experimental uncertainty.

The profiles of the streamwise velocity component are shown in figures 3.7 to 3.9, for stations 8 (x/L = 0.920), 10 (x/L = 1.020) and 12 (x/L = 1.120), respectively. No boundary layer velocity results were provided by the methods COUSTEIX/BERRUE and SMITH. With the exception of MÜLLER, NAKKASYAN and CEBECI/HUANG results, all methods appear to compute streamwise velocities very well at station 8, although no set of results lies wholly within the experimental error band (about 1% for mean velocities). All calculations except those of CROSS and HOEKSTRA deviate markedly from the experimental data at station 10 and deteriorate further by station 12.

Similar trends can be noted in the corresponding profiles for the crossflow velocity component, shown in figures 3.10 to 3.12, but the discrepancies are on the whole much larger here. At station 8 the crossflow angle β_w is only about 13°, but at station 12 it has risen to 26°. Most methods seriously underestimate the crossflow at station 12 and this would be expected to contribute to the poor performance for the streamwise velocity (figure 3.9). The integral method of CROSS yields good agreement with experimental crossflow profiles at all three stations.

A more revealing demonstration of accuracy is obtained after comparing measured and calculated Reynolds stresses. The streamwise (figures 3.13 to 3.15) and crosswise shear stresses (figures 3.16 to 3.18) are plotted versus the coordinate normal to the wall for stations 7 (x/L = 0.895), 9 (x/L = 0.995) and 11 (x/L = 1.095), respectively. The wall shear stress component determined with Stanton tubes is also indicated in the graphs and connected with a dashed line to the data obtained by hot wire. Calculated shear stress is available only from the field methods. The calculations scatter widely about the measured data. The experimental error is ± 10% or ± 0.02 x 10^{-2}, whichever is the greatest. Most calculation results still fall, completely or

partly, outside this fairly large uncertainty range. For the stream-
wise shear stress component most methods tend to overestimate the
magnitude, but the HOEKSTRA method tends to underestimate it. The
NAKKASYAN results are in fair agreement at station 7, but not anymore
at station 9 and 11. For the crosswise shear stresses, the HOEKSTRA
and SCHNEIDER models appear to perform best. NAKKASYAN computes a
clearly too small crosswise shear stress level, while most of the
others tend to overestimate it.

It is interesting to study the results of the calculation methods
using a non-isotropic eddy viscosity. Compared to methods with an
isotropic eddy viscosity, the non-isotropic model used in the HUMPHREYS
calculations is seen to confer rather small benefit for the crosswise
shear stresses, notably at station 11. On the other hand NAKKASYAN
seems to introduce such a strong anisotropy that the crosswise shear
stresses are almost annihilated. The calculations by SCHNEIDER with a
non-isotropic eddy viscosity appear to bring the crosswise shear
stress fairly close to the measurements. The crosswise shear stresses
computed with HOEKSTRA's isotropic eddy viscosity method are also in
fair agreement with experiment. The modified eddy viscosity model
employed by him leads to an overall low level of the total shear
stress and the streamwise shear stresses are consistently too low
(figures 3.13 to 3.15), as noted earlier.

In figures 3.19 to 3.23 are presented the results of various
additional calculations carried out by the participants to test
different assumptions. Figures 3.19 to 3.20 show the effects of
changing turbulence models used for the HOEKSTRA and NAKKASYAN results.
In figure 3.19, HOEKSTRA version 2 uses a fairly standard algebraic
isotropic eddy viscosity model, while in version 1 a modified isotropic

eddy viscosity model is applied, which takes into account pressure
gradient effects on the eddy viscosity magnitude (see Chapter 2 and
Humphreys & Lindhout 1987). The agreement with experiment is seen to
be much better with version 1. Note that this version has been applied
to this test case only. Calculations with various degrees of anisotropy
of the eddy viscosity were performed with the NAKKASYAN method. Figure
3.20 shows the large effect of the anisotropy on the calculations.
Best agreement is obtained with version 3 having the strongest anisotropy.

The COUSTEIX/BERRUE method has been applied with different empirical
assumptions. They were derived from similarity solutions using an
isotropic and a non-isotropic eddy viscosity model. The latter one is
the standard version of this calculation method. The difference in
results obtained with the two versions of this integral method turned
out to be very small.

Figure 3.21 shows the effect computed with the CROSS method of
assuming a slightly different initial wall crossflow angle β_w. Not
very much happens before about $x/L = 1.1$. The results of the two
calculations then begin to draw apart and the second run, with in-
creased initial β_w, appears not to be able to proceed further down-
stream than $x/L = 1.2$.

If the pressure distribution is modified, even greater changes
are seen. In figure 3.22 are shown two sets of calculations performed
with the HUMPHREYS method, version 1 using the measured wall pressure
C_{pw}, as prescribed for the Workshop, and version 2 using a pressure
distribution computed from the measured external flow angles (van den
Berg & Elsenaar 1972). Although the static pressure variation across
the boundary layer is negligible up to $x/L = 1.1$ and reaches only
$C_{pe} - C_{pw} \cong 0.01$ at $x/L = 1.3$ (near separation), the difference in
computed results appears to be disproportionally large.

Similar results are evident in the four sets of calculations carried out with the SCHNEIDER method (figure 3.23). Version 1 used C_{pw} together with the external velocity vector direction computed from C_{pw} assuming swept infinite wing conditions, as prescribed for the Workshop. Version 2 assumed measured edge pressures C_{pe} and measured flow angles at the boundary layer edge. The difference between both angles is of the order of 1° between x/L = 1.1 and 1.3. Versions 3 and 4 took (C_{pw}, measured angle) and (C_{pe}, computed angle), respectively. With irrotational inviscid conditions, pressure and flow angle cannot strictly be prescribed independently, as has been done in versions 2 to 4. The effect of these changes appears to be very large downstream of x/L = 1.1.

Figures 3.21 to 3.23 demonstrate that with these direct mode calculations the boundary layer becomes sensitive to its flow-defining conditions at x/L = 1.1, some five boundary layer thicknesses from the separation line. The possibility that such calculations could be sensitive to the prescribed pressure distribution close to separation has been recognized for some time by various workers, in the case of BEEL72 by the experimenters themselves (Elsenaar, van den Berg & Lindhout 1975), amongst others. Recently de Bruin (1983) investigated systematically the effect of pressure modification for this flow. The study confirmed the sensitivity to small changes in the prescribed pressure distribution for x/L > 1.1, but only for those calculations which approach separation. With a turbulence model leading to a boundary layer with no tendency to separate, calculations were not sensitive to small modifications in the prescribed pressure distribution. Most calculations applied to this test case do not give results close to separation.

The numerical difficulties near separation can be resolved by using inverse solutions and prescribing the measured boundary layer thickness distribution instead of the pressure distribution. Such inverse calculations have been performed by Cousteix & Houdeville (1981), Smith (1984) and others. Inverse calculations were not required for the Berlin Workshop, because few suitable inverse calculation methods were available at the time.

Table 3.2 Survey of computed results for the BEEL72 test case

figures	quantities	CEBECI HUANG	COUSTEIX BERRUE	CROSS	HOEKSTRA	HUMPHREYS	LINDHOUT DE BRUIN
3.4 -3.6	R_θ, β_w, C_f	X	X	X	X	X	X
3.7 -3.12	U, W	X		X	X	X	X
3.13-3.18	τ_x, τ_z	X			X	X	X
3.19-3.24	R_θ, β_w, C_f		various versions	various versions	various versions	various versions	

figures	quantities	MULLER	NAKKASYAN	PATEL KROGSTAD BAEK	SCHNEIDER	SMITH
3.4 -3.6	R_θ, β_w, C_f	X	X	X	X	X
3.7 -3.12	U, W	X	X	X	X	
3.13-3.18	τ_x, τ_z	X	X	X	X	
3.19-3.24	R_θ, β_w, C_f		various versions		various versions	
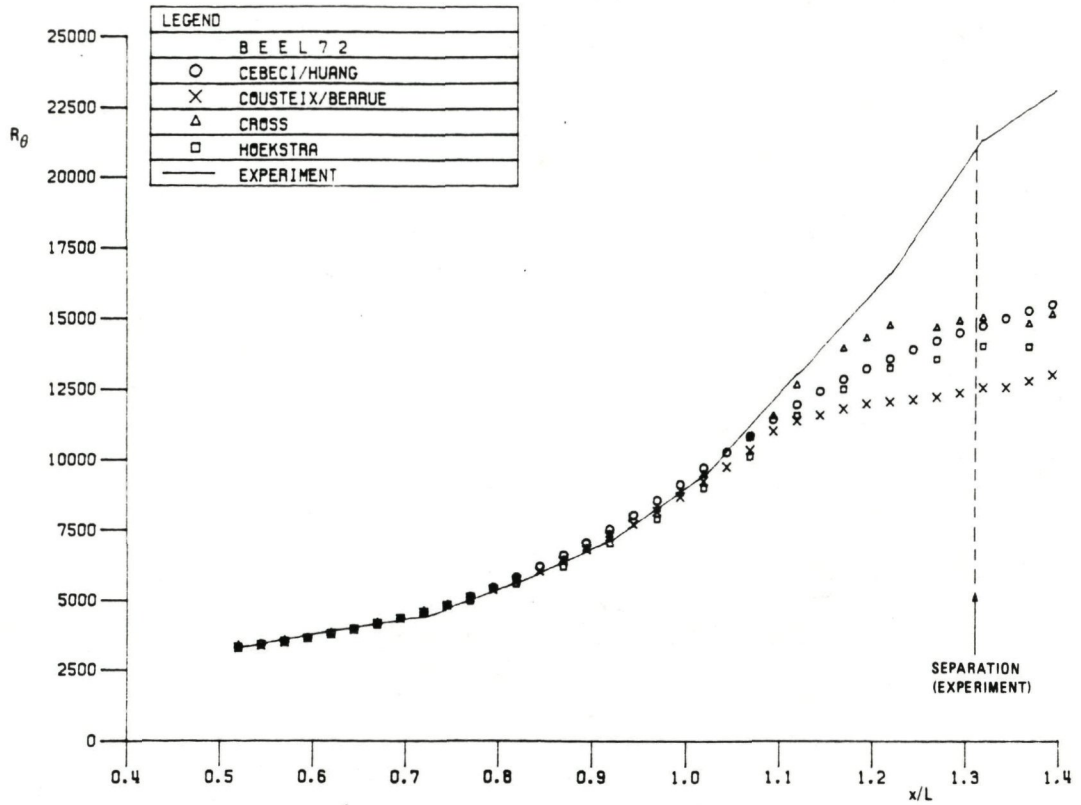
Fig. 3.4a Variation of momentum thickness Reynolds number with x/L
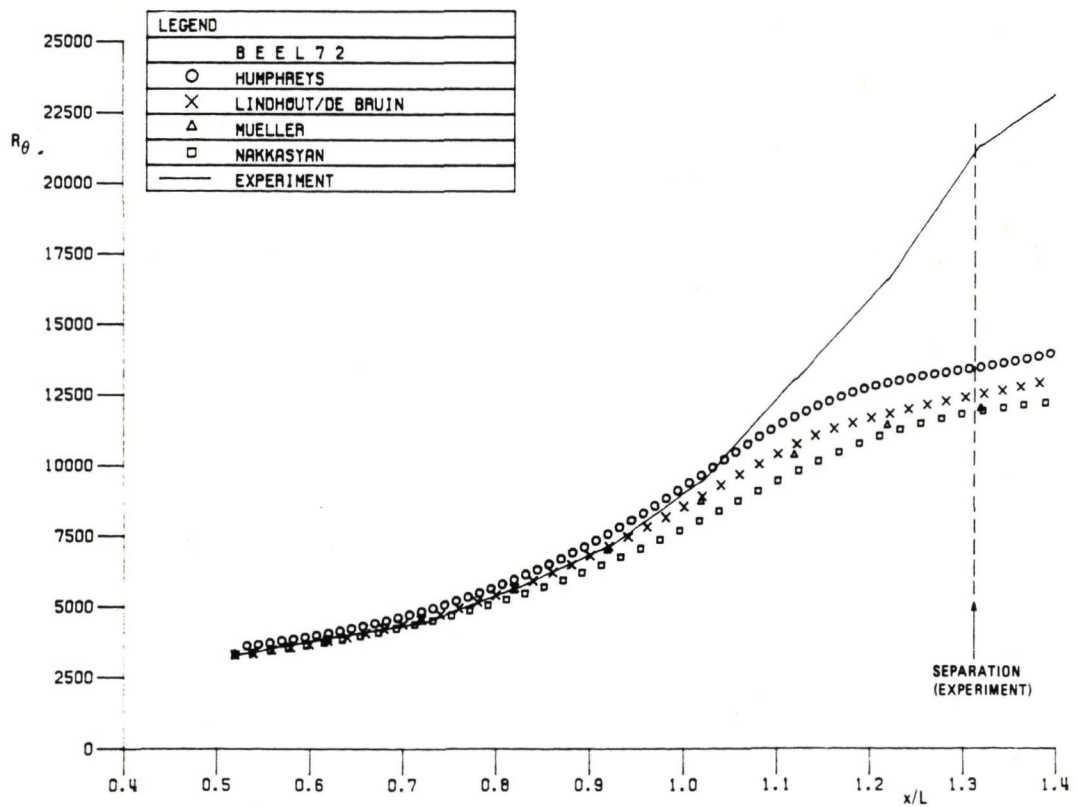
Fig. 3.4b Variation of momentum thickness Reynolds number with x/L
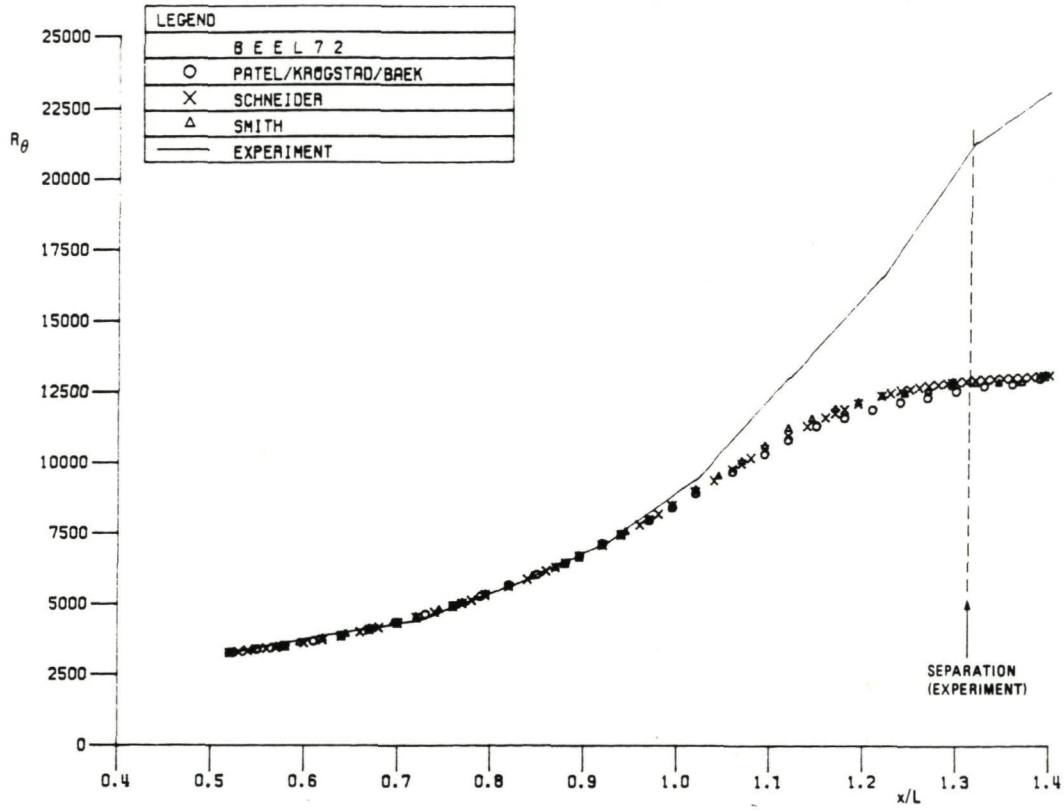
Fig. 3.4c Variation of momentum thickness Reynolds number with x/L
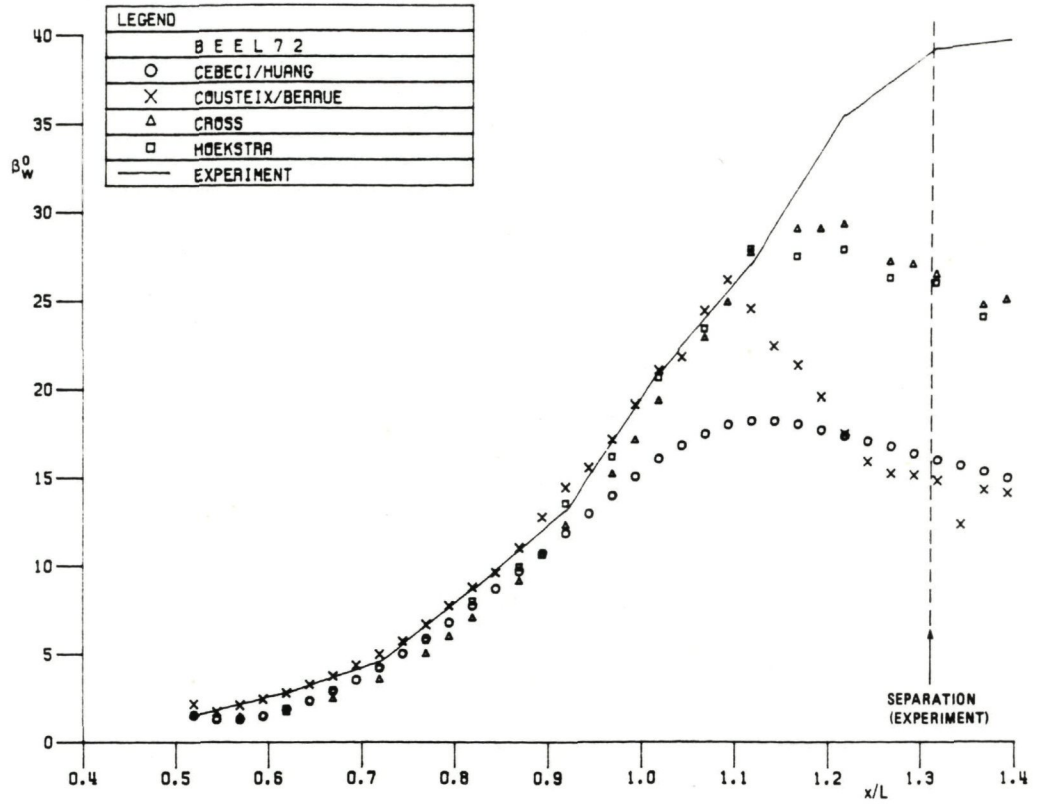
Fig. 3.5a   Variation of wall flow angle with x/L
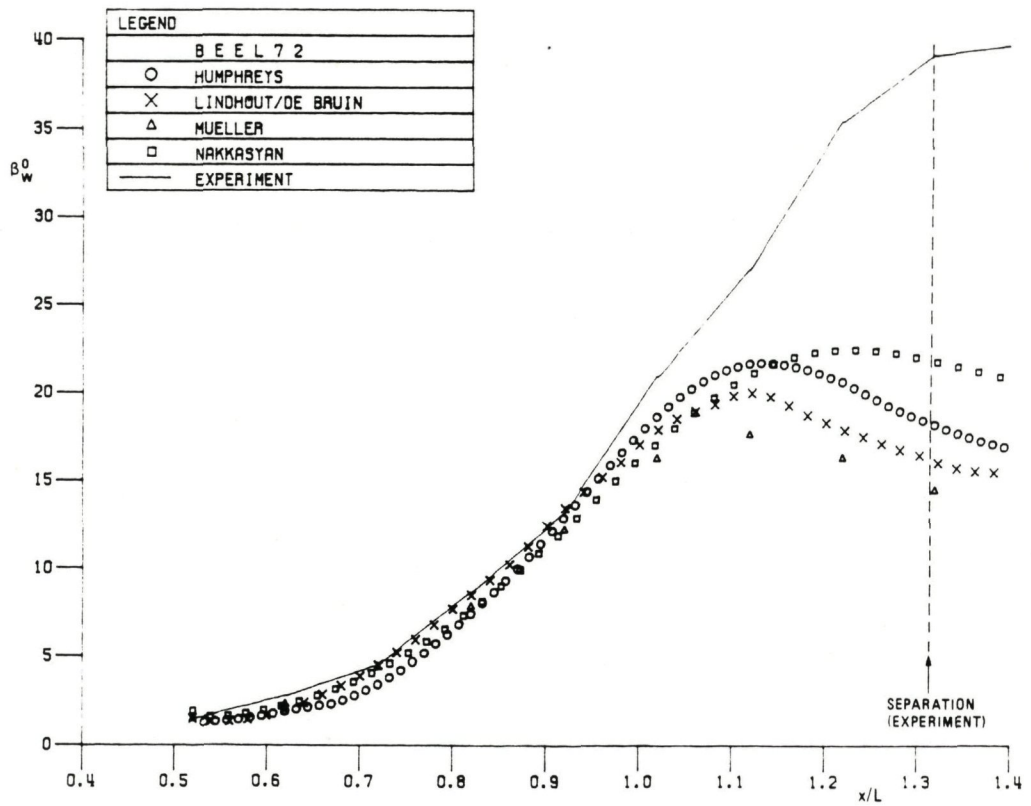
Fig. 3.5b   Variation of wall flow angle with x/L
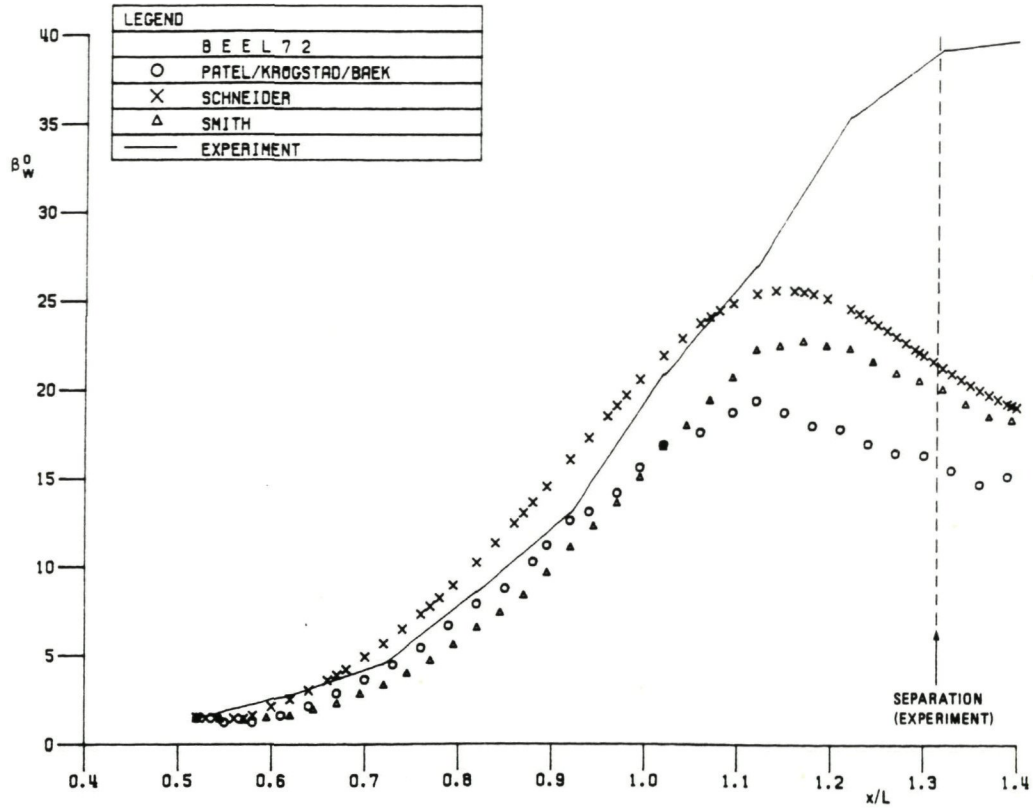
Fig. 3.5c Variation of wall flow angle with x/L
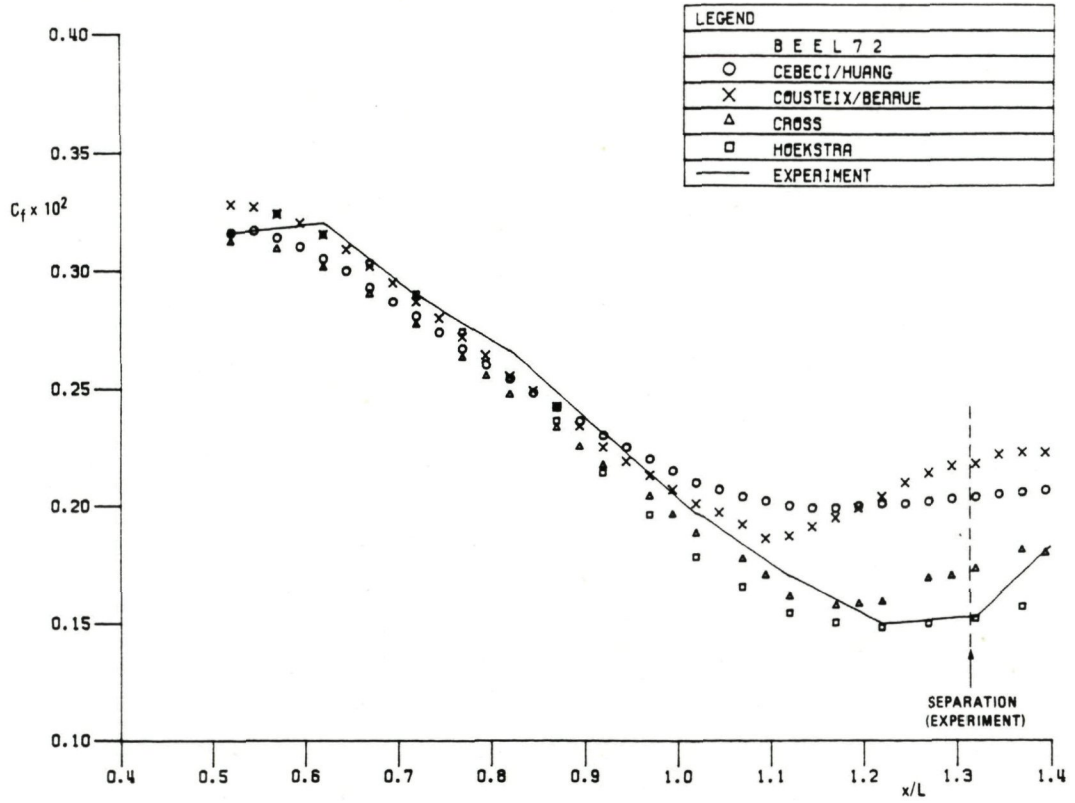
Fig. 3.6a   Variation of skin friction with x/L
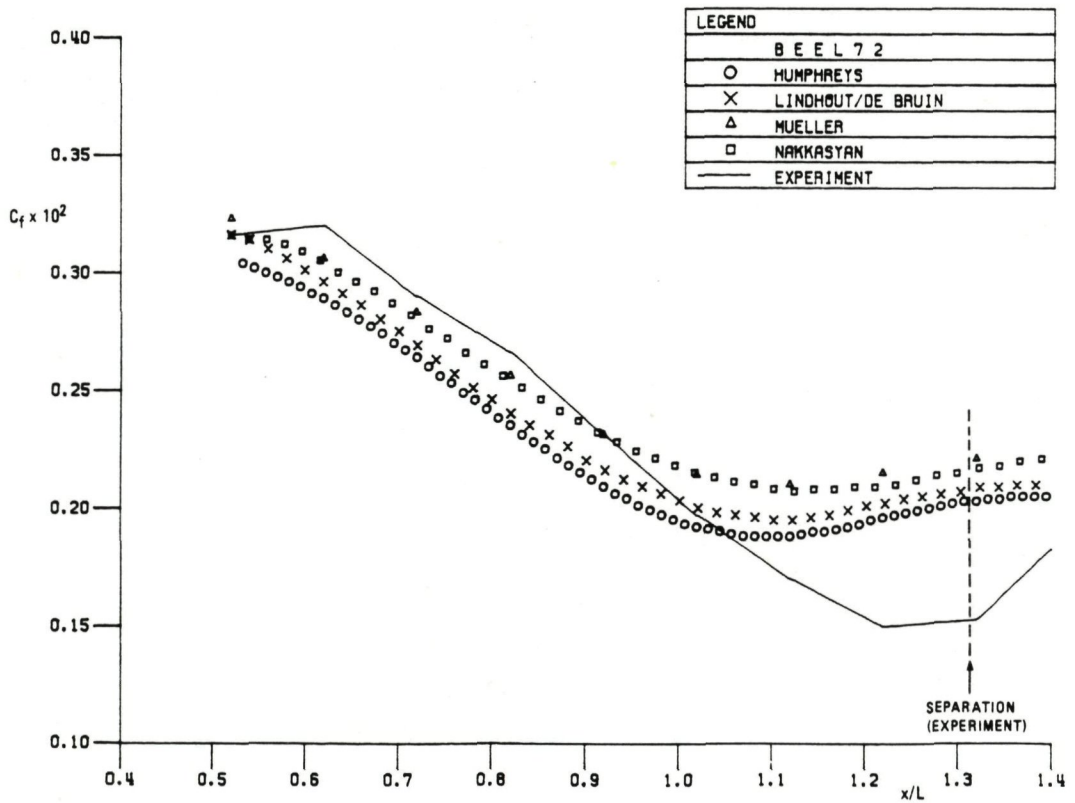
Fig. 3.6b   Variation of skin friction with x/L
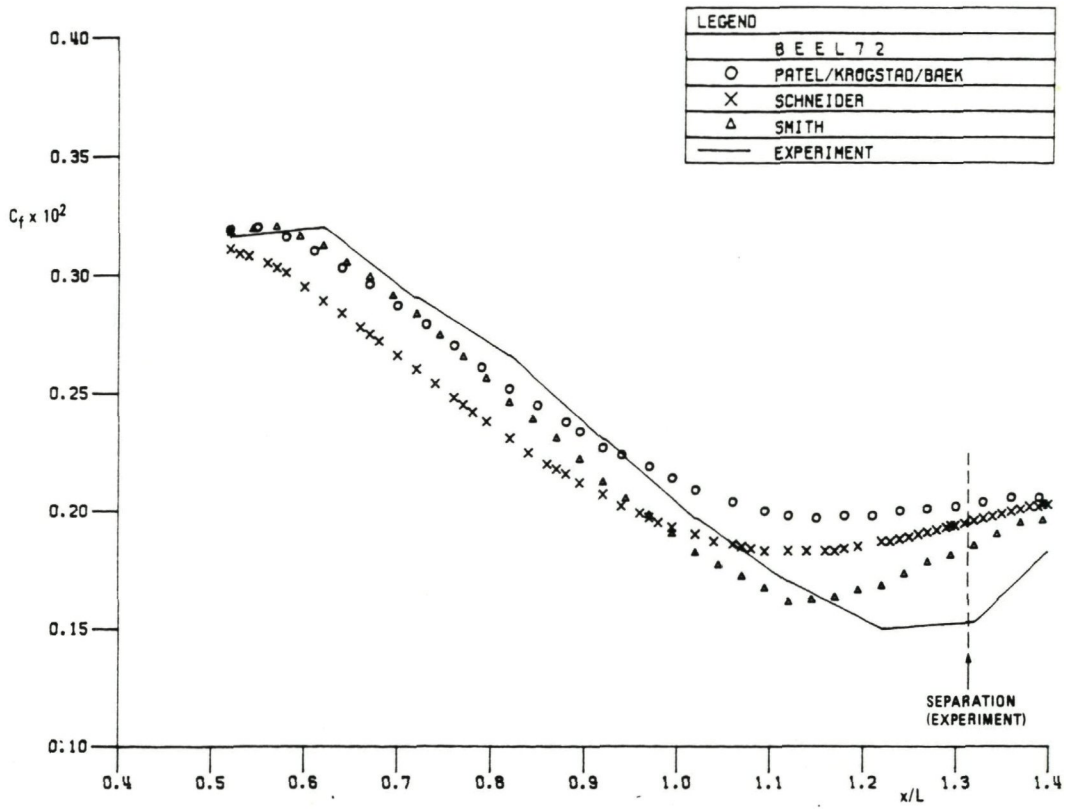
Fig. 3.6c Variation of skin friction with x/L
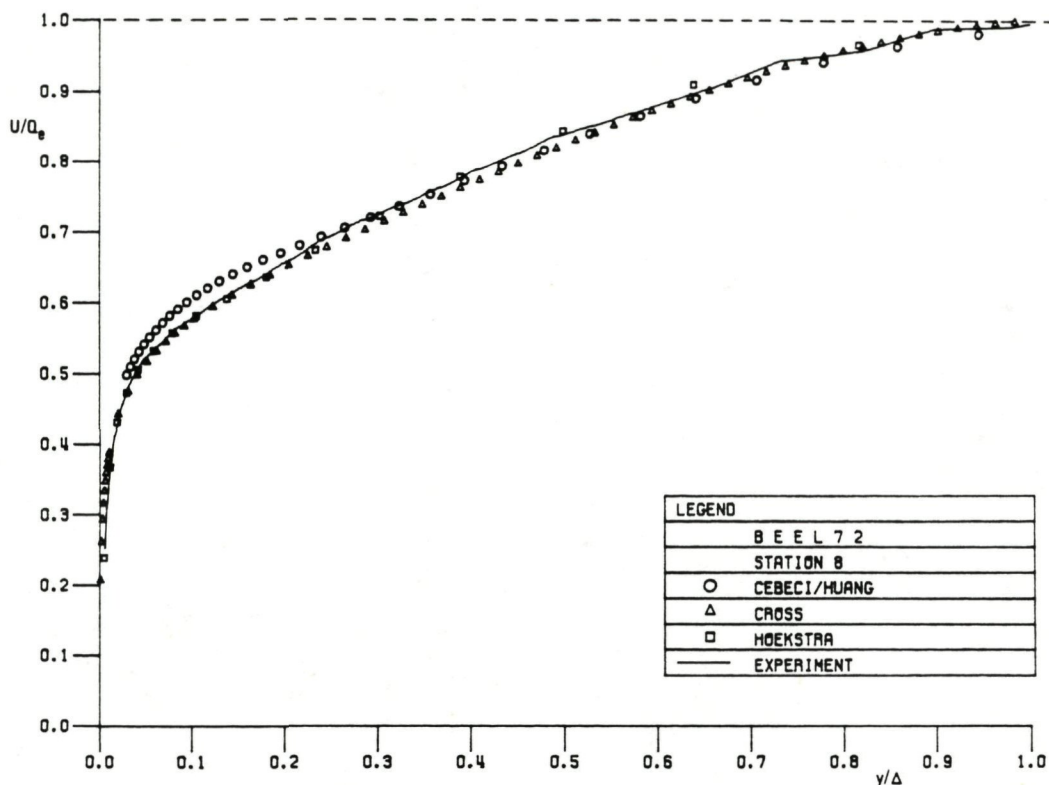
Fig. 3.7a   Streamwise velocity profiles at station 8   (x/L = 0.920)
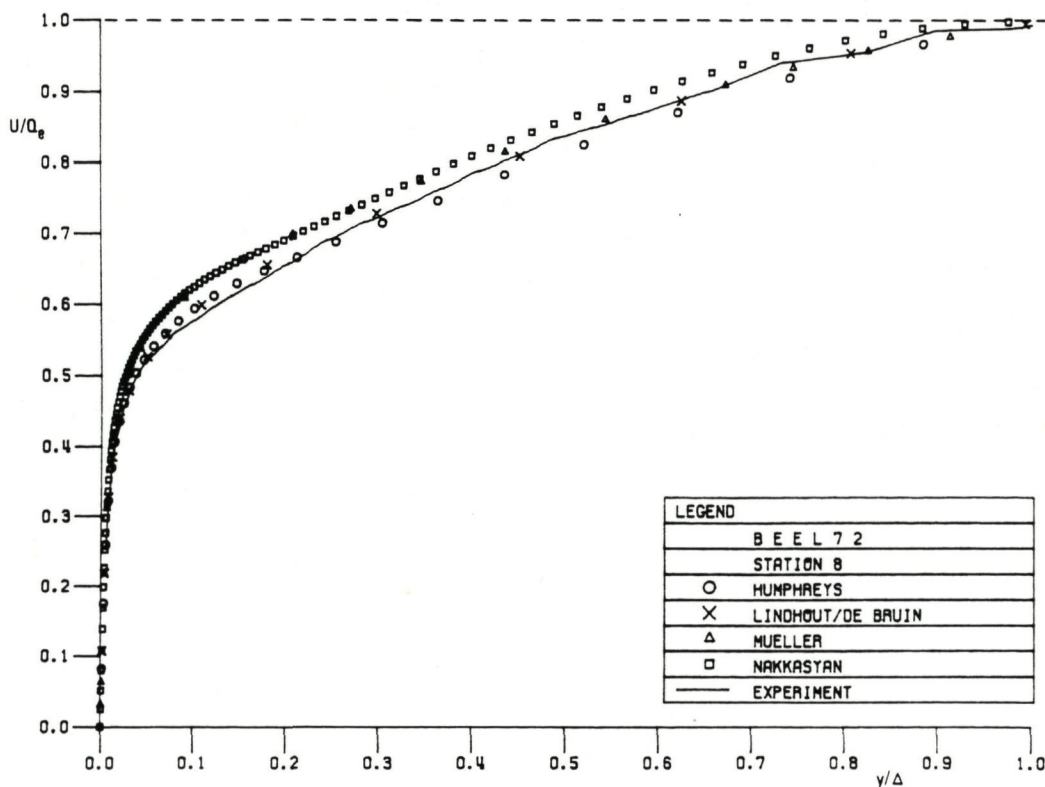
Fig. 3.7b   Streamwise velocity profiles at station 8   (x/L = 0.920)
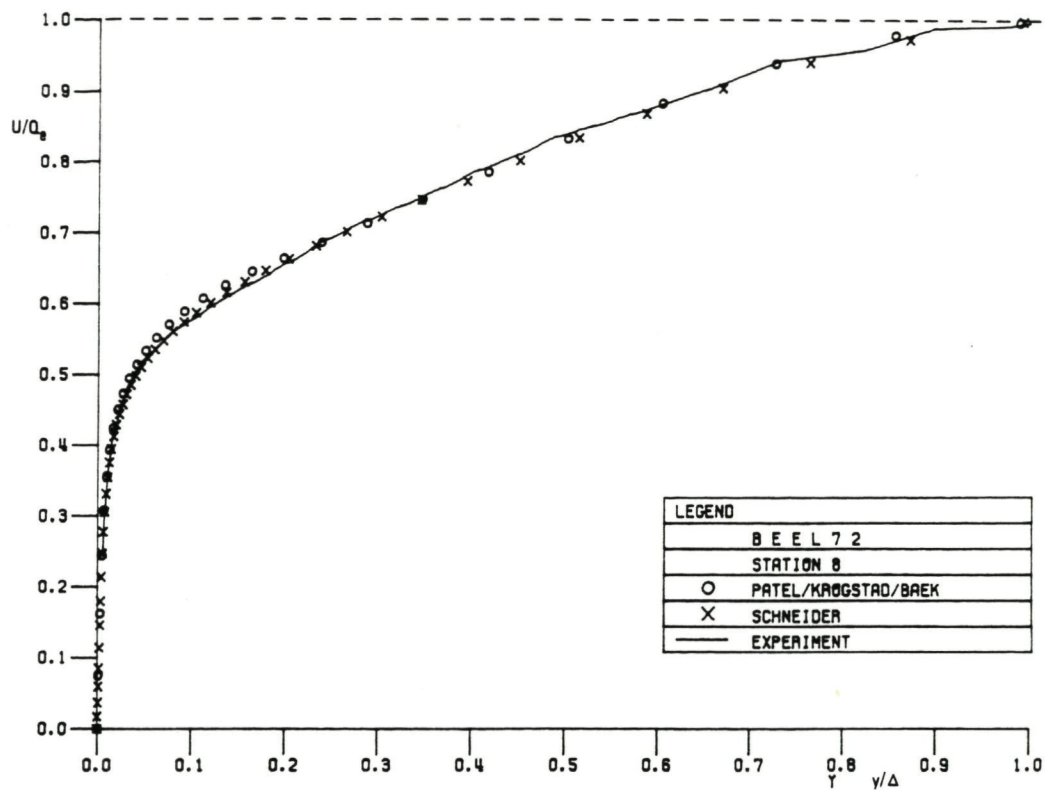
Fig. 3.7c   Streamwise velocity profiles at station 8 (x/L = 0.920)
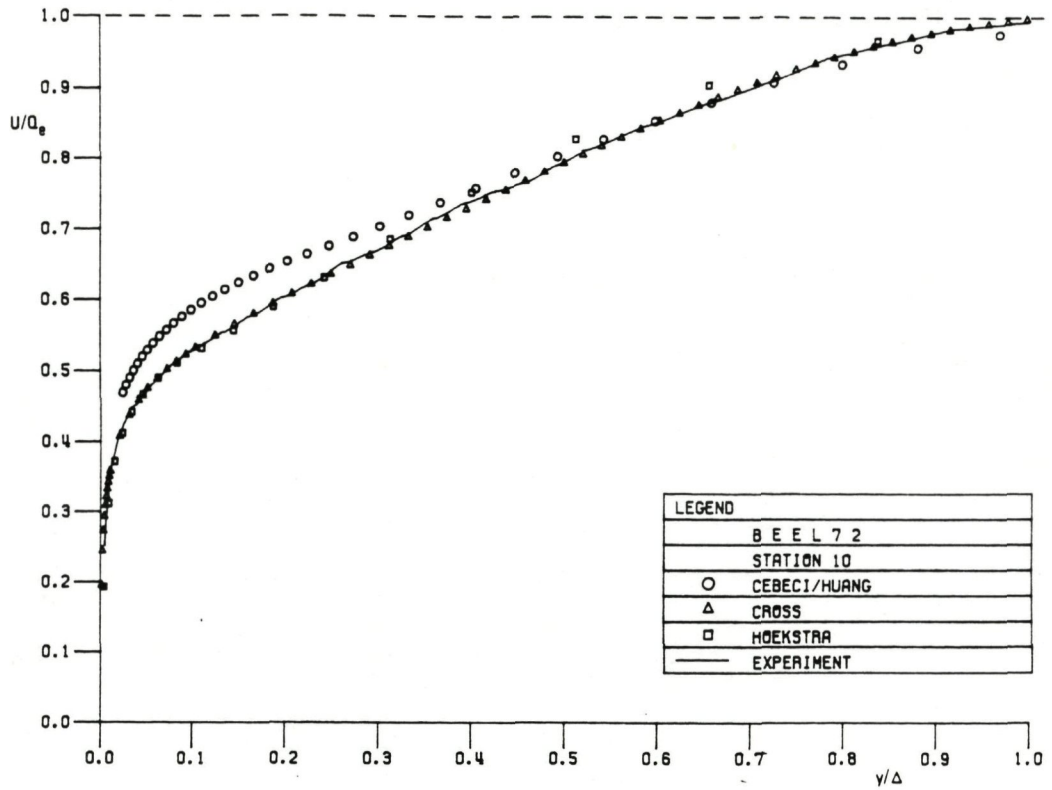
Fig. 3.8a Streamwise velocity profiles at station 10 (x/L = 1.020)
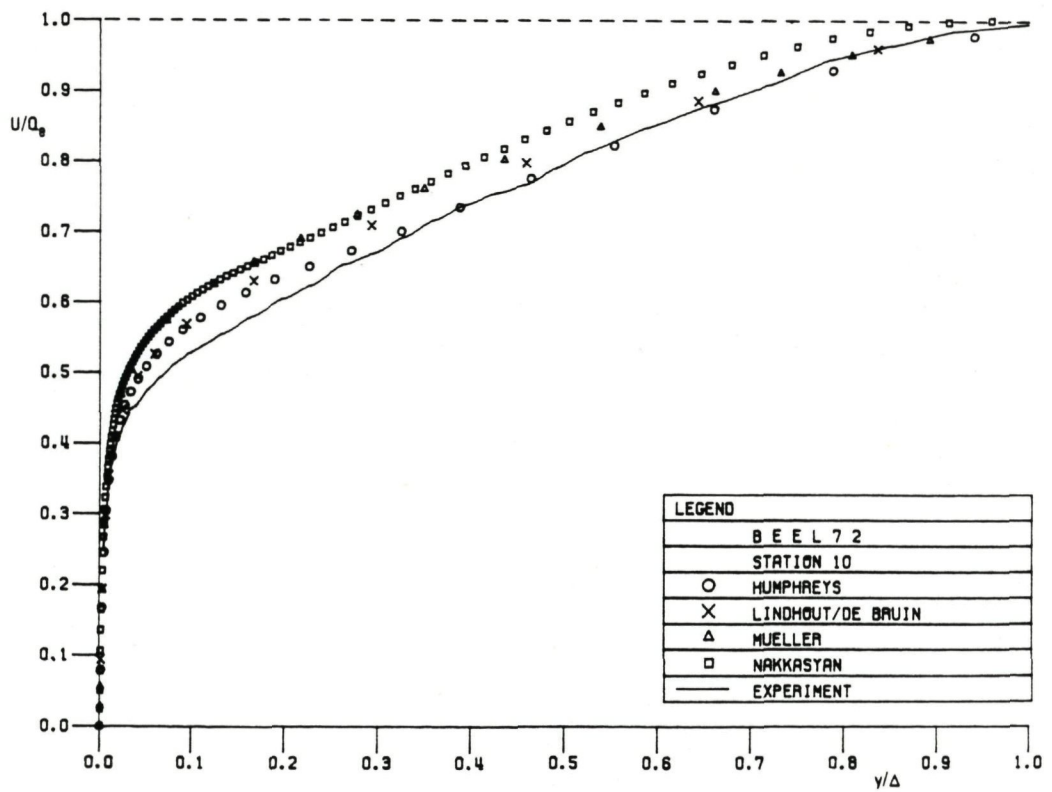
Fig. 3.8b Streamwise velocity profiles at station 10 (x/L = 1.020)
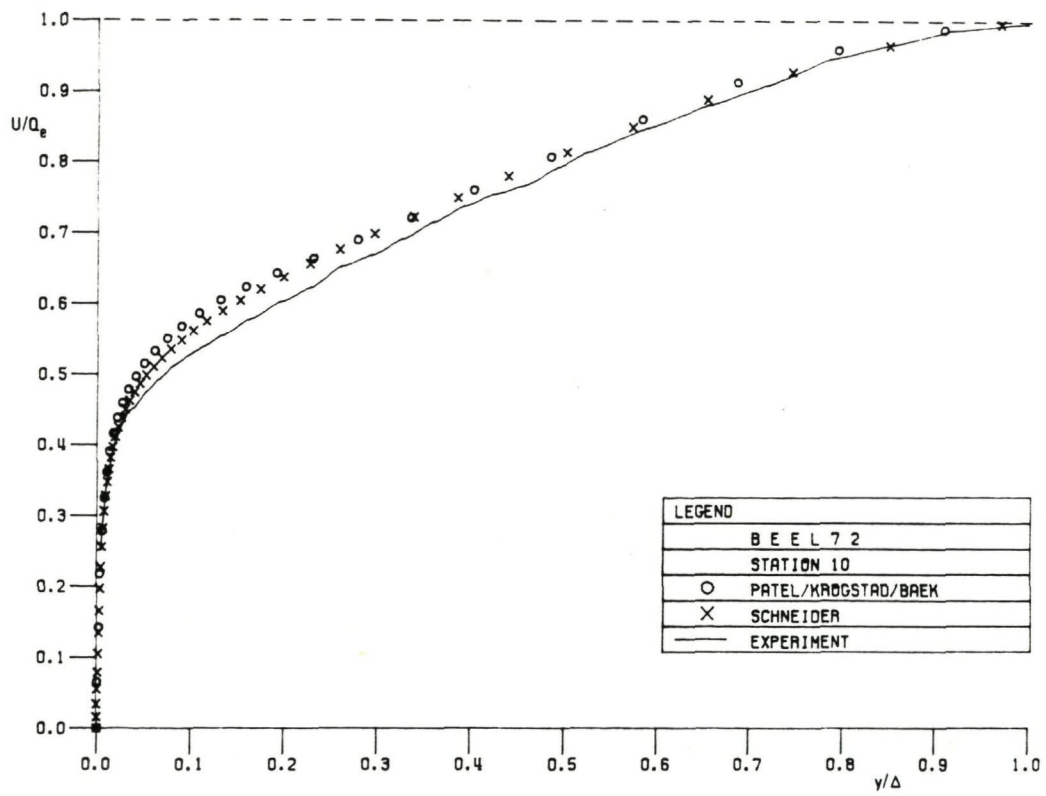
Fig. 3.8c   Streamwise velocity profiles at station 10 (x/L = 1.020)
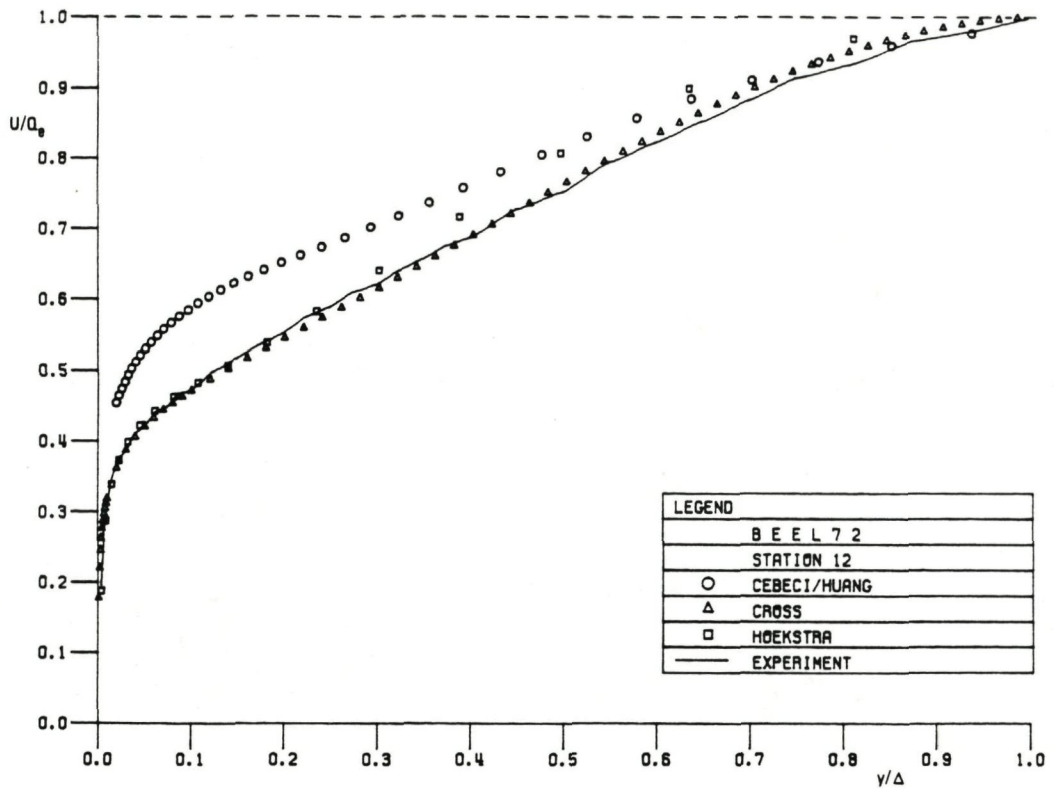
Fig. 3.9a   Streamwise velocity profiles at station 12 (x/L = 1.120)
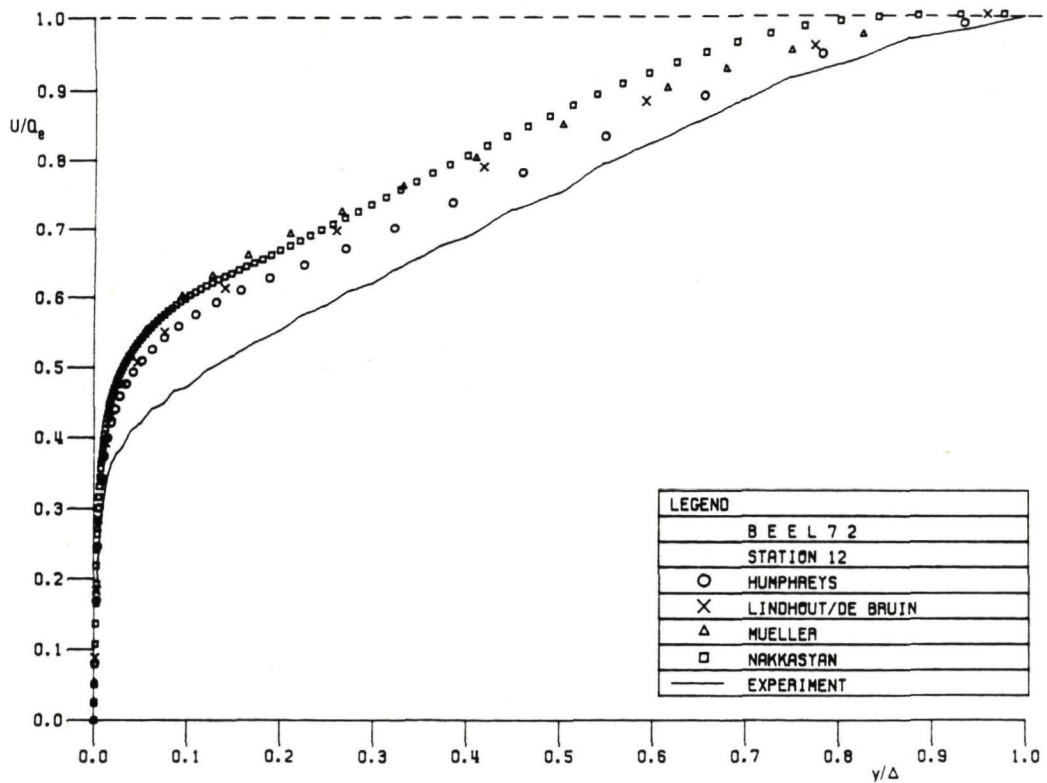
Fig. 3.9b   Streamwise velocity profiles at station 12 (x/L = 1.120)
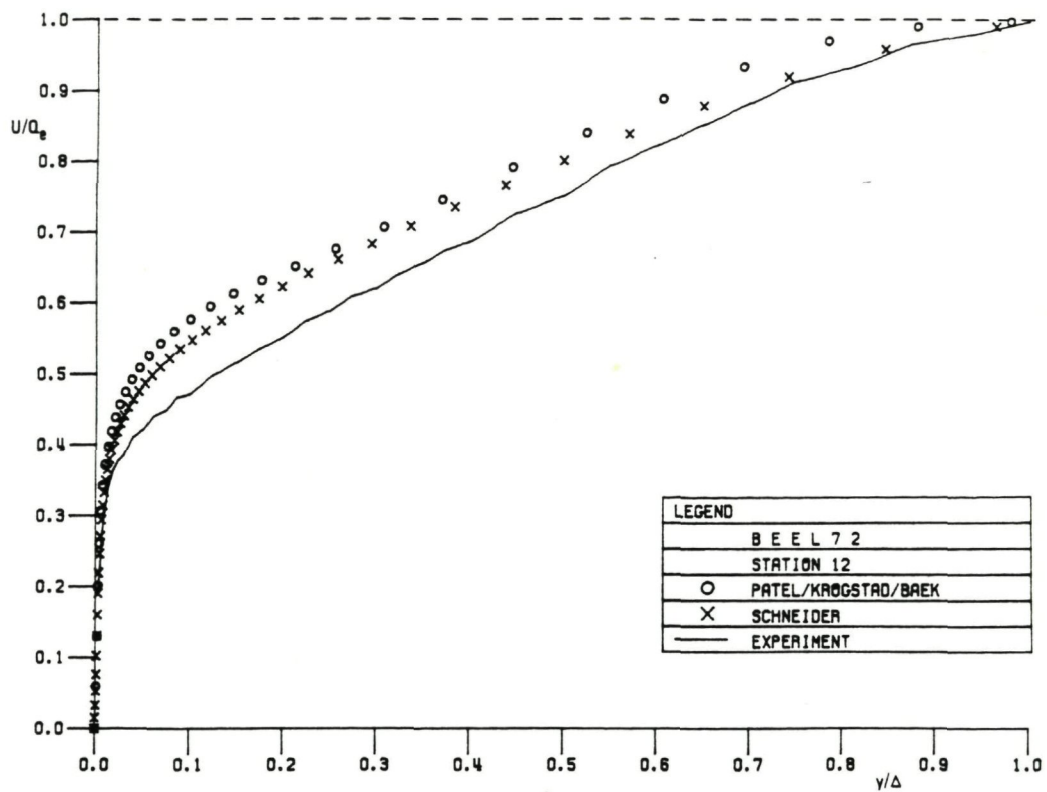
Fig. 3.9c   Streamwise velocity profiles at station 12 (x/L = 1.120)
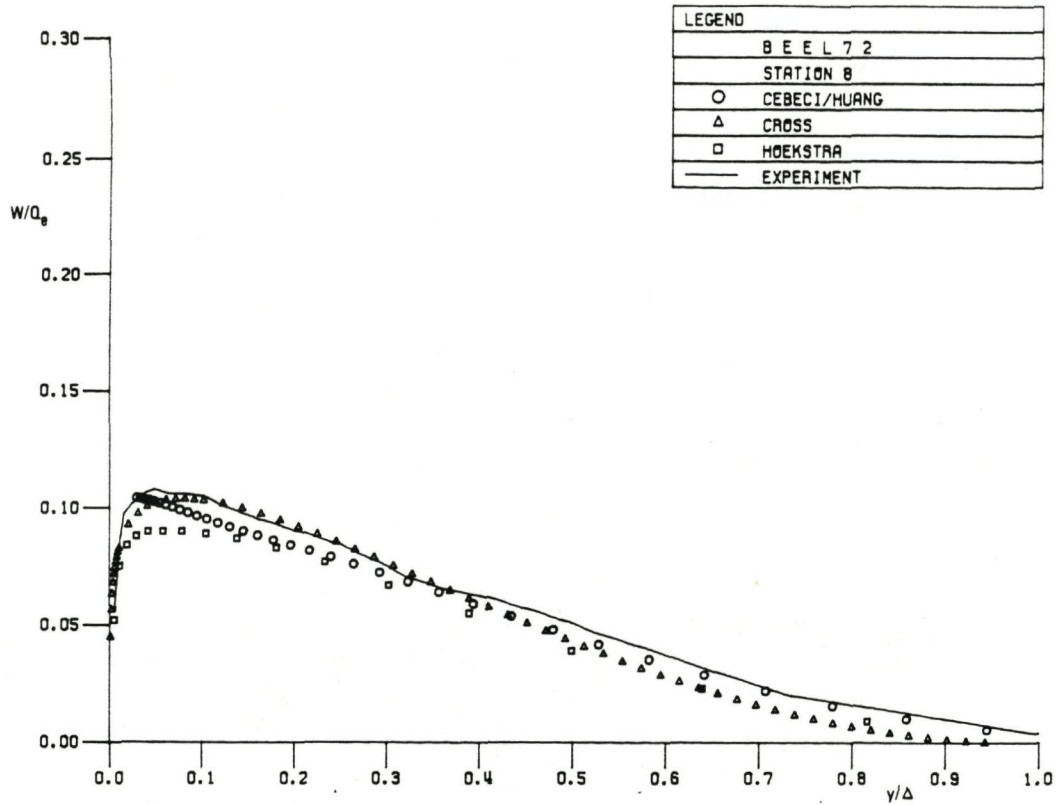
Fig. 3.10a   Crosswise velocity profiles at station 8 (x/L = 0.920)
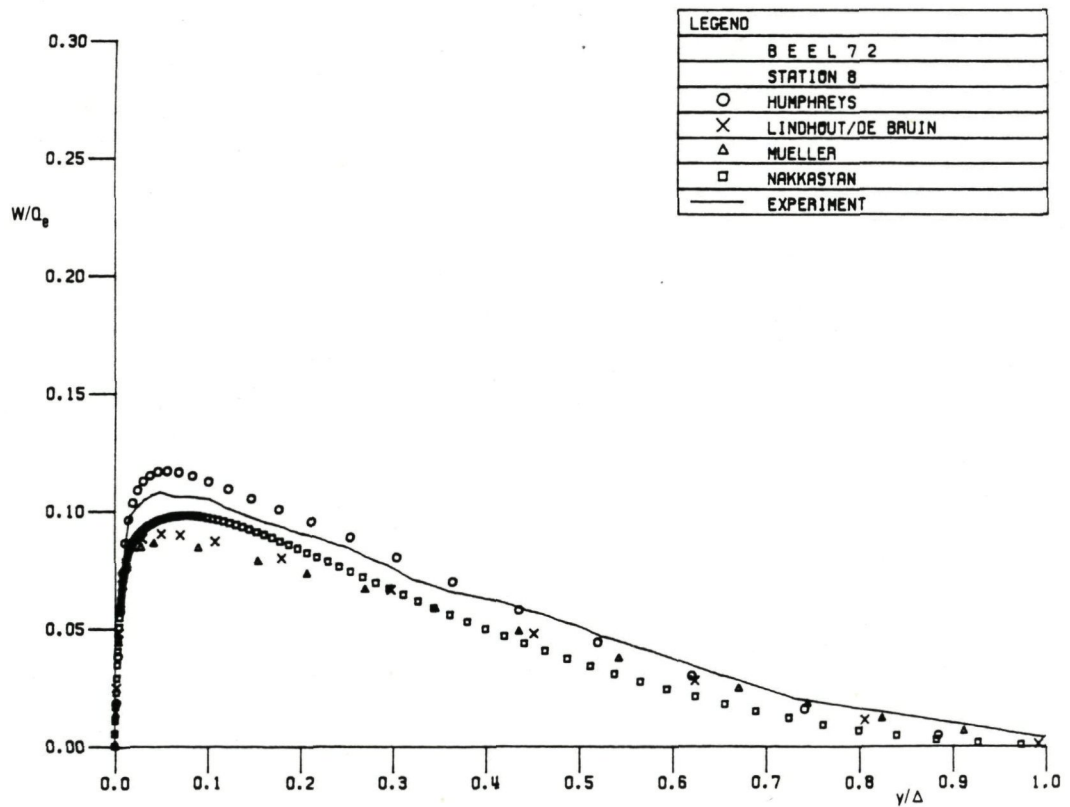
Fig. 3.10b   Crosswise velocity profiles at station 8 (x/L = 0.920)
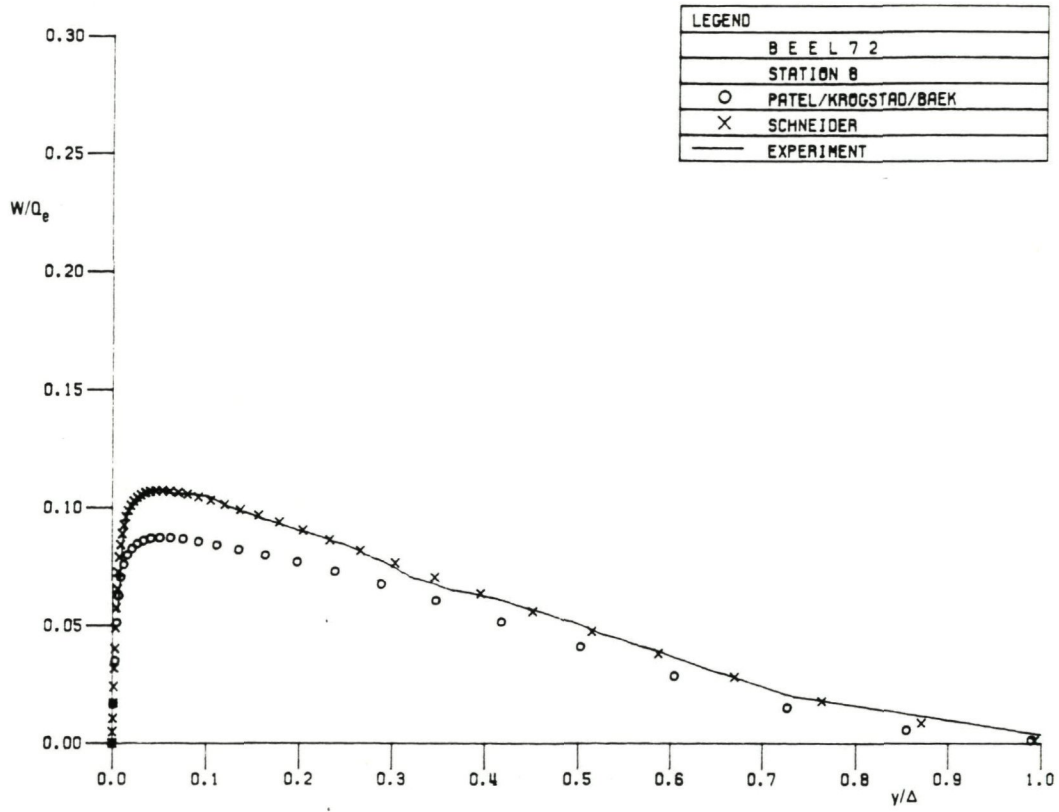
Fig. 3.10c   Crosswise velocity profiles at station 8 (x/L = 0.920)
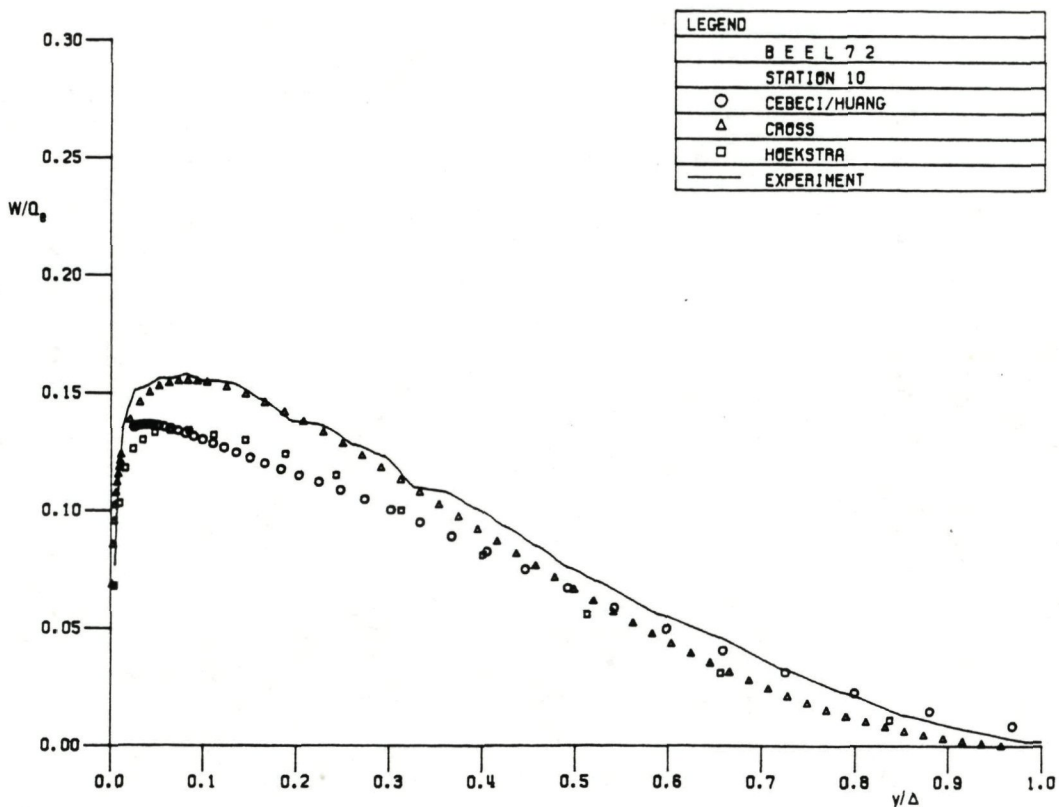
Fig. 3.11a   Crosswise velocity profiles at station 10 (x/L = 1.020)
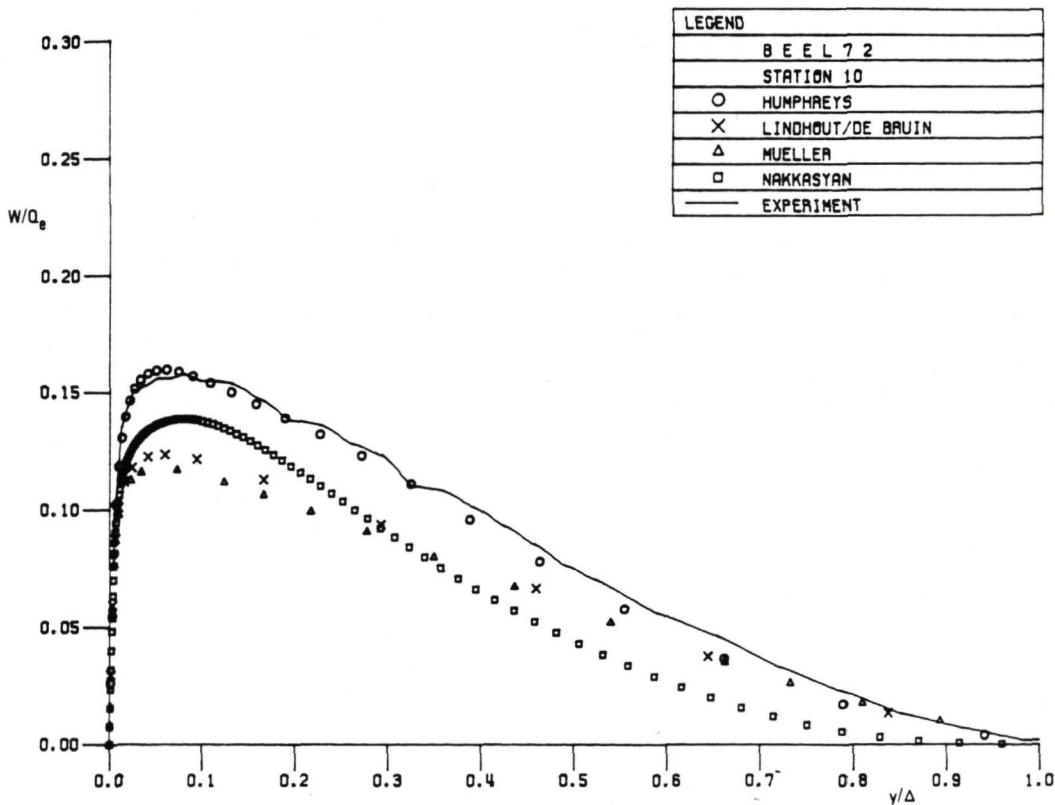
Fig. 3.11b   Crosswise velocity profiles at station 10 (x/L = 1.020)
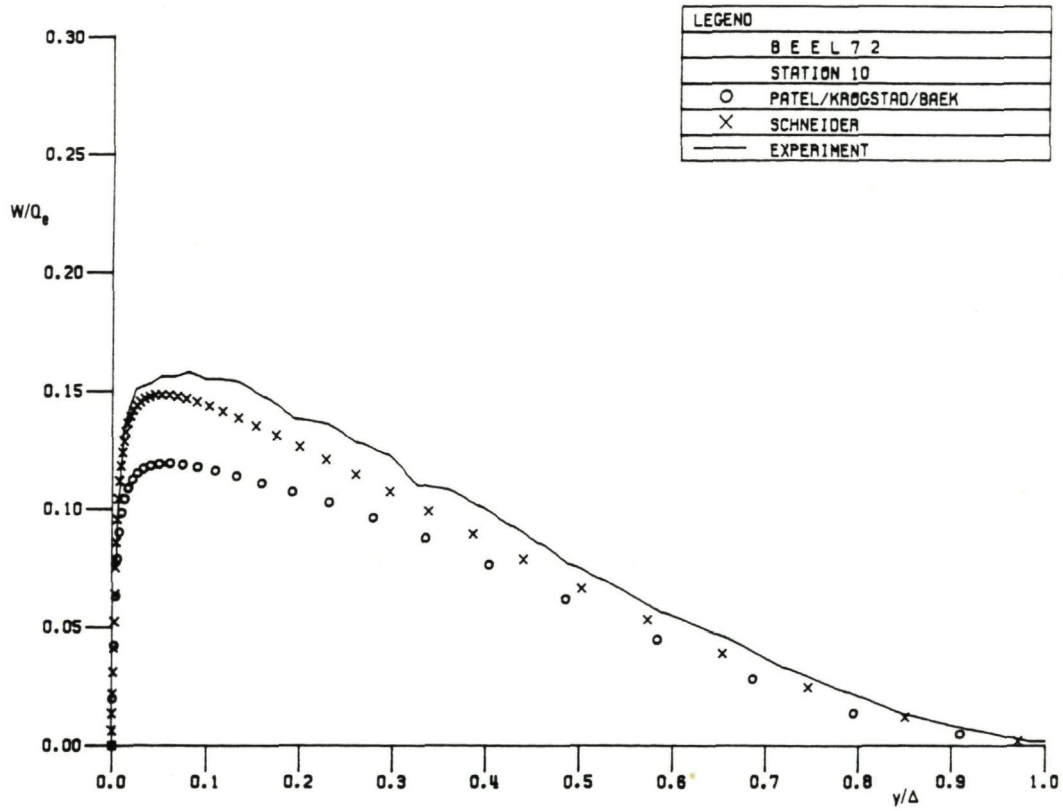
Fig. 3.11c   Crosswise velocity profiles at station 10 (x/L = 1.020)
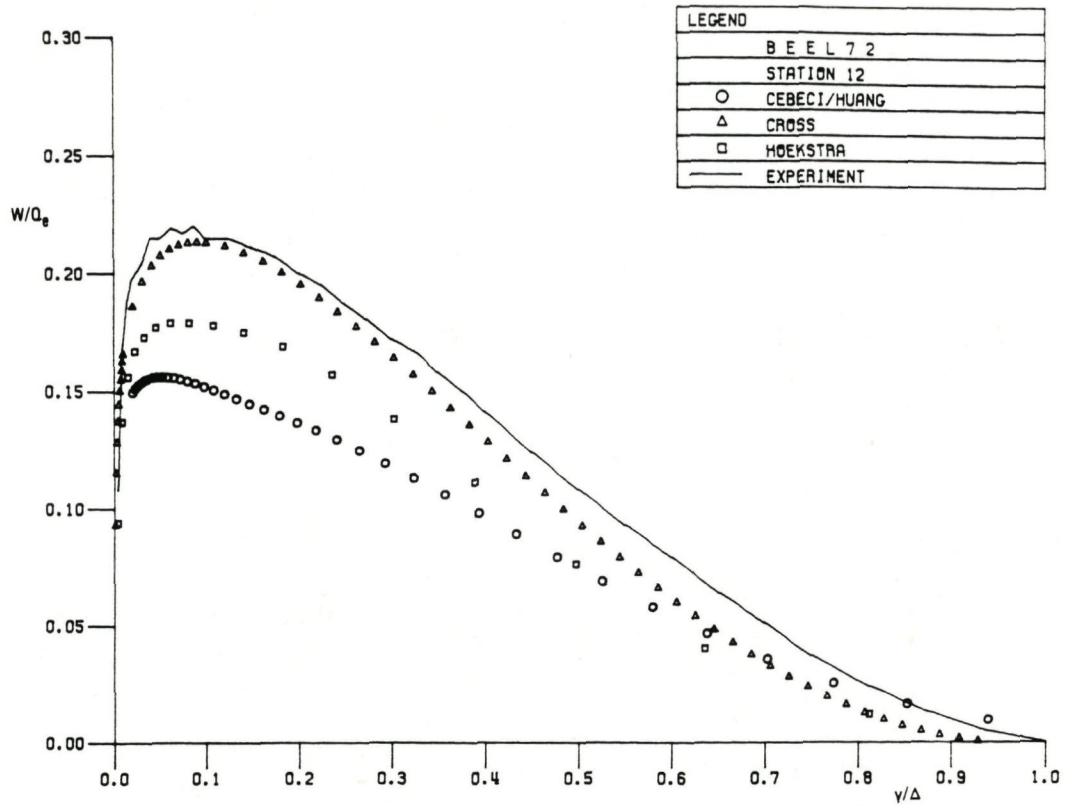
Fig. 3.12a Crosswise velocity profiles at station 12 (x/L = 1.120)
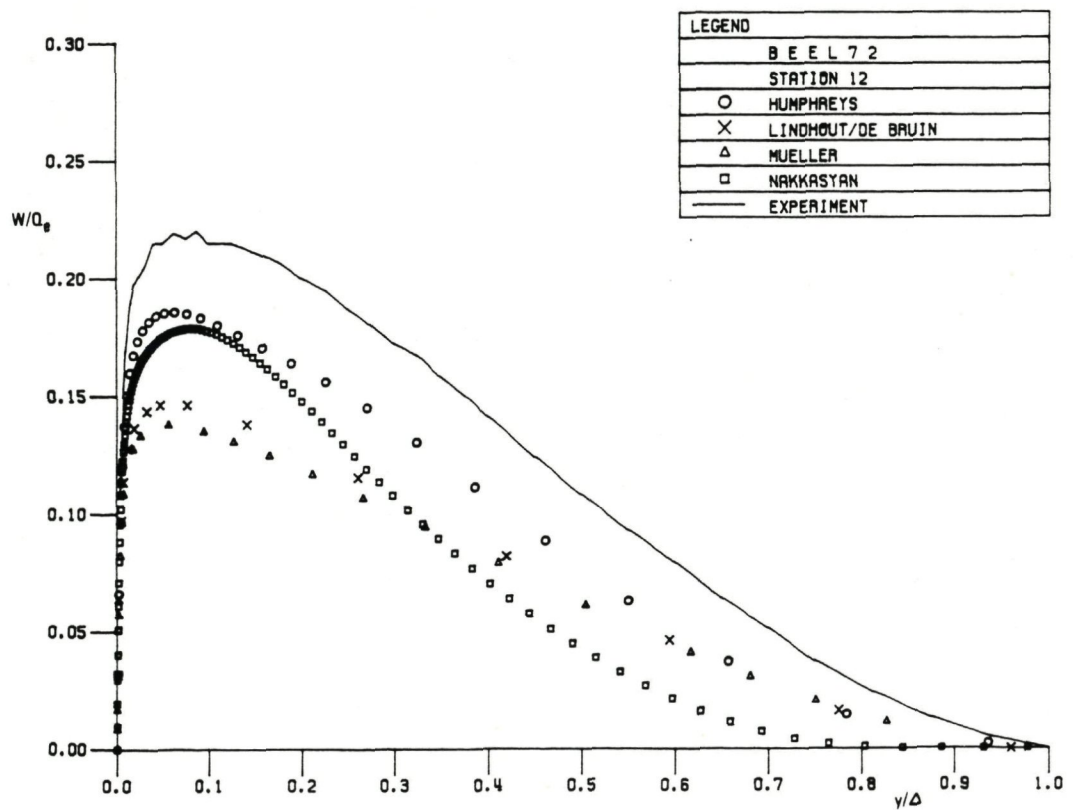
Fig. 3.12b Crosswise velocity profiles at station 12 (x/L = 1.120)
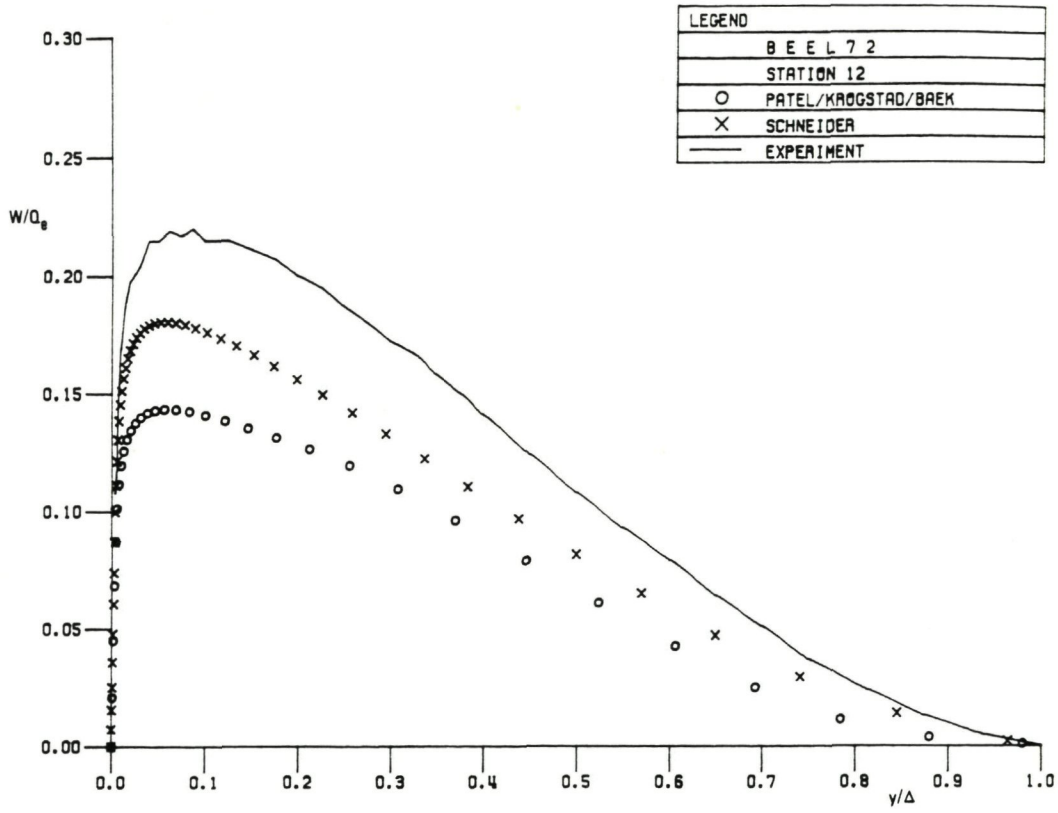
Fig. 3.12c Crosswise velocity profiles at station 12 (x/L = 1.120)
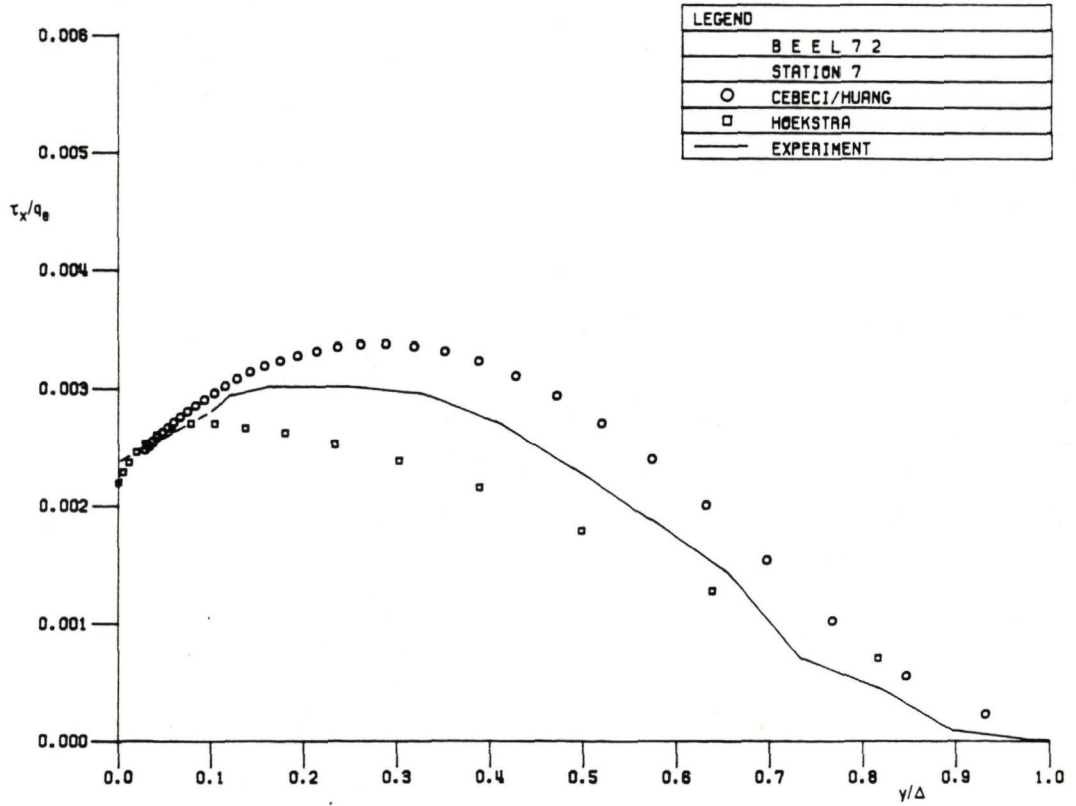
Fig. 3.13a   Streamwise shear stresses at station 7 (x/L = 0.895)
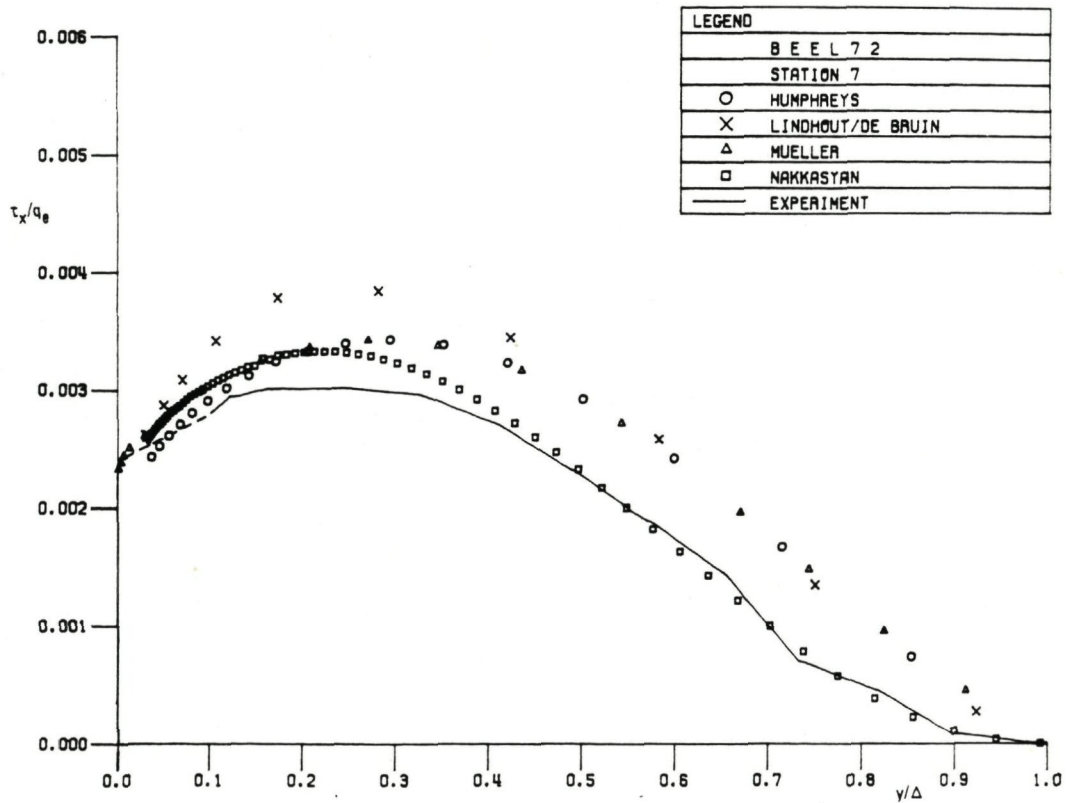
Fig. 3.13b   Streamwise shear stresses at station 7 (x/L = 0.895)
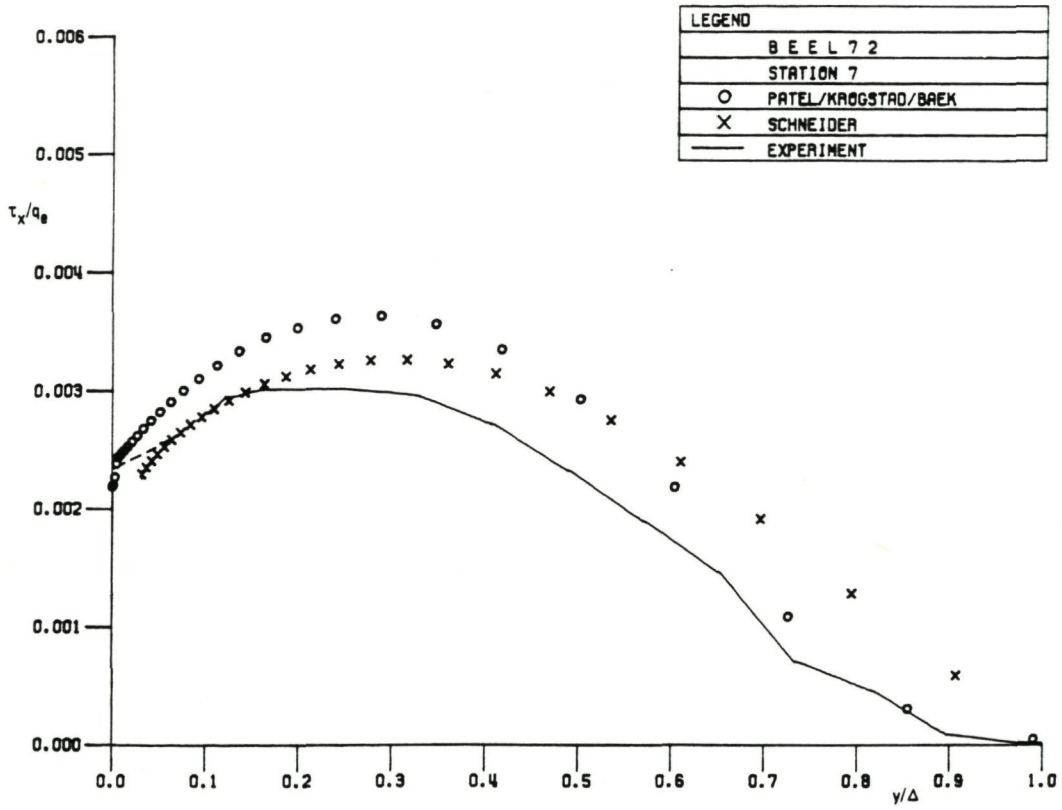
Fig. 3.13c   Streamwise shear stresses at station 7 (x/L = 0.895)
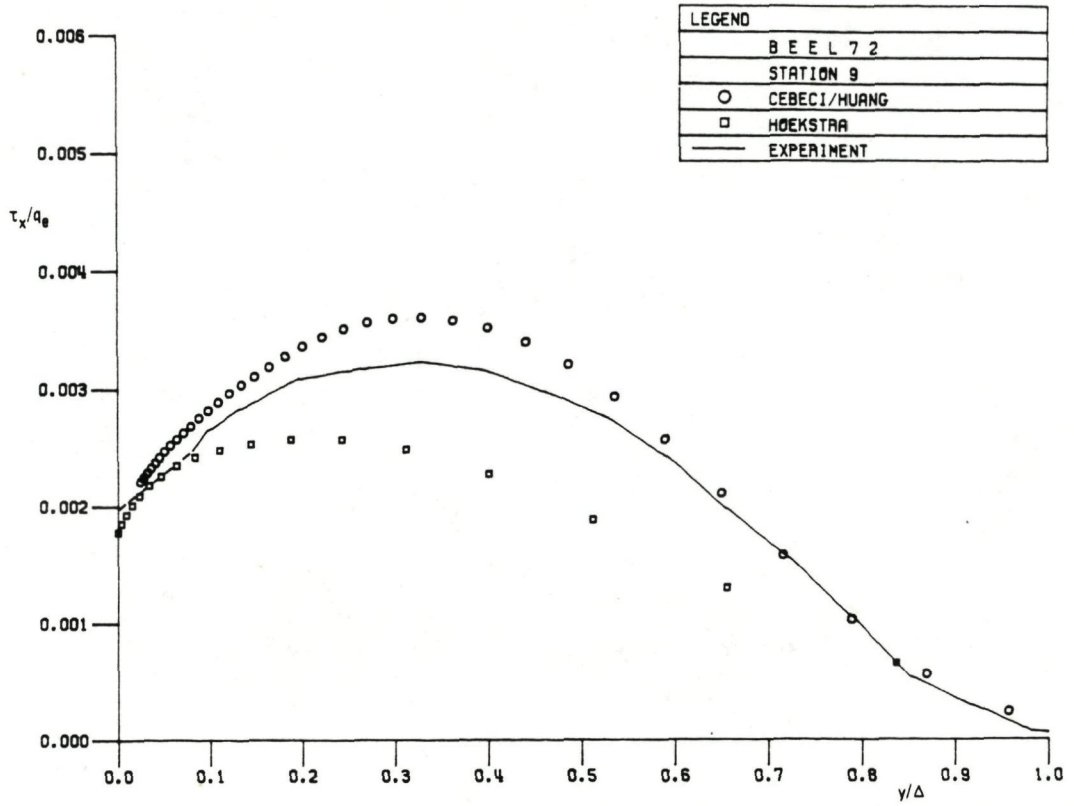
Fig. 3.14a   Streamwise shear stresses at station 9 (x/L = 0.995)
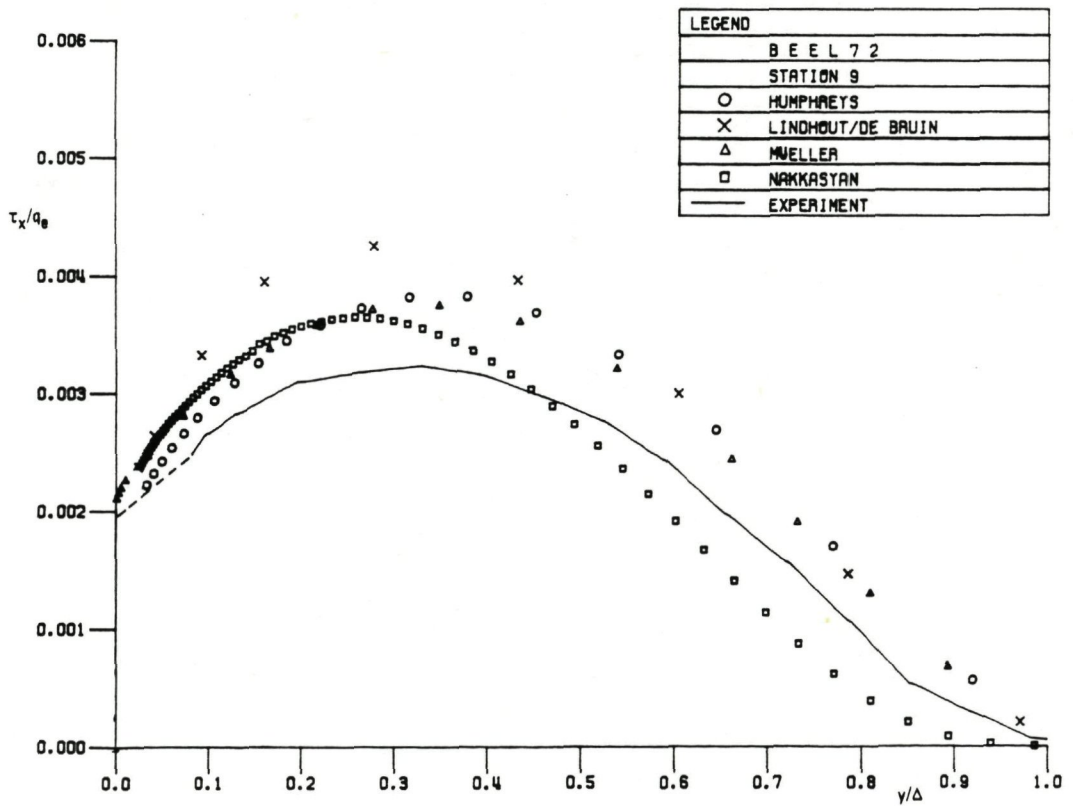
Fig. 3.14b   Streamwise shear stresses at station 9 (x/L = 0.995)
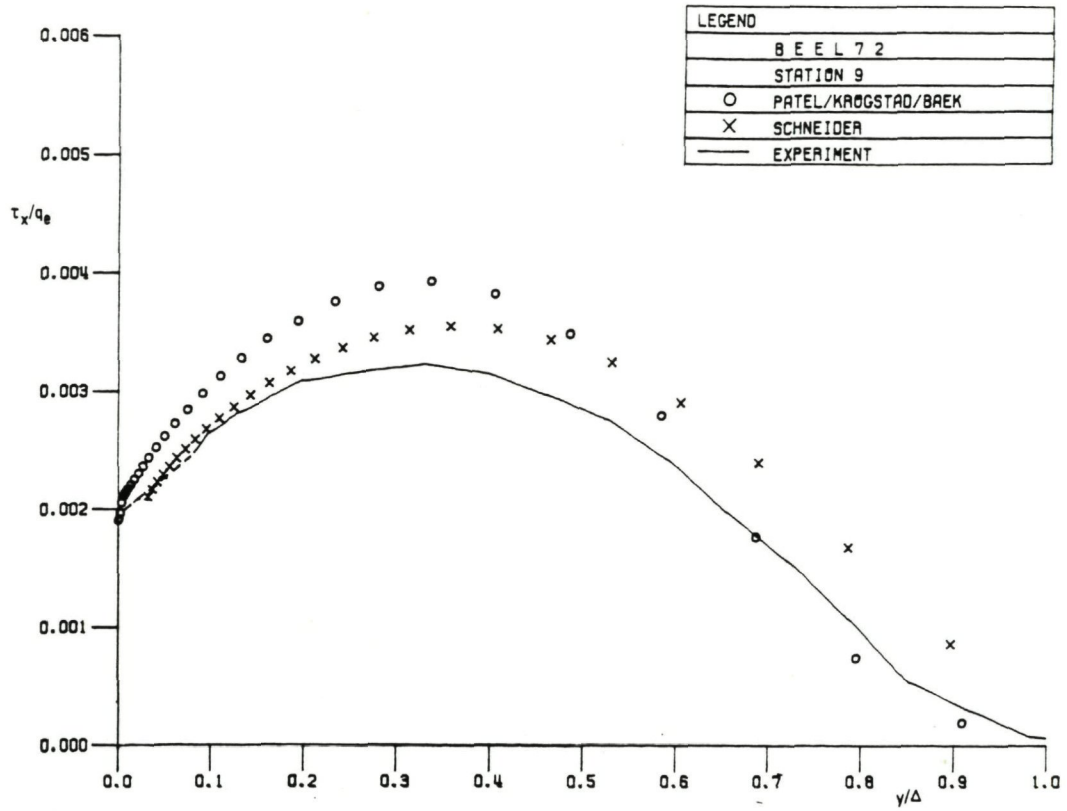
Fig. 3.14c   Streamwise shear stresses at station 9 (x/L = 0.995)
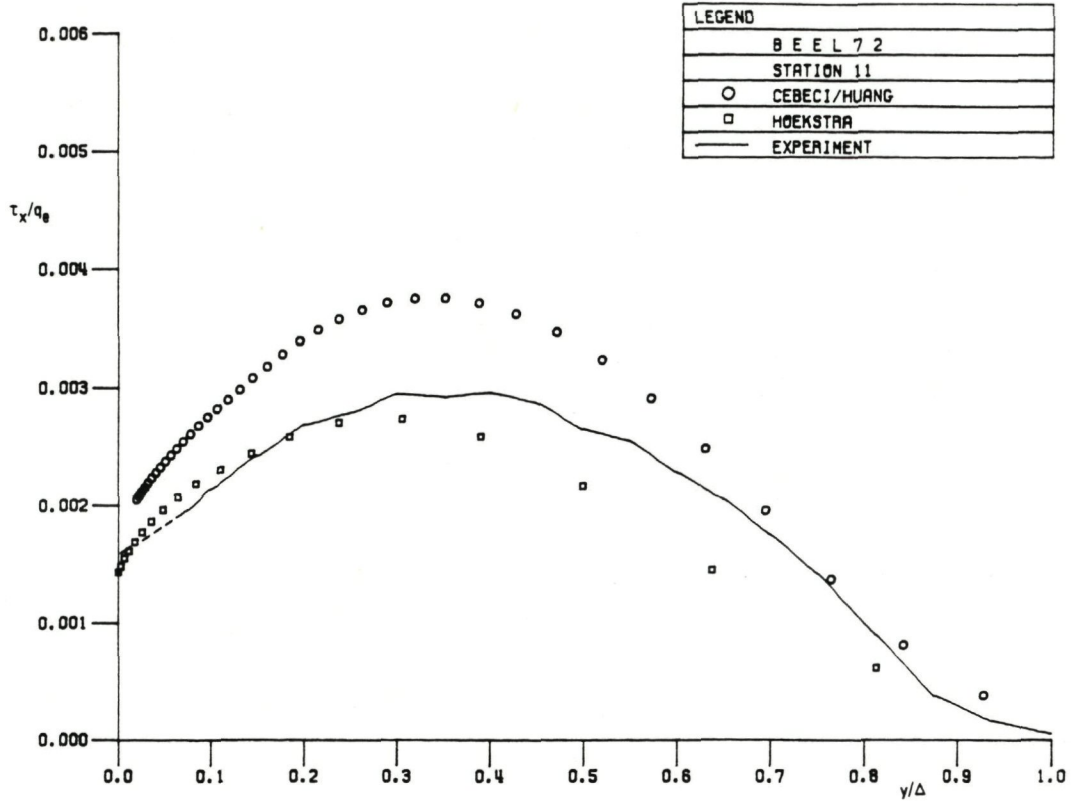
Fig. 3.15a Streamwise shear stresses at station 11 (x/L = 1.095)
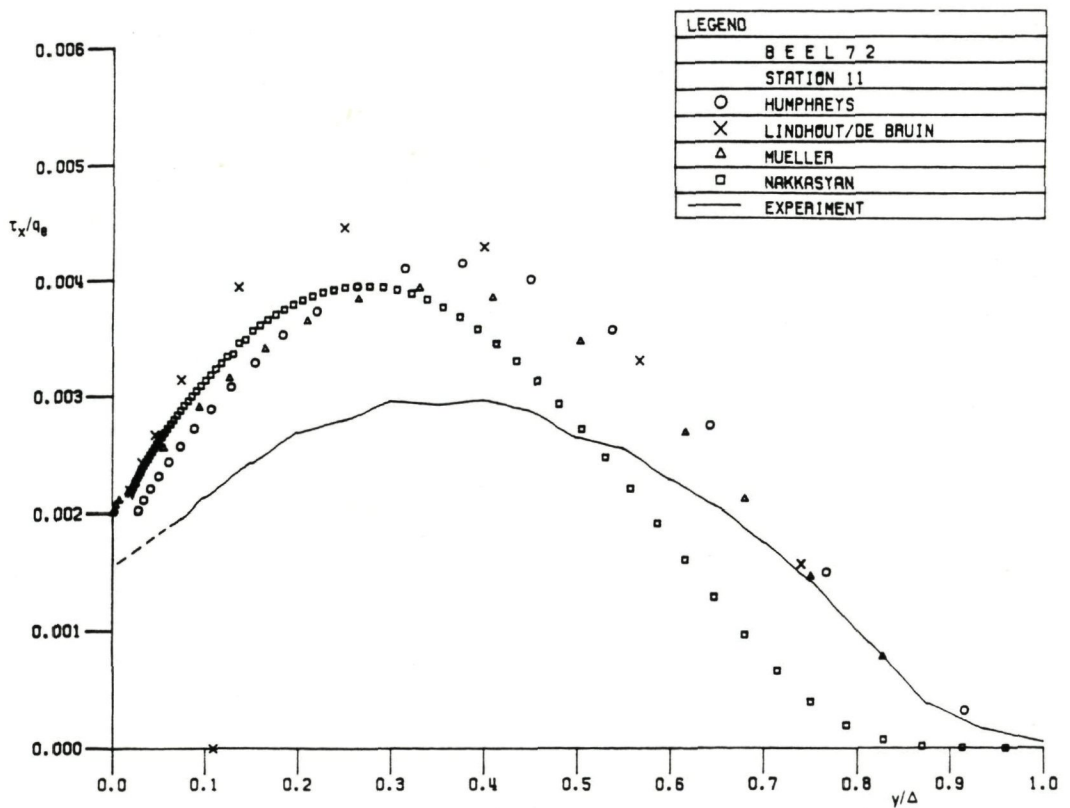
Fig. 3.15b Streamwise shear stresses at station 11 (x/L = 1.095)
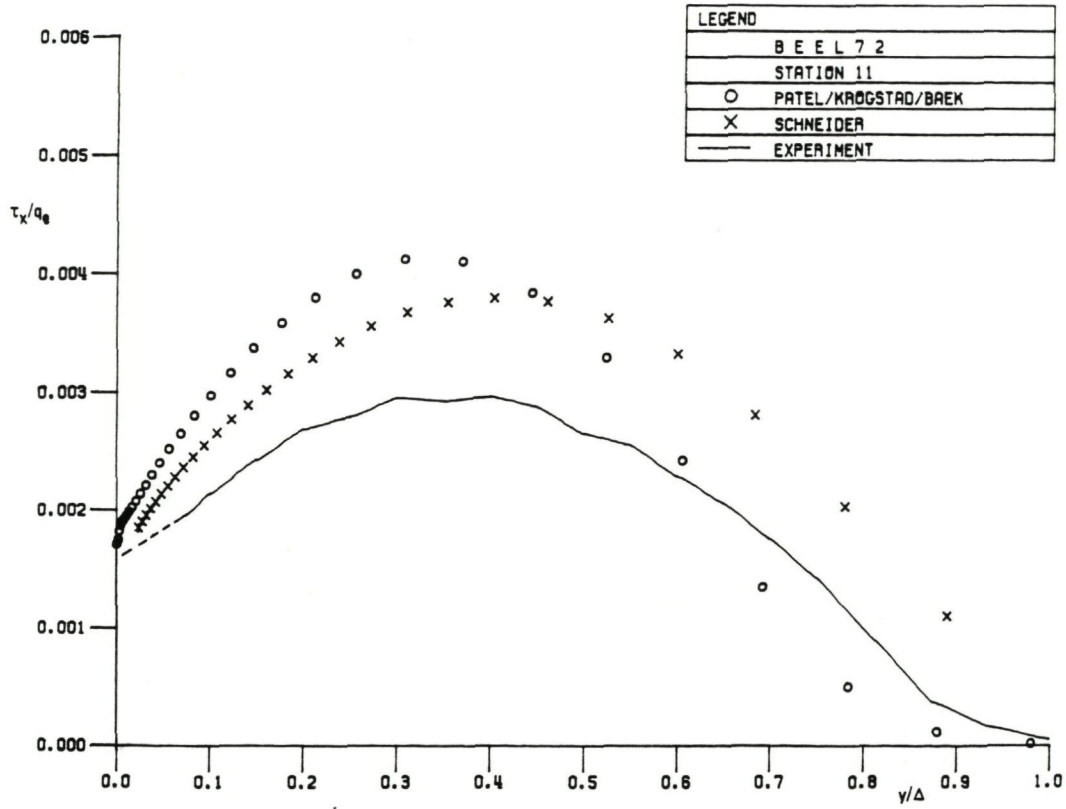
Fig. 3.15c Streamwise shear stresses at station 11 (x/L = 1.095)
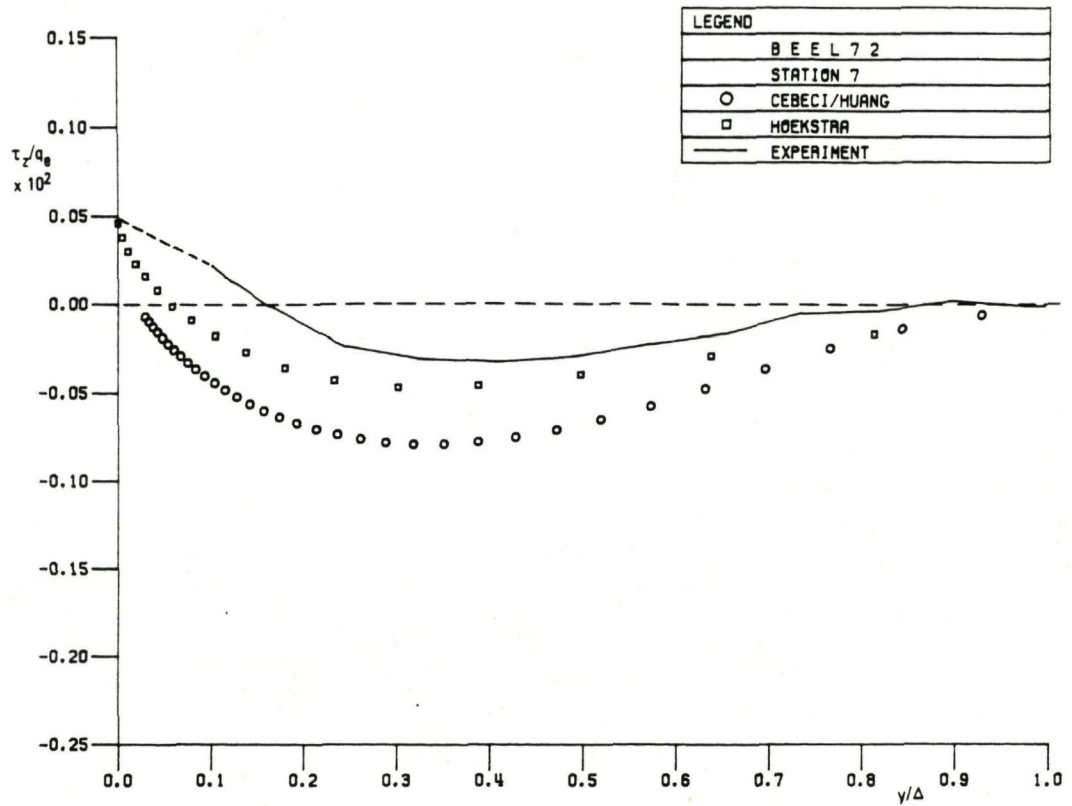
Fig. 3.16a Crosswise shear stresses at station 7 (x/L = 0.895)
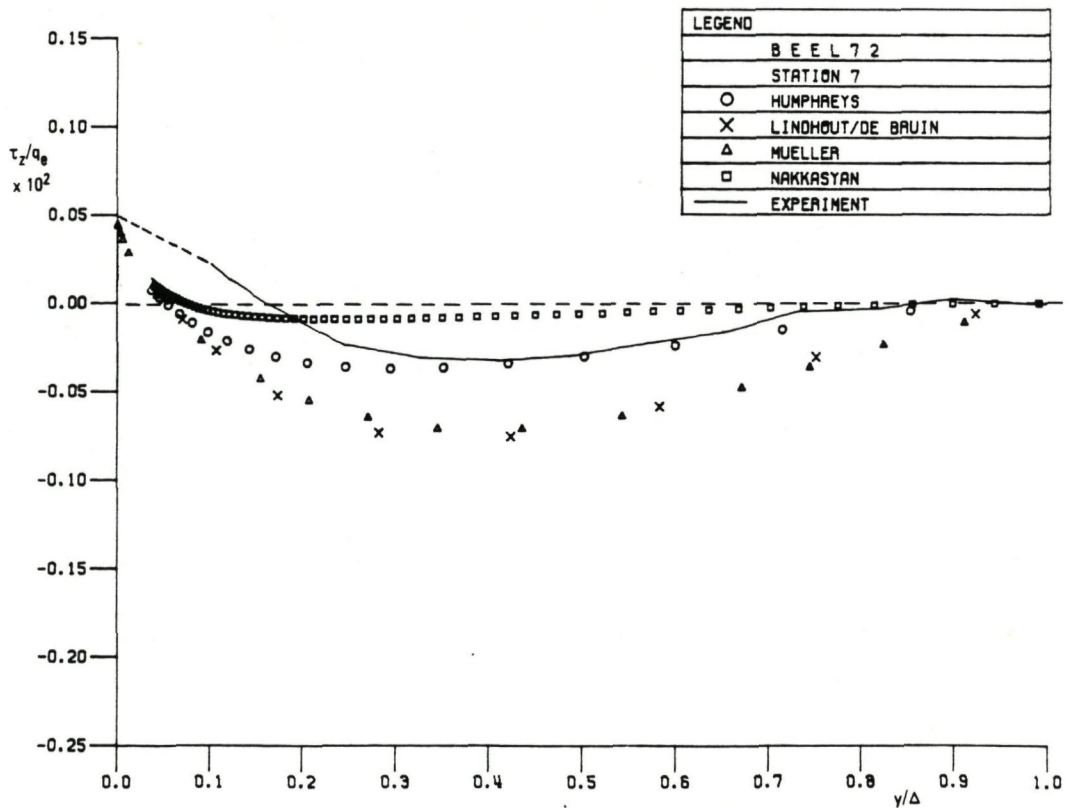
Fig. 3.16b Crosswise shear stresses at station 7 (x/L = 0.895)
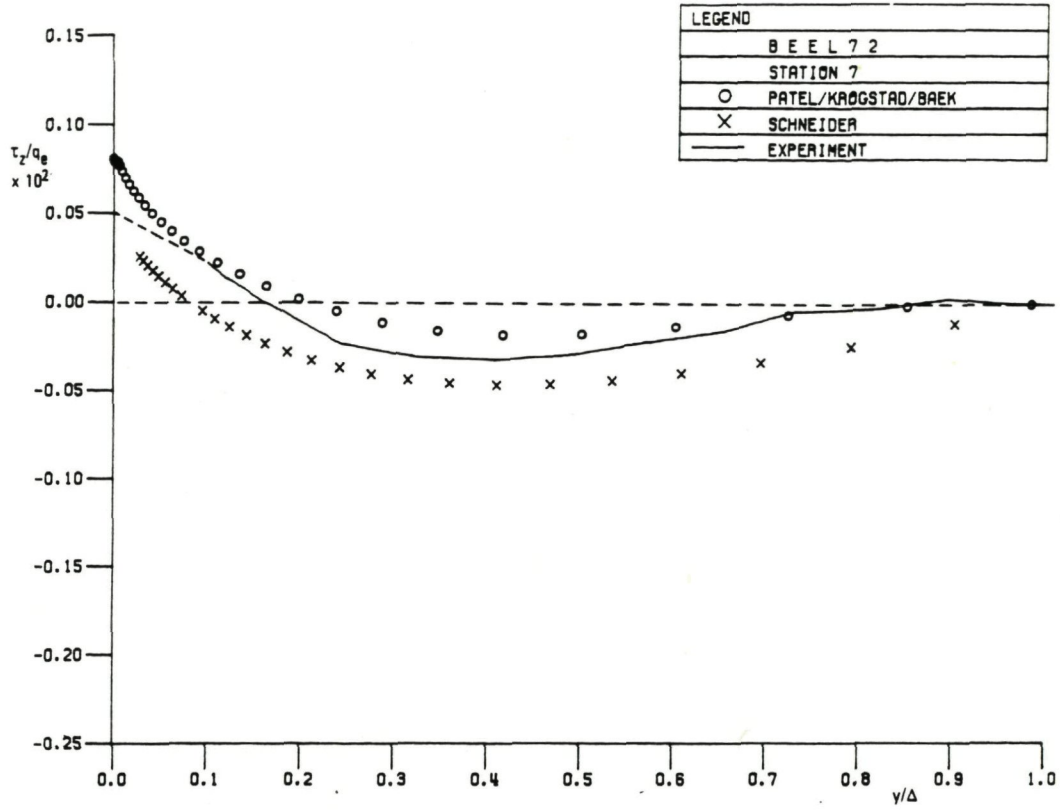
Fig. 3.16c   Crosswise shear stresses at station 7 (x/L = 0.895)
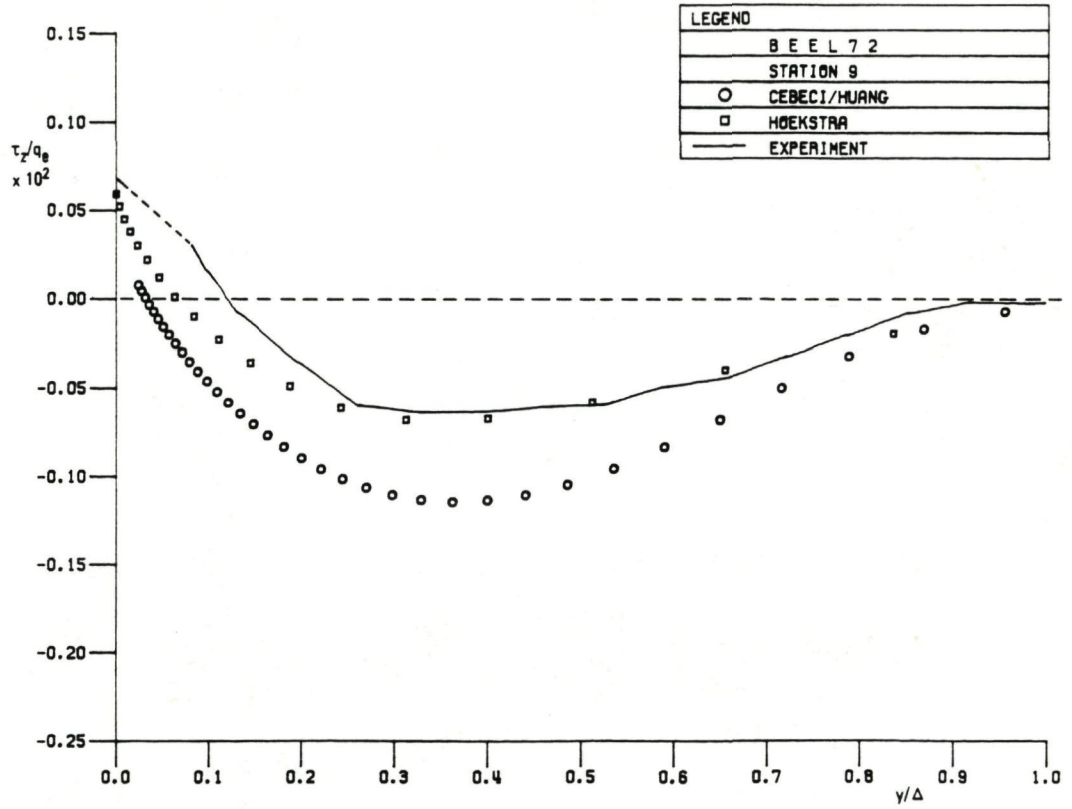
Fig. 3.17a   Crosswise shear stresses at station 9 (x/L = 0.995)
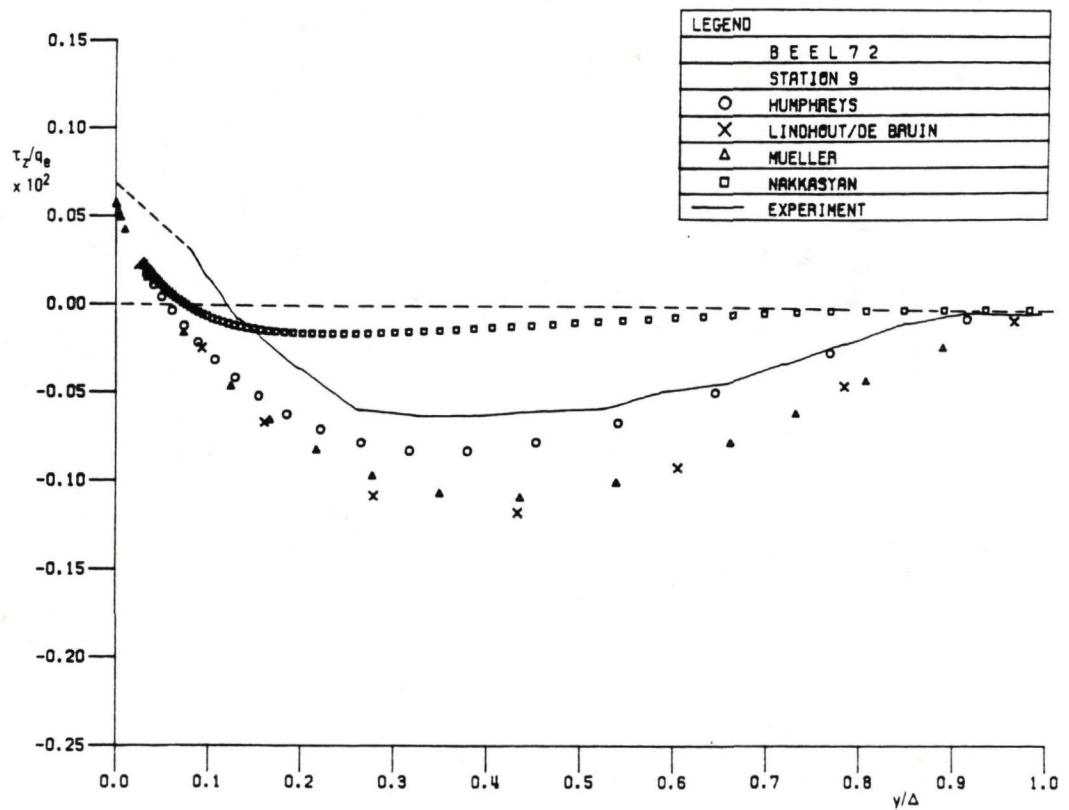
Fig. 3.17b   Crosswise shear stresses at station 9 (x/L = 0.995)
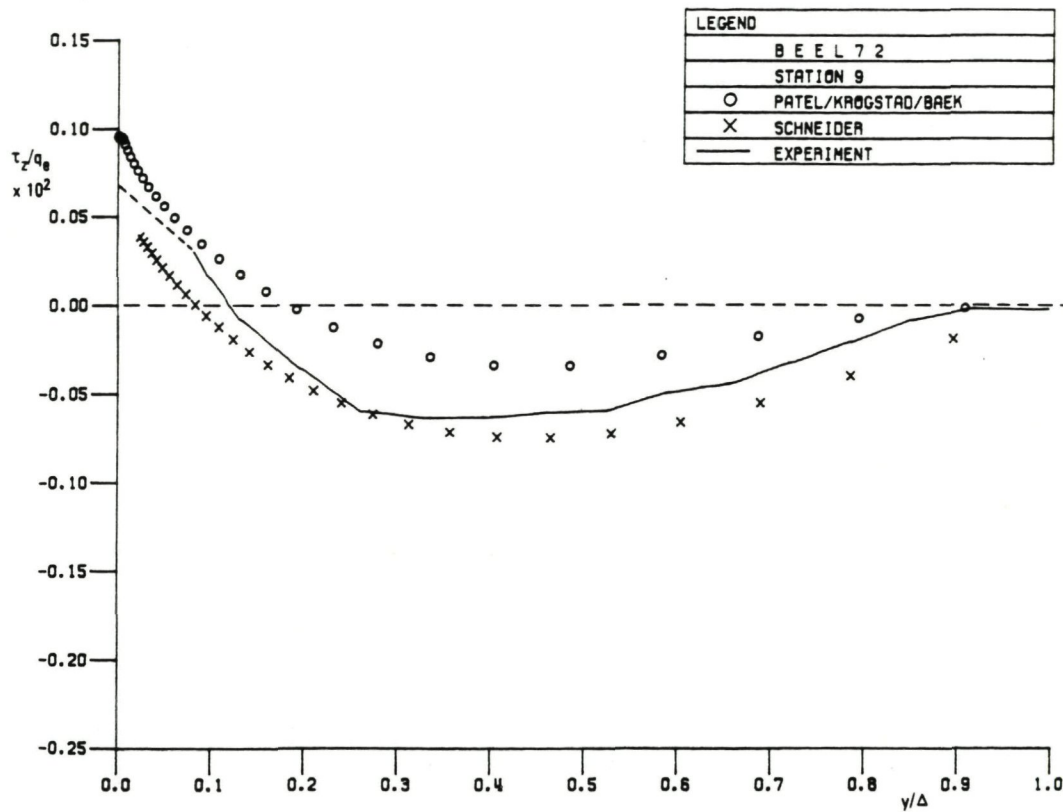
Fig. 3.17c   Crosswise shear stresses at station 9 (x/L = 0.995)
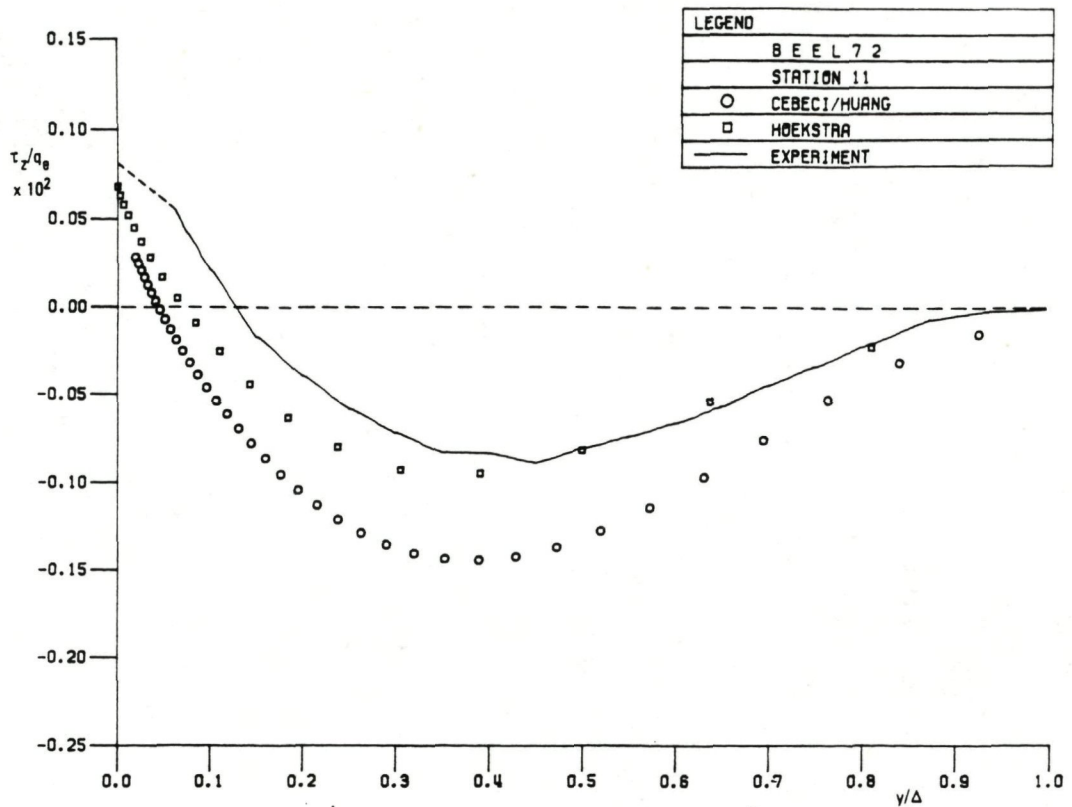
Fig. 3.18a   Crosswise shear stresses at station 11 (x/L = 1.095)
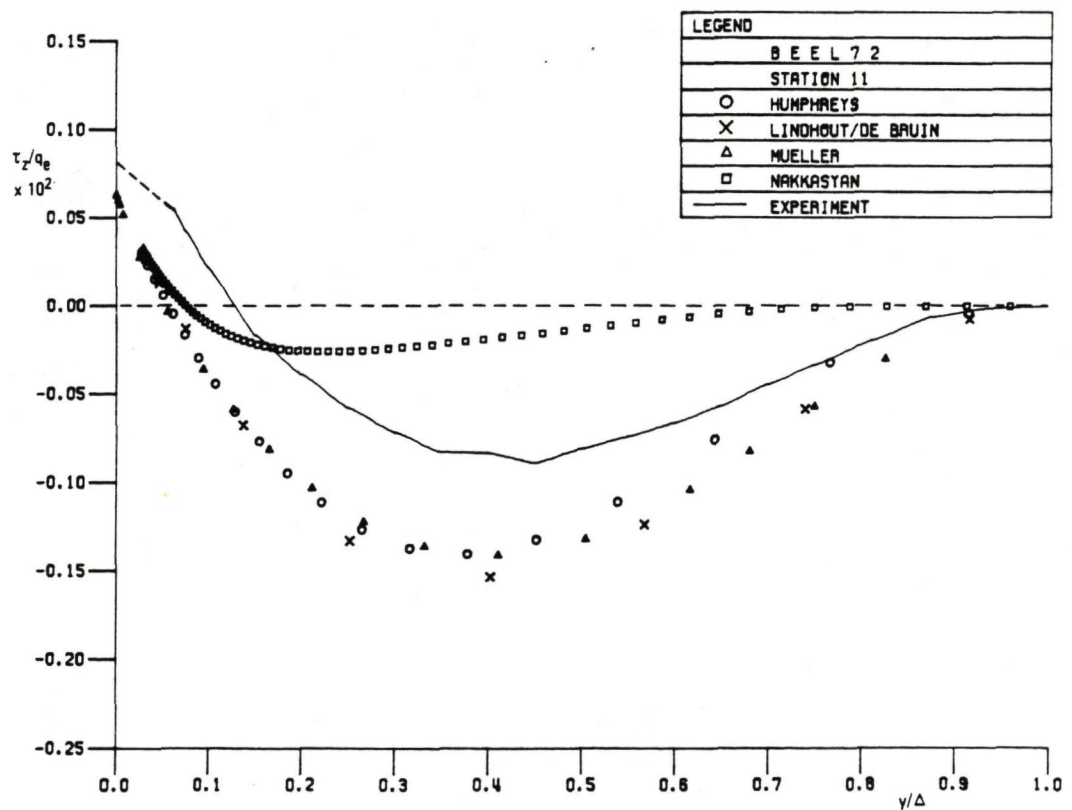
Fig. 3.18b   Crosswise shear stresses at station 11 (x/L = 1.095)
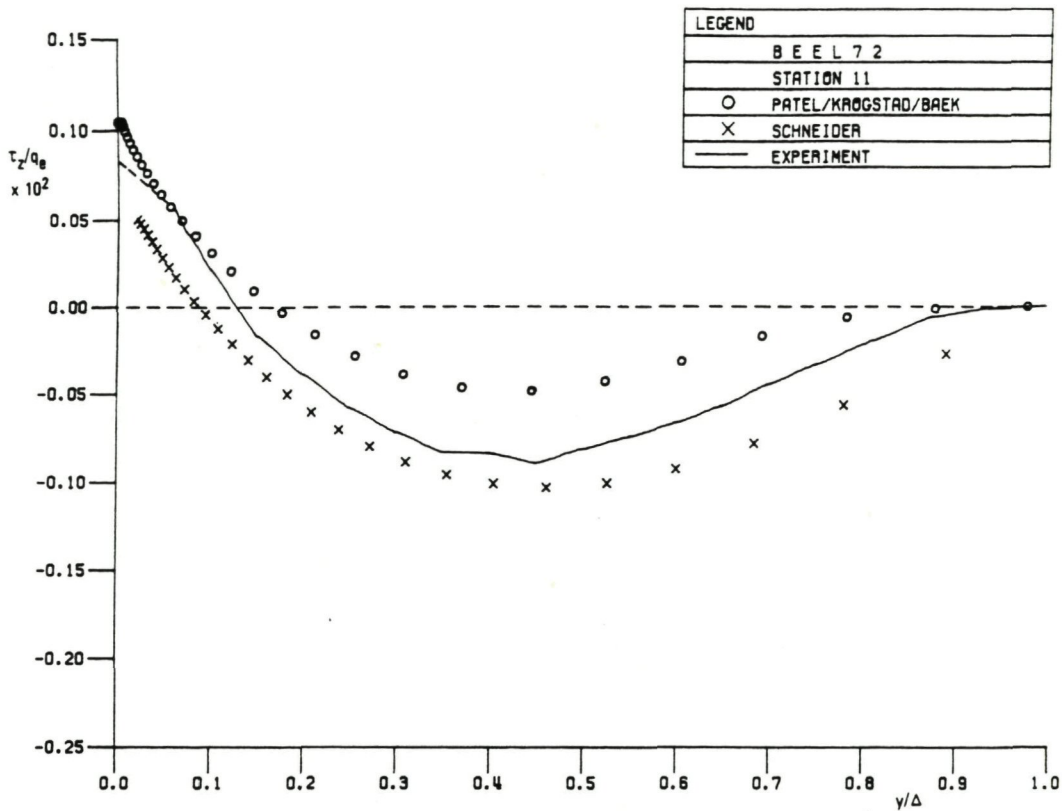
Fig. 3.18c Crosswise shear stresses at station 11 (x/L = 1.095)
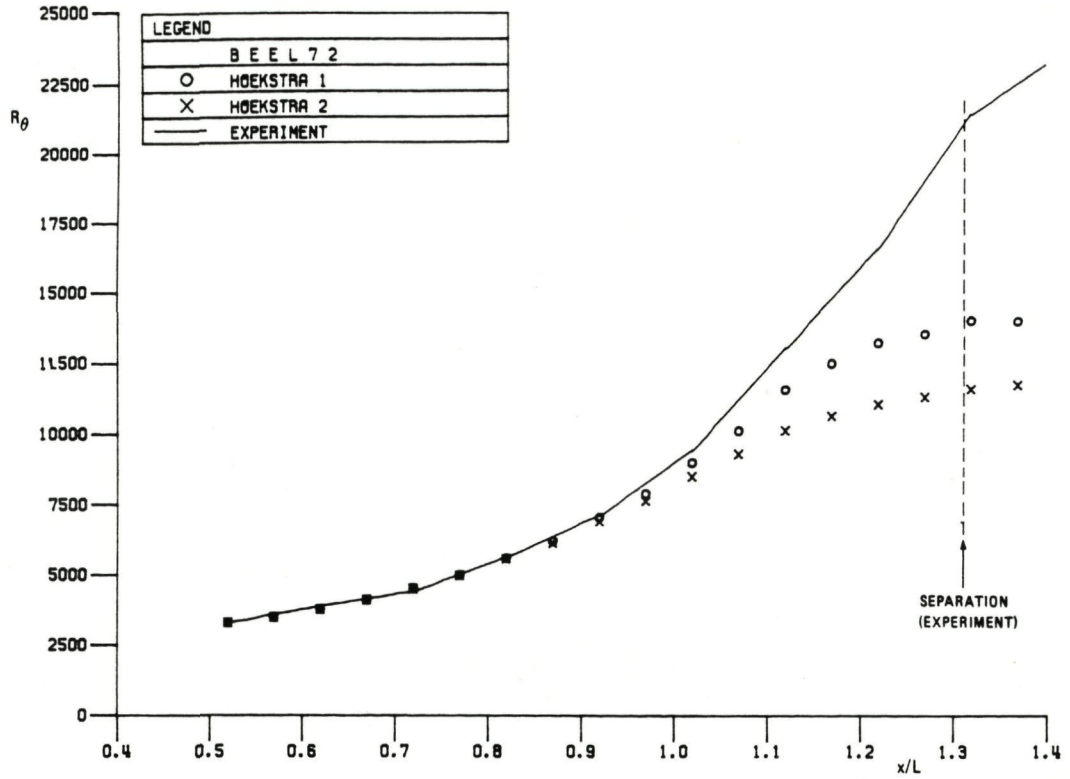
Fig. 3.19a   Effect of empirical assumptions in Hoekstra's isotropic
eddy viscosity method. Version 1: advanced model leading
here to reduced eddy viscosities. Version 2: standard
eddy viscosity model
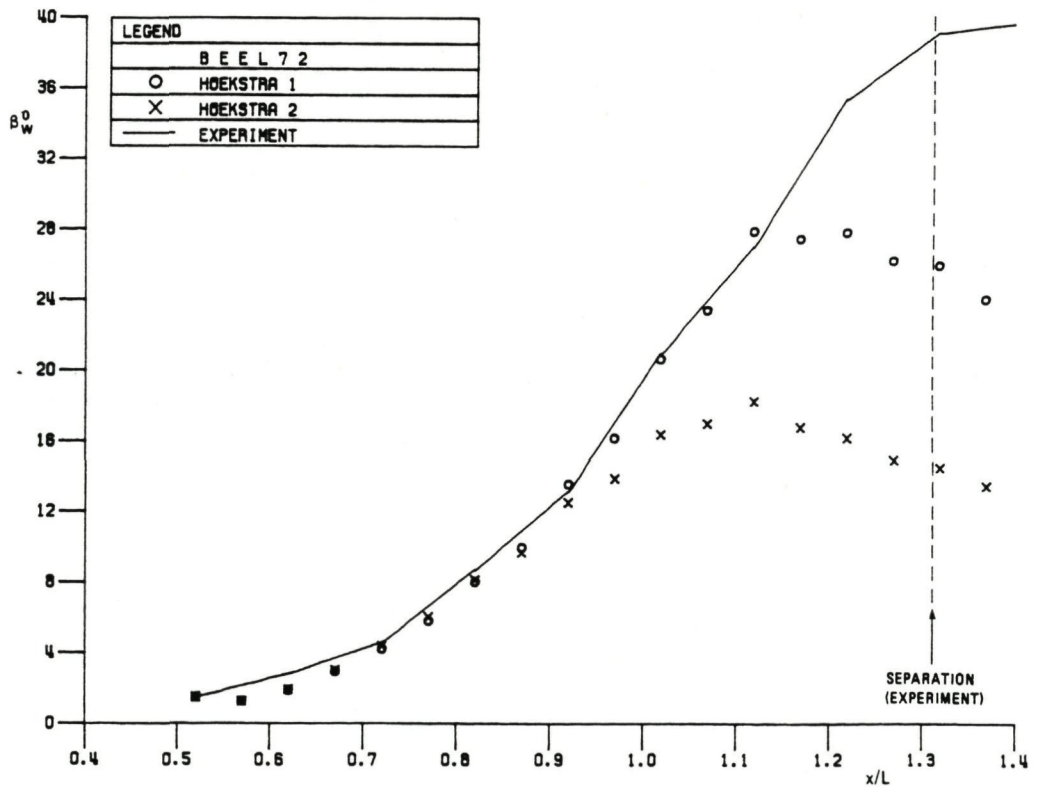
Fig. 3.19b   Effect of empirical assumptions in Hoekstra's isotropic
eddy viscosity method. Version 1: advanced model leading
here to reduced eddy viscosities. Version 2: standard
eddy viscosity model
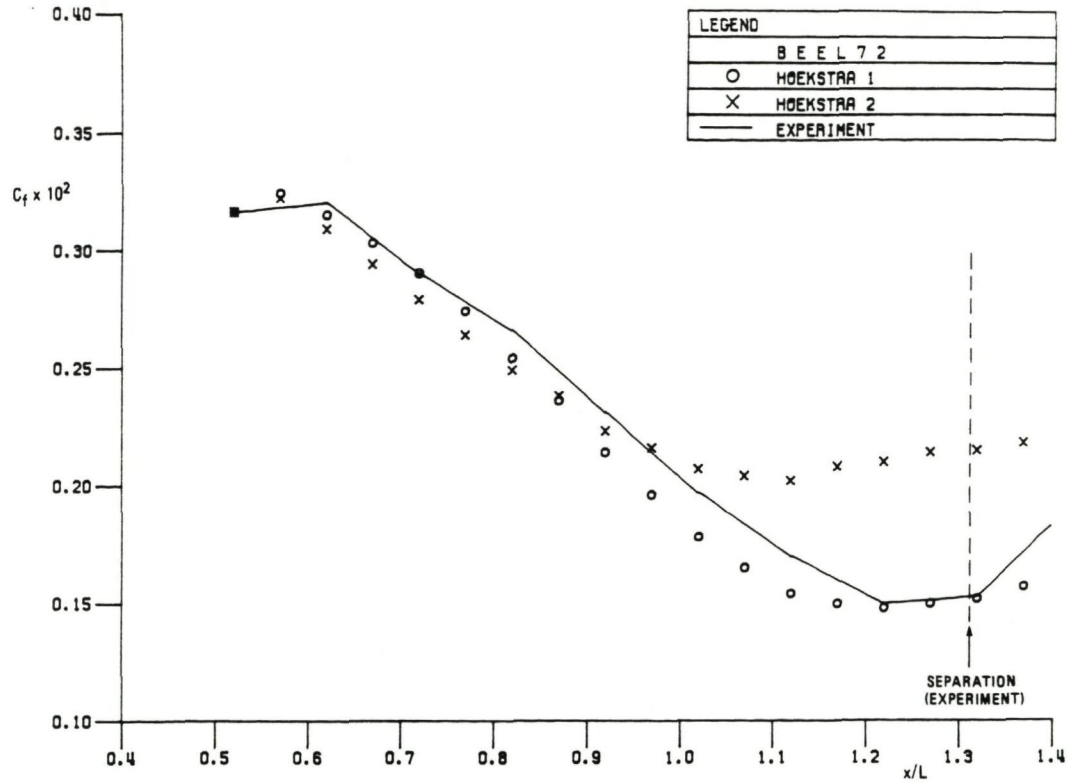
Fig. 3.19c   **Effect of empirical assumptions in Hoekstra's isotropic eddy viscosity method. Version 1: advanced model leading here to reduced eddy viscosities. Version 2: standard eddy viscosity model**
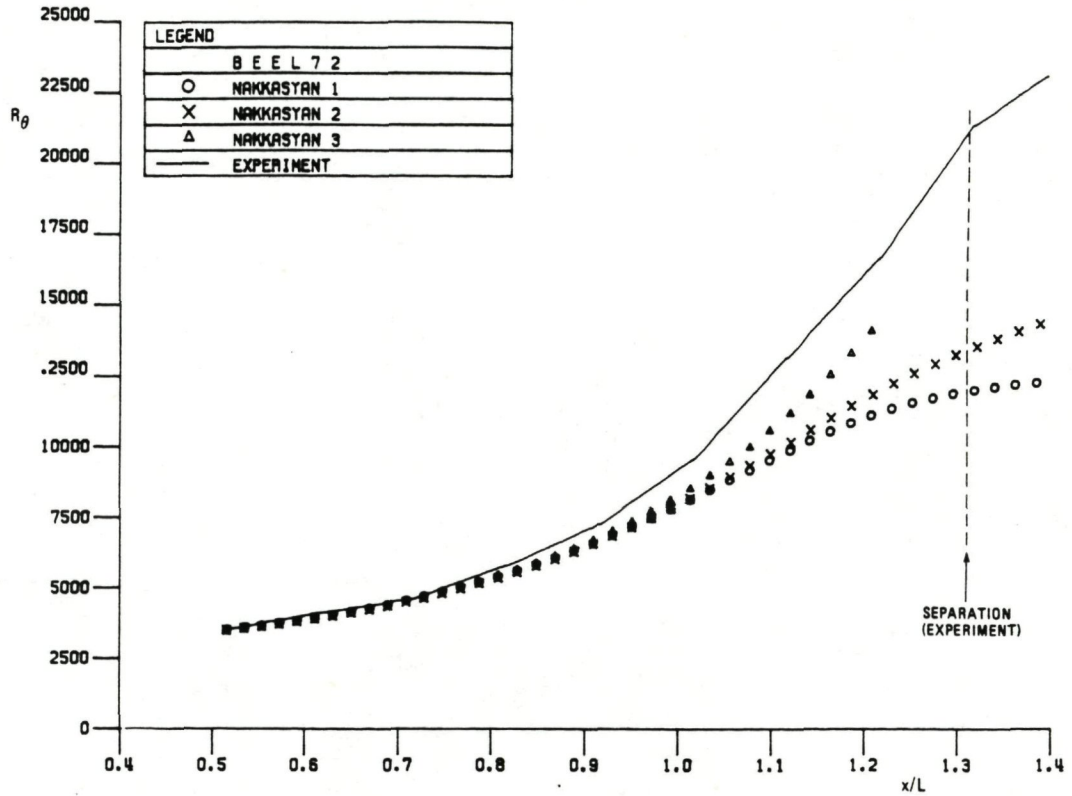
Fig. 3.20a   Effect of empirical assumptions in Nakkasyan's non-
isotropic eddy viscosity model. Version 1-3: various
degrees of non-isotropy of the eddy viscosity
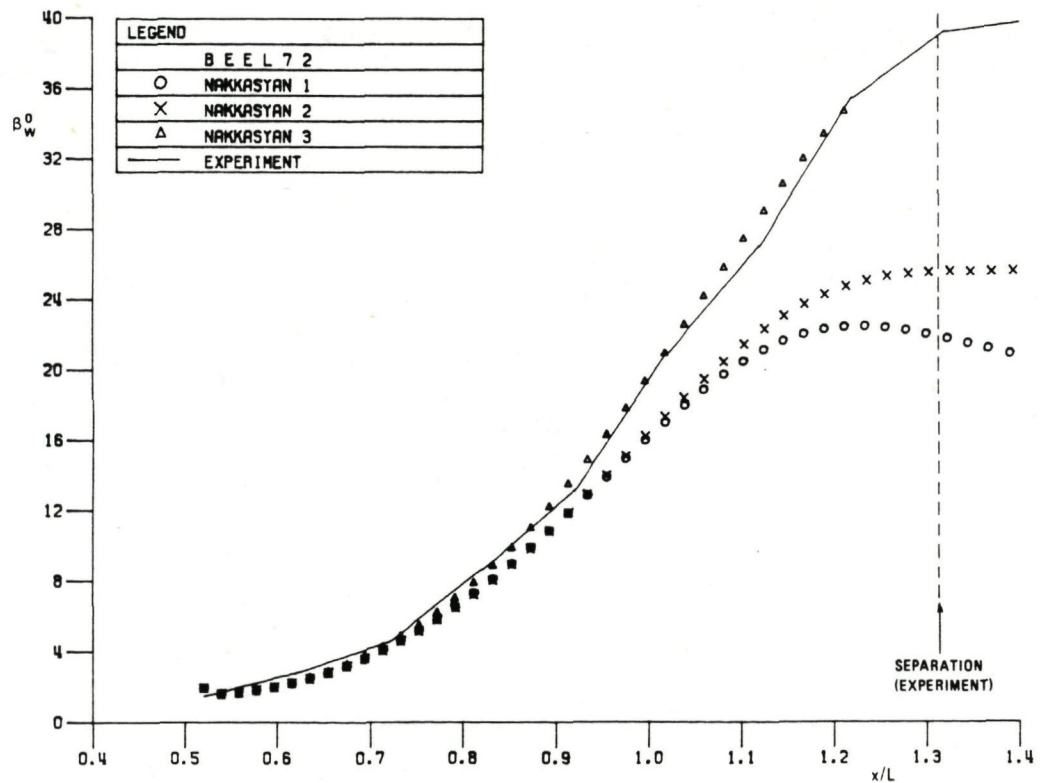
Fig. 3.20b   Effect of empirical assumptions in Nakkasyan's non-
isotropic eddy viscosity model. Version 1-3: various
degrees of non-isotropy of the eddy viscosity
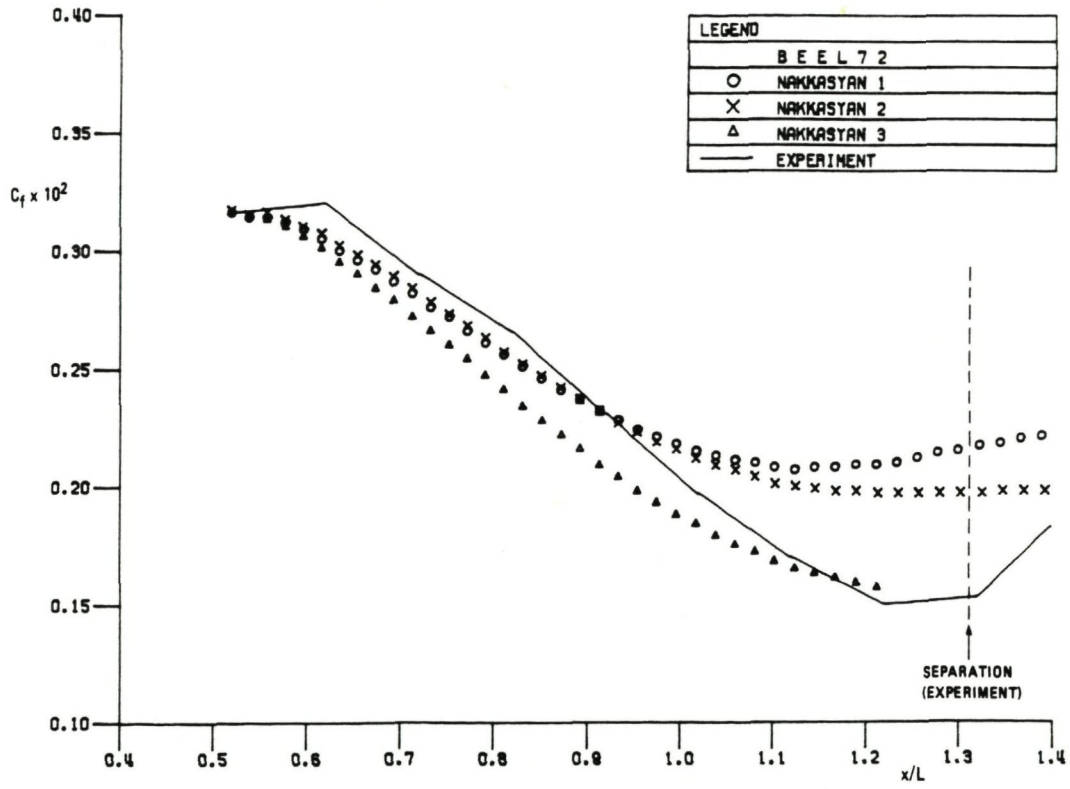
Fig. 3.20c   **Effect of empirical assumptions in Nakkasyan's non-isotropic eddy viscosity model. Version 1-3: various degrees of non-isotropy of the eddy viscosity**
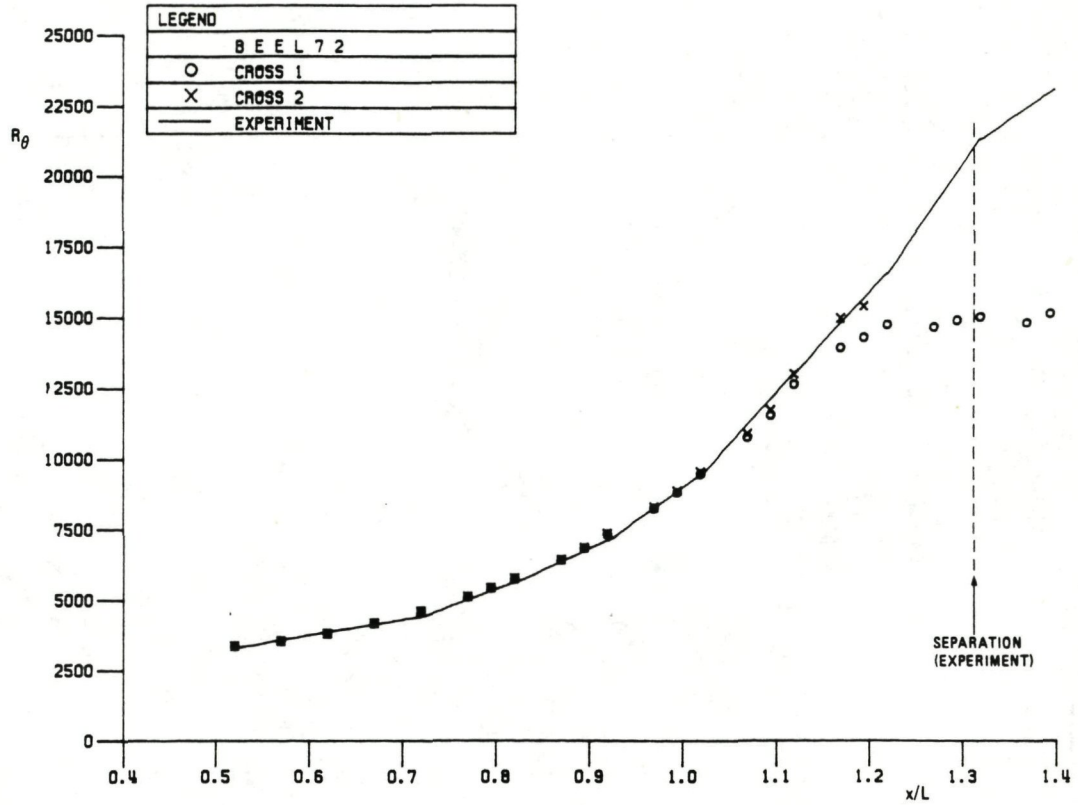
Fig. 3.21a   Effect of assumed crossflow at the initial station.
Version 1: $\beta_{w_i} = 1.5^o$. Version 2: $\beta_{w_i} = 2.0^o$

Fig. 3.21b   Effect of assumed crossflow at the initial station
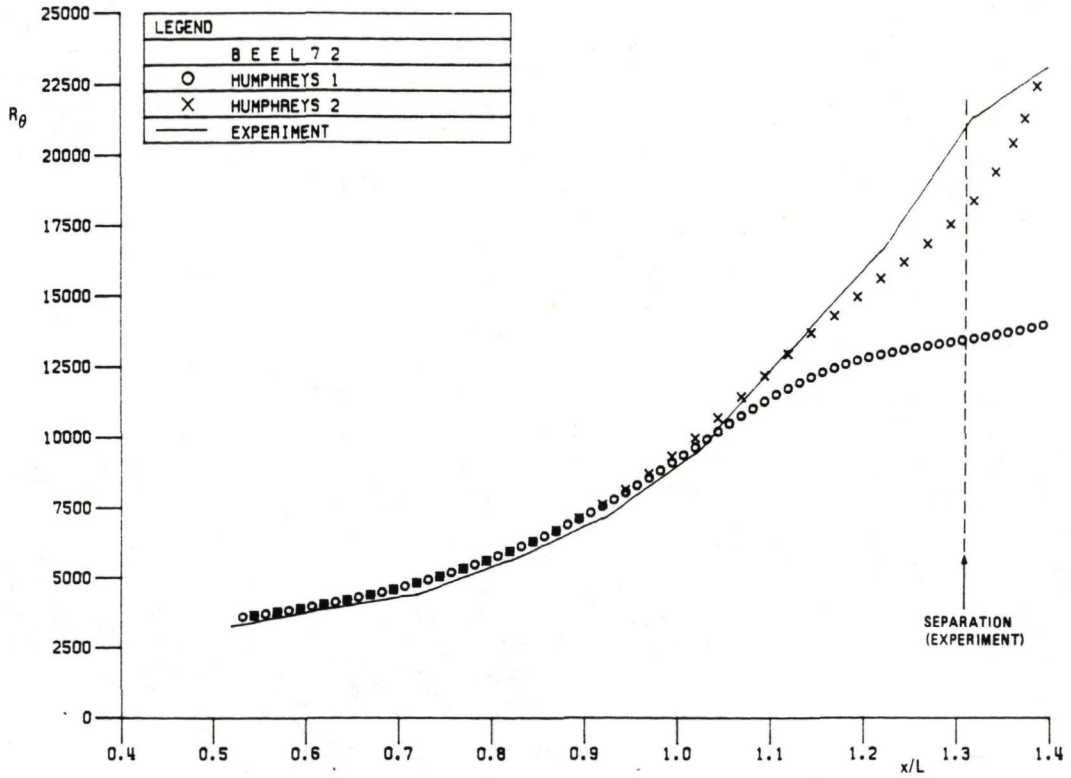Version 1: $\beta_{w_i} = 1.5^o$. Version 2: $\beta_{w_i} = 2.0^o$

Fig. 3.21c   Effect of assumed crossflow at the initial station.
Version 1: $\beta_{w_i} = 1.5°$. Version 2: $\beta_{w_i} = 2.0°$

Fig. 3.22a   Effect of assumed pressure distribution for Humphreys' non-
               isotropic eddy viscosity method. Version 1: wall pressure
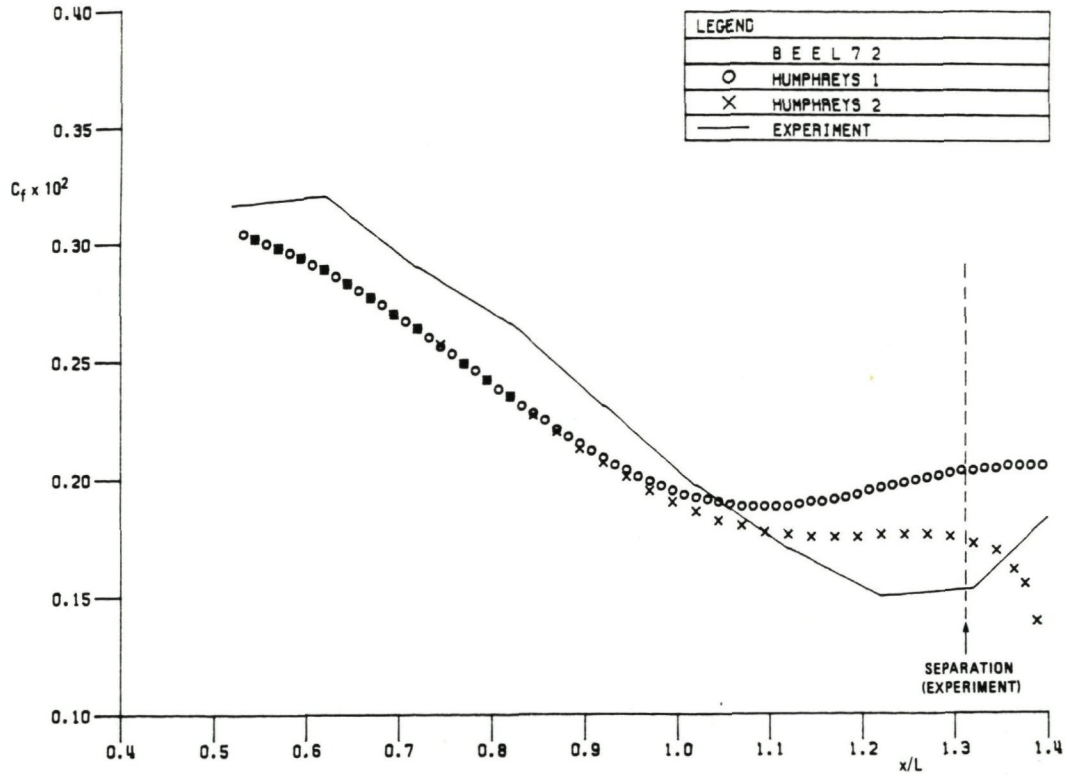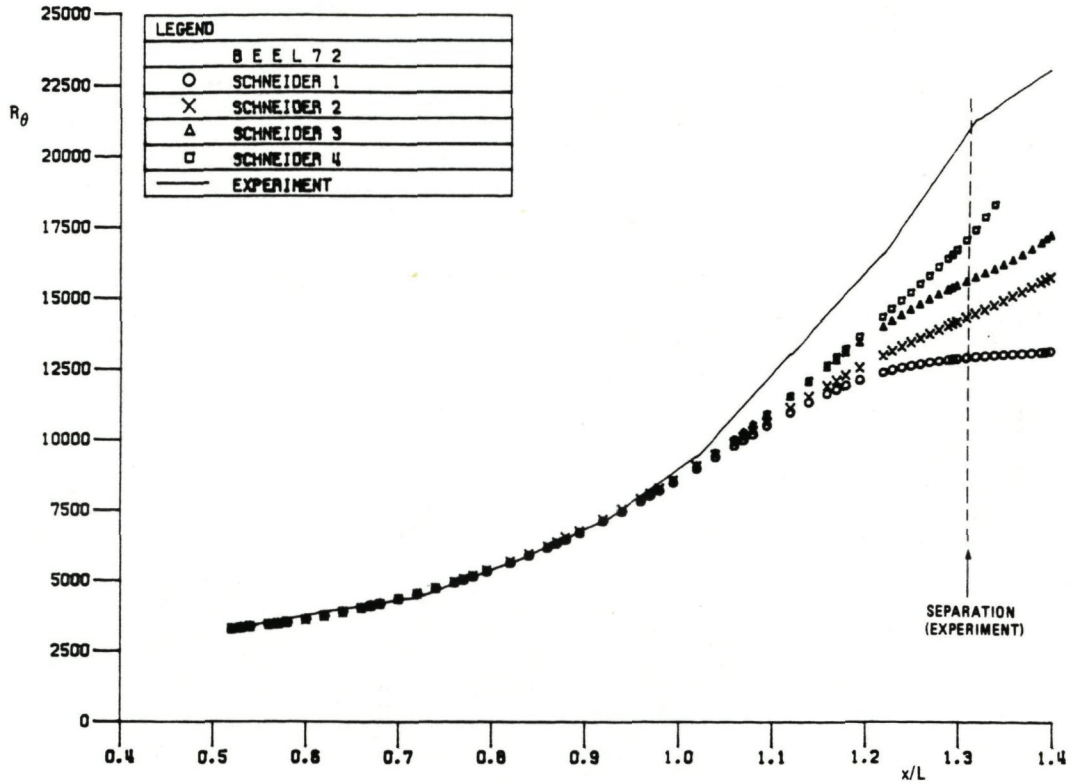   distribution. Version 2: external pressure distribution
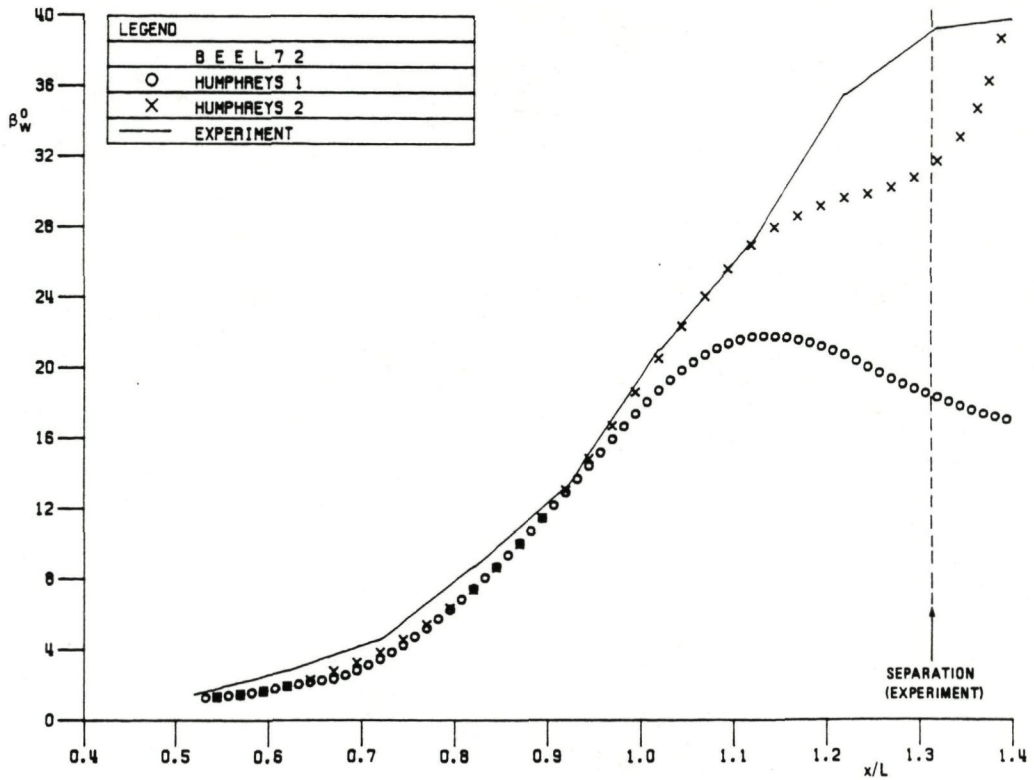
Fig. 3.22b   Effect of assumed pressure distribution for Humphreys' non-
               isotropic eddy viscosity method. Version 1: wall pressure
               distribution. Version 2: external pressure distribution

Fig. 3.22c   **Effect of assumed pressure distribution for Humphreys' non-isotropic eddy viscosity method. Version 1: wall pressure distribution. Version 2: external pressure distribution**

Fig. 3.23a Effect of assumed pressure distribution for Schneider's non-isotropic eddy viscosity method. Version 1: wall pressure distribution. Version 2-4: various modifications.
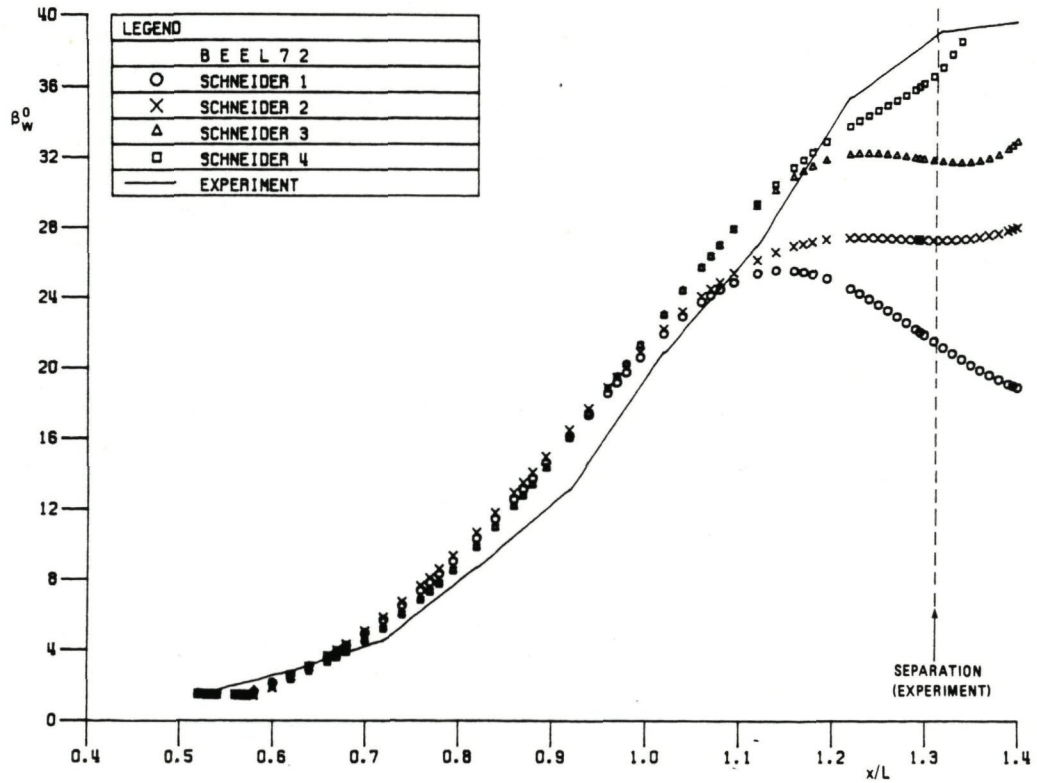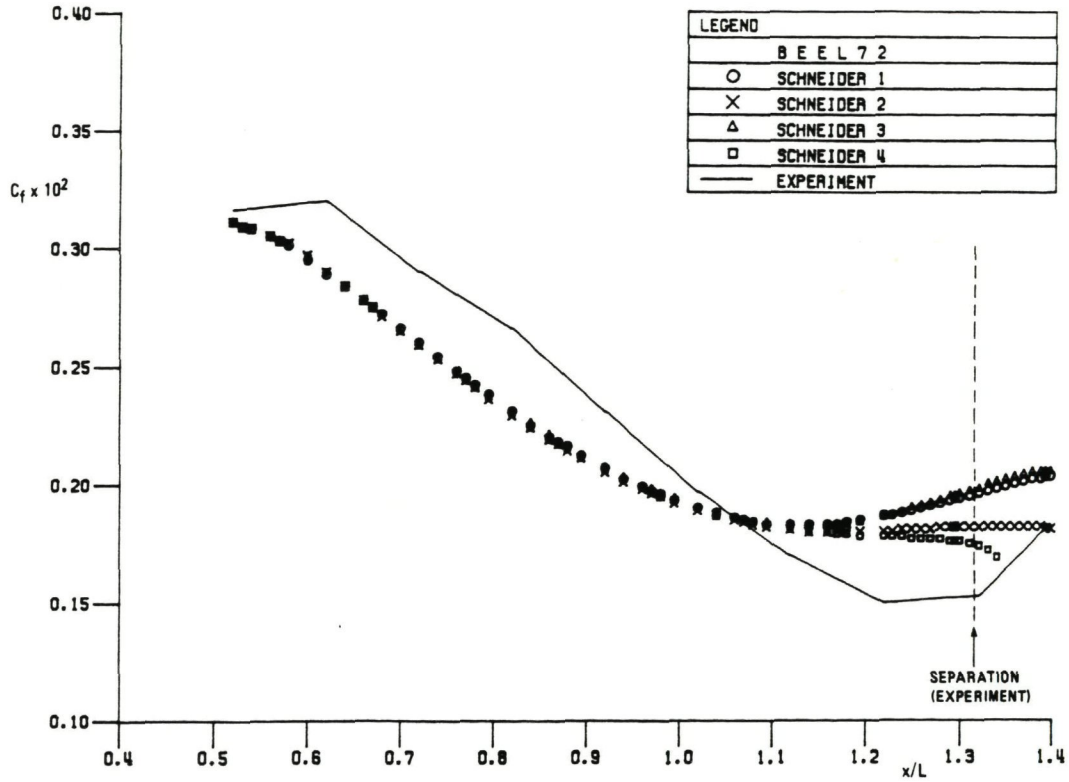

Fig. 3.23b Effect of assumed pressure distribution for Schneider's non-isotropic eddy viscosity method. Version 1: wall pressure distribution. Version 2-4: various modifications.

Fig. 3.23c   **Effect of assumed pressure distribution for Schneider's non-isotropic eddy viscosity method. Version 1: wall pressure distribution. Version 2-4: various modifications.**

4   TEST CASE DEFE77

This test case concerns the boundary layer in front of a cylinder
standing on a flat wall in a wind tunnel. The experiment is described
in Dechow (1977) and Dechow & Felsch (1977). Far upstream the boundary
layer is two-dimensional. The non-circular cylinder induces a pressure
distribution driving the boundary layer to three-dimensionality. In
figure 4.1 the displacement body and the test region are sketched.
Measurements were performed along the symmetry line (AS) at two
stations and along an outer streamline (BC) at ten stations. The first
of these ten stations is situated in the region with collateral flow
and the last station is downstream of the three-dimensional
separation line. In figure 4.2 the measuring stations and the station
numbering system are indicated. Comparisons with calculations will be
made at stations (4,1), (4,2), (5,2) and (6,2).

The boundary layer was tripped to turbulent flow with a wire of
about 1 mm diameter far upstream of the displacement body. At the
line along which the initial conditions are specified R_Θ is about
4500. For the stations which are of interest for the Workshop
comparisons the pressure variation through the boundary layer is at
most about ΔC_p = 1% (occurring at station (6,2)). Outside the region
considered, closer to the cylinder, much larger pressure variations
occur. The participants were provided with the wall pressure
distribution. The mean velocity profiles were measured with single hot
wires and the Reynolds shear stresses with an X-wire. The magnitude
of the shear stress at the wall was determined with a Preston tube.
The direction of the mean velocity was measured down to 0.2 mm above
the plate ($y^+ \cong 10$). These values have been employed in the comparisons
with the computed limiting streamline angles at the wall. Checks
performed with surface hot films showed discrepancies up to 10 degrees
but values taken from oil flow patterns compare quite well (Dechow 1977).
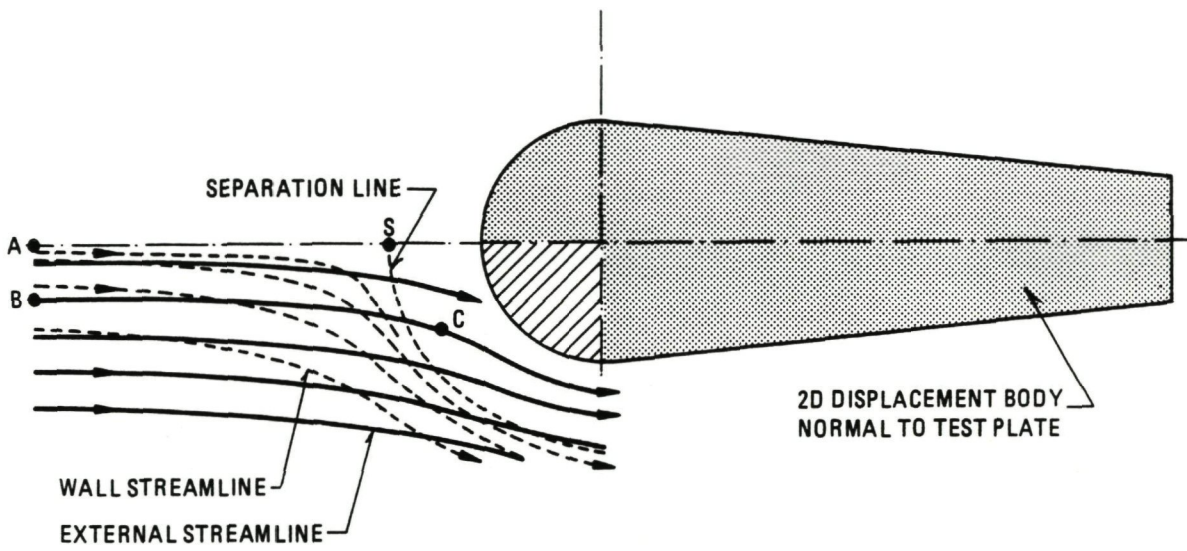
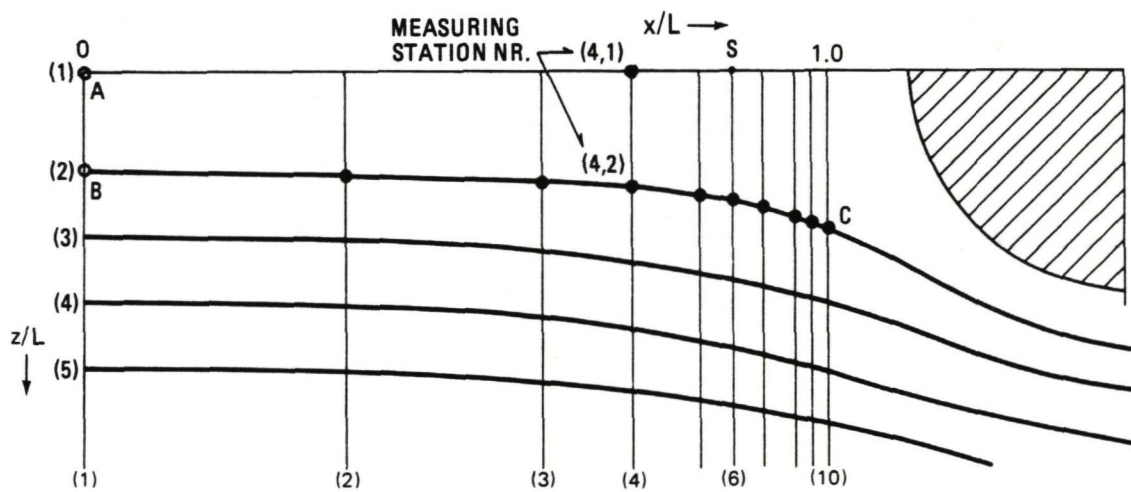Fig. 4.1   DEFE77 test set-up

Fig. 4.2   Position of measuring stations

The error estimates by Dechow (1977) for the measured velocities and Reynolds stresses are given in Appendix B. An impression of the numerical accuracy of the various calculations may be obtained from table 4.1. The table contains mainly data on the effect of step size changes on the calculated wall flow angle and wall shear stress. Four of the seven calculation methods carried out such studies and the results suggest that the numerical accuracy is acceptable.

This test case has been computed by two integral methods (COUSTEIX/-BERRUE and CROSS) and five field methods (CEBECI/HUANG, HOEKSTRA, MÜLLER, PATEL/KROGSTAD/BAEK and LINDHOUT/DE BRUIN). All the field methods employ an eddy viscosity model, including a van Driest damping factor with pressure gradient correction. According to Bradshaw (1973) the turbulence structure can seriously be affected by extra rates of strain. For instance, the divergence of streamlines, which occurs near the symmetry line, can substantially increase the Reynolds shear stress. None of the methods, applied to this test case, takes into account such effects. Moreover, the streamwise length of the region over which the flow develops to separation in this case is only about 15 initial boundary layer thicknesses. Therefore history effects become very important and may nearly freeze the shear stresses (van den Berg 1982). It can be expected that there is a lagging behind of the Reynolds shear stress magnitude and direction. Only the COUSTEIX/-BERRUE integral method takes into account a difference between the shear stress direction and the direction of the velocity gradient through its global empirical assumptions.

Initial conditions are provided at A and B, station (1,1) and (1,2), far upstream of the displacement body (figure 4.1). Participants were asked to interpolate linearly the initial velocity profiles between A and B.

Table 4.1 Results of numerical accuracy studies for DEFE77 test case

(a) Stepsize variation

results submitted	stepsize factor	coordinate direction	station number	effect on calculations
COUSTEIX/BERRUE	2	x,z		$\Delta\beta_w < 1.8°$
CROSS	2	x,z	4,2	$\Delta\beta_w = .7°$ $\Delta C_f^w = 2.1\%$
MÜLLER	2	x		$\Delta\beta_w < .5°$ $\Delta C_f^w < 1\%$
PATEL/KROGSTAD/BAEK	1.5	x	4,2	$\Delta C_f = .5\%$

(b) Integral momentum balance

results submitted	station number	local error
MÜLLER	5,2	$\Omega_x = .8\%$ $\Omega_z = .05\%$

The computable region associated with the initial conditions along AB has the following boundaries: The symmetry line AS, where S is the separation point, the outer streamline BC and the separation line through S. The last station for which computational results are asked for is station (6,2), situated a small distance upstream of the separation line.

Some methods are programmed to absorb information on a side line, in this case the symmetry line, and treat it as an inflow boundary. In the CEBECI/HUANG method attachment line computations are performed until separation is found on the symmetry line close to $x/L = 0.8$. HOEKSTRA computed the symmetry line solution simultaneously with the computations in the rest of the field. PATEL/KROGSTAD/BAEK followed a similar procedure, but they had to modify the pressure distribution close to separation to avoid oscillations. MÜLLER had the same complaint. Most likely the second derivative of the pressure, as derived from the experimental data, is not accurate enough in the plane of symmetry. In order to avoid these difficulties MÜLLER applied Hall's scheme with which it is possible to perform the computation without using extra information from the symmetry line. With that scheme the computational domain shrinks with each marching step.

The participants were asked to produce global results along the external streamline BC and detailed velocity and shear stress profiles at station (4,1) on the symmetry line and at stations (4,2), (5,2) and (6,2) along BC. The integral methods COUSTEIX/BERRUE and CROSS computed the global behaviour of boundary layers, but did not give detailed profiles, although CROSS gave a velocity profile on the symmetry line. The PATEL/KROGSTAD/BAEK method did not present global quantities along the external streamline BC, since this was not a coordinate line of the computation. MÜLLER submitted no results on the symmetry line for the reason discussed in the preceding paragraph. A summary of the results presented is given in table 4.2.

The results of the seven calculation methods, which were applied to this test case, will be discussed next in some detail. The local momentum thickness Reynolds number, R_Θ, is depicted in figure 4.3. The irregularities in the experimental data line are probably due to measurement scatter. The horizontal axis runs to $x/L = 0.9$ which is the approximate position where separation occurs along BC. The HOEKSTRA method closely follows the measured momentum thickness development until $x/L = 0.6$. The predictions of three methods (CROSS, MULLER and LINDHOUT/DE BRUIN) coincide up to $x/L = 0.75$, but have a steeper slope than the measured one. The COUSTEIX/BERRUE calculation has an elevated starting value for the momentum thickness, but the calculated slope compares well with the measurements. The two data points obtained with the CEBECI/HUANG method deviate from the general trend.

In figure 4.4 the limiting streamline angles, β_w, are depicted. The computations follow the measured angles well, apart from CROSS, which underpredicts the wall flow angle for the whole range. The friction coefficient, C_f, see figure 4.5, is computed with reasonable accuracy over almost the whole range. Close to separation all methods show a minimum after which the skin friction increases again.

In figure 4.6 and 4.7 the streamwise velocity profiles and the streamwise shear stresses at station (4,1) on the symmetry line are depicted. The computed velocity profiles show a slight overestimation of the velocity near the region of maximum shear stress, which itself is overestimated by 30%. If the extra rate of strain due to streamline divergence had had a dominant effect the measured shear stresses would have been larger than the computed ones, which is not the case. If the history effects were important, the Reynolds stresses could be considered as "frozen" in the experiment, leading to smaller stresses, as can indeed be observed.

Figure 4.8 depicts the streamwise velocity profiles at station (4,2) along the external streamline BC. Figure 4.9 shows the crosswise velocity profiles and figures 4.10 and 4.11 the streamwise and crosswise shear stresses. All methods follow the variations of the experimental crosswise velocity, even close to the wall. Shear stresses are over-estimated, the streamwise stresses are computed about 30% too high. The measured crosswise shear stresses almost vanish along a normal, except close to the wall. The small crosswise stresses can be explained by assuming that the turbulence properties behave as if frozen. These experimental findings are not reproduced by the calculations.

The methods of HOEKSTRA, MULLER, PATEL/KROGSTAD/BAEK and LINDHOUT/ DE BRUIN have calculated velocity and shear stress profiles downstream of station (4,2). The results at stations (5,2) and (6,2) are shown in figures 4.12 to 4.19. Mean velocity profiles are computed in broad agreement with experiment, though the deviations exceed the experimental error range (± .02 in the plotted velocity ratios), especially at station (6,2). The computed streamwise shear stresses are too large. The magnitude of the crosswise shear stresses in the outer region of the boundary layer is very much overestimated in the calculations. The differences between computed and measured shear stresses are much larger than the stated experimental error (± 10%). On the whole, the Reynolds stresses, particularly the crosswise component, are very poorly predicted in all the calculations.

Table 4.2 <u>Survey of computed results for the DEFE77 test case</u>

figures	quantities	CEBECI HUANG	COUSTEIX BERRUE	CROSS	HOEKSTRA	LINDHOUT DE BRUIN	MÜLLER	PATEL KROGSTAD BAEK
4.3 – 4.5	R_Θ, β_w, c_f along BC	X	X	X	X	X	X	
4.6	U at (4,1)	X		X	X	X		X
4.7	τ_x at (4,1)				X	X		X
4.8 4.9	U,W at (4,2)	X			X	X	X	X
4.10 4.11	τ_x, τ_z at (4,2)				X	X	X	X
4.12 4.13	U,W at (5,2)				X	X	X	X
4.14 4.15	τ_x, τ_z at (5,2)				X	X	X	X
4.16 4.17	U,W at (6,2)				X	X	X	X
4.18 4.19	τ_x, τ_z at (6,2)				X	X	X	X
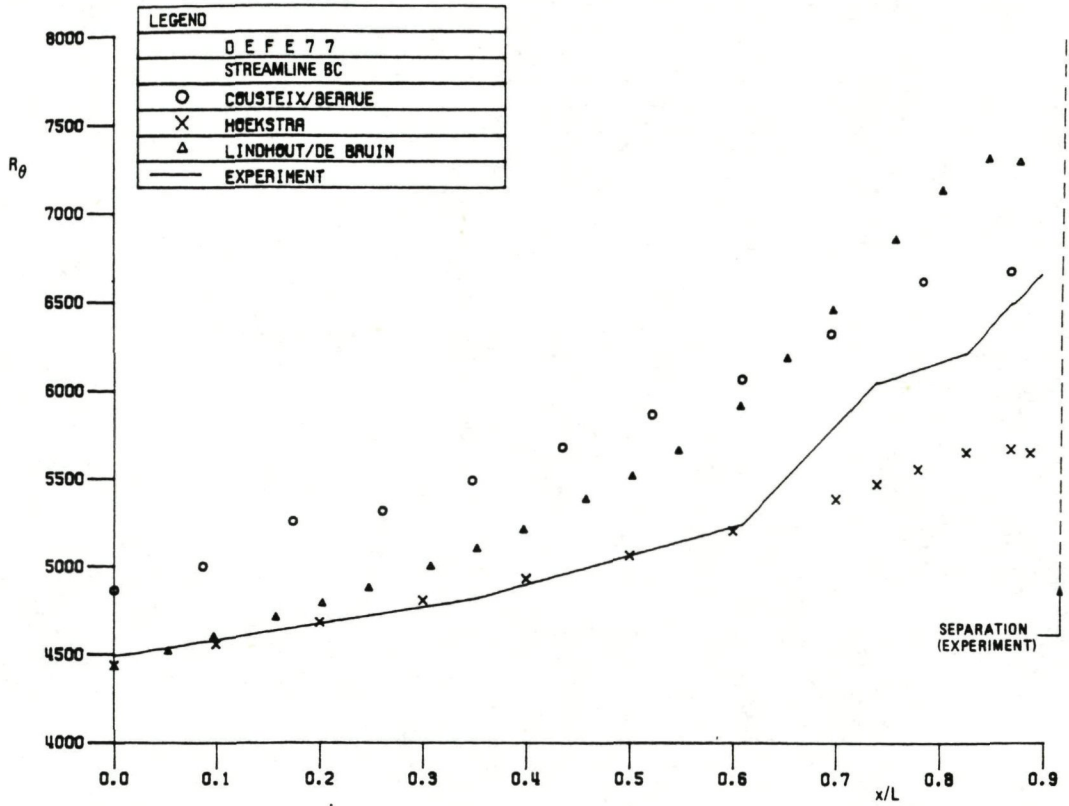
Fig. 4.3a   Variation of the momentum thickness Reynolds number
along the external streamline BC
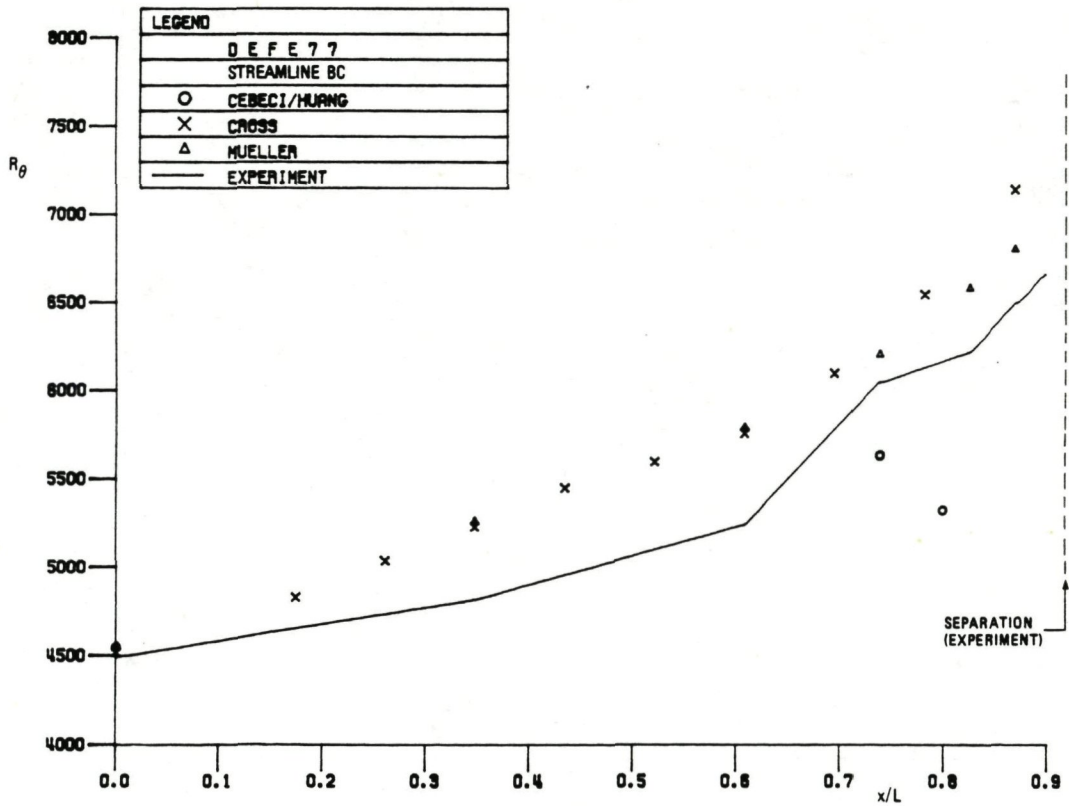
Fig. 4.3b   Variation of the momentum thickness Reynolds number
along the external streamline BC
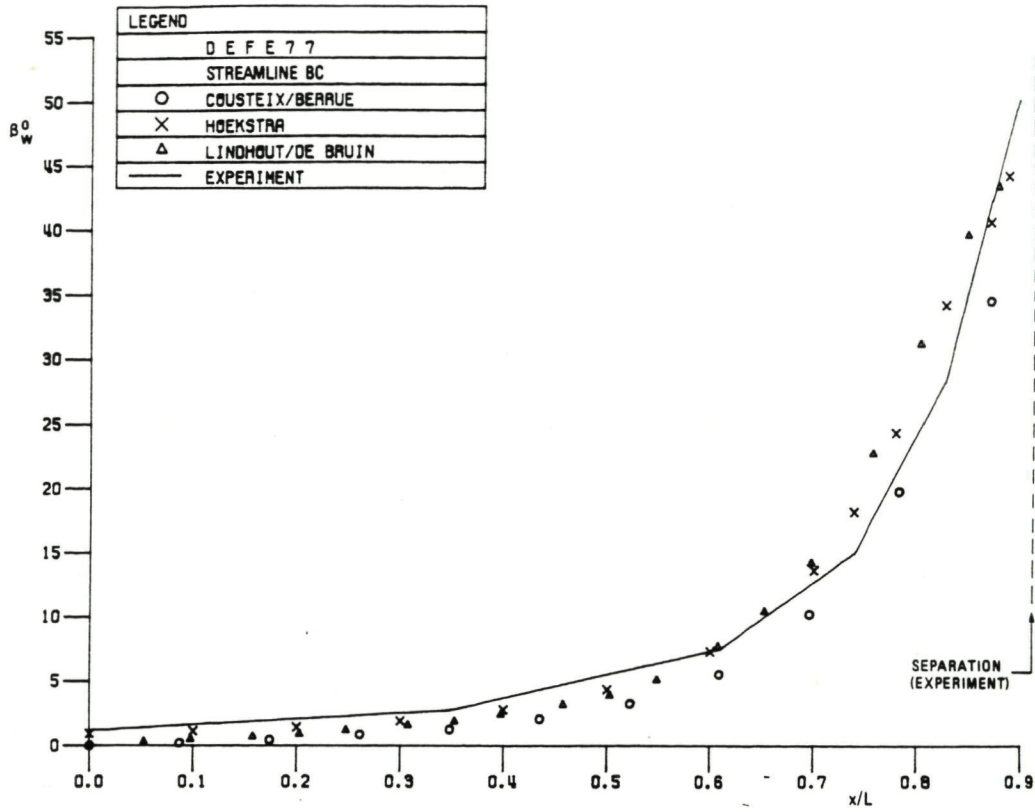
Fig. 4.4a   Variation of wall flow angle along the external
            streamline BC
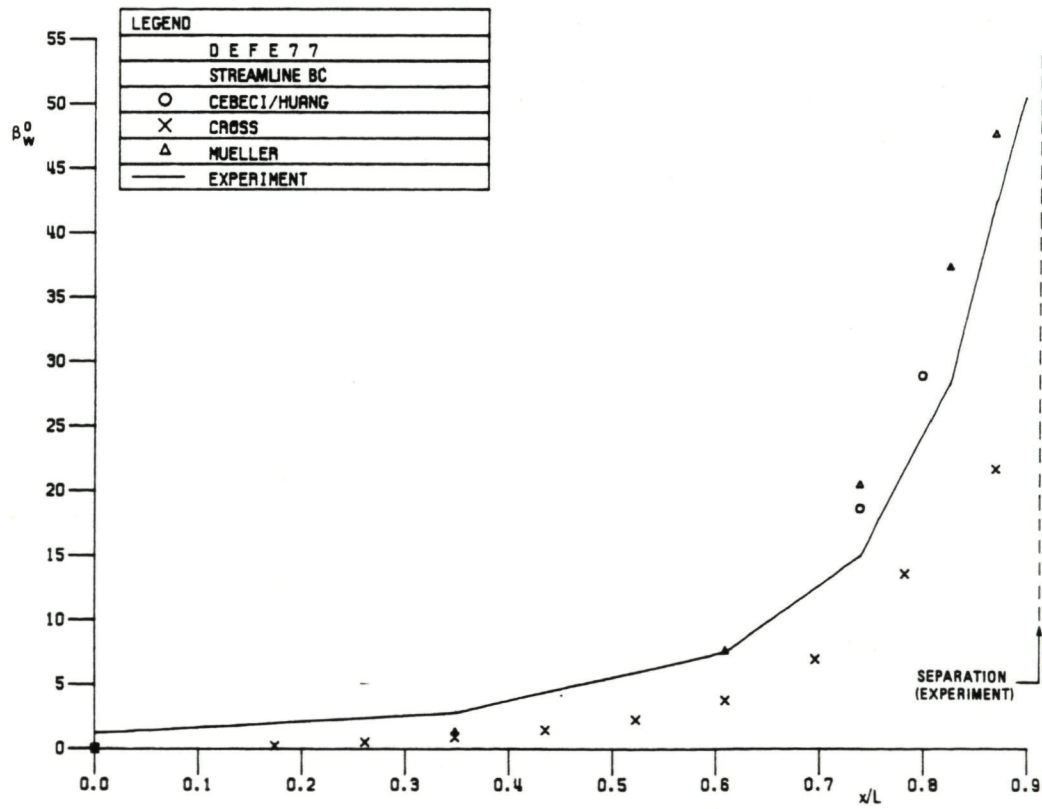
Fig. 4.4b   Variation of wall flow angle along the external
            streamline BC
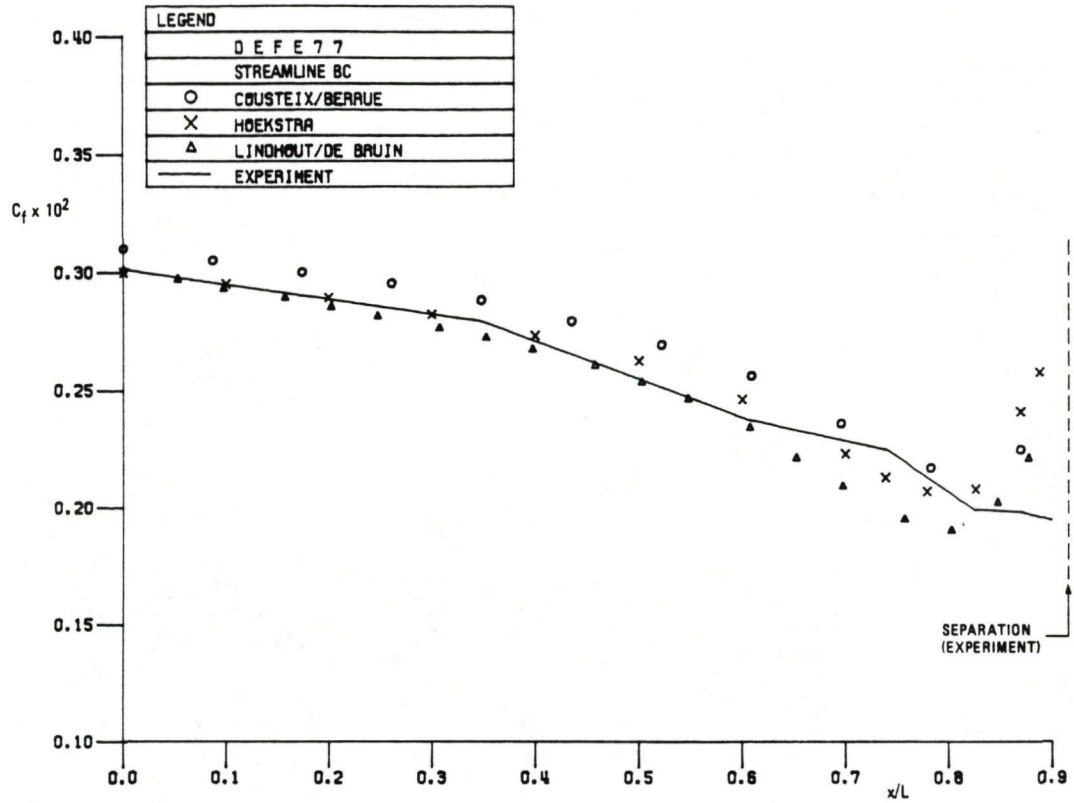
Fig. 4.5a   Variation of skin friction along the external
streamline BC
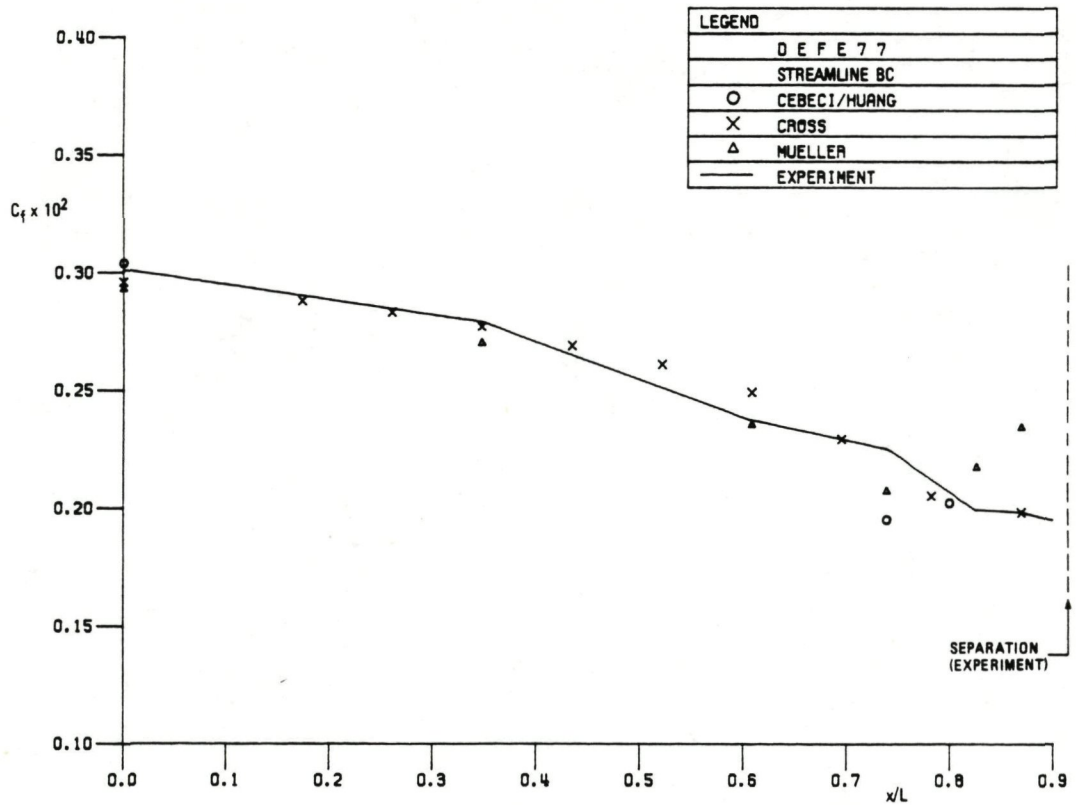
Fig. 4.5b   Variation of skin friction along the external
streamline BC
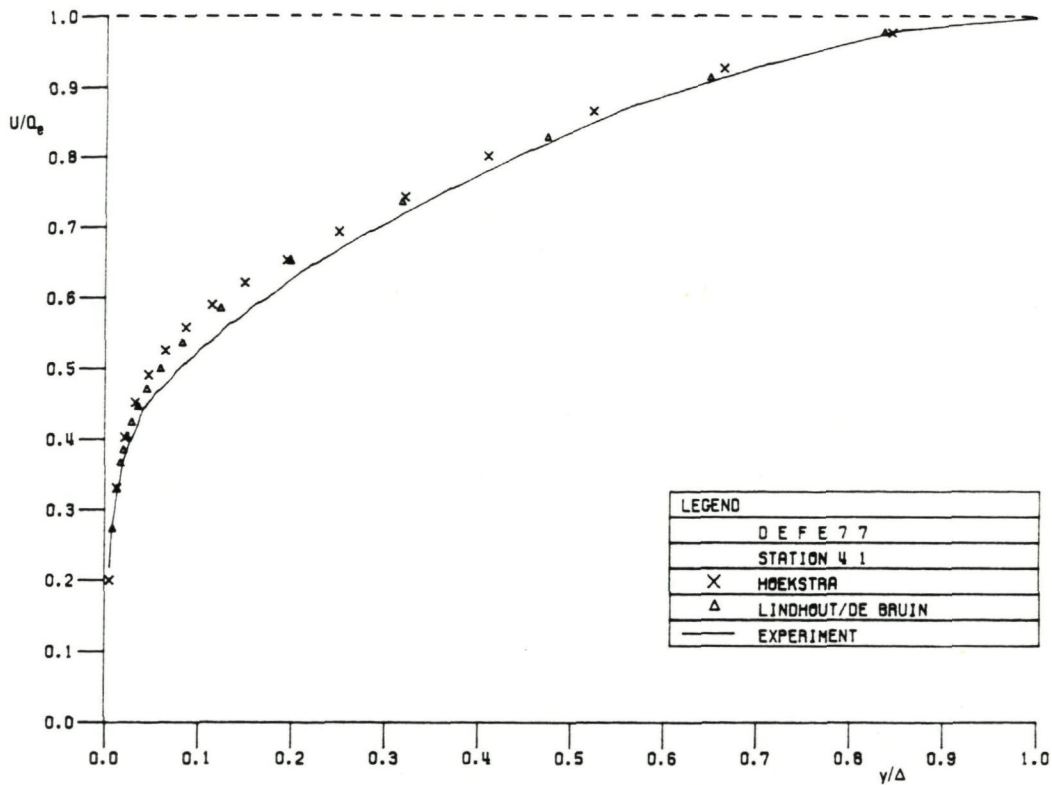
Fig. 4.6a   Streamwise velocity profiles at station 4, 1
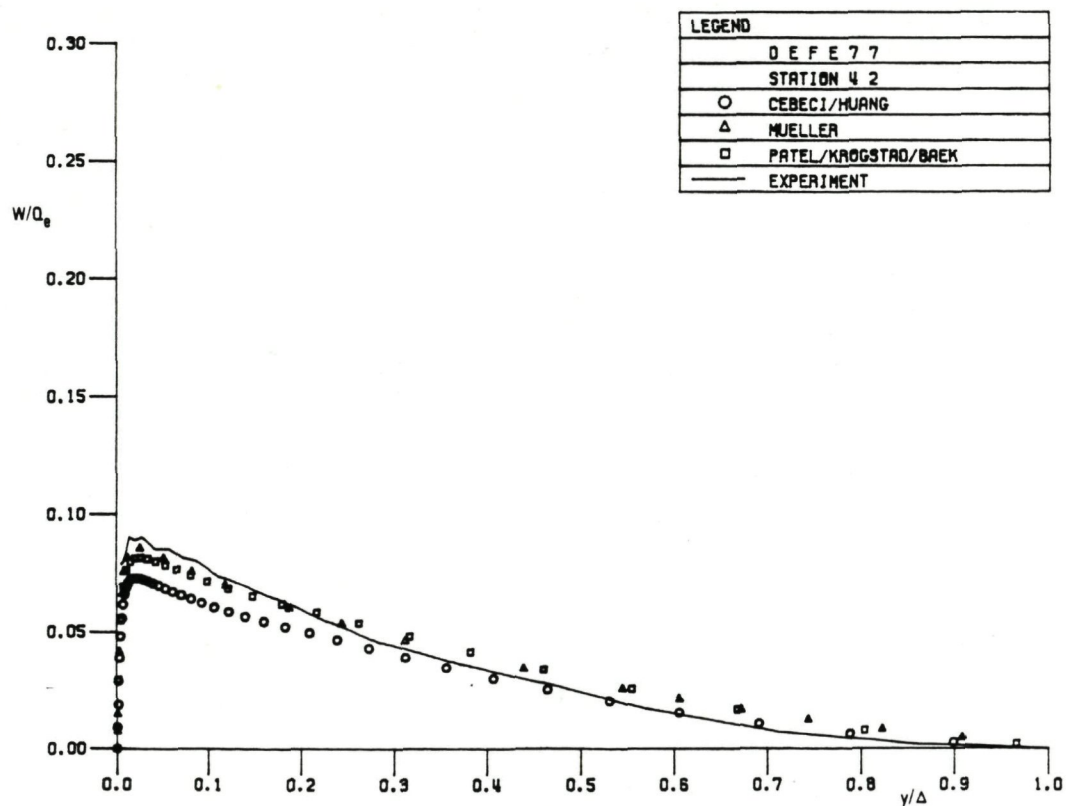   (x/L = 0.739) on the symmetry line
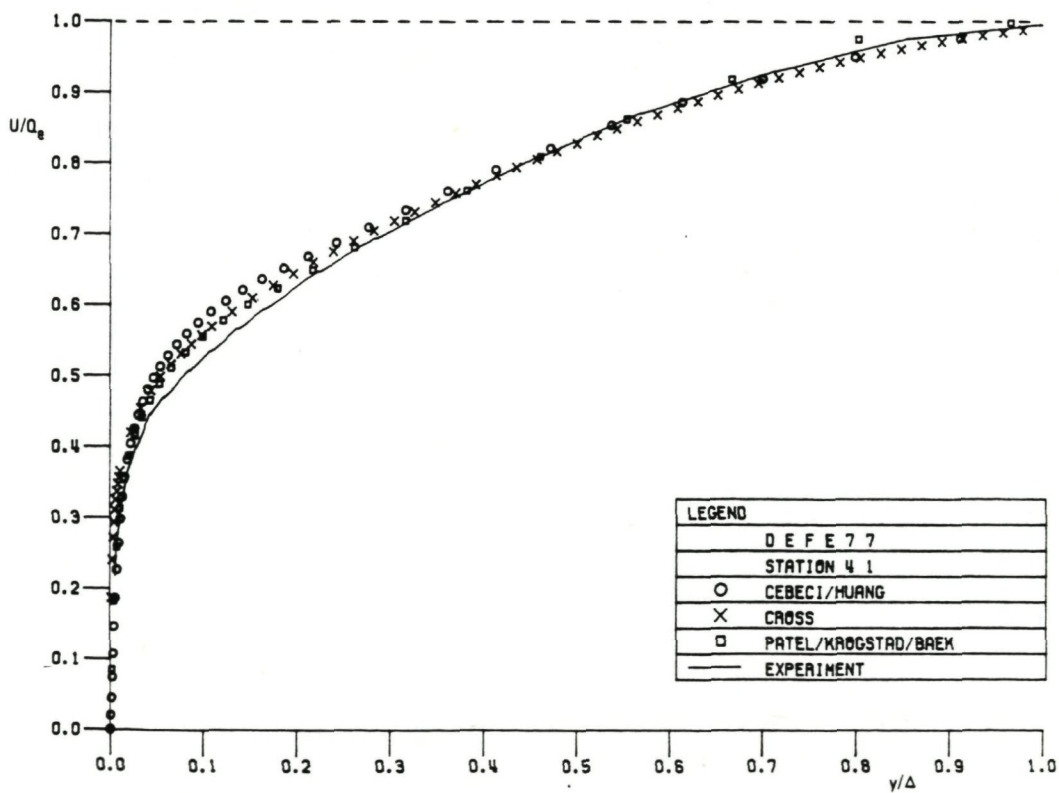
Fig. 4.6b   Streamwise velocity profiles at station 4, 1
   (x/L = 0.739) on the symmetry line
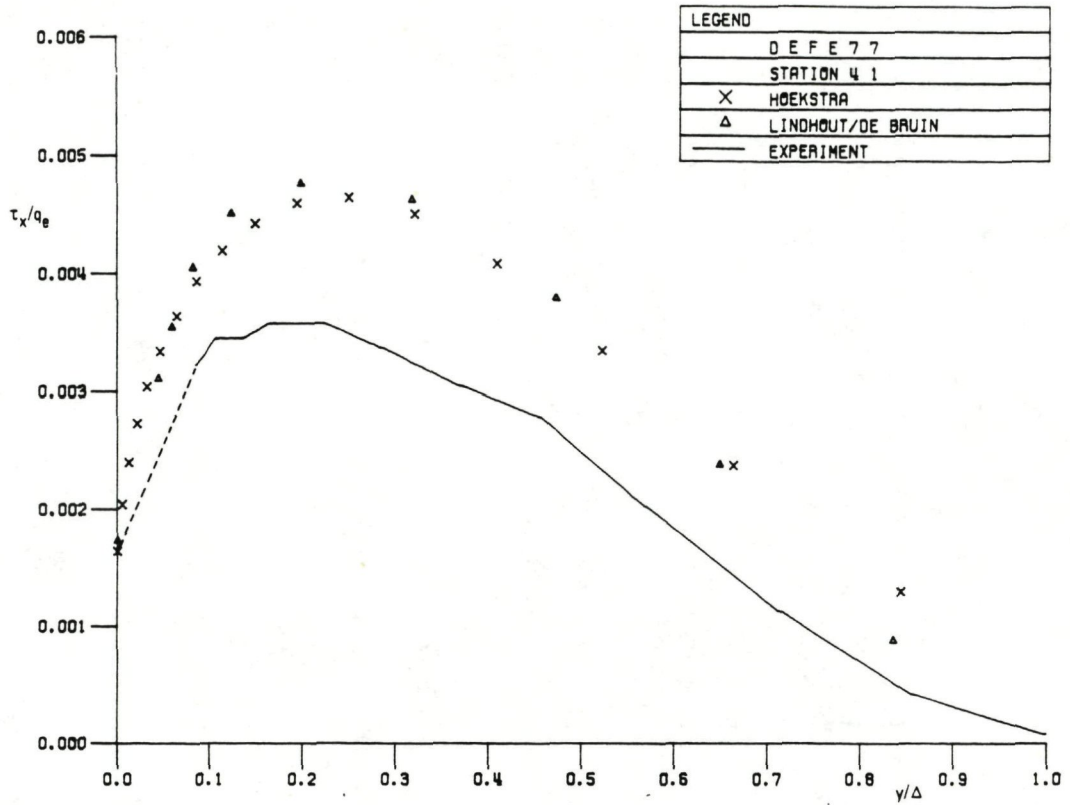
Fig. 4.7a   Streamwise shear stresses at station 4, 1
(x/L = 0.739) on the symmetry line
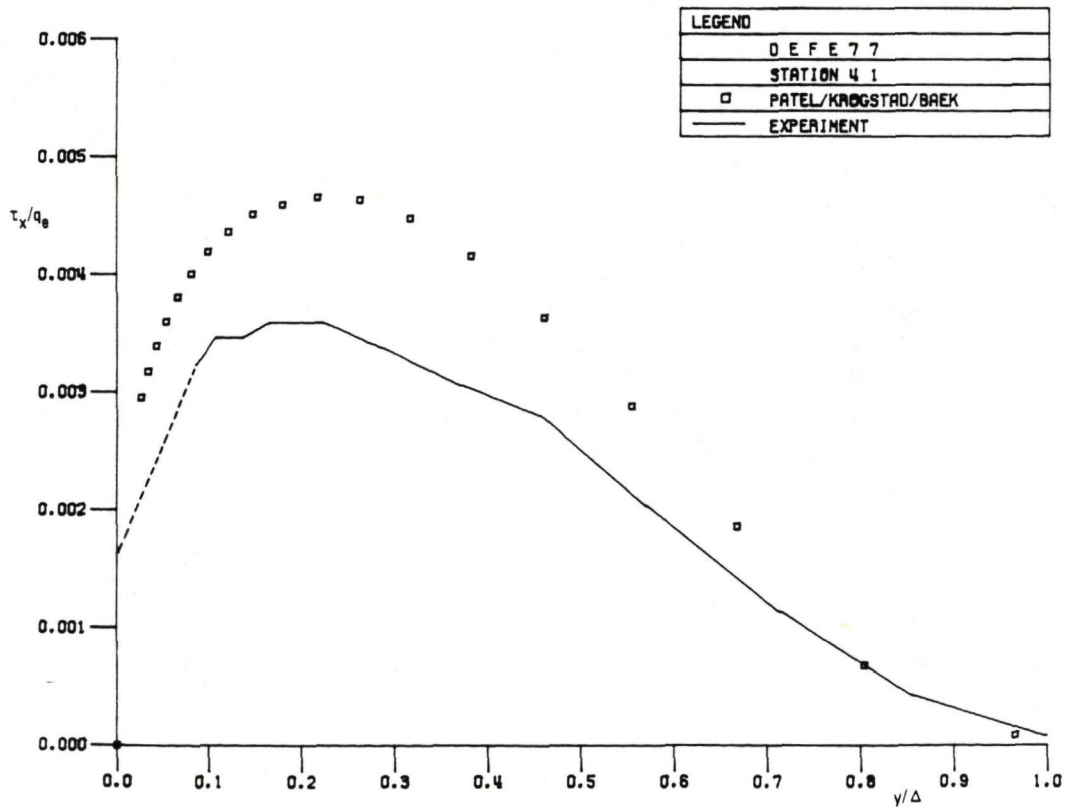
Fig. 4.7b   Streamwise shear stresses at station 4, 1
(x/L = 0.739) on the symmetry line
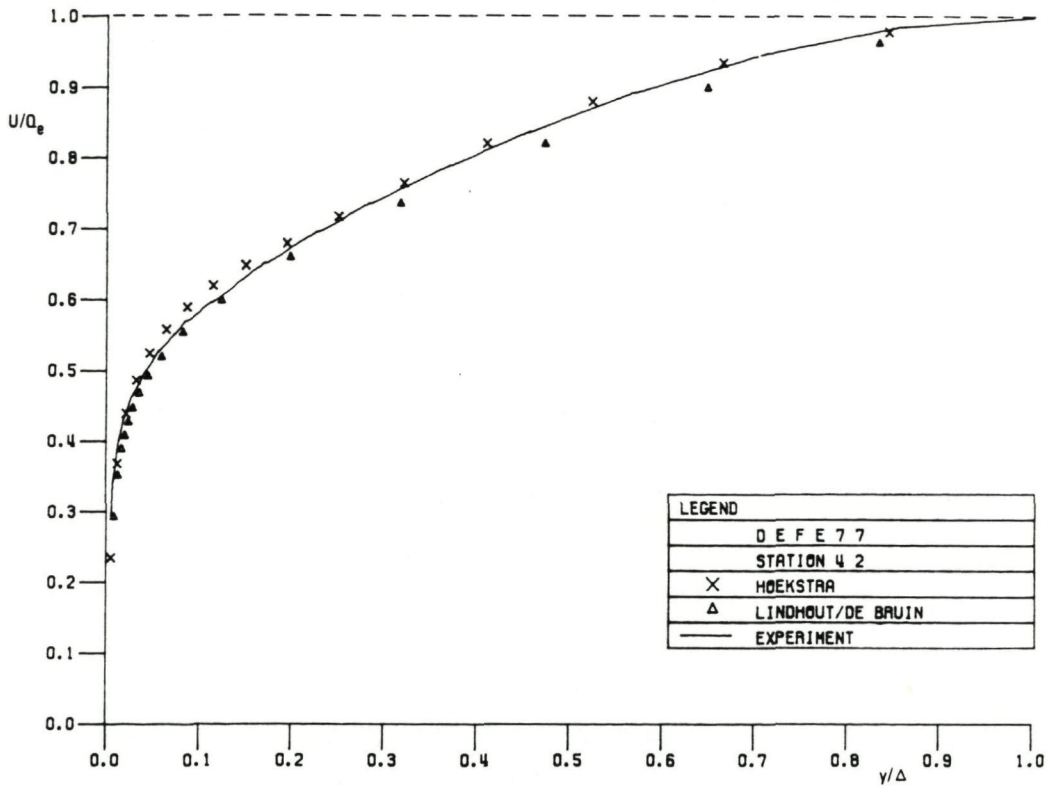
Fig. 4.8a   Streamwise velocity profiles at station 4, 2
            (x/L = 0.739) on the external streamline BC
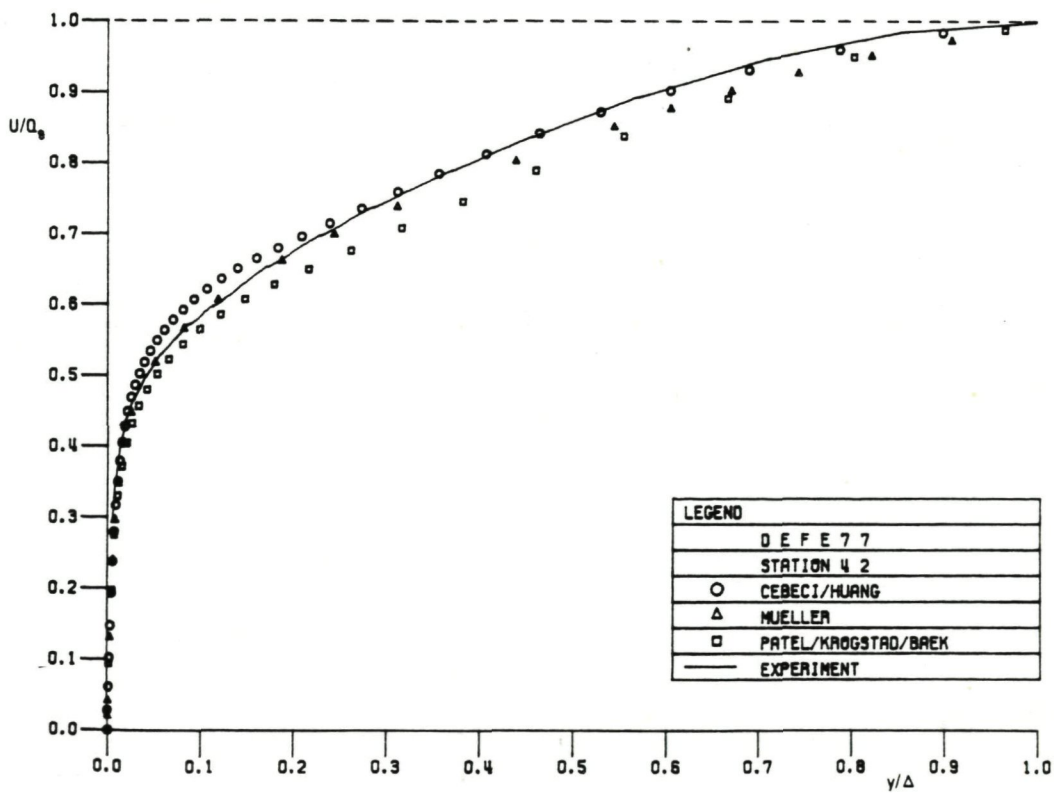
Fig. 4.8b   Streamwise velocity profiles at station 4, 2
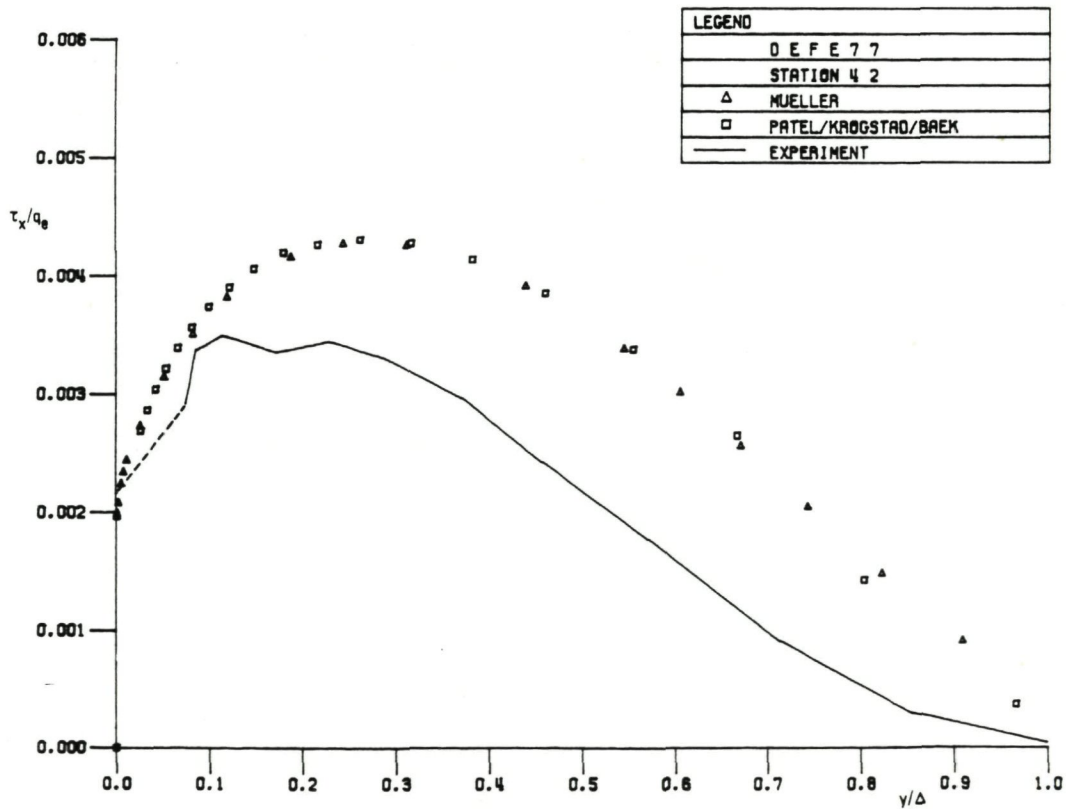   (x/L = 0.739) on the external streamline BC
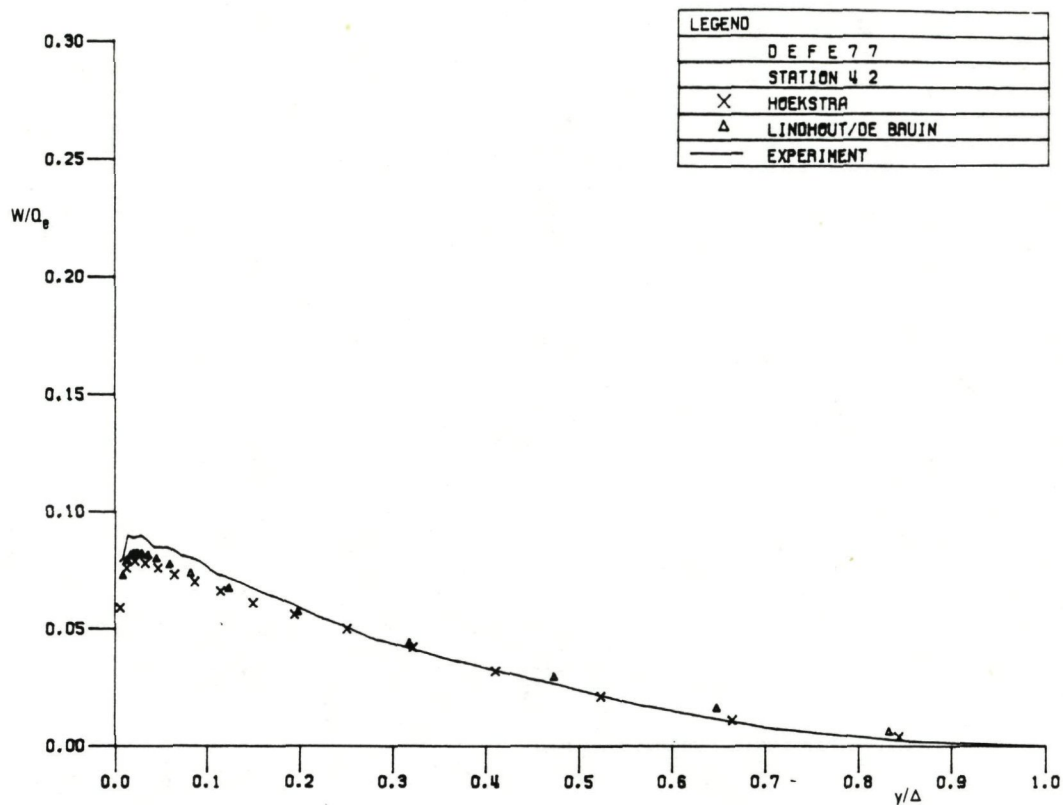
Fig. 4.9a   Crosswise velocity profiles at station 4, 2
(x/L = 0.739) on the external streamline BC

Fig. 4.9b   Crosswise velocity profiles at station 4, 2
(x/L = 0.739) on the external streamline BC
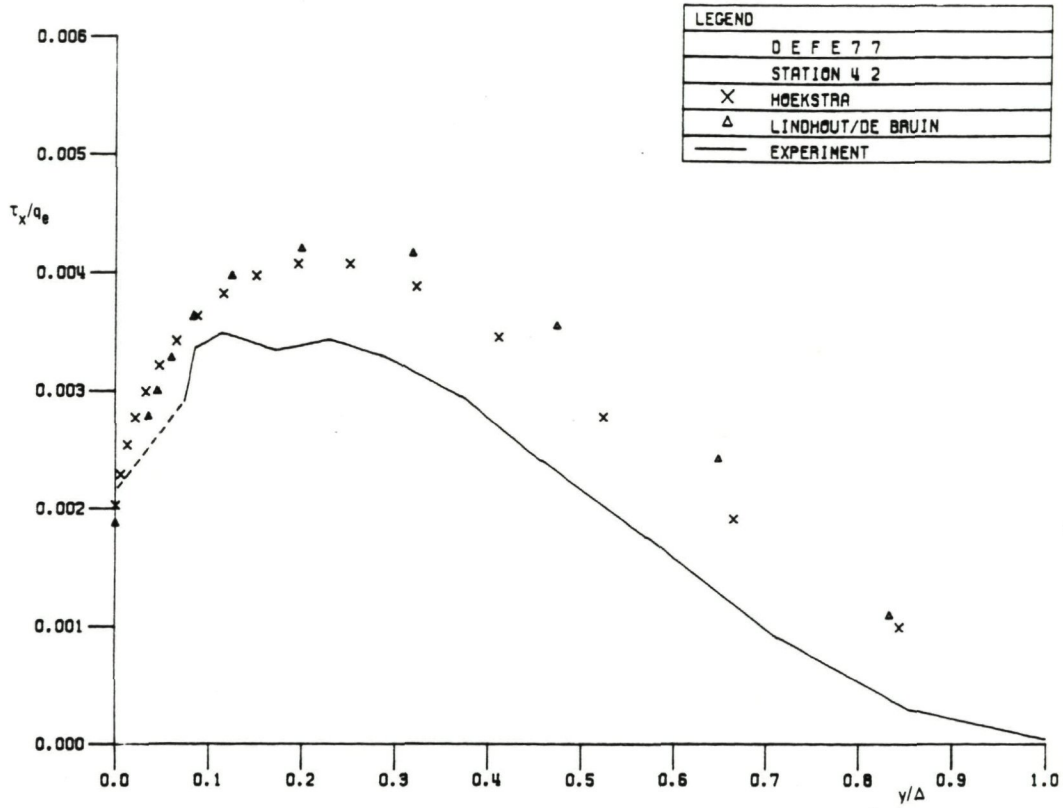
Fig. 4.10a Streamwise shear stresses at station 4, 2
(x/L = 0.739) on the external streamline BC

Fig. 4.10b Streamwise shear stresses at station 4, 2
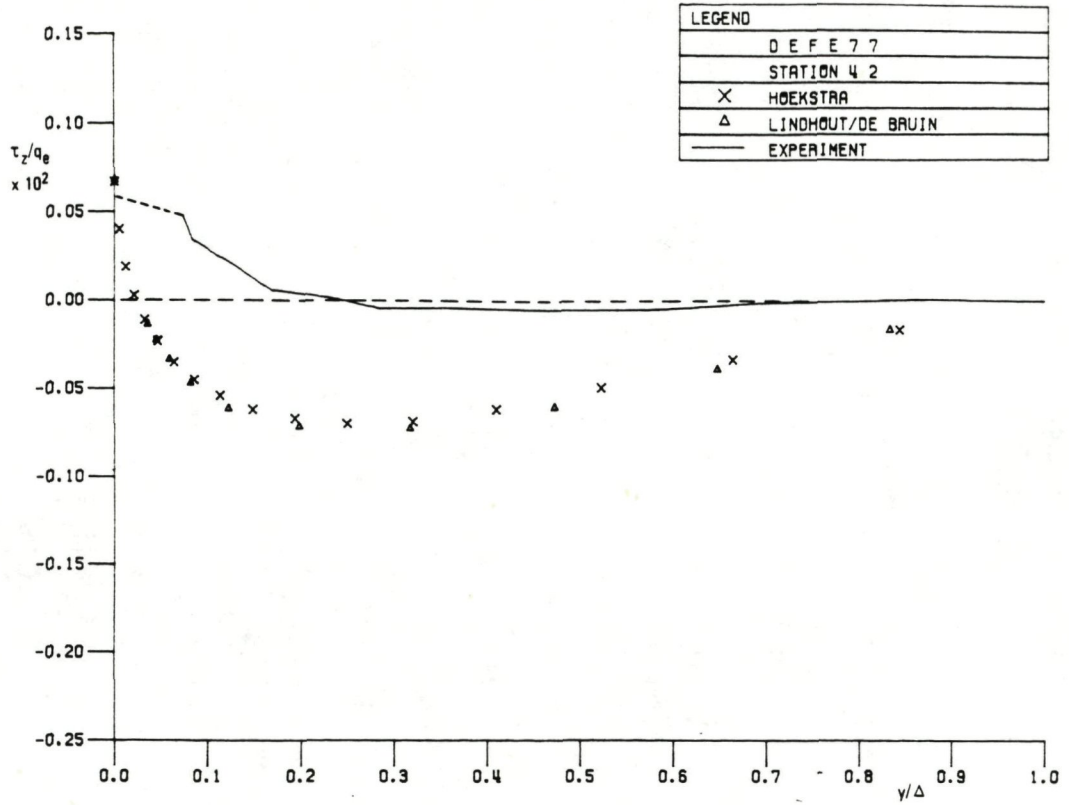(x/L = 0.739) on the external streamline BC

Fig. 4.11a   Crosswise shear stresses at station 4, 2
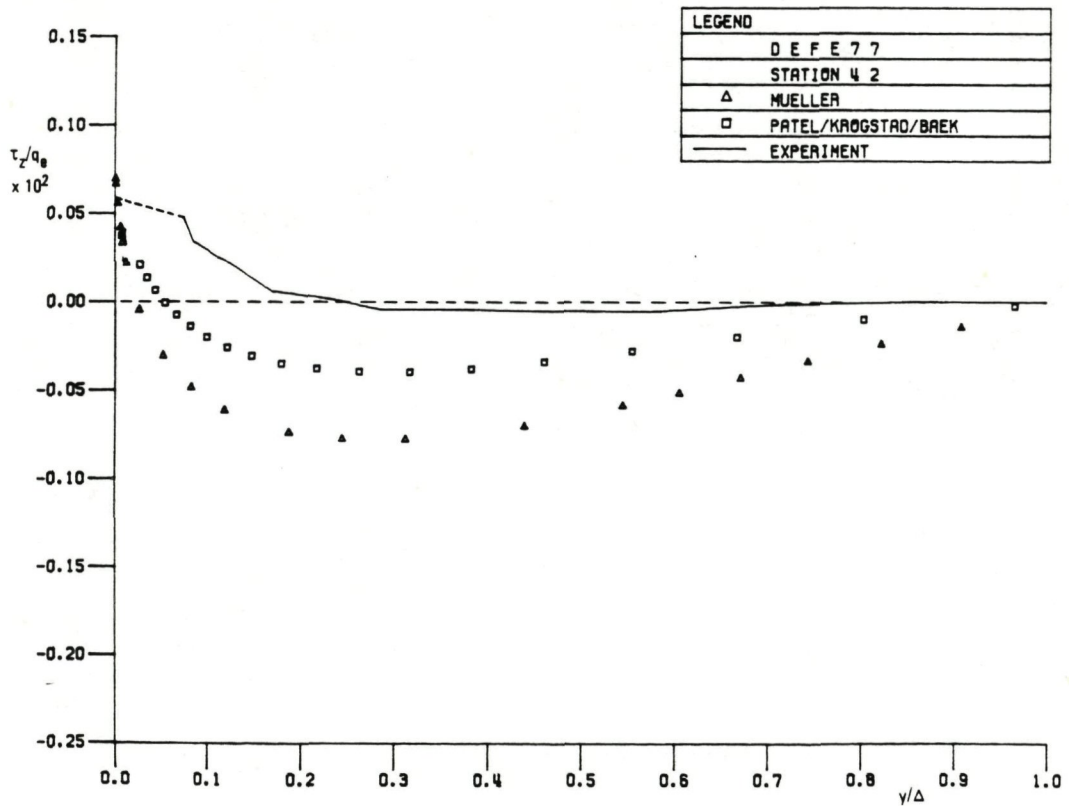(x/L = 0.739) on the external streamline BC

Fig. 4.11b   Crosswise shear stresses at station 4, 2
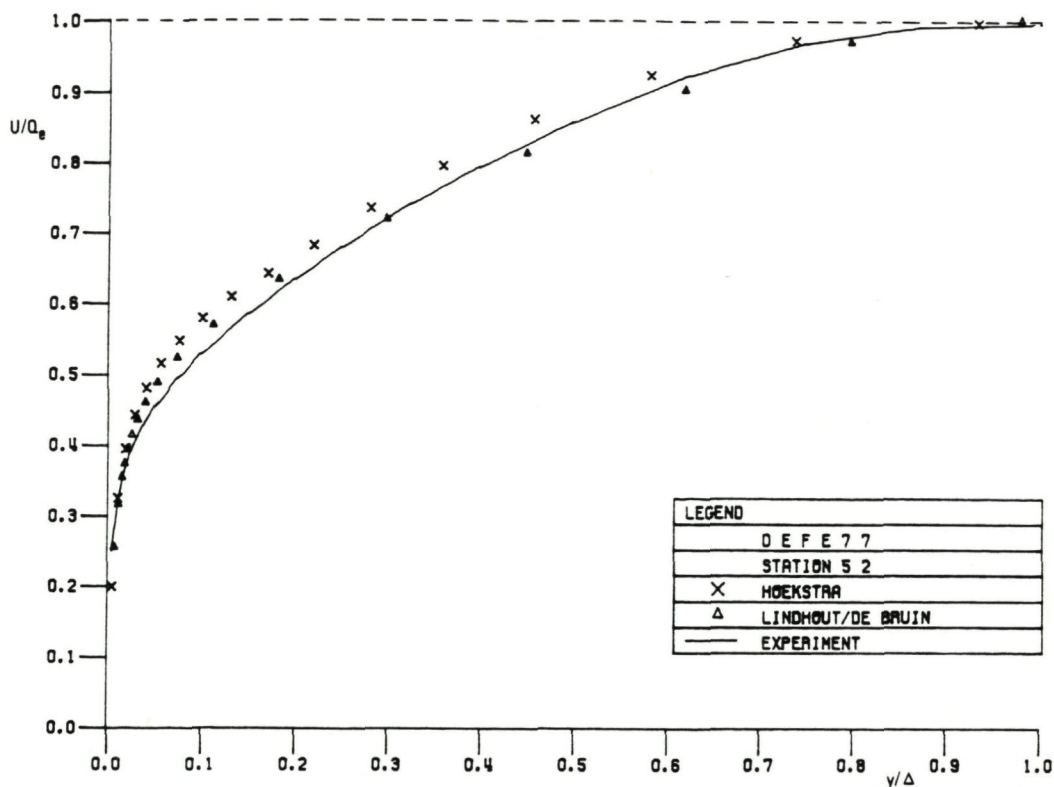(x/L = 0.739) on the external streamline BC

Fig. 4.12a   Streamwise velocity profiles at station 5, 2
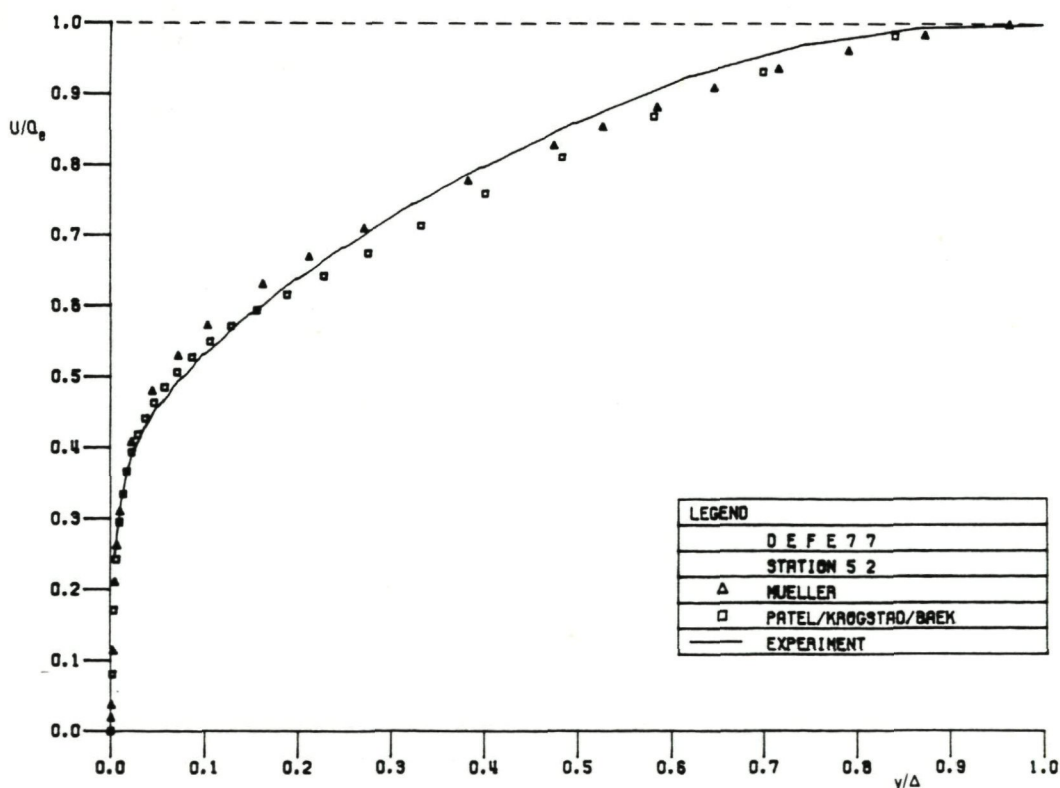   (x/L = 0.826) on the external streamline BC

Fig. 4.12b   Streamwise velocity profiles at station 5, 2
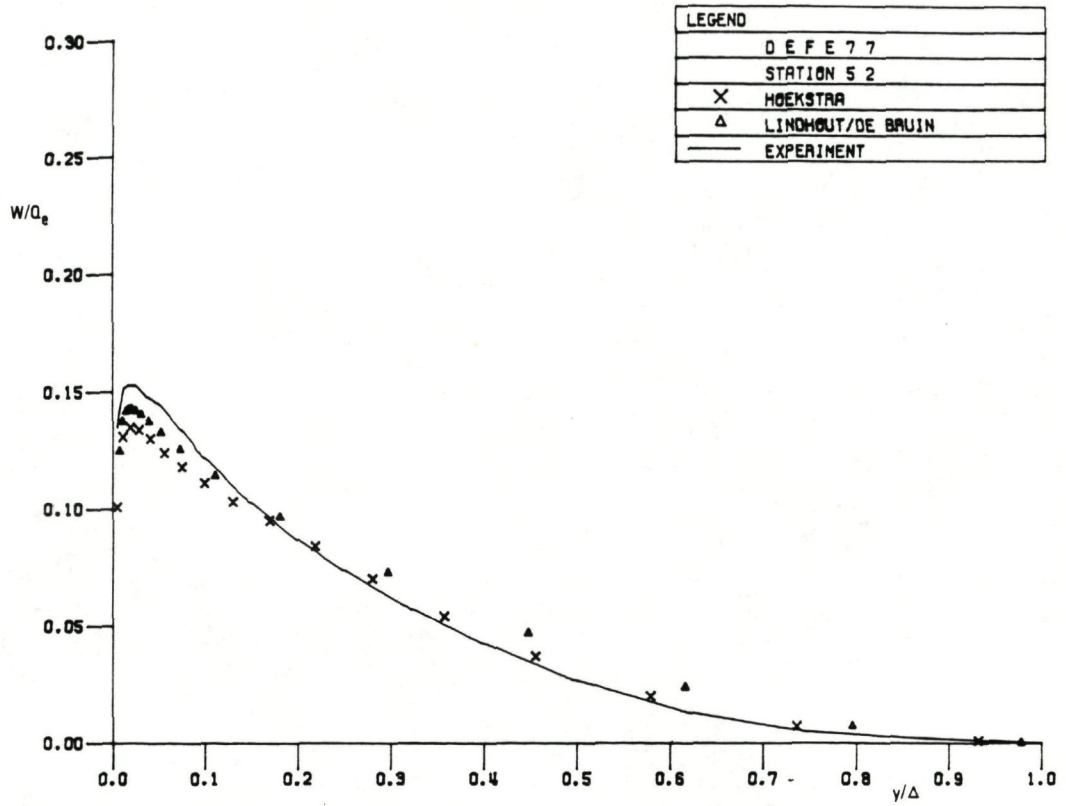   (x/L = 0.826) on the external streamline BC

Fig. 4.13a   Crosswise velocity profiles at station 5, 2
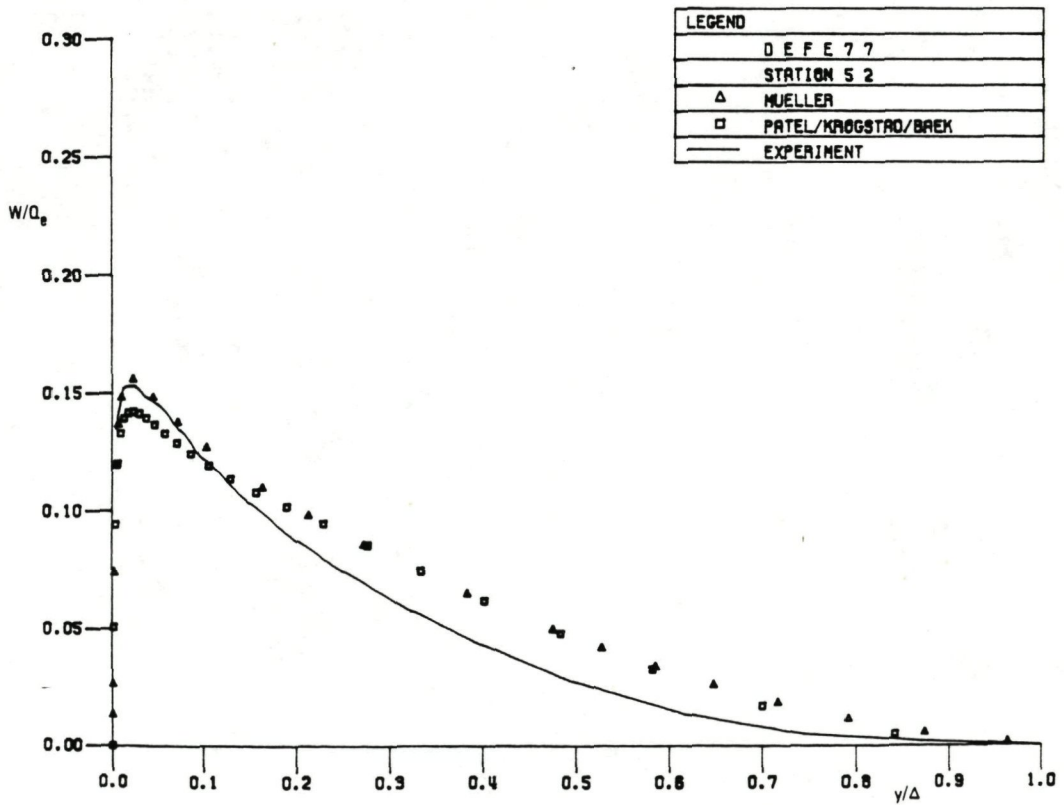(x/L = 0.826) on the external streamline BC

Fig. 4.13b   Crosswise velocity profiles at station 5, 2
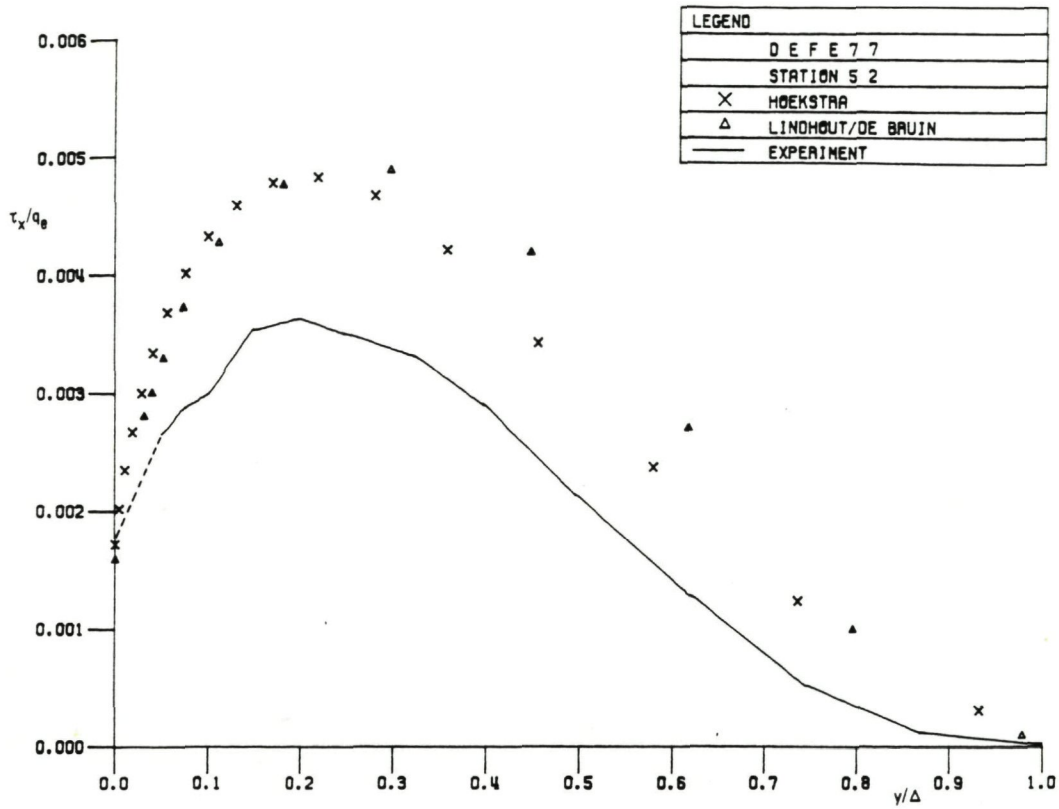(x/L = 0.826) on the external streamline BC

Fig. 4.14a   Streamwise shear stresses at station 5, 2
(x/L = 0.826) on the external streamline BC

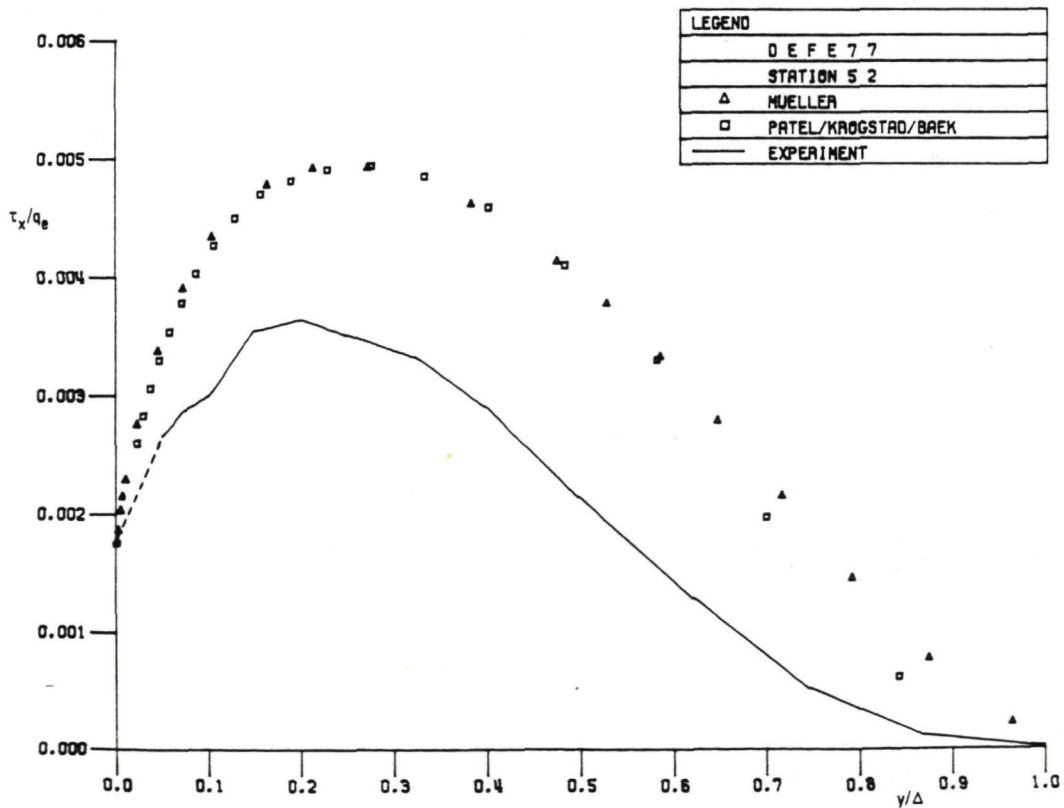Fig. 4.14b   Streamwise shear stresses at station 5, 2
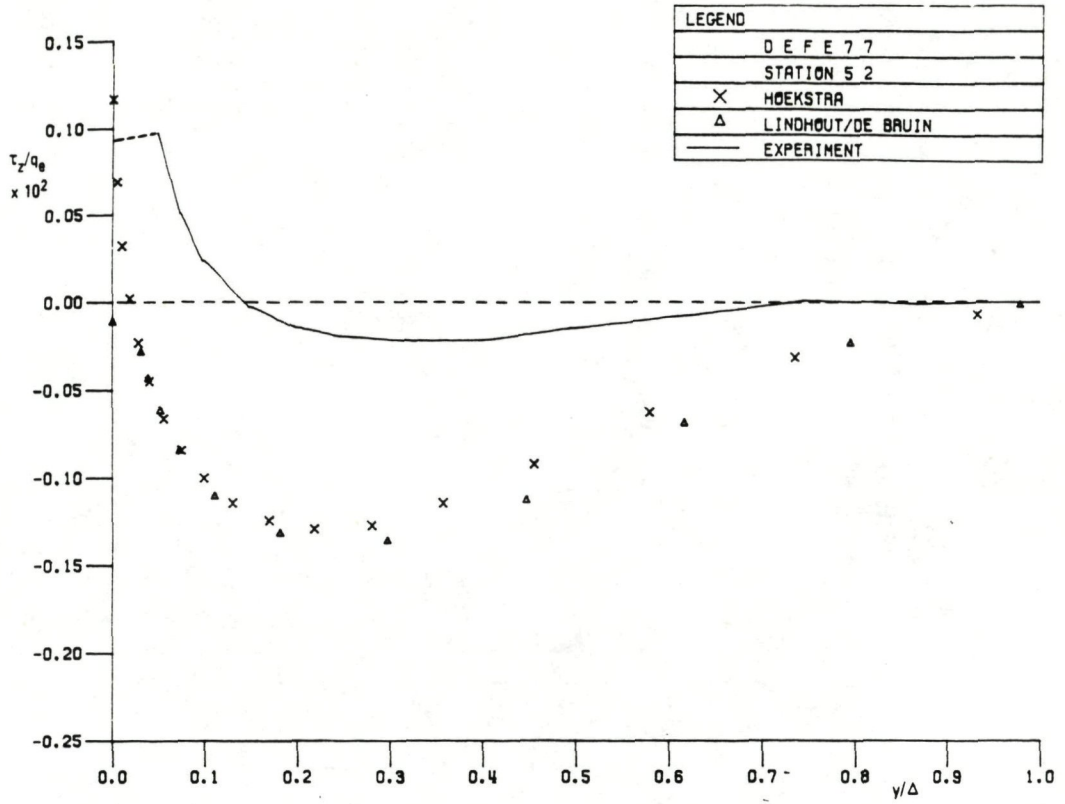(x/L = 0.826) on the external streamline BC

Fig. 4.15a   Crosswise shear stresses at station 5, 2
(x/L = 0.826) on the external streamline BC

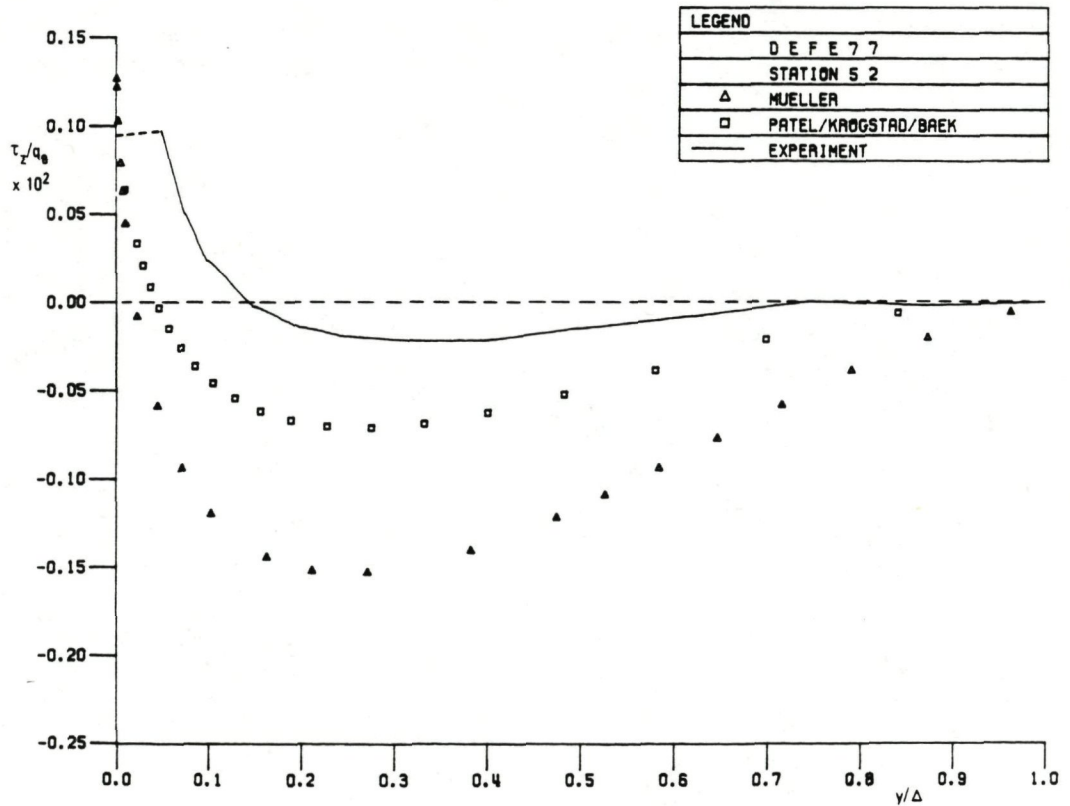

Fig. 4.15b   Crosswise shear stresses at station 5, 2
(x/L = 0.826) on the external streamline BC

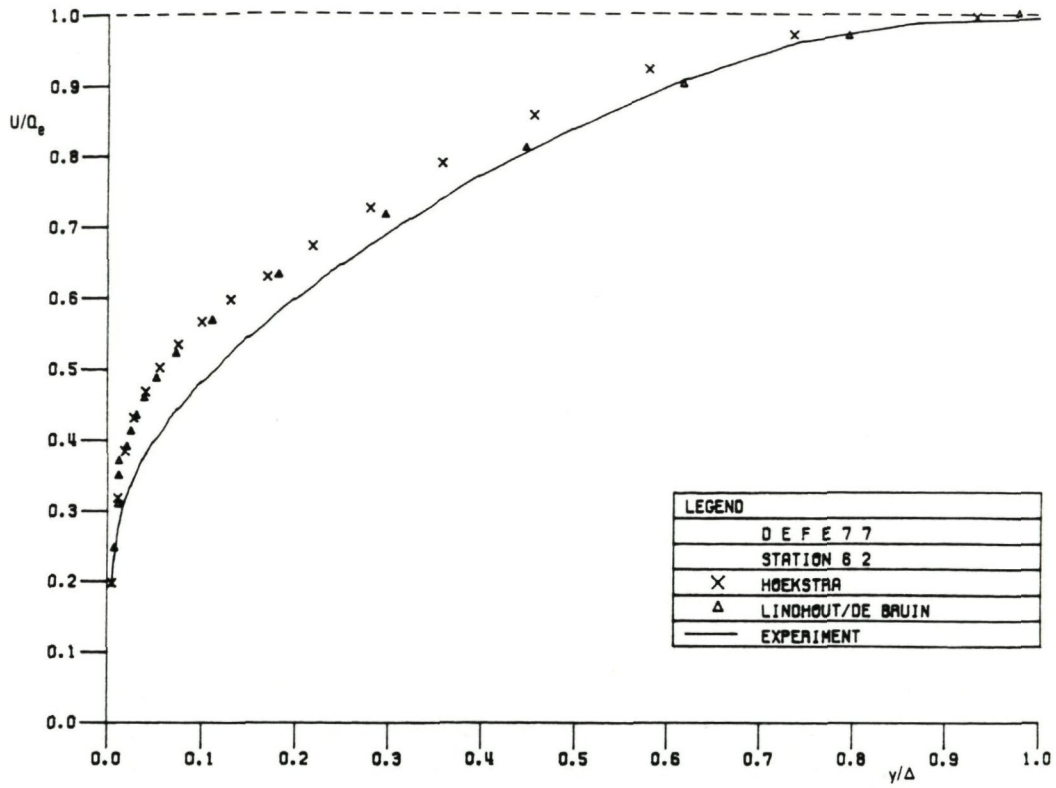Fig. 4.16a   Streamwise velocity profiles at station 6, 2
(x/L = 0.871) on the external streamline BC

Fig. 4.16b   Streamwise velocity profiles at station 6, 2
(x/L = 0.871) on the external streamline BC

Fig. 4.17a   Crosswise velocity profiles at station 6, 2
(x/L = 0.871) on the external streamline BC

Fig. 4.17b   Crosswise velocity profiles at station 6, 2
(x/L = 0.871) on the external streamline BC

Fig. 4.18a   Streamwise shear stresses at station 6, 2
             (x/L = 0.871) on the external streamline BC

Fig. 4.18b   Streamwise shear stresses at station 6, 2
             (x/L = 0.871) on the external streamline BC
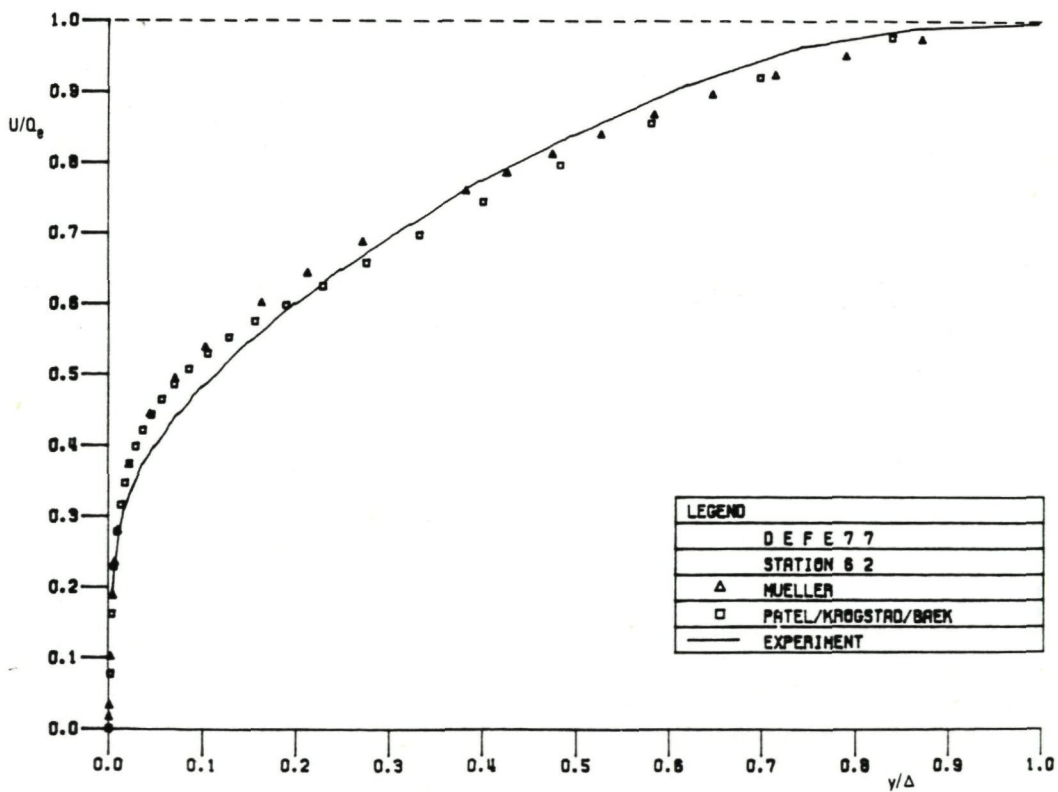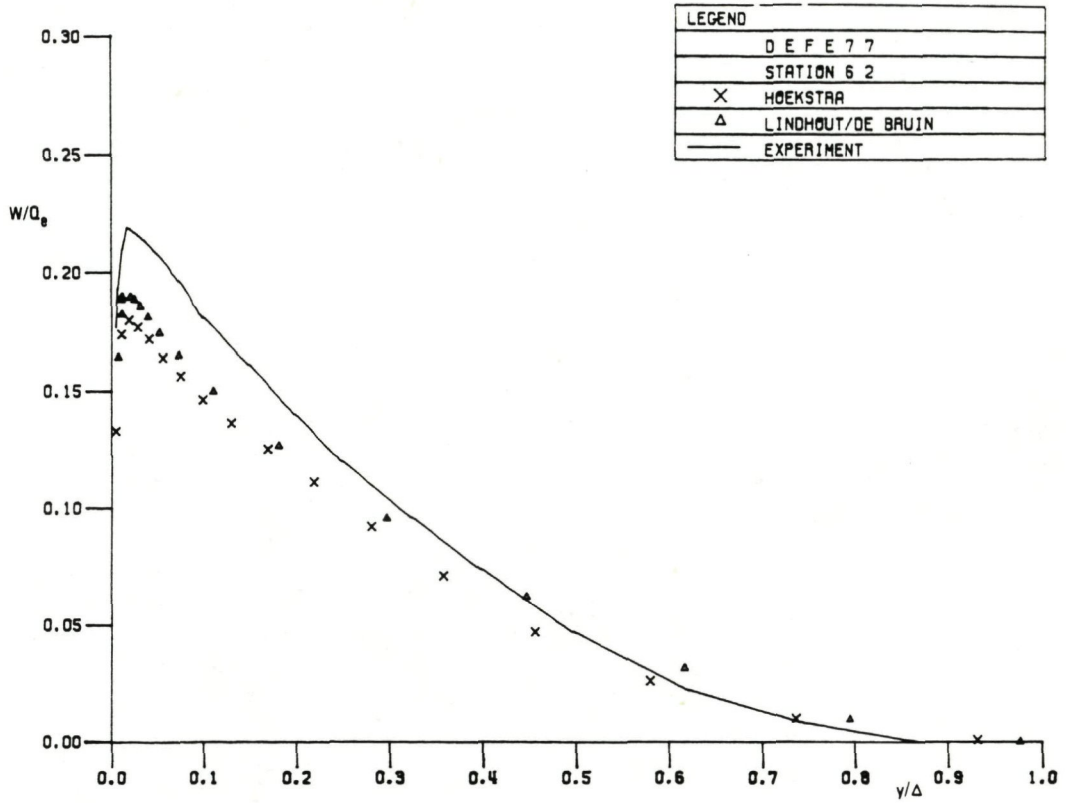
Fig. 4.19a   Crosswise shear stresses at station 6, 2
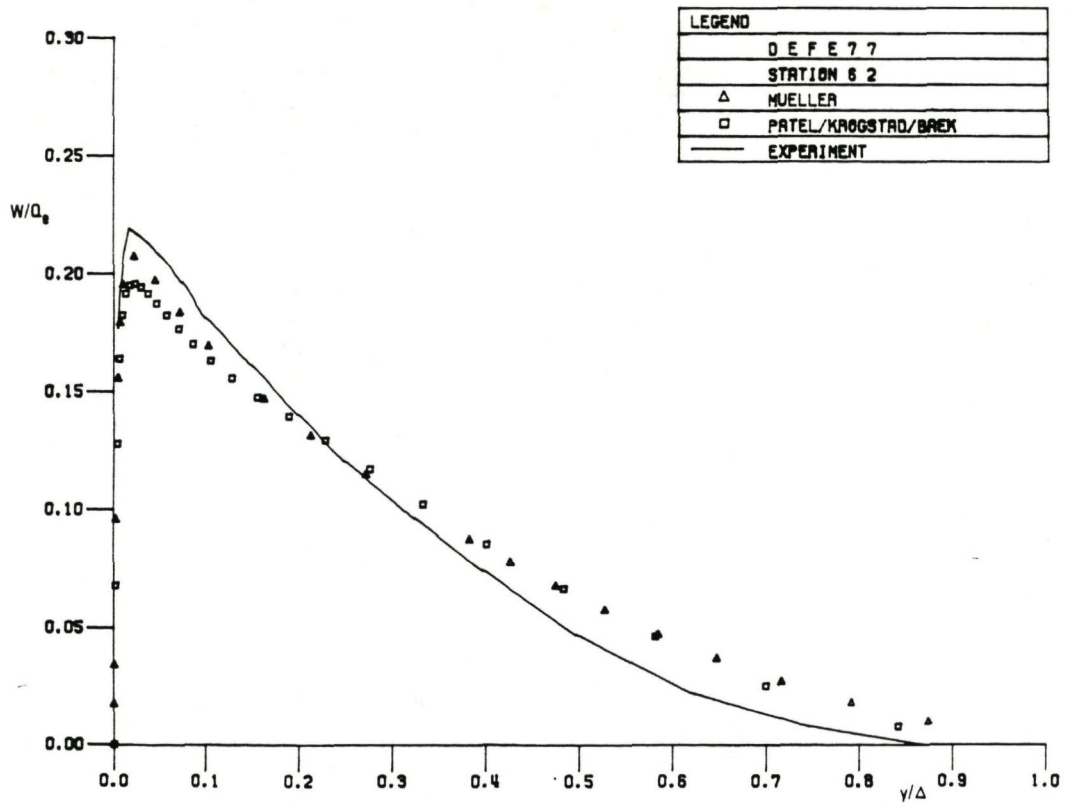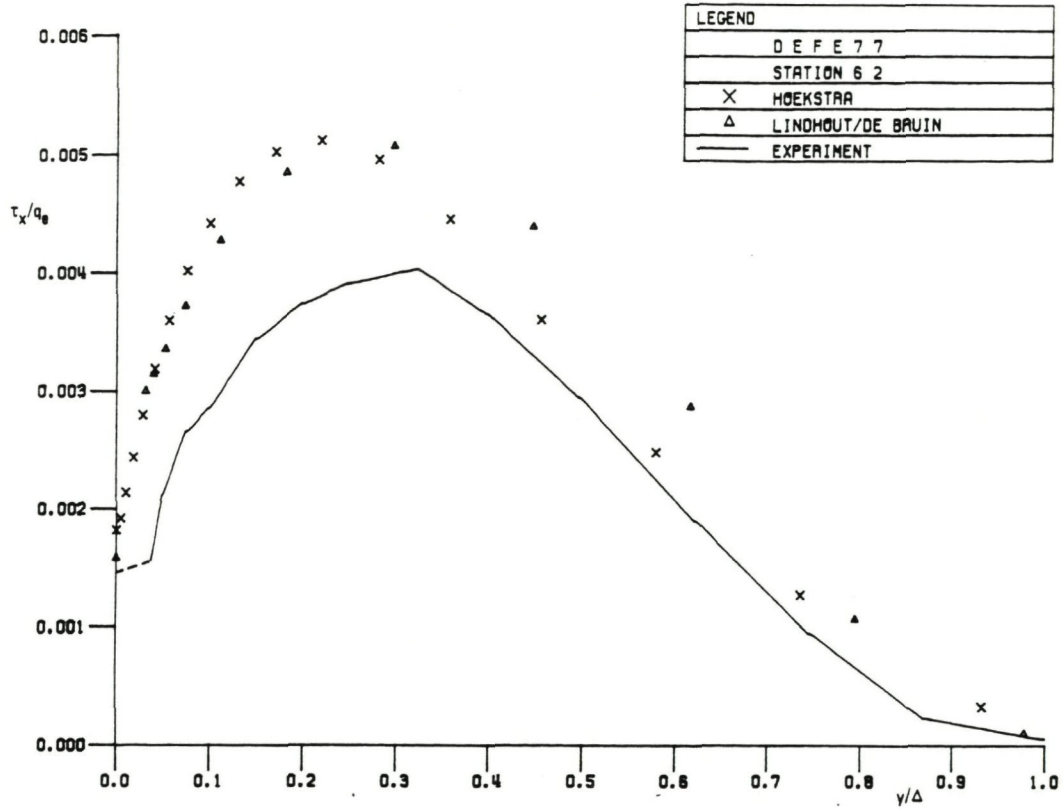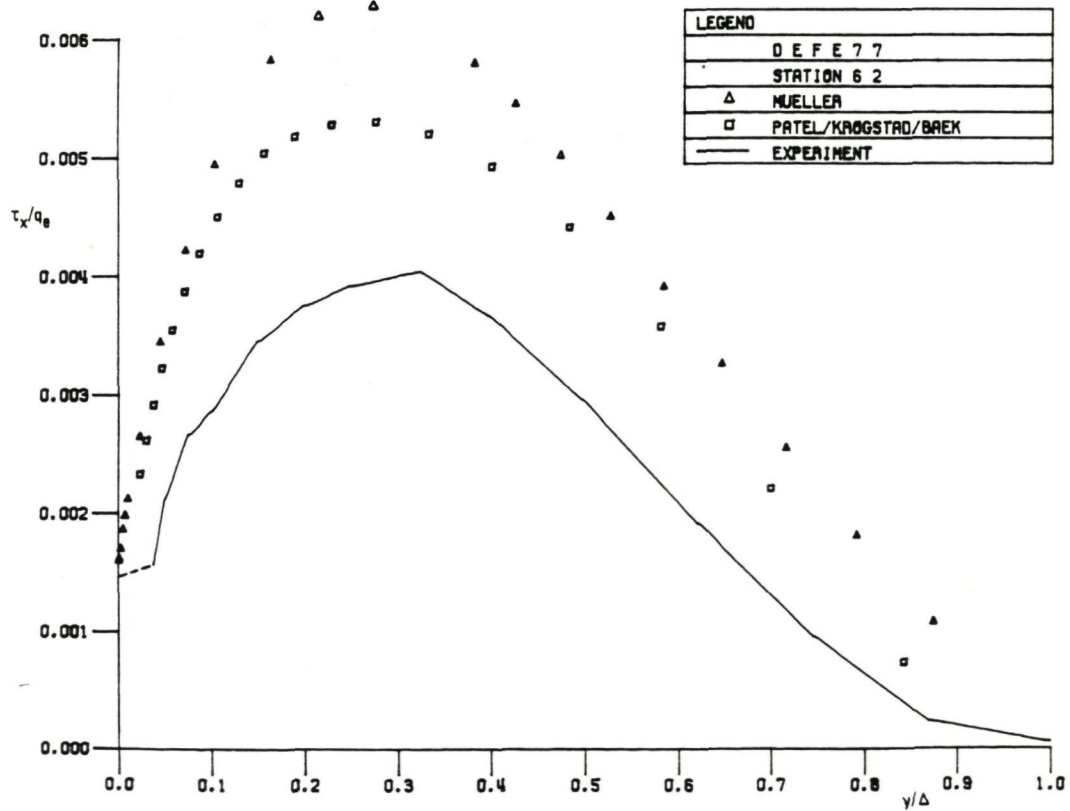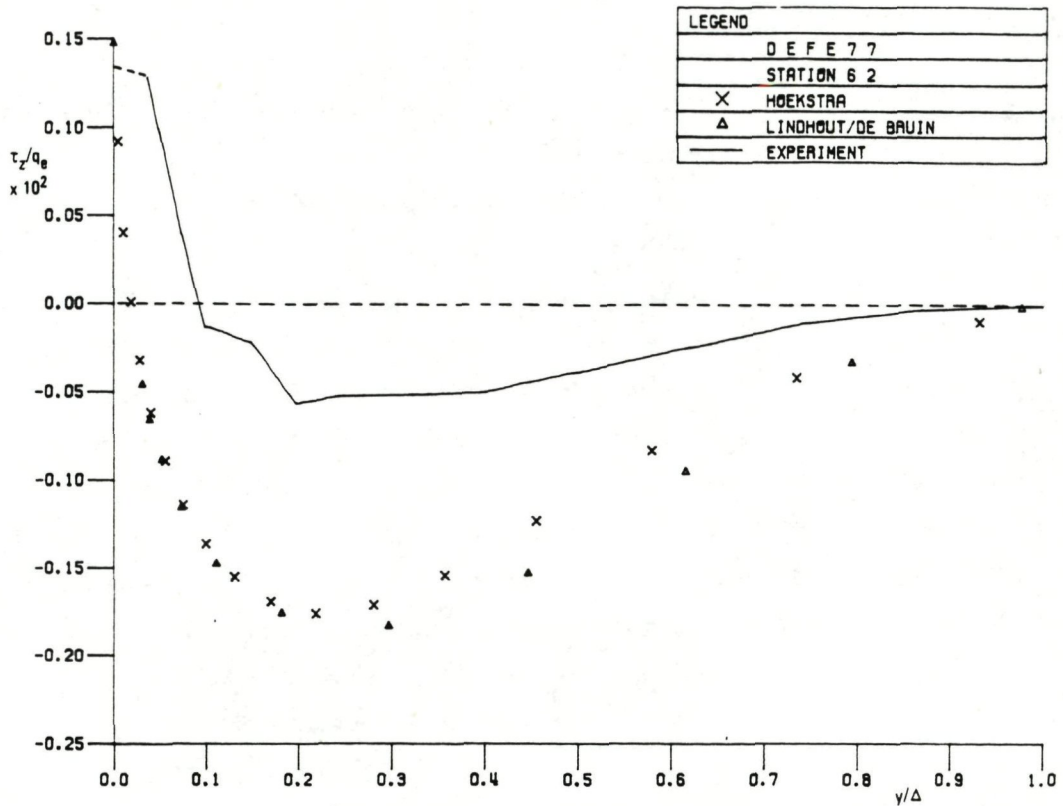(x/L = 0.871) on the external streamline BC

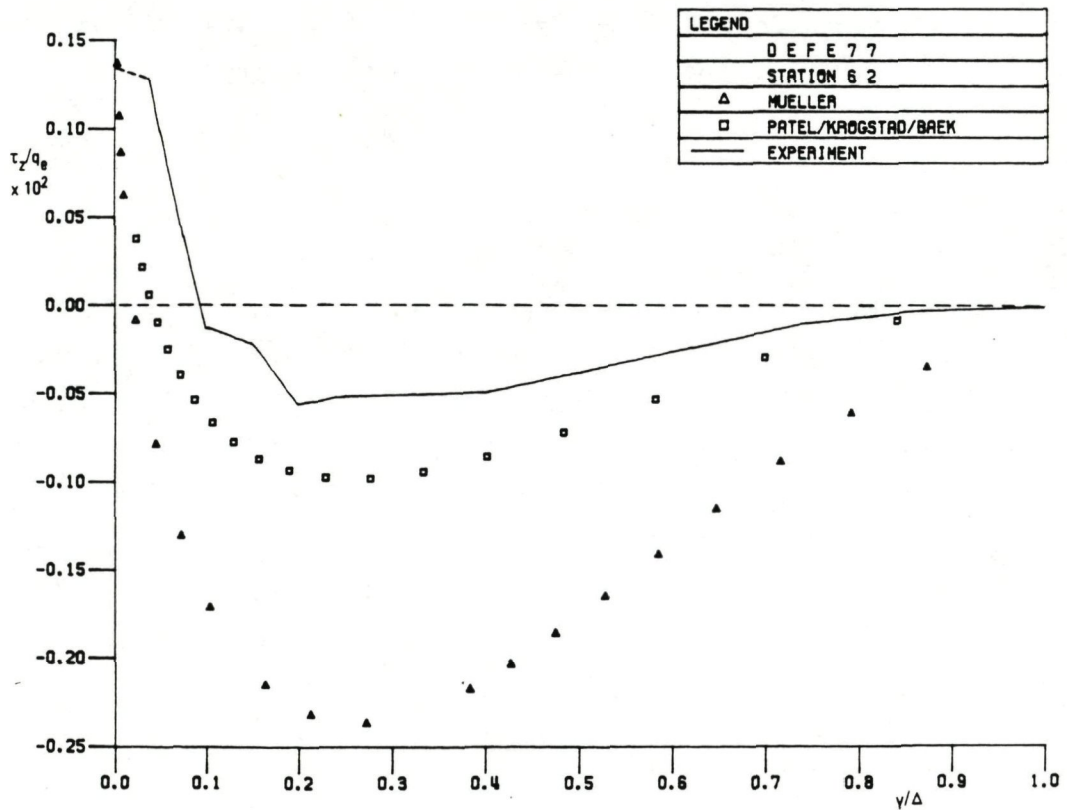Fig. 4.19b   Crosswise shear stresses at station 6, 2
(x/L = 0.871) on the external streamline BC

5   TEST CASE LOHM73

       This test case concerns the three-dimensional turbulent boundary
layer flow which occurs when an initially two-dimensional boundary
layer encounters a local transverse motion of the bounding surface.
The interesting feature of the flow is that the three-dimensionality
is created here solely by the transverse shear forces. Such a boundary
layer flow may be generated on a cylinder with a stationary front
section and a rotating aft section as sketched in figure 5.1. The
effect of the abrupt transverse surface motion becomes evident first
in a thin layer near the surface, which grows downstream. Far down-
stream an equilibrium three-dimensional boundary layer flow develops.
The flow may be viewed from the stationary coordinate system, as was
done above, or from a rotating coordinate system attached to the
rotating cylinder section. In the latter coordinate system the boundary
layer is initially three-dimensional and decays to a two-dimensional
one far downstream. The flow development in both coordinate systems is
illustrated in the polar plots of figure 5.2.

       This type of flow has been investigated by several workers
(Lohmann 1976, Bissonette & Mellor 1974, Fulachier, Arzoumanian &
Dumas 1982) with globally similar results. The experimental invest-
igation by Lohmann (1976) was selected here as the test case for
several reasons, but mainly because in his experiment the boundary
layer thickness was smallest compared with the cylinder radius. Even
in this case, however, the ratio of the boundary layer thickness to
the cylinder radius is not really small: $\delta/R \cong 0.2$. Consequently it
may be necessary to employ the momentum equations with transverse
curvature terms for the boundary layer computations. This was done by
most of the participants, in many cases also with an allowance for
transverse curvature effects on the turbulence. The surface curvature
will particularly affect the turbulence properties in the boundary
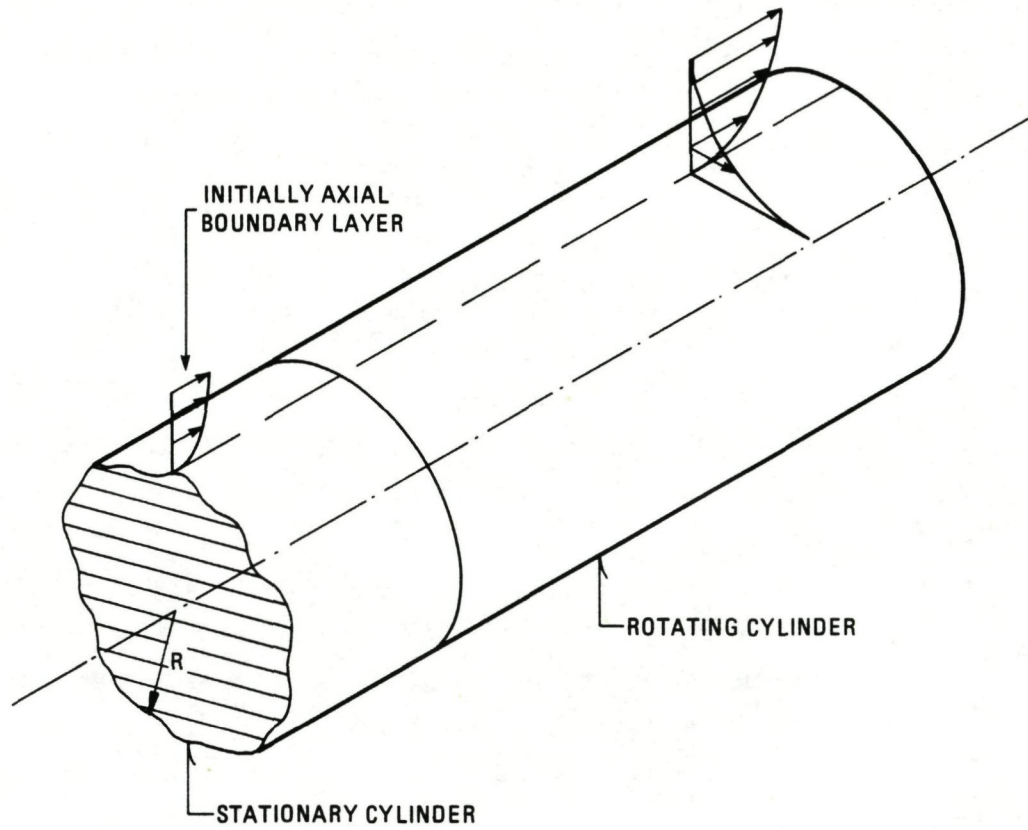layer on the rotating part of the cylinder, however.

Fig. 5.1   LOHM73 test set-up

STATIONARY COORDINATE SYSTEM   ROTATING COORDINATE SYSTEM
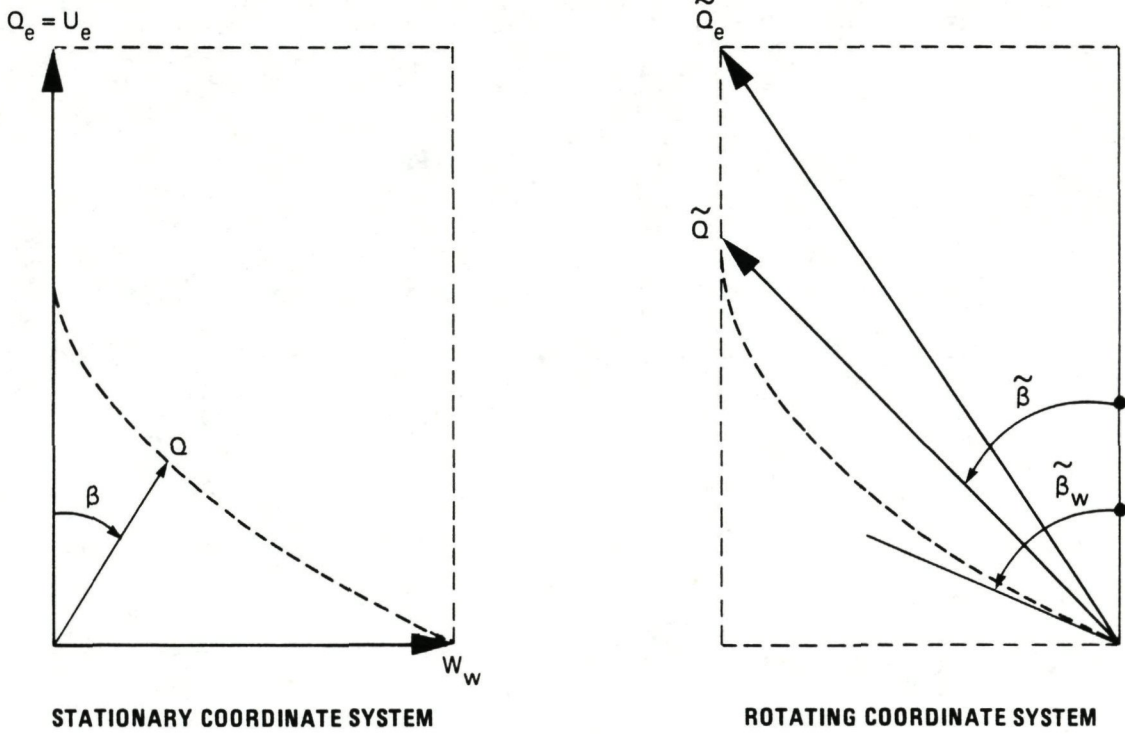
Fig. 5.2   Polar plot in stationary and rotating coordinate system

An equivalent Richardson number (Bradshaw 1973) can be defined to
express the severity of the curvature effects in the rotating part of
the flow:

$$Ri = \frac{2 \frac{W}{r^2} \frac{\partial}{\partial r} (Wr)}{(\partial U/\partial r)^2 + (\partial W/\partial r)^2} \qquad (5.1)$$

Assuming $\partial W/\partial r$ = order (W_w/δ) and U = order (W), one obtains
Ri = order (δ/R). Since $\delta/R \cong 0.2$, the rotation Richardson number is
not small in this flow. No explicit allowance for the effects of
rotation on the turbulence was made, however, in any of the calculation
methods applied to this test case. Only the PATEL/KROGSTAD/BAEK method
was applied with a correction to the eddy viscosity in extra calculations,
which will be discussed at the end of this chapter. The effects of
rotation on the turbulence may have been taken into account implicitly
in the calculation methods which employ transport equations for the
Reynolds stresses.

The boundary layer was tripped to turbulence by a strip of sand-
paper far upstream on the stationary part of the cylinder. In the
measurement range the Reynolds number based on the boundary layer
momentum thickness varies between R_Θ = 2500 and 3500. Low Reynolds
number effects may have played some role in this flow. In the majority
of the calculation methods applied, an allowance for low Reynolds
number effects was included in the turbulence model.

Experimental data were obtained at two rotational speeds. Here
only the case with a surface to free-stream velocity ratio W_w/U_e = 1.411
is considered.

At the transition from the stationary front section to the rotating
aft section of the cylinder a small axial gap existed in the experiment.

In the calculations a discontinuous change of the surface boundary
condition at the transition had to be assumed. Significant changes in
the boundary layer flow occur just downstream of this discontinuity.
It was not possible to cope with the discontinuity correctly. However,
Navier-Stokes solutions obtained for comparable conditions, such as
the flow near a plate leading edge, show that the effects may be
expected to remain local (Van de Vooren & Dijkstra 1970). In figure
5.3 the results of two calculation methods, which use similar turbulence
models, are compared in a small region downstream of the discontinuity.
In the calculations of LINDHOUT/DE BRUIN the wall flow angle, β_w, is
seen to drop from 90° to less than 70° over a very short distance:
$\Delta x < 0.5 L \cong 0.5 \delta$. These calculations have been included in this
graph, because they were carried out with different step sizes,
varying between $\Delta x/L = 10^{-4}$ to 10^{-1}. The calculation results are seen
to converge well. The results of CEBECI/HUANG, also included in the
graph, are specially valuable, since in this calculation the dis-
continuous change of the boundary condition at $x = 0$ was smoothed. It
was assumed that between $-0.5 < x/L < 0$, the transverse surface
velocity $W_w = W_{wo} \sin \{\pi (x/L - 0.5)\}$. Figure 5.3 shows that at some
distance downstream of the discontinuity the agreement between both
calculations is reasonable, especially when noting that the smoothing
was applied upstream of the discontinuity implying an early start of
the transverse surface velocity. On the whole it seems that the
discontinuity does not play an essential role.

After the substantial changes in the wall region of the boundary
layer immediately downstream of the discontinuity, the further changes
take place only gradually. As will appear later, the measurement
region in the experiment is not large enough for the boundary layer to
reach equilibrium. In fact, at the most downstream station, the outer
region of the boundary layer is still unaffected by the change in the
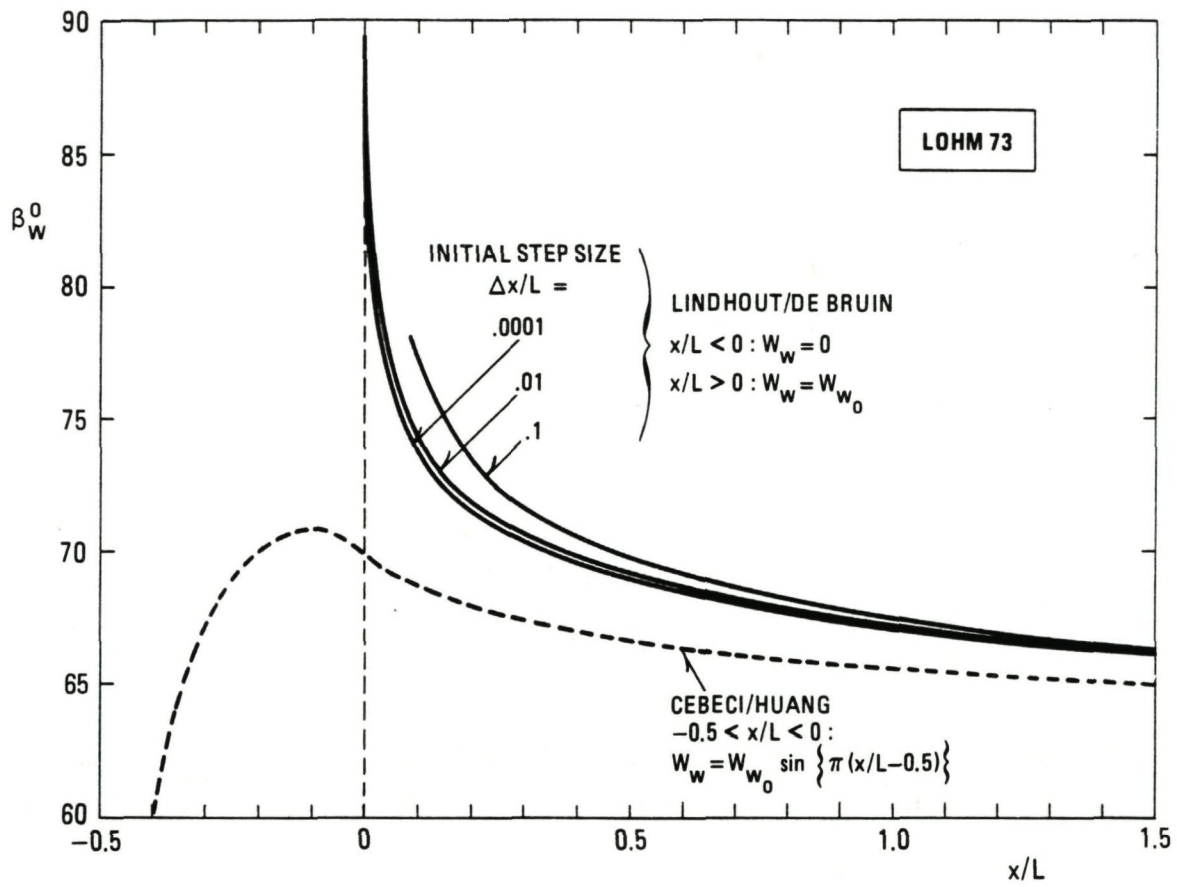surface boundary condition.

Fig. 5.3 Calculated wall flow angle variations near x = 0

Eight calculation methods were applied to this test case. In five methods (CEBECI/HUANG, HOEKSTRA, LINDHOUT/DE BRUIN, PATEL/KROGSTAD/BAEK, PIERCE/AQUILAR/TREVENTI) algebraic eddy viscosity models were used. The method of GALMES/LAKSHMINARAYANA employed the k-ε turbulence model with no wall functions. The method of GIBSON/YOUNIS is the most complex, using seven transport equations for turbulence quantities, but with wall functions to describe the flow in the wall region. One integral method, COUSTEIX/BERRUE, was applied to this test case. In most calculation methods an isotropic eddy viscosity was assumed. The stress transport model of GIBSON/YOUNIS is an exception and also the integral method of COUSTEIX/BERRUE. In the latter method an anisotropy factor, defined with respect to the local flow direction, is introduced for the eddy viscosity. The effect of the anisotropy enters through the corresponding integral relations employed for this method.

As mentioned in the beginning of this section (see also figure 5.2) the flow may be viewed from a coordinate system attached to the fixed part of the cylinder or from a coordinate system attached to the rotating part of the cylinder. It should be noted that the anisotropy factor in the method of COUSTEIX/BERRUE takes on different values, depending on what coordinate system is used, and that several of the other turbulence models are not invariant to change in coordinate system. The fixed coordinate system was used in all calculations with the exception of those of LINDHOUT/ DE BRUIN. The boundary layer thickness parameter δ_{95}, which occurs in the latter method, is affected by the choice of the moving coordinate system for the calculations. This thickness parameter, which is defined as the wall distance with a velocity magnitude defect of 5%, is more than 40% smaller than in the fixed coordinate system.

The experimental data were employed earlier as a test case by Higuchi and Rubesin (1979), who used three different turbulence models. The results of these calculations will not be considered in

the present comparison, as they were not carried out for precisely the same boundary conditions. However the results of these authors agree broadly with the calculation results to be discussed below.

Before comparing the calculated and measured data, the accuracy of the data should be considered. The computational uncertainties near the discontinuous change of the surface boundary condition have already been discussed earlier. Most participants investigated the effect of grid size variations on their calculation results. As appears from table 5.1, numerical convergence seems to have been achieved to a satisfactory degree. The experimental accuracy estimates are given in Appendix B.

Table 5.1 Results of numerical accuracy studies for LOHM73 test case

Stepsize variation

results submitted	stepsize factor	coordinate direction	station number	effect on calculations
CEBECI/HUANG	2	x, y	5	ΔC_f = .2%
COUSTEIX/BERRUE	2	x		$\Delta \beta_w$ < .01°
GIBSON/YOUNIS	$\sim$ 2	x, y		ΔC_f < .2%
PATEL/KROGSTAD BAEK	1.5	x	5	ΔC_f = .5%

Figure 5.4 shows the development of the Reynolds number, R_Θ, which is directly proportional to the streamwise boundary layer momentum thickness, Θ, as the external velocity is constant in this test case. The momentum thickness growth is small over the measurement range. The irregularities in the experimental line should probably be attributed mainly to data scatter. Most of the differences in the calculated results apparent in figure 5.4 are due to differences in the assumed initial conditions.

Figure 5.5 shows the computed and measured variation of the wall flow angle, β_w, in the fixed coordinate system. At the front end of the rotating cylinder, at $x = 0^+$, the wall flow angle should be $\beta_w = 90°$. This condition can generally not be satisfied by integral methods, because of the limited possibilities of the velocity profile families used in these methods. The integral method of COUSTEIX/BERRUE gives $\beta_w \cong 63°$ instead of $90°$. Nor does the field method of GIBSON/ YOUNIS produce the right wall flow angle at $x = 0^+$. These calculations give an angle as low as $\beta_w \cong 11°$ there, probably because of the application of simple two-dimensional wall functions, while in the wall region the actual flow near $x = 0^+$ is dominated by the three-dimensionality. Although a very advanced turbulence model is used for the outer region of the boundary layer in this method, the results obtained are not satisfactory near $x = 0^+$ due to the treatment of the inner region. It is not known why $\beta_w = 76°$ at $x = 0^+$ in the calculations of PATEL/KROGSTAD/BAEK. CEBECI/HUANG have $\beta_w = 69°$ at $x = 0$, caused by smoothing the discontinuous change in surface boundary condition.

Considering the differences in wall flow angle at $x = 0^+$ in the various calculations, it is remarkable that the computed wall flow angles further downstream still agree reasonably well, both with each other and with the experimental data, see figure 5.5. This is probably because of the low momentum of the crossflow, which occurs only in a very thin region initially.

Far downstream the wall flow angle should tend to $\beta_w = \tan^{-1}$ $(W_w/U_\infty) = 54.7°$. Here the wall flow angles at the downstream end of the measurement region are still roughly 5° larger. After the drop in wall flow angle immediately downstream of $x = 0^+$, further decrease in wall flow angle takes place only very slowly, both according to the calculations and the experiment.

The skin friction results are plotted in figure 5.6. Boundary layer calculations, as carried out here, should in theory lead to an infinite skin friction immediately downstream of the discontinuous change in surface boundary condition, $C_f = \infty$ at $x = 0^+$. In the calculations a large finite value is found at $x = 0^+$, which decreases fast downstream. Exceptionally the integral method of COUSTEIX/BERRUE does not produce this effect, but there seems to be little detrimental influence on the computed skin friction values further downstream. The methods of CEBECI/HUANG, PIERCE/AQUILAR/TREVENTI, PATEL/KROGSTAD/BAEK and HOEKSTRA employ nearly the same turbulence model (an algebraic eddy viscosity model). The latter two, however, compute comparatively large skin friction values in the upstream part of the measurement region. The reason for the large skin friction values from PATEL/-KROGSTAD/BAEK and HOEKSTRA is not clear.

The velocity profiles in the external streamline direction, in axial direction, at station 3 (x/L = 3.0), station 5 (x/L = 8.0) and station 8 at the end of the measurement range (x/L = 16.0) are plotted in figures 5.7 - 5.9. The results of the integral method are not included in these plots. Generally the agreement between calculations and measurements is reasonably good at station 3, though in the wall region the calculated velocities are somewhat high. At stations 5 and 8 the agreement is less satisfactory. The deviations from the experiment exceed the estimated experimental error (about ± 1%). The results of the method of GIBSON/YOUNIS with a multi-equation transport model of turbulence are an exception with the good prediction of the streamwise velocity profile at station 8. The method of GALMES/ LAKSHMINARAYANA with a k-ε model appears to compute the streamwise velocity consistently high at all three stations.

Figures 5.10 - 5.12 give plots of the crosswise velocity, the velocity component in the circumferential direction. Crosswise velocities occur only in the lower part of the boundary layer. Even at the most downstream position, station 8, a substantial part of the boundary layer is still collateral and apparently not affected by the changed surface boundary condition, which created the flow three-dimensionality. The data comparison shows consistently low values of the crossflow velocities by the method of GALMES/LAKSHMINARAYANA. The other calculations are in better agreement with experiment at station 3 and 5 (experimental accuracy estimate is ± .03 in W/Q_e). At station 8 larger differences can be seen, notably due to high cross-flows in two of the calculations (PATEL/KROGSTAD/BAEK and HOEKSTRA), while two other calculations using nearly the same algebraic eddy viscosity model do not produce this.

The streamwise shear stress results are plotted in figures 5.13 - 5.15. The experimental shear stress data were obtained from hotwire measurements. The accuracy is estimated to be only ± 20%, so that the experimental error band is rather wide here. The streamwise component of the wall shear stress, obtained in the experiment from Clauser plots, is also indicated in the graph and connected to the hot wire data by a dashed line. The calculation results at station 3 are seen to scatter a good deal, but this is mainly due to two of the data sets. The calculations of LINDHOUT/DE BRUIN yield very low shear stress values in the boundary layer outer region. This is very probably connected with the fact that the flow was computed in the moving coordinate system without adapting the turbulence model, as discussed earlier. The calculations of GALMES/LAKSHMINARAYANA exhibit a dis-continuity in the slope of the streamwise shear stress profile at station 3. A more detailed investigation of the data showed that the computed variation of the turbulence energy k in their k-ε model has a similar form. This behaviour possibly originates from the dis-continuity at x = 0, which is only 3 to 4 boundary layer thicknesses

upstream. At station 5 and 8 these effects are no longer visible. The general trend, apparent from the plots, is a tendency to overestimate the streamwise shear stresses somewhat as compared with experiment at station 3 and 5. At station 8 a clear trend is not apparent.

The crosswise shear stress data are plotted in figures 5.16 - 5.18. There are no crosswise shear stresses in the outer part of the boundary layer, as should be expected since the flow is still collateral there (figures 5.10 - 5.12). A clear conclusion can be drawn from the comparison of the calculations and measurements in these figures. At the more downstream stations all calculations are seen to underestimate the crosswise shear stresses substantially. The calculation results obtained with the more advanced turbulence models are no better. As the streamwise stresses are predicted roughly correctly, a non-isotropic eddy viscosity is needed to compute the higher crosswise shear stresses found in this experiment. Note that differences up to a factor of two are found between the crosswise shear stress in the calculations and the experiment.

As discussed earlier, the flow has a two-layer structure with the transverse flow restricted to the inner layer. Once the inner layer has grown beyond a quarter of the boundary layer thickness, the large eddy structure in the outer region of the boundary layer is affected by the transverse flow. According to Lohmann (1976) this leads to a general increase in turbulence level. The associated crosswise shear stress increment, which is found in the experiment, is apparently not reproduced in any of the calculations, see figures 5.17 and 5.18.

Some interesting additional calculations on the curvature effects in this experiment were carried out with the PATEL/KROGSTAD/BAEK method. Using the rotation Richardson number defined in equation (5.1), the following correction was applied on the standard eddy viscosity model:

$$\nu_{t_c} = \nu_t \, (1 - 4.5 \, Ri)^2 \tag{5.2}$$

The calculation results with and without curvature correction are compared in figure 5.19. The curvature correction appears to affect the calculated skin friction values particularly. Although the change in turbulence model has a distinct influence, it cannot be concluded that a better agreement with the experimental data is obtained.

The most important discrepancy which emerges for this test case is the substantial underestimation of the crosswise shear stresses at the more downstream stations by all calculation methods. The crossflow velocity, which is shear stress driven, is not underpredicted, but may become so further downstream beyond the measurement range of the experiment.

Table 5.2   Survey of computed results for the LOHM73 test case

figures	quantities	CEBECI HUANG	COUSTEIX BERRUE	GALMES LAKSHM.	GIBSON YOUNIS	HOEKSTRA	LINDHOUT DE BRUIN	PATEL KROGSTAD BAEK	PIERCE AQUILAR TREVENTI
5.4 -5.6	R_θ, β_w, c_f	X	X	X	X	X	X	X	X
5.7 -5.12	U, W	X		X	X	X	X	X	X
5.13-5.18	τ_x, τ_z	X		X	X	X	X	X	X
5.19	R_θ, β_w, c_f							various versions	
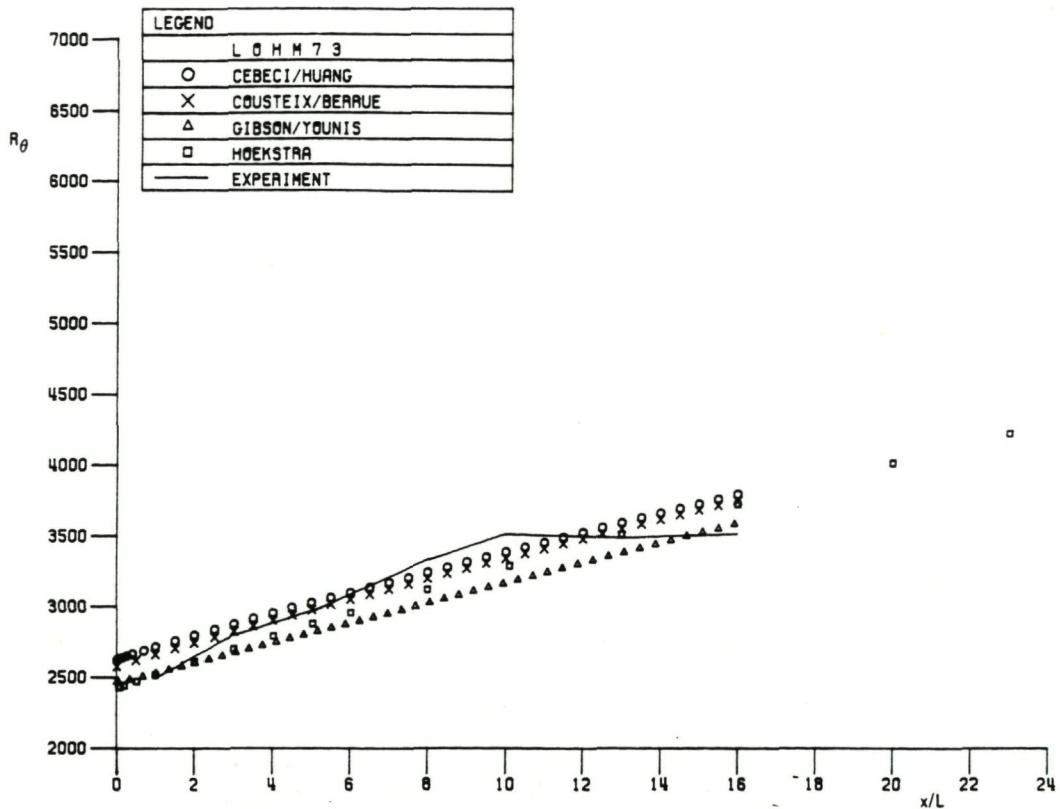
Fig. 5.4a   Variation of momentum thickness Reynolds number
with axial distance
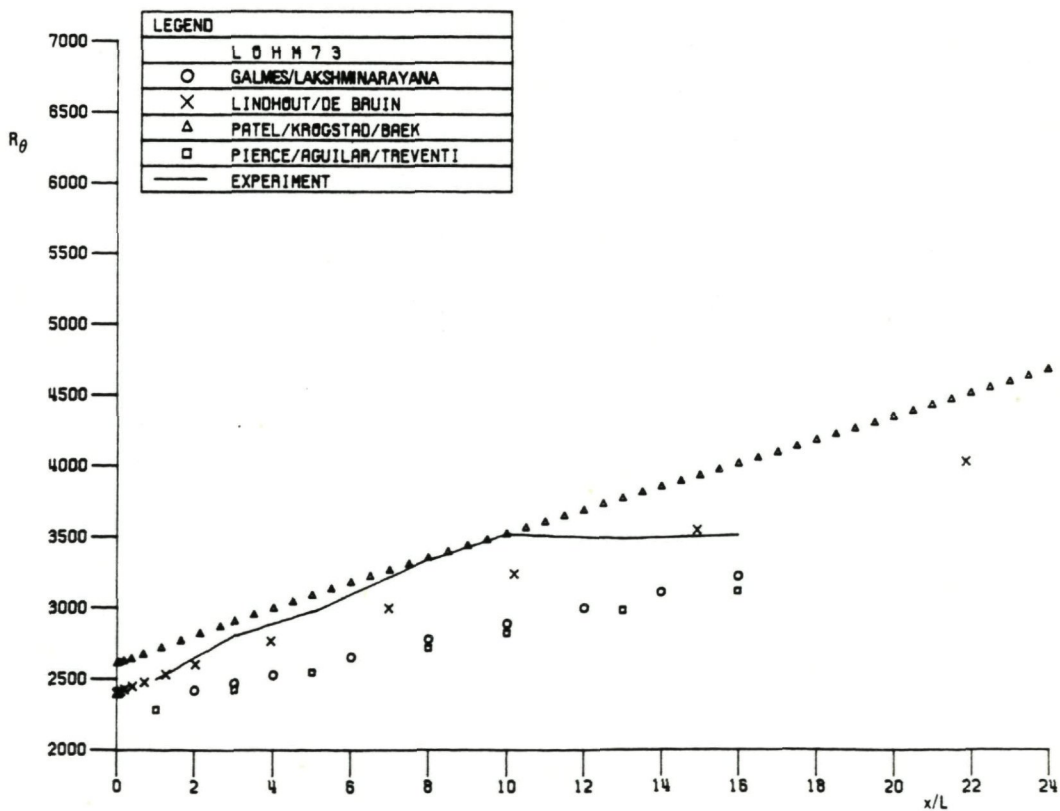
Fig. 5.4b   Variation of momentum thickness Reynolds number
with axial distance
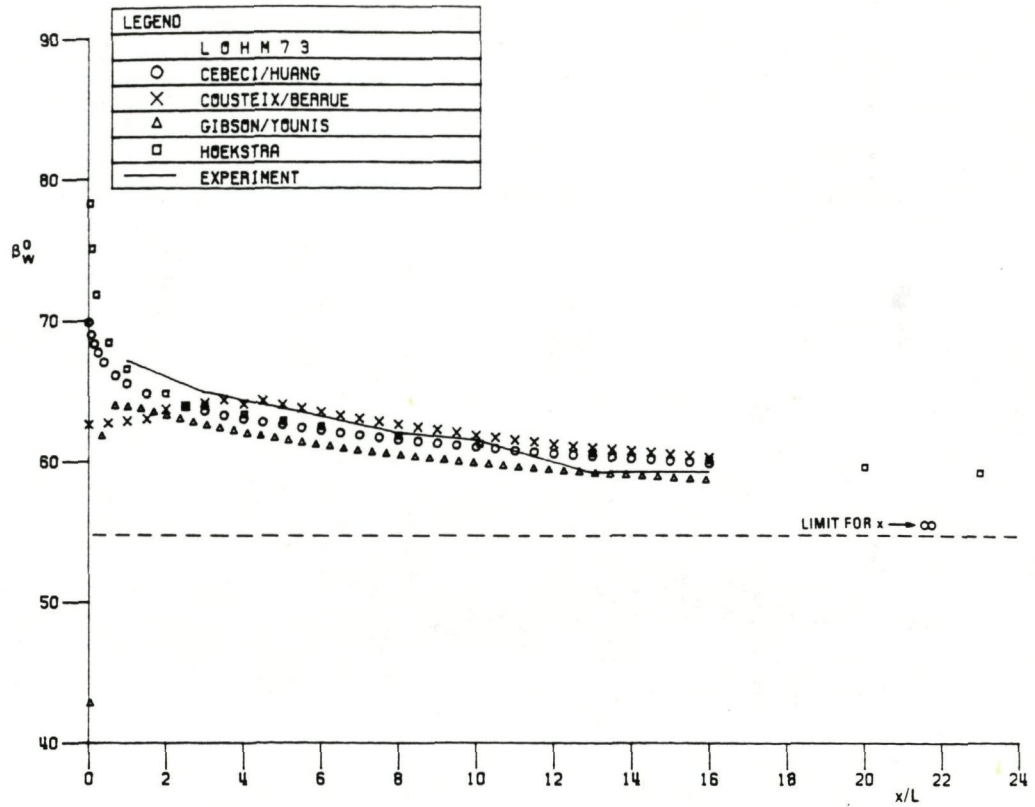
Fig. 5.5a   Variation of wall flow angle with axial distance
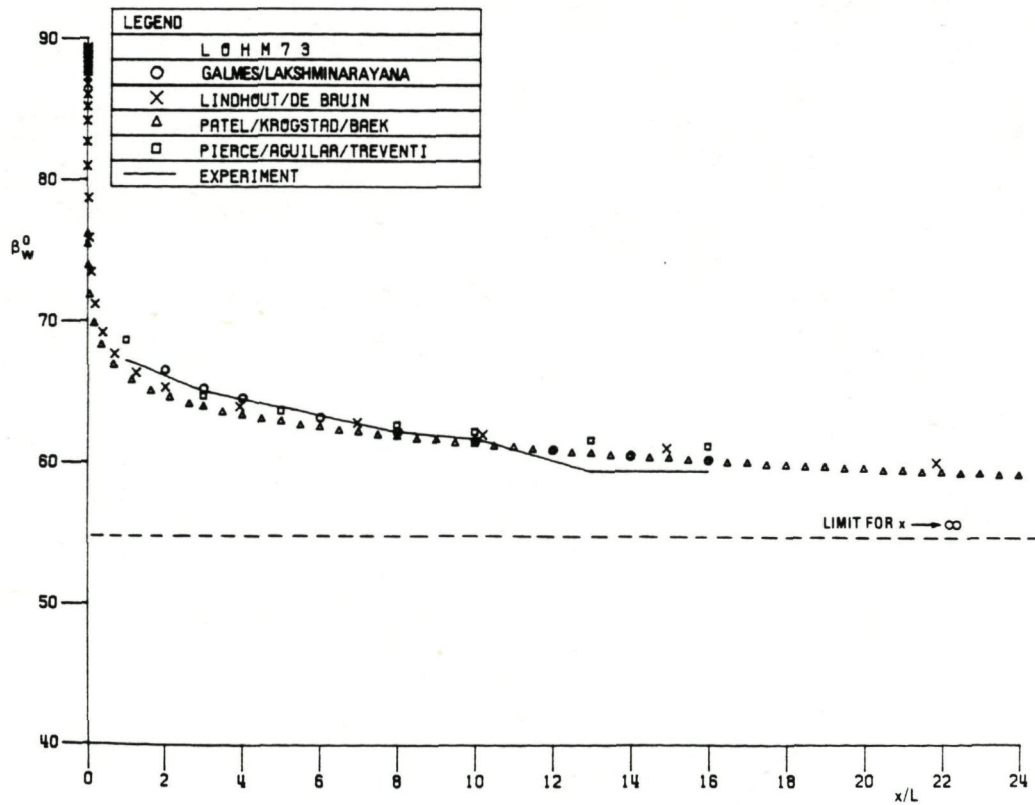
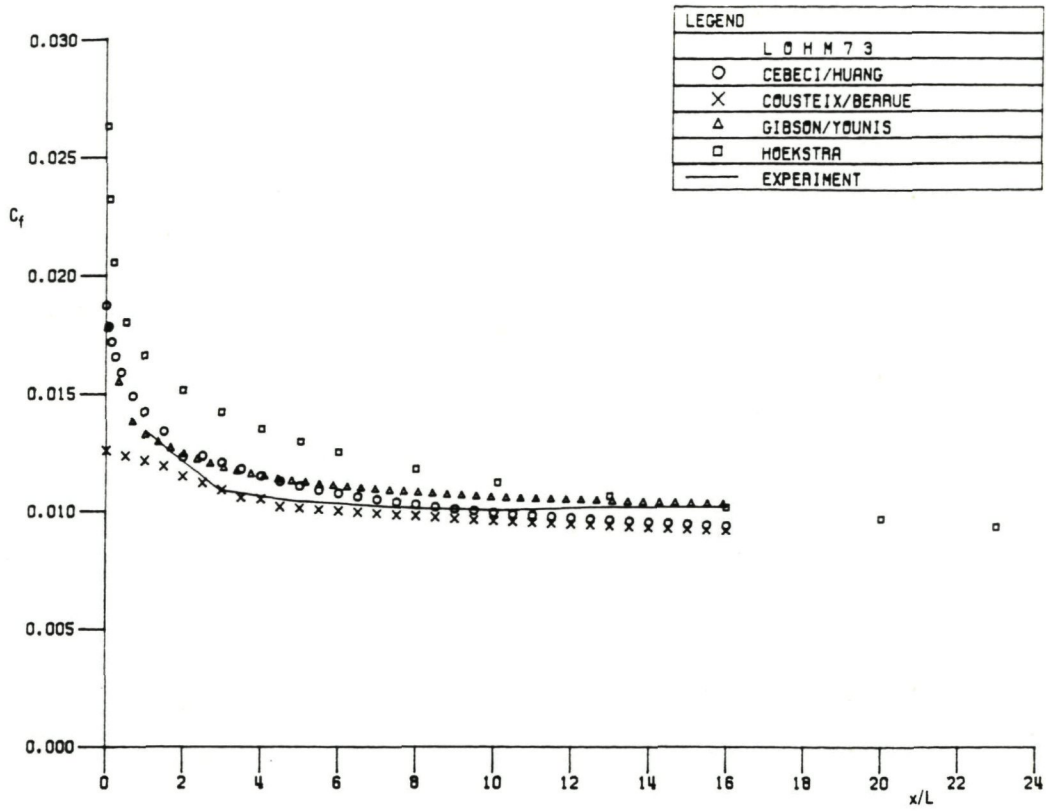Fig. 5.5b   Variation of wall flow angle with axial distance

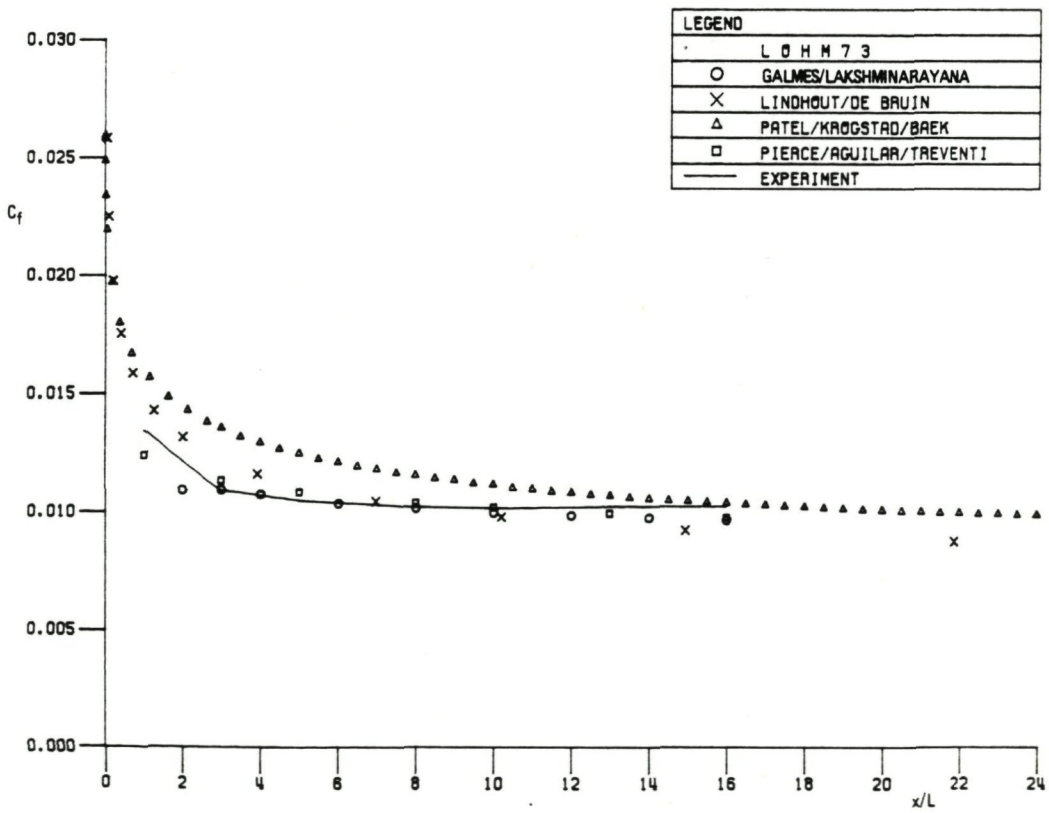Fig. 5.6a   Variation of skin friction with axial distance

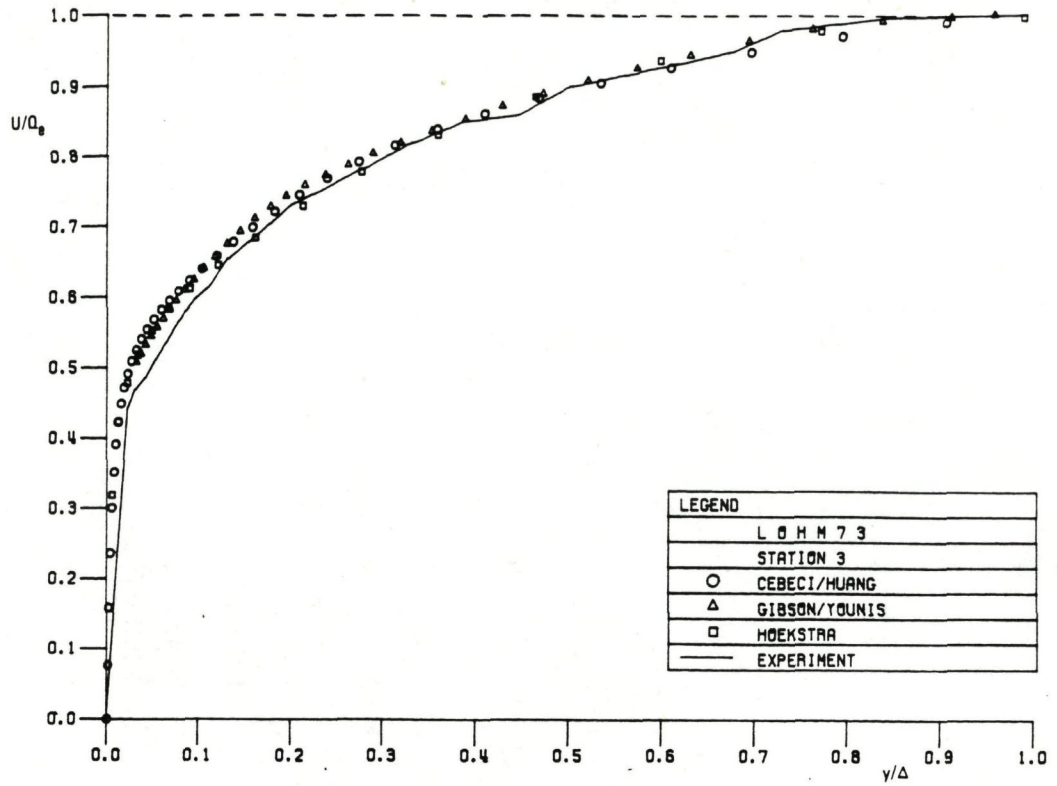Fig. 5.6b   Variation of skin friction with axial distance

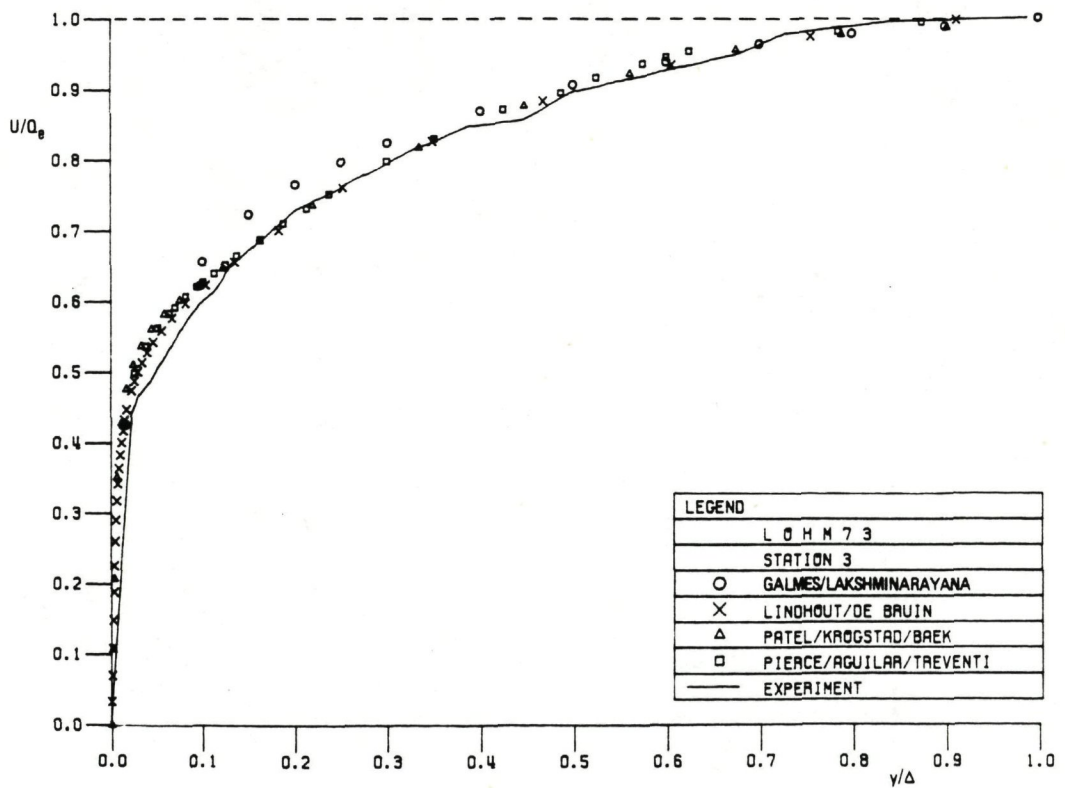Fig. 5.7a   Streamwise velocity profiles at station 3   (x/L = 3.0)

Fig. 5.7b   Streamwise velocity profiles at station 3   (x/L = 3.0)
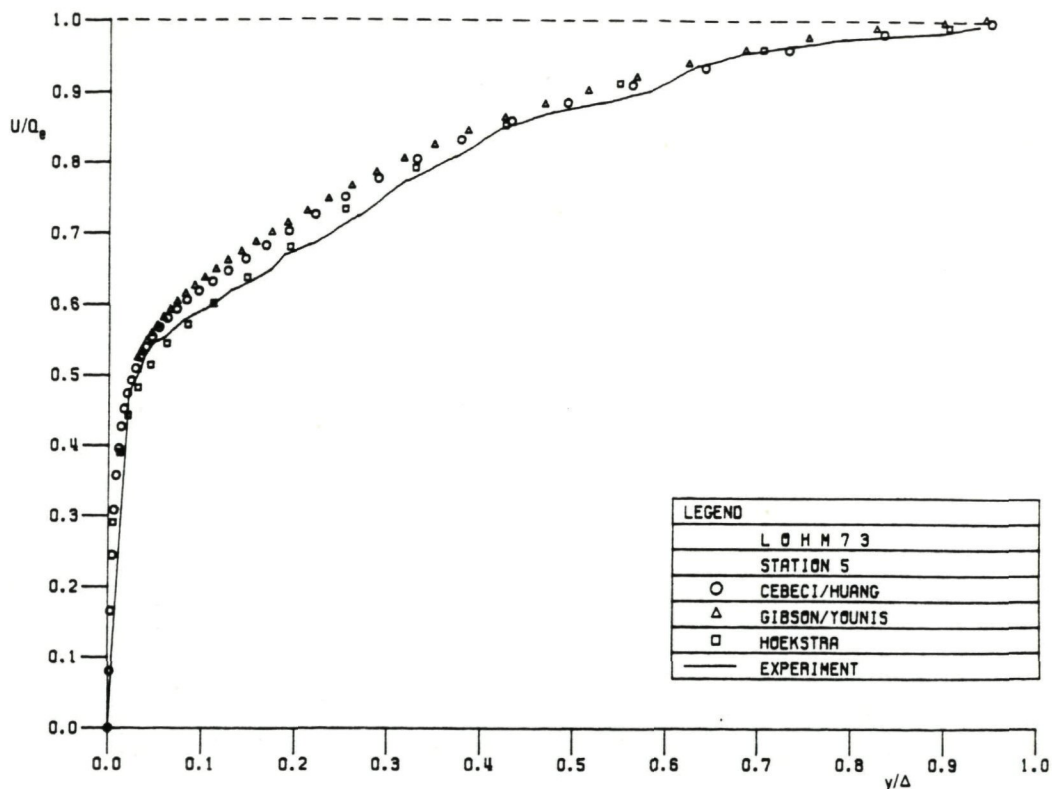
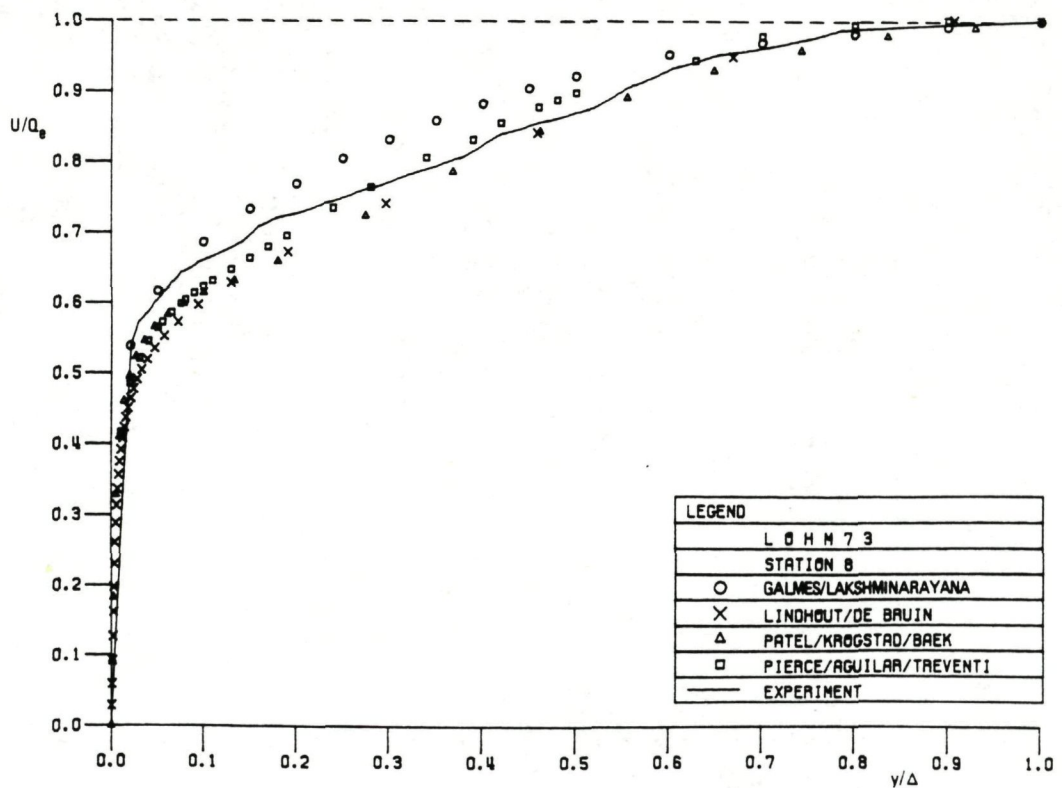Fig. 5.8a   Streamwise velocity profiles at station 5 (x/L = 8.0)
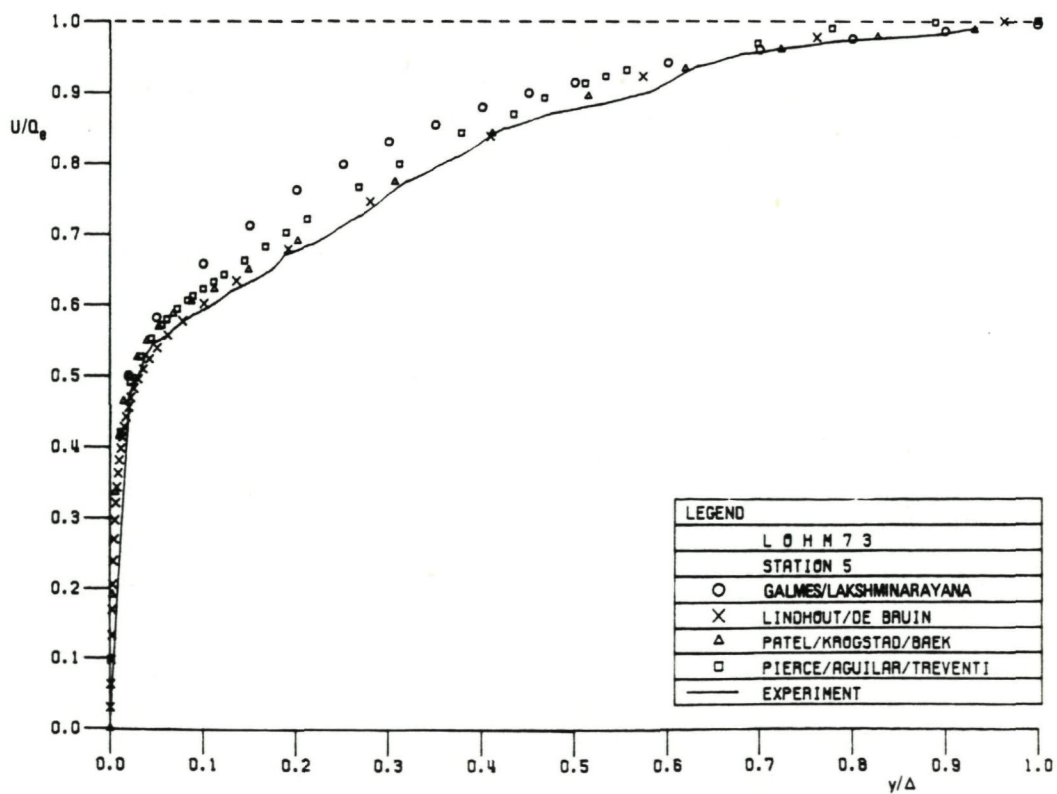
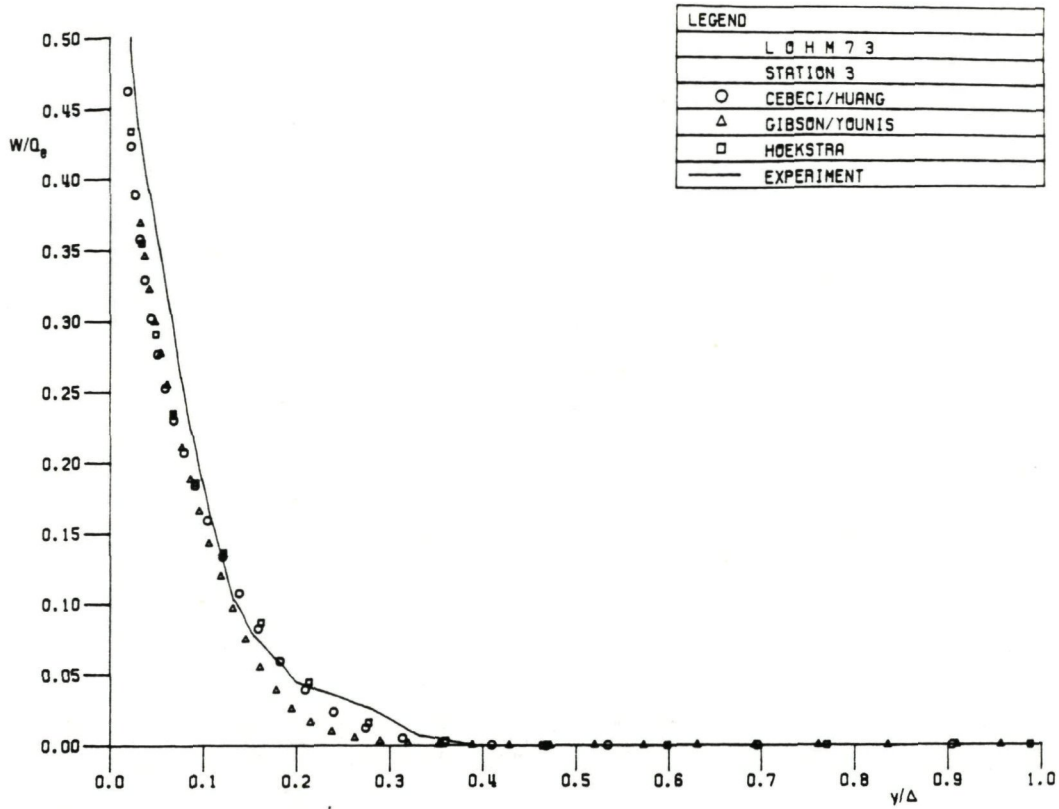Fig. 5.8b   Streamwise velocity profiles at station 5 (x/L = 8.0)
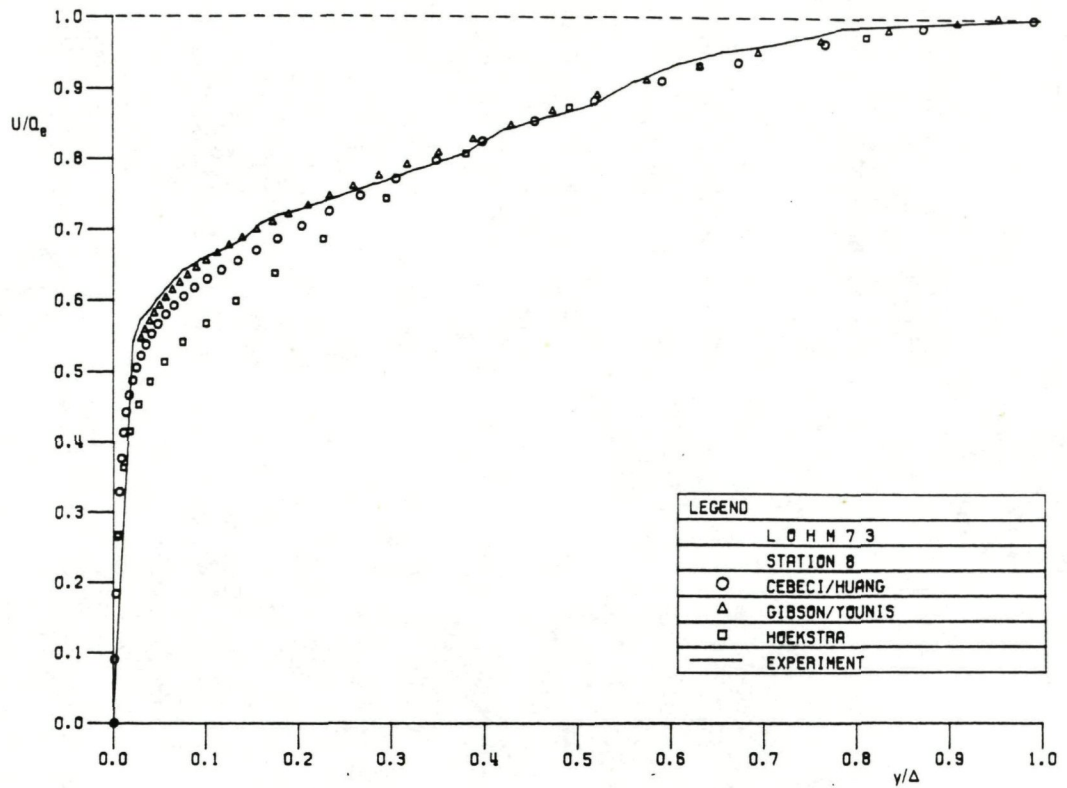
Fig. 5.9a   Streamwise velocity profiles at station 8 (x/L = 16.0)

Fig. 5.9b   Streamwise velocity profiles at station 8 (x/L = 16.0)

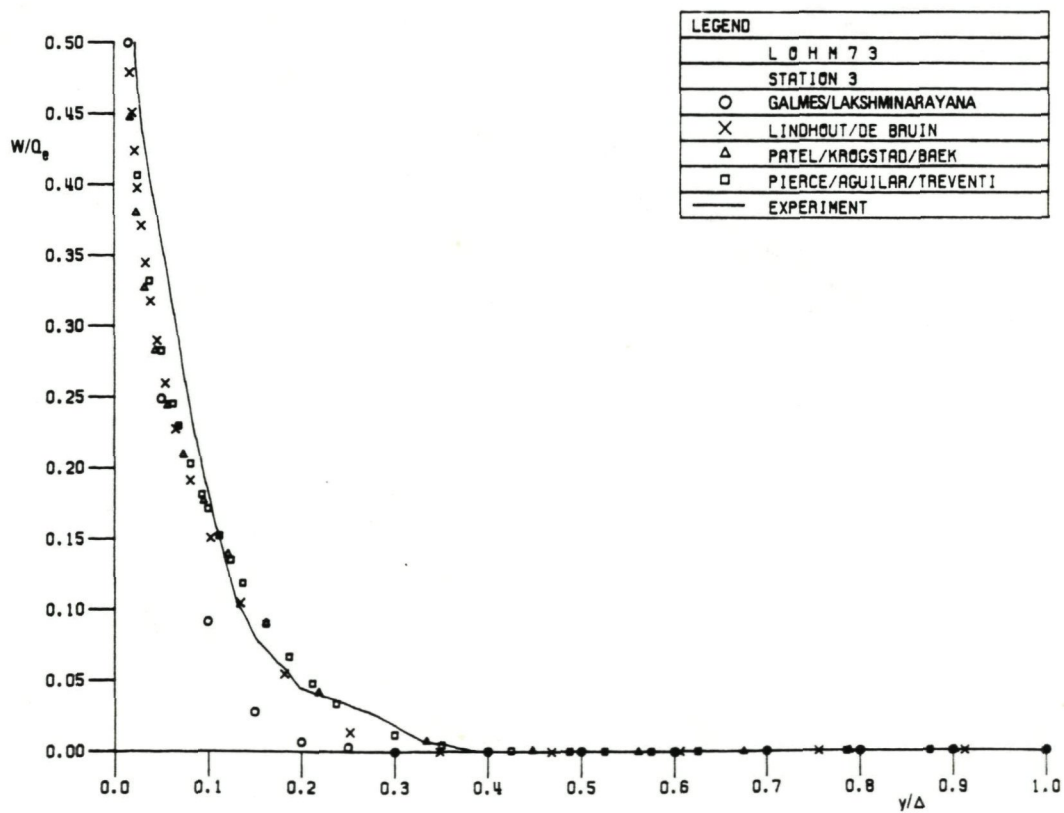Fig. 5.10a   Crosswise velocity profiles at station 3 (x/L = 3.0)

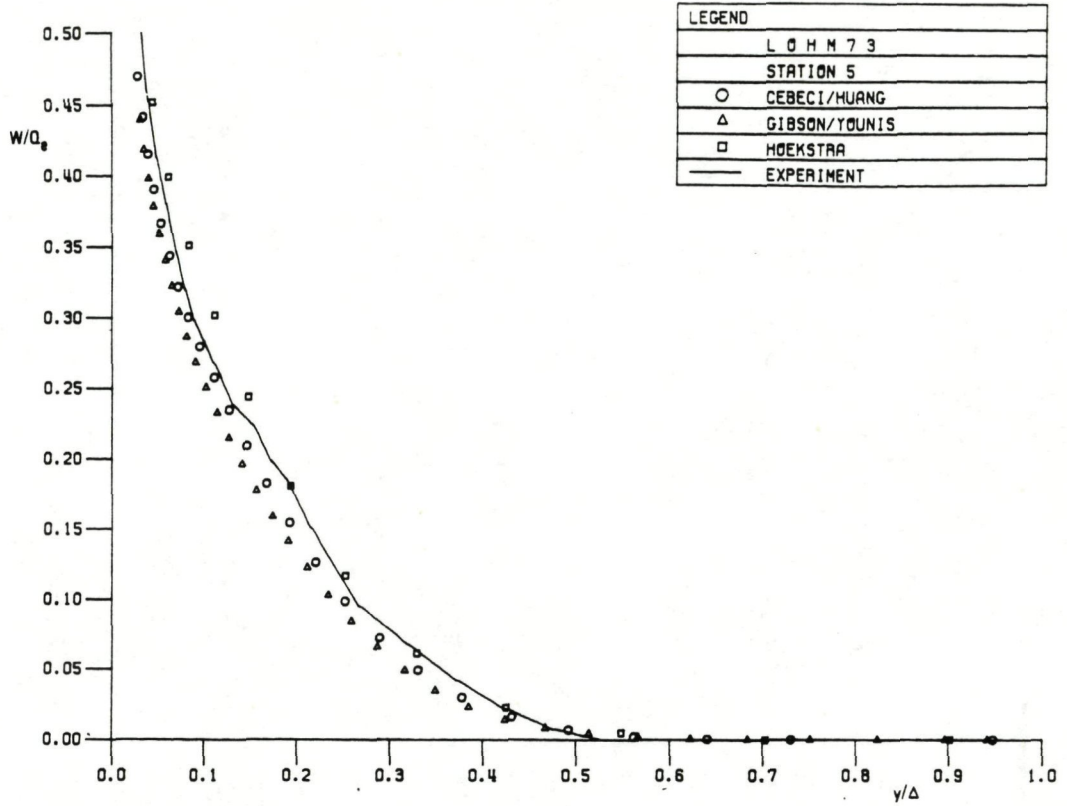Fig. 5.10b   Crosswise velocity profiles at station 3 (x/L = 3.0)

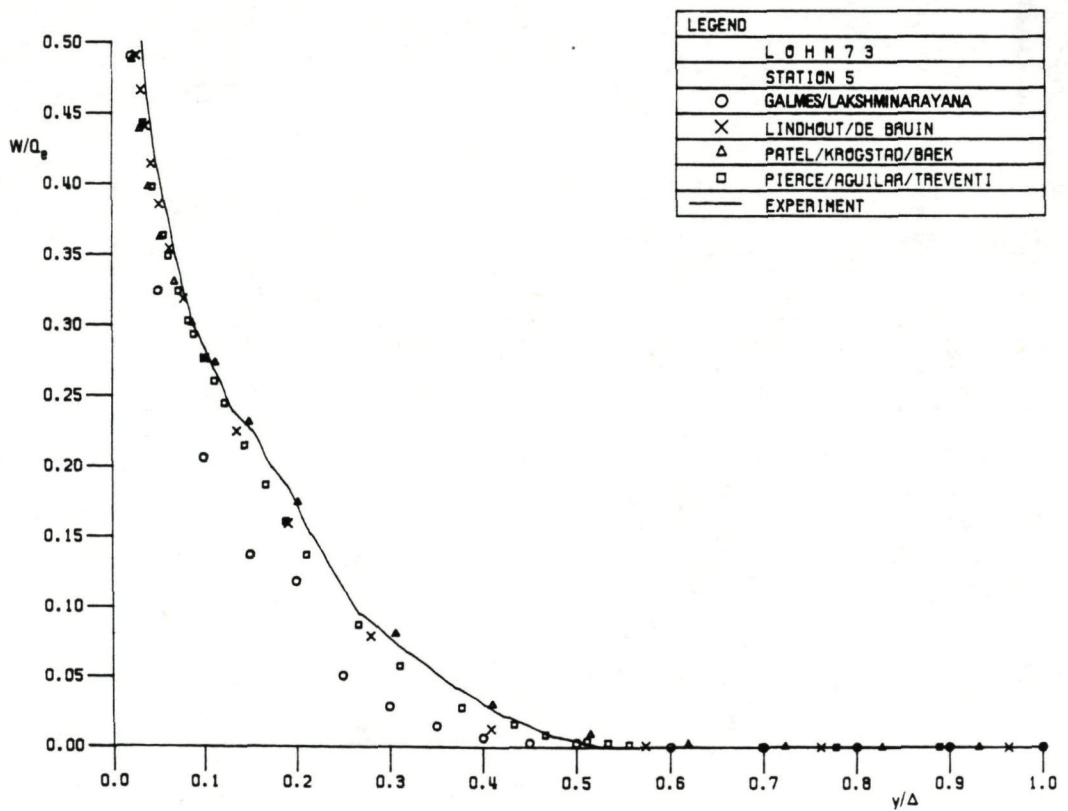Fig. 5.11a Crosswise velocity profiles at station 5 (x/L = 8.0)

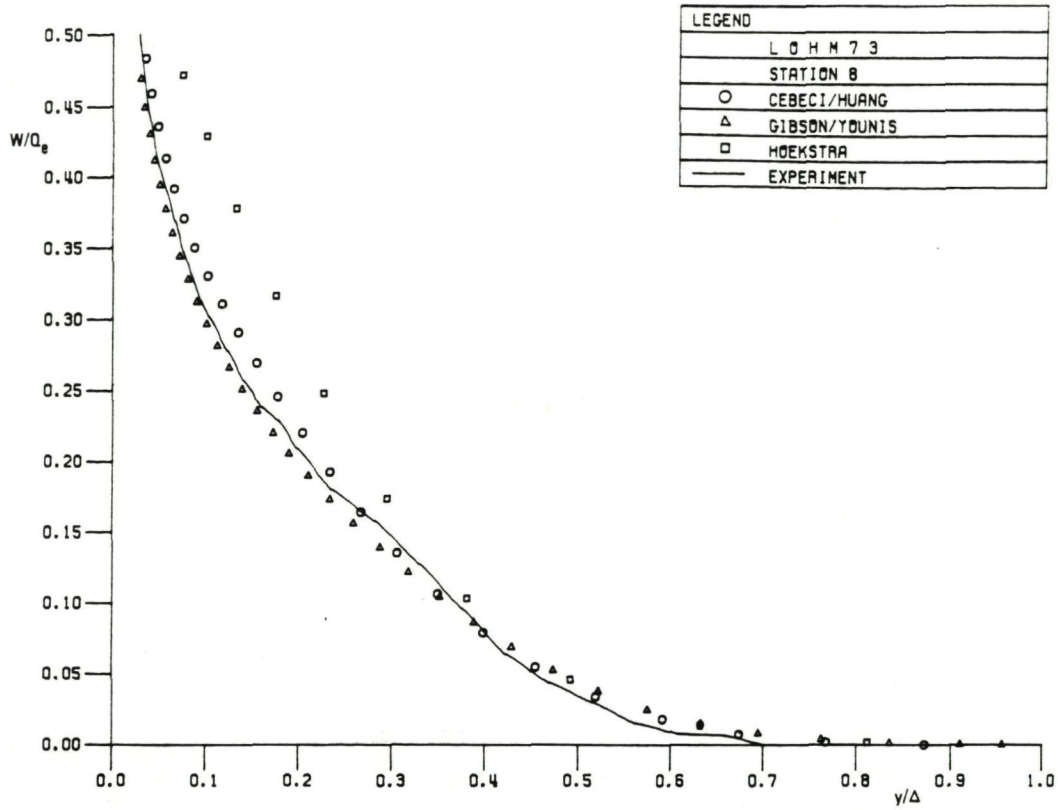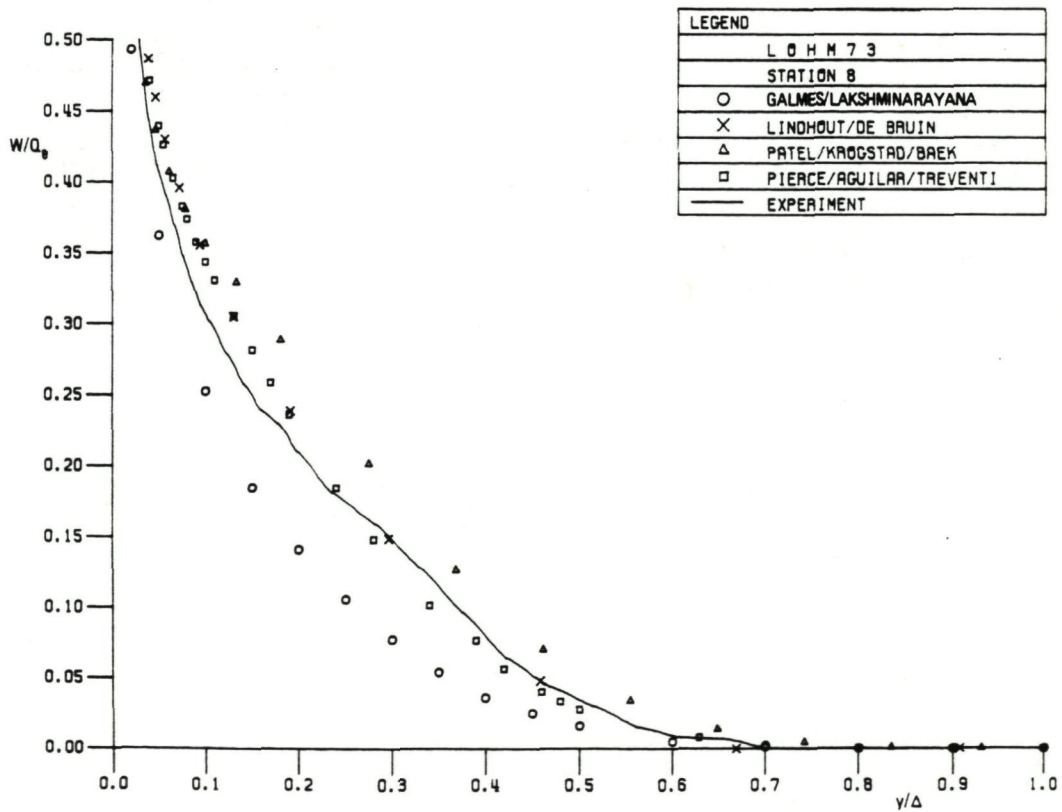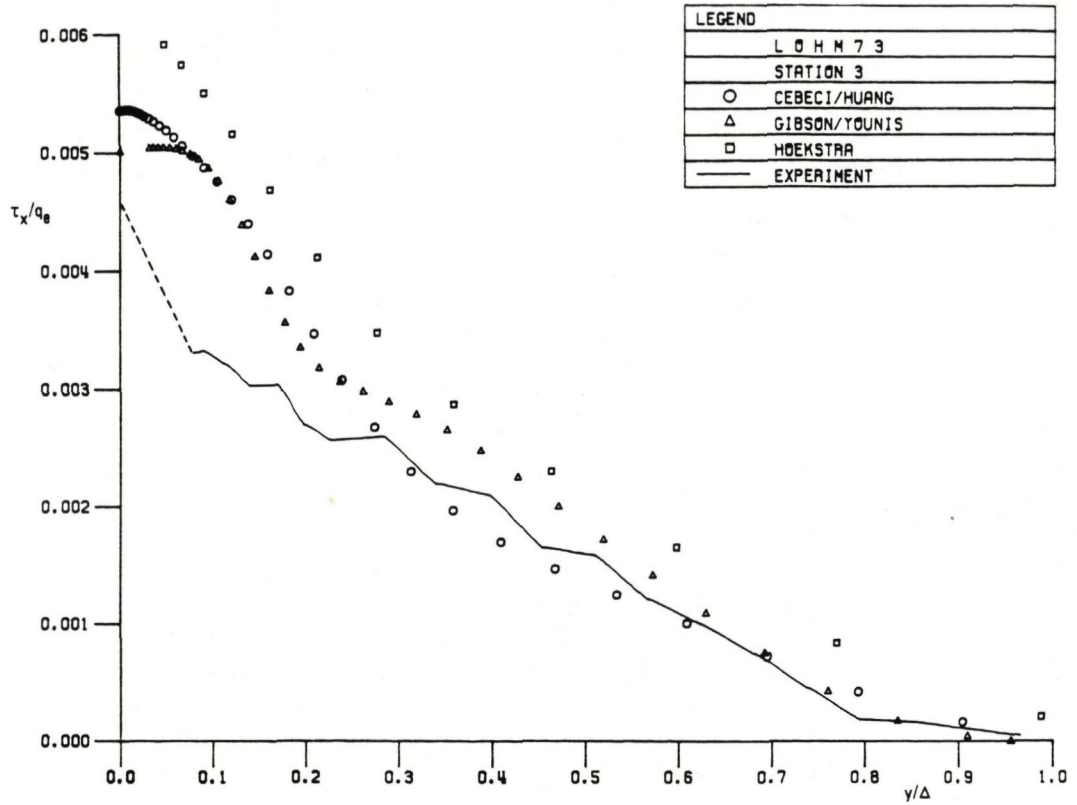Fig. 5.11b Crosswise velocity profiles at station 5 (x/L = 8.0)

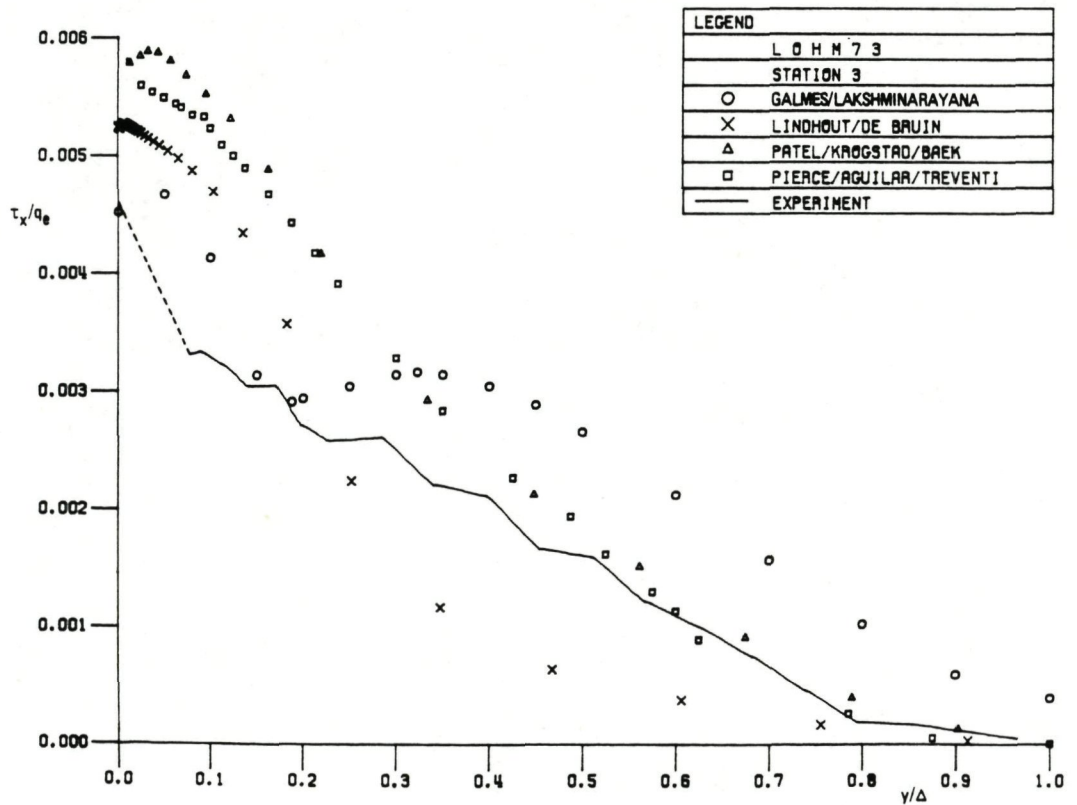Fig. 5.13a   Streamwise shear stresses at station 3 (x/L = 3.0)

Fig. 5.13b   Streamwise shear stresses at station 3 (x/L = 3.0)

Fig. 5.14a   Streamwise shear stresses at station 5 (x/L = 8.0)

Fig. 5.14b   Streamwise shear stresses at station 5 (x/L = 8.0)

Fig. 5.15a   Streamwise shear stresses at station 8 (x/L = 16.0)
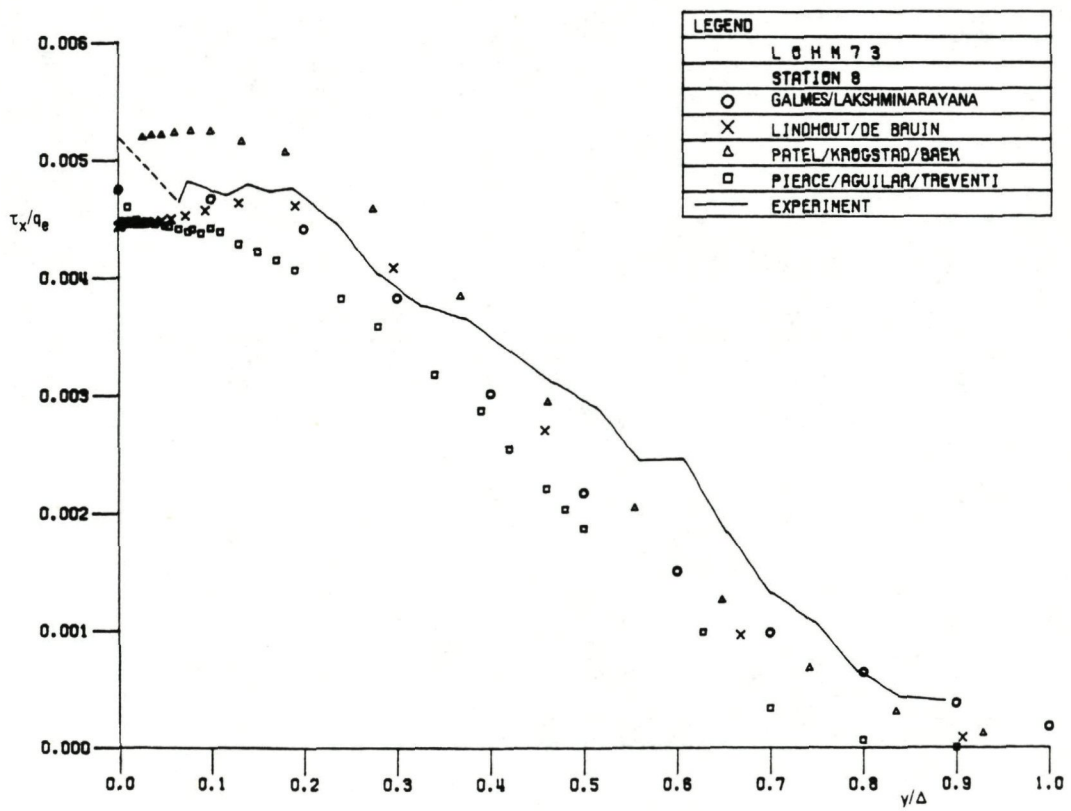
Fig. 5.15b   Streamwise shear stresses at station 8 (x/L = 16.0)
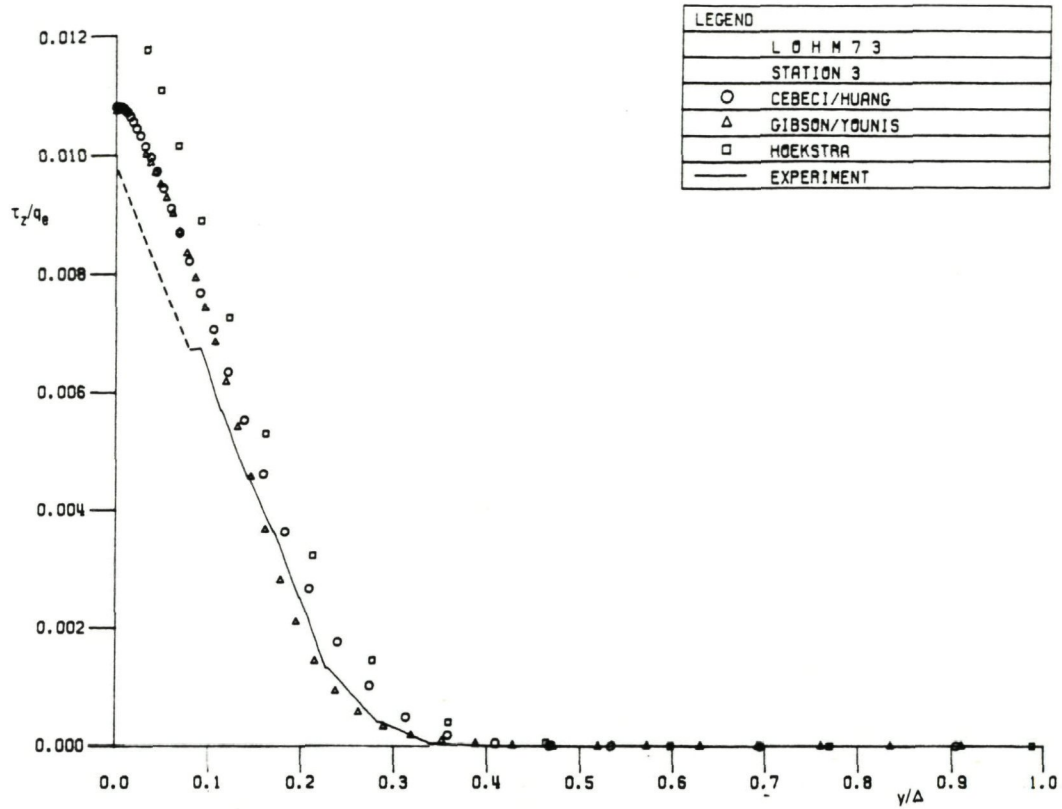
Fig. 5.16a   Crosswise shear stresses at station 3 (x/L = 3.0)
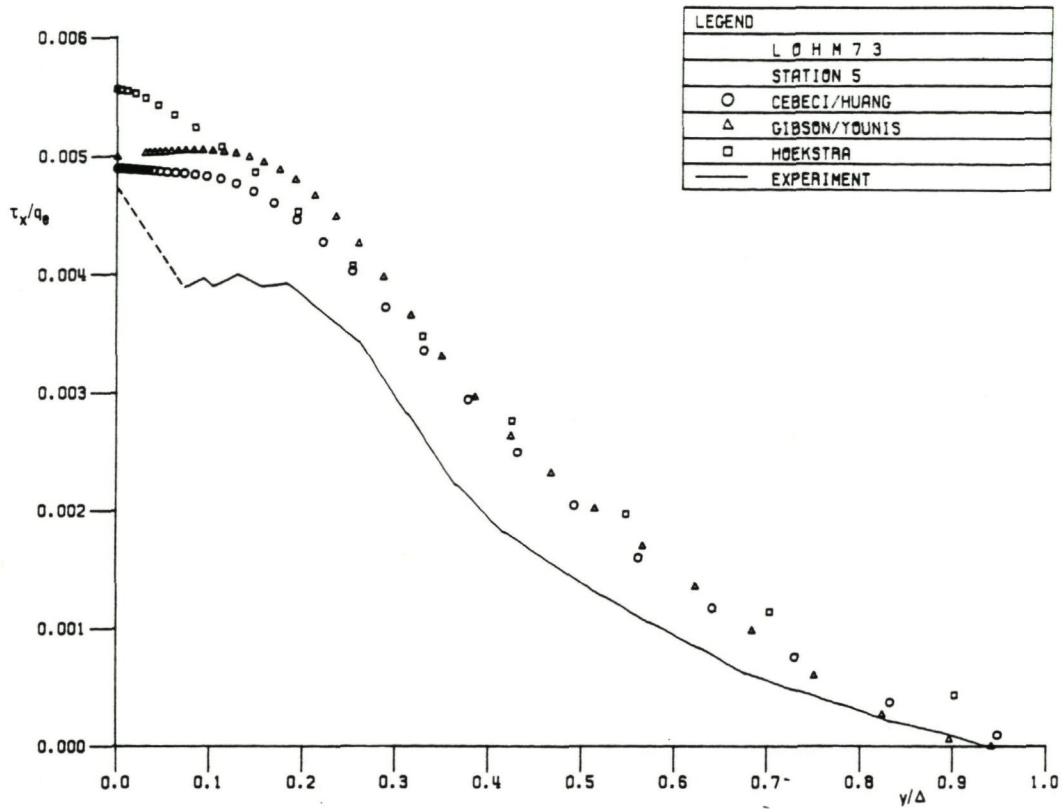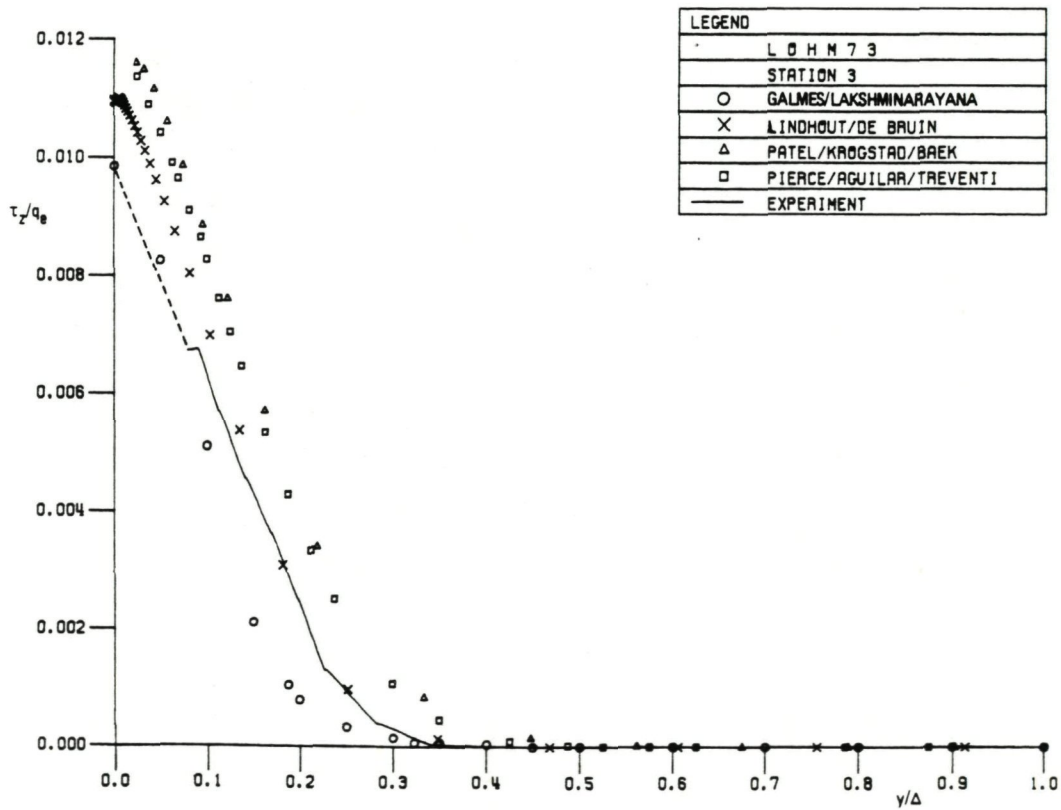

Fig. 5.16b   Crosswise shear stresses at station 3 (x/L = 3.0)
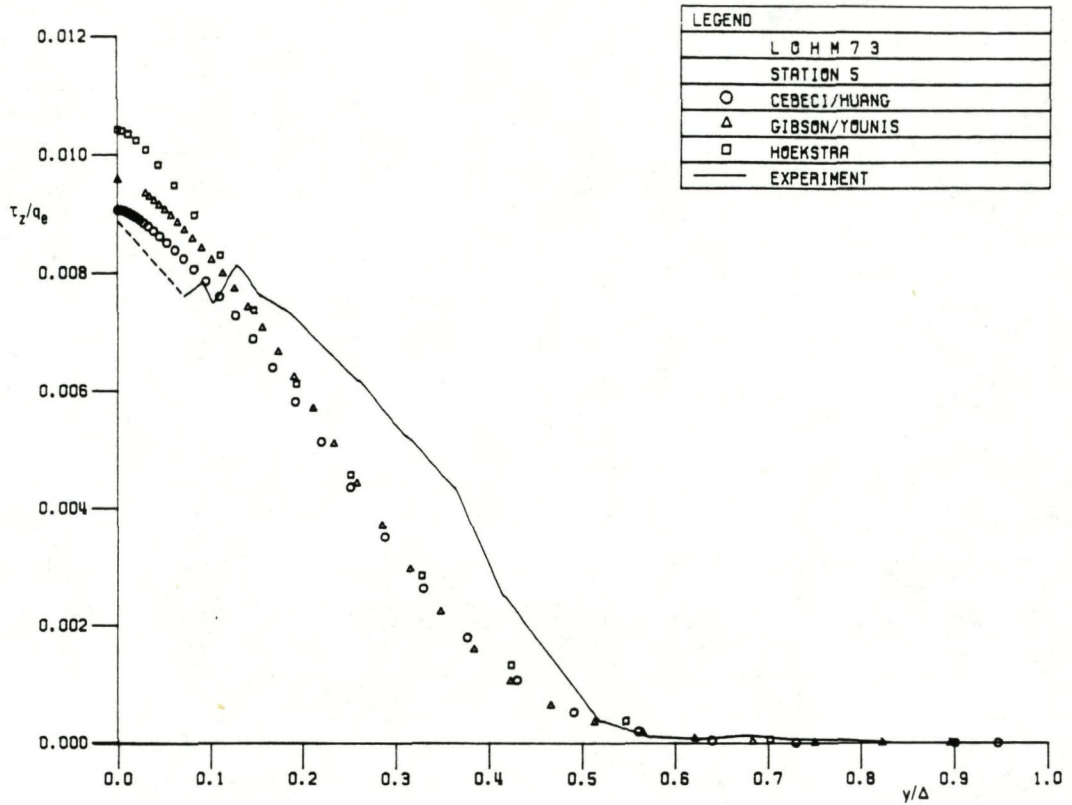
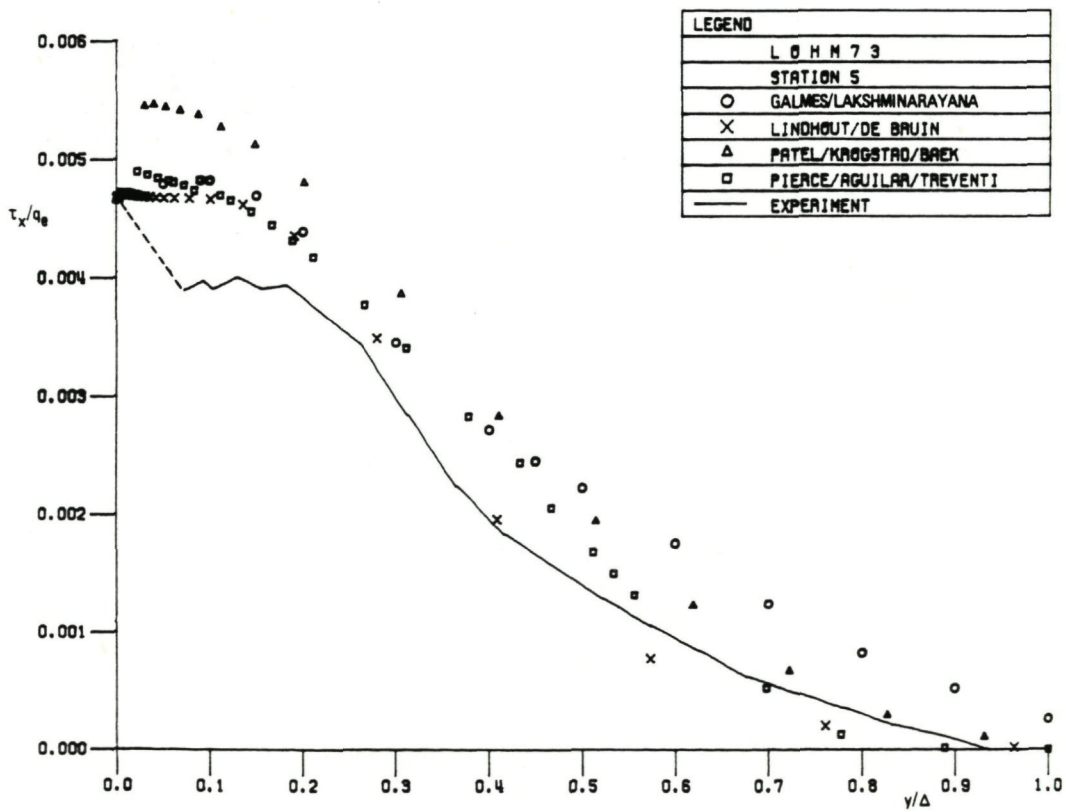Fig. 5.17a   Crosswise shear stresses at station 5 (x/L = 8.0)
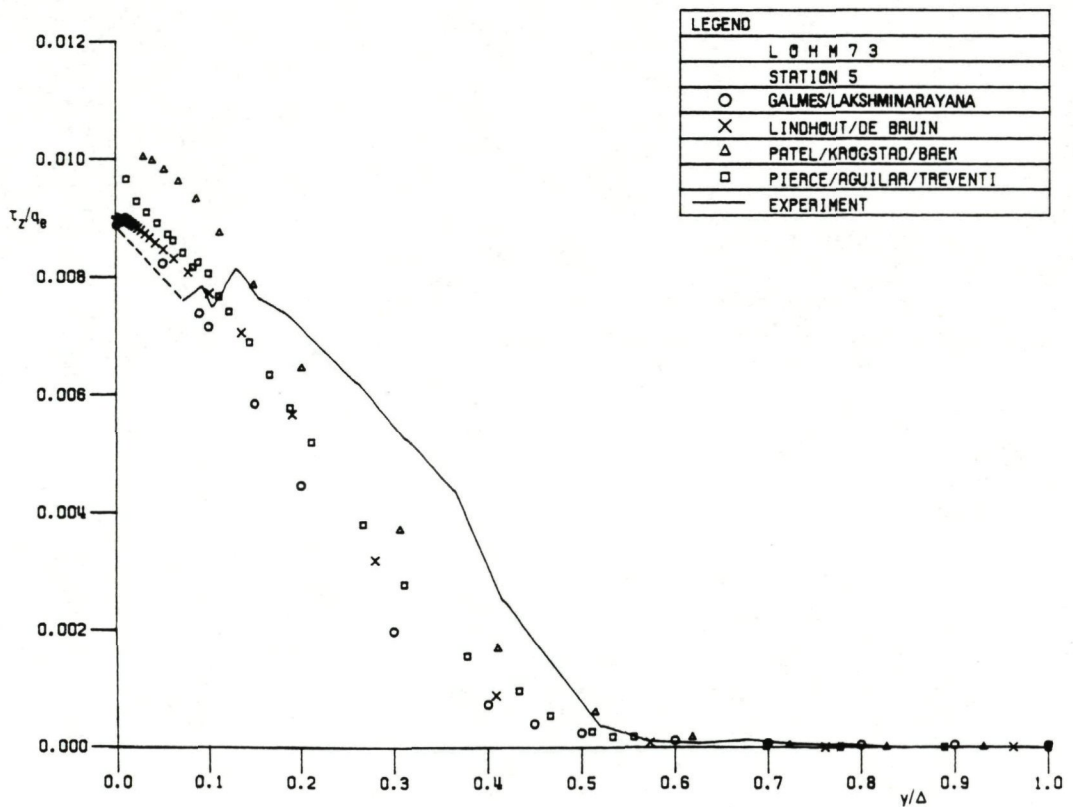
Fig. 5.17b   Crosswise shear stresses at station 5 (x/L = 8.0)
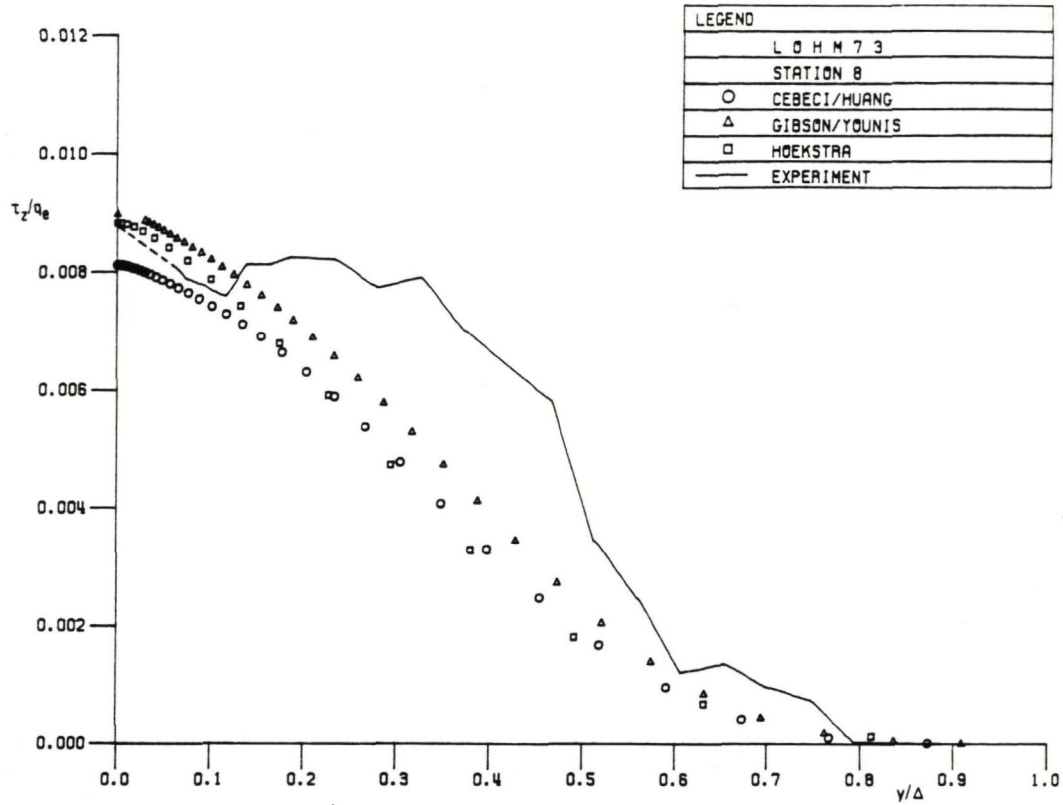
Fig. 5.18a   Crosswise shear stresses at station 8 (x/L = 16.0)
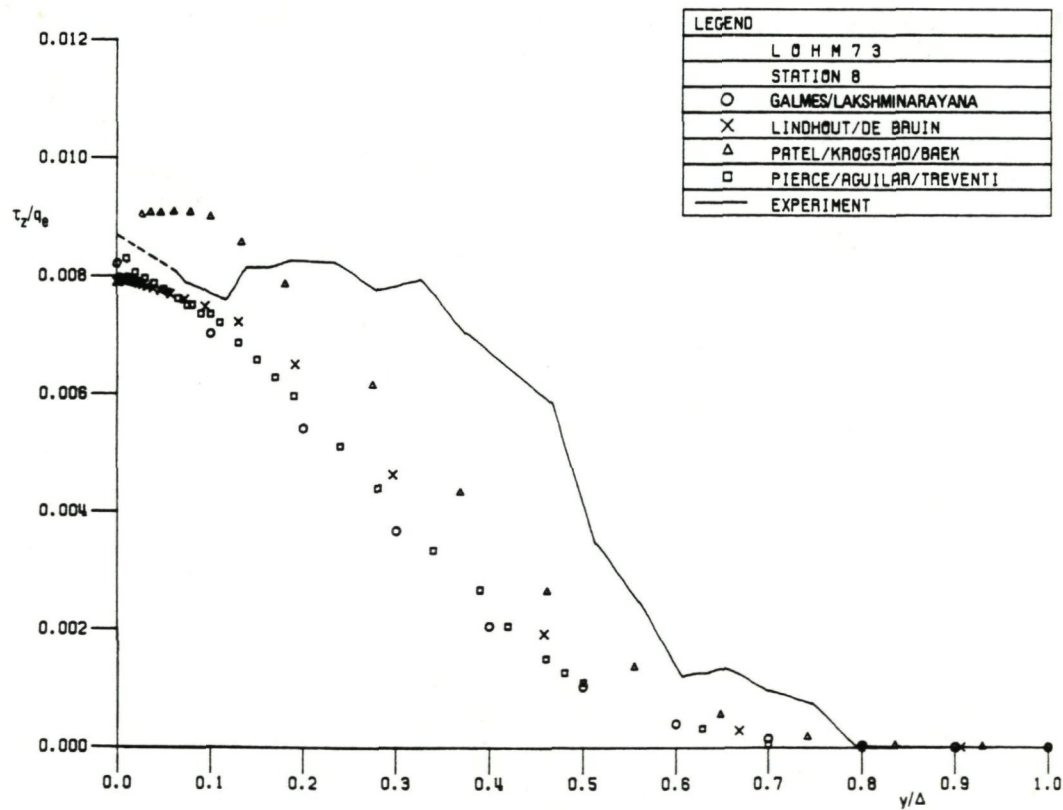
Fig. 5.18b   Crosswise shear stresses at station 8 (x/L = 16.0)
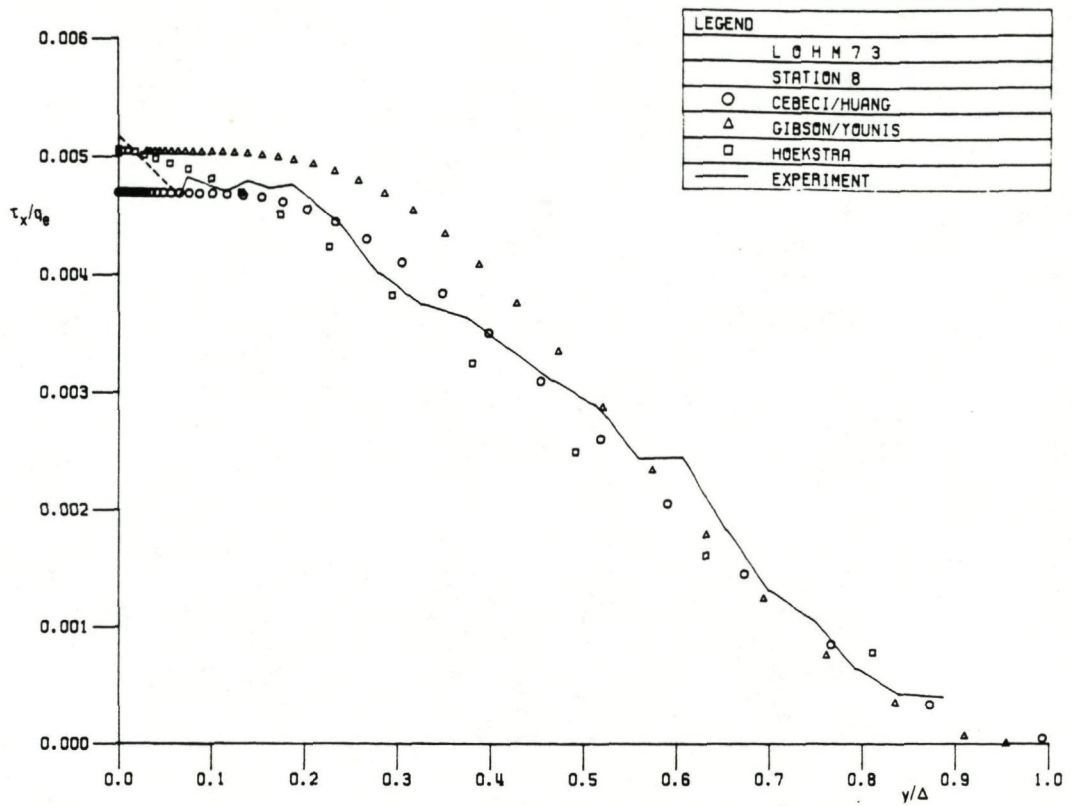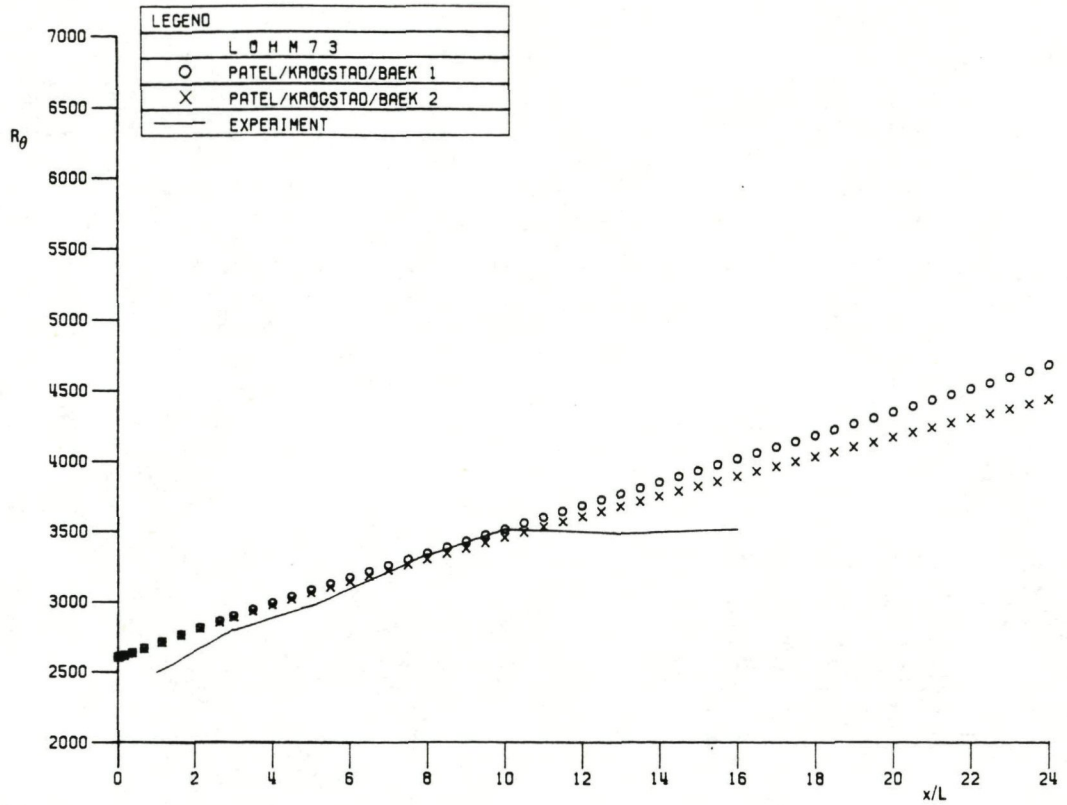
Fig. 5.19a   Effect of streamline curvature correction in turbulence
model. Version 2: with curvature correction
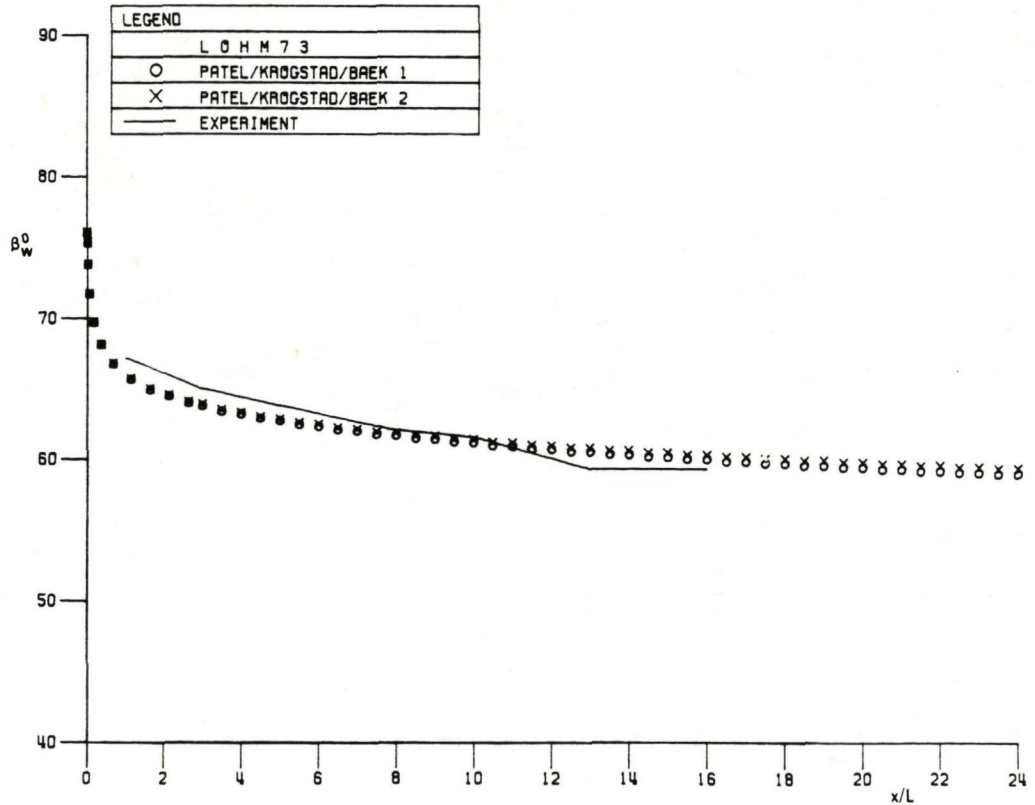
Fig. 5.19b   Effect of streamline curvature correction in turbulence
model. Version 2: with curvature correction
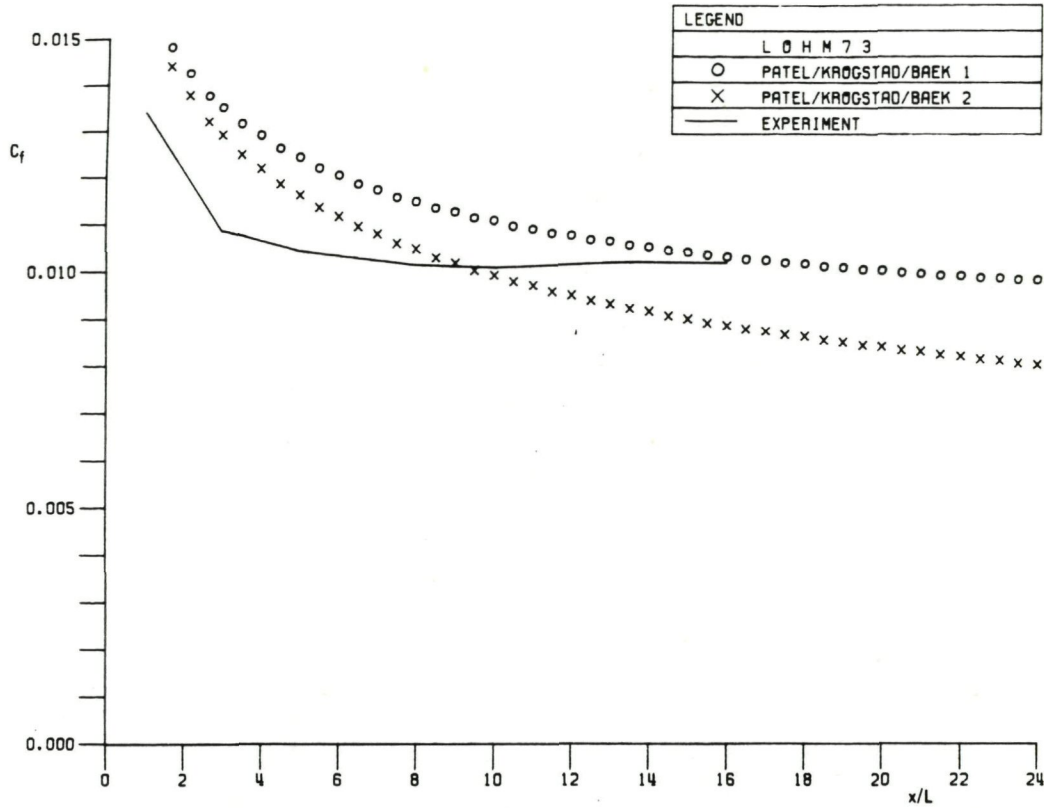
Fig. 5.19c Effect of streamline curvature correction in turbulence
model. Version 2: with curvature correction

6   TEST CASE MUKR 79

This test case is based on an experiment performed by Müller and
Krause. The experiment is extensively described in Müller (1979),
Müller & Krause (1979) and Müller (1982a). Measurements were carried out
in a turbulent boundary layer on a flat plate with a pressure distribu-
tion induced on it. As sketched in figure 6.1, the pressure distribu-
tion on the test plate was induced by two guiding plates on the
surface, with a third plate added to generate an adverse pressure
gradient. Due to the induced surface pressure distribution the origin-
ally collateral boundary layer is skewed considerably downstream. The
position of the measuring stations and the coordinate system employed
is indicated in figure 6.2. The station identification here is based
on sequence numbers in the x- and z-directions.

The boundary layer on the test plate was tripped near the plate
leading edge by fixing a wire of 5 mm diameter on the surface. This
large diameter wire not only made the boundary layer turbulent, but
also increased the boundary layer thickness at the leading edge
substantially. The boundary layer at the initial line of the measurement
region (see figure 6.1) has not recovered yet from the influence of
the wire. Figure 6.3 compares the eddy viscosity, as deduced form the
measurements, at a station on the initial line with the corresponding
value in two-dimensional equilibrium conditions. It appears that the
measured eddy viscosity is large in the outer region of the boundary
layer. This would be a particular interesting test case, therefore,
for calculation methods which take into account the initial turbulence
conditions of the boundary layer. No such calculation methods were,
however, applied to this test case in the Berlin Workshop.

PRESSURE–INDUCING PLATES

INITIAL LINE

TRIPPING WIRE

MEASURING STATION

TEST PLATE

WALL STREAMLINE

EXTERNAL STREAMLINE

Fig. 6.1   MUKR79 test set-up
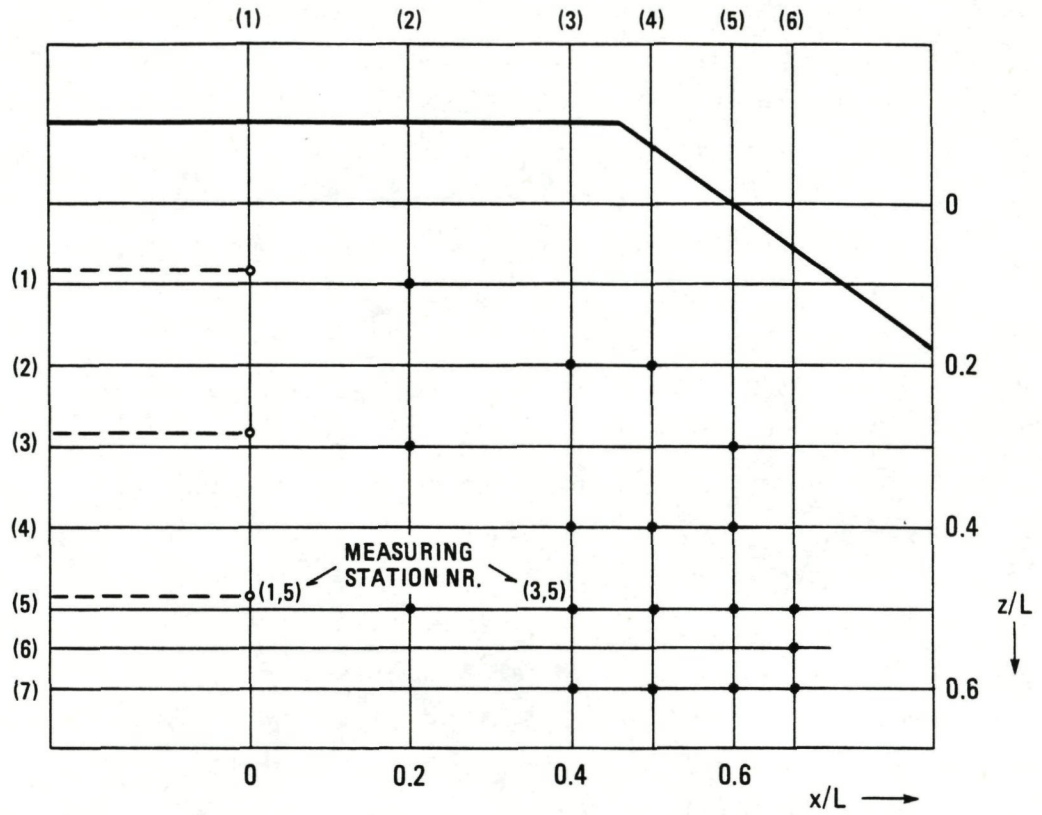
Fig. 6.2   Position of measuring stations

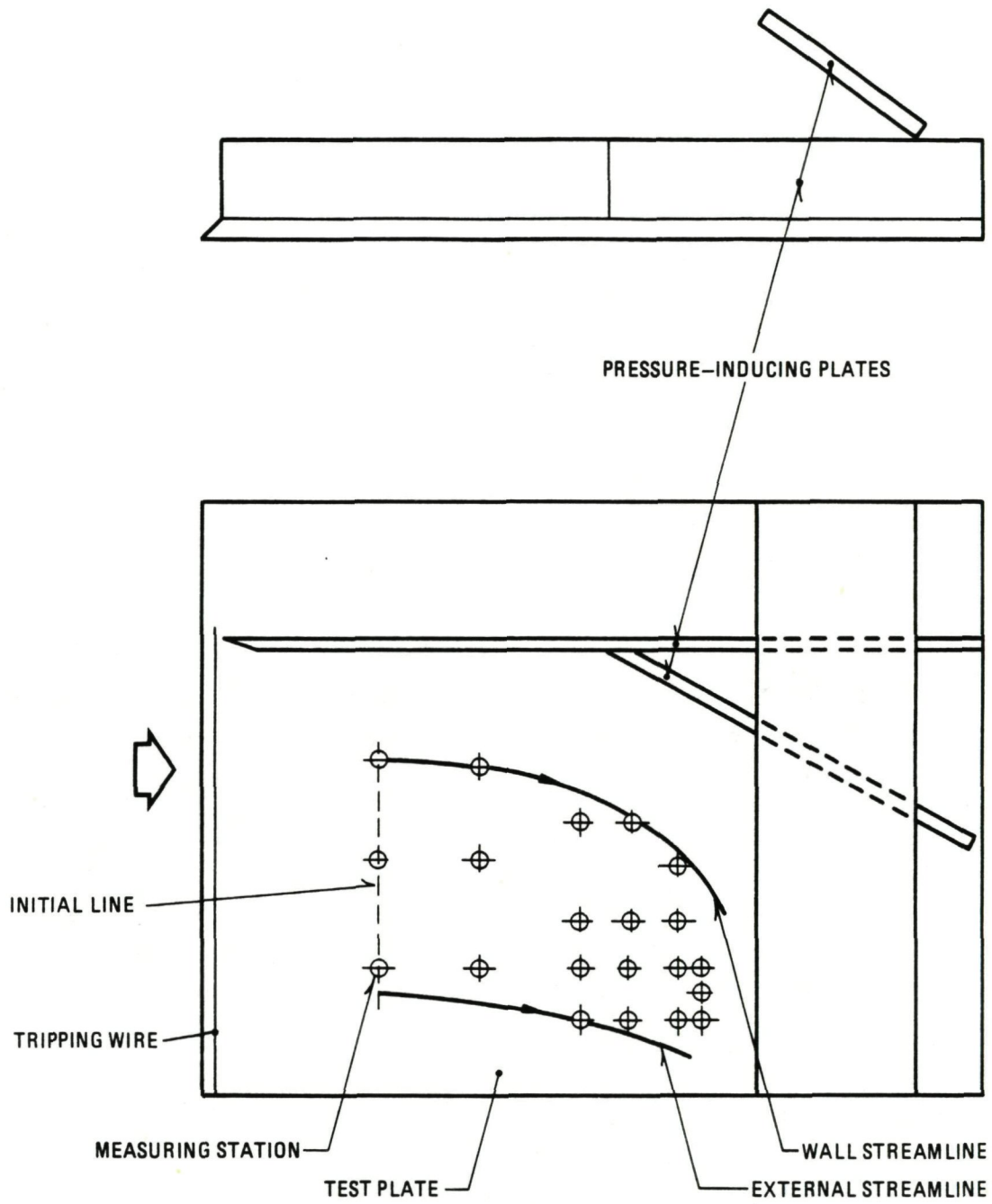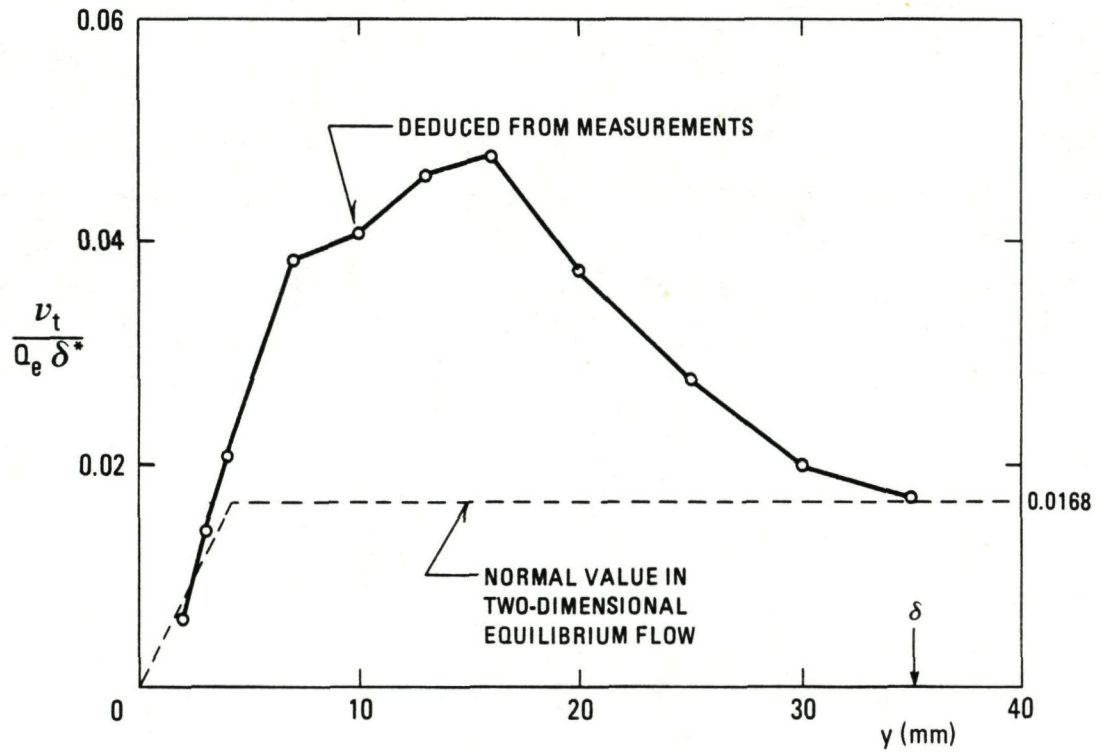Fig. 6.3   Measured eddy-viscosity at initial station (1, 5)

Three comparison calculations were performed. The method of CROSS
is an integral method, while those of MÜLLER and PATEL/KROGSTAD/BAEK
are field methods with an algebraic isotropic eddy viscosity model.
The eddy viscosity variation represented by the dashed line in figure
6.3 is nearly identical with the assumption made in the method of
PATEL/KROGSTAD/BAEK. The turbulence model in the method of MÜLLER
employs a mixing length formulation.

Numerical accuracy studies were performed by all three participants.
These studies comprised the effect of step size variations on the
calculation results and in one case also a momentum integral balance
check. The results are given in table 6.1. Experimental accuracy
estimates are given in Appendix B.

In figure 6.4 the calculated and measured momentum thickness
Reynolds numbers are compared. Figure 6.4a shows the development of R_θ
with x/L at z/L = 0.5, the development in approximately the streamwise
direction. The results show some scatter. The data from MÜLLER are
consistently higher than those of the other methods. Figures 6.4b and
6.4c show the variation of R_θ with z/L at x/L = 0.4 and 0.6. The
spanwise extent over which calculation results are given, differs for
the three calculations. This is probably due to different lengths of
the initial line used in the calculations, which leads to computational
regions of different width downstream of the initial line. In the
calculations of PATEL/KROGSTAD/BAEK side boundary conditions at z = 0
were assumed. For the comparisons attention should be focussed on the
region where experimental data are given, which corresponds roughly
with the region of determinacy of the line segment with measured
initial data.

Table 6.1   Results of numerical accuracy studies for MUKR79 test case

a. Stepsize variation

results submitted	stepsize factor	coordinate direction	station number	effect on calculations
CROSS	2	x, z	5,5	$\Delta\beta_w = 2.6°$ $\Delta C_f = 1.5\%$
MÜLLER	2	x		$\Delta\beta_w < 3°$ $\Delta C_f < 3\%$
PATEL/KROG-STAD/BAEK	1.5	x	5,5	$\Delta C_f = .5\%$

b. Integral momentum balance

results submitted	station number	local error
MULLER	5,5	$\Omega_x = .9\%$ $\Omega_z = 2.5\%$

Figure 6.5a shows the streamwise variation of the wall flow angle, β_w. The calculation results of CROSS are seen to correspond best with experimental data. Both field methods overestimate the wall flow angle increase, especially the method of PATEL/KROGSTAD/BAEK. This is even more evident from the results in figure 6.5c. The fact that in the experiment the wall flow angle was set equal to the flow angle at $y = 0.2$ mm ($y^+ \cong 10$) may contribute to the discrepancy.

The skin friction results are given in figure 6.6. The experimental data plotted are the Preston tube results given in Müller 1979. The experimental uncertainty for these data is estimated as $\pm 1.5 \times 10^{-4}$. The agreement between the calculations and experiment in figure 6.6 may be regarded as satisfactory, apart from the slightly high skin friction values from CROSS in part of the flow, see figure 6.6b.

Figure 6.7 shows the streamwise velocity profiles at four stations. The velocity profiles of the CROSS integral method are members of a three-dimensional version of Coles' profile family. The results of MÜLLER agree best with experiment. As shown by the velocity profiles, the boundary layer thickness calculated by CROSS and PATEL/KROGSTAD/-BAEK is slightly too small at all stations. This trend is also apparent in the crossflow profiles, see figure 6.8. The crossflow velocity component is computed consistently low by MÜLLER, while for the other calculation methods deviations in both directions occur. The relative positions of the three sets of computed crossflow results is the same for all stations shown.

To check the empirical assumptions made about the Reynolds shear stresses, it is best to compare directly measured and calculated shear stresses. This is done in figures 6.9 and 6.10. The integral method of CROSS does not give shear stress profiles.

The streamwise shear stresses (experimental error estimate ± 10%) at four stations are depicted in figures 6.9a to d. The streamwise component of the skin friction is also indicated in the graphs by connecting the wall value to the first shear stress data point from the wall by a dashed line. On the whole the calculated shear stresses appear to yield the correct trends, notably the MÜLLER results. The streamwise shear stresses calculated by PATEL/KROGSTAD/BAEK are too high at station (6,5).

The crosswise shear stresses (experimental error estimate ± 15%) at the four stations are plotted in figure 6.10a to d. At the wall distance where $W/y = 0$ (see figure 6.8), the crosswise shear stress should change sign in an eddy viscosity calculation method. This is not the case for the results of PATEL/KROGSTAD/BAEK. The crosswise shear stress is negative over the larger part of the boundary layer. The magnitude of the calculated crosswise shear stresses is in some cases significantly smaller (see figure 6.10b) than the magnitude of the measured crosswise shear stresses. The results of PATEL/KROGSTAD/- BAEK are much less satisfactory than those of MÜLLER.

The most striking fact to emerge from the analysis again concerns the crosswise shear stress. In the other pressure-driven flows (BEEL72 and DEFE77) too small positive or too large negative crosswise shear stresses were generally computed with isotropic eddy viscosity models (chapters 3 and 4). Here the calculations give too large positive or too small negative crosswise shear stresses. In the MUKR79 experiment a comparatively large crosswise eddy viscosity was deduced from the measurements (Müller & Krause, 1979), while a comparatively small crosswise eddy viscosity was reported for the other experiments (Elsenaar et al 1975, Dechow & Felsch 1977).

Tabel 5.3 <u>Survey of computed results for the MUKR79 test case</u>

figures	quantities	CROSS	MÜLLER	PATEL KROGSTAD BAEK
6.4-6.6	R_Θ, β_w, C_f	X	X	X
6.7-6.8	U, W	X	X	X
6.9-6.10	τ_x, τ_z		X	X
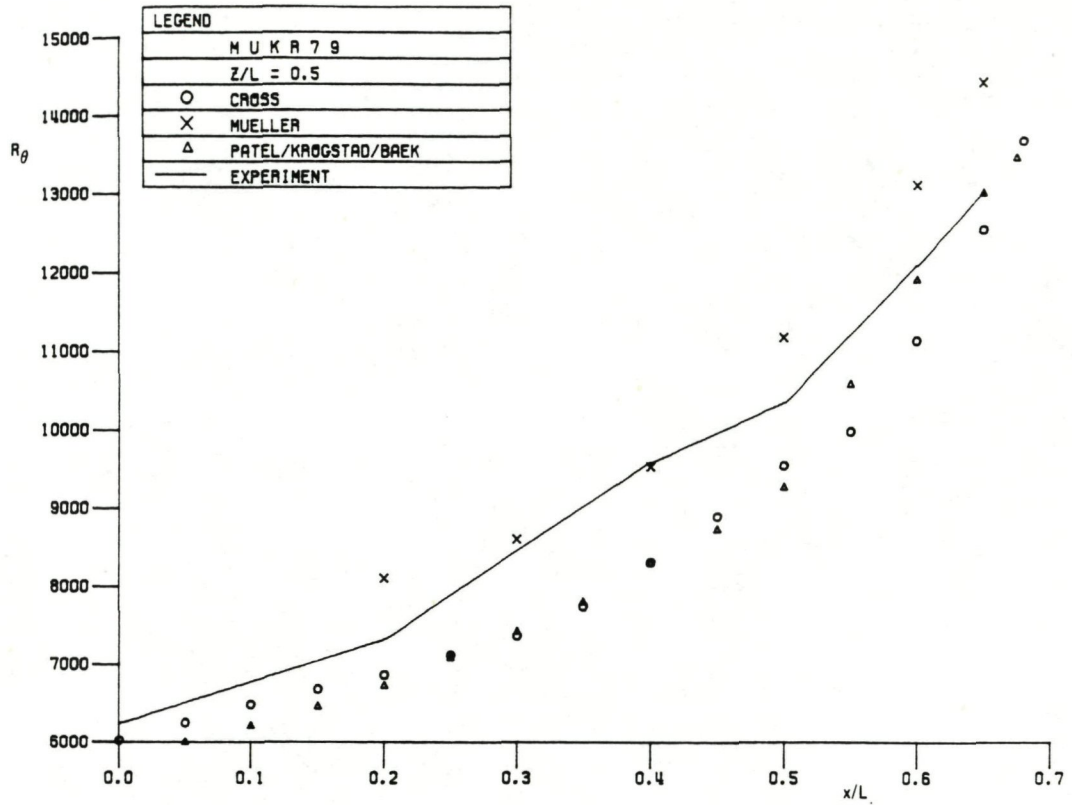
Fig. 6.4a Variation of momentum thickness Reynolds number
with x/L at z/L = 0.5
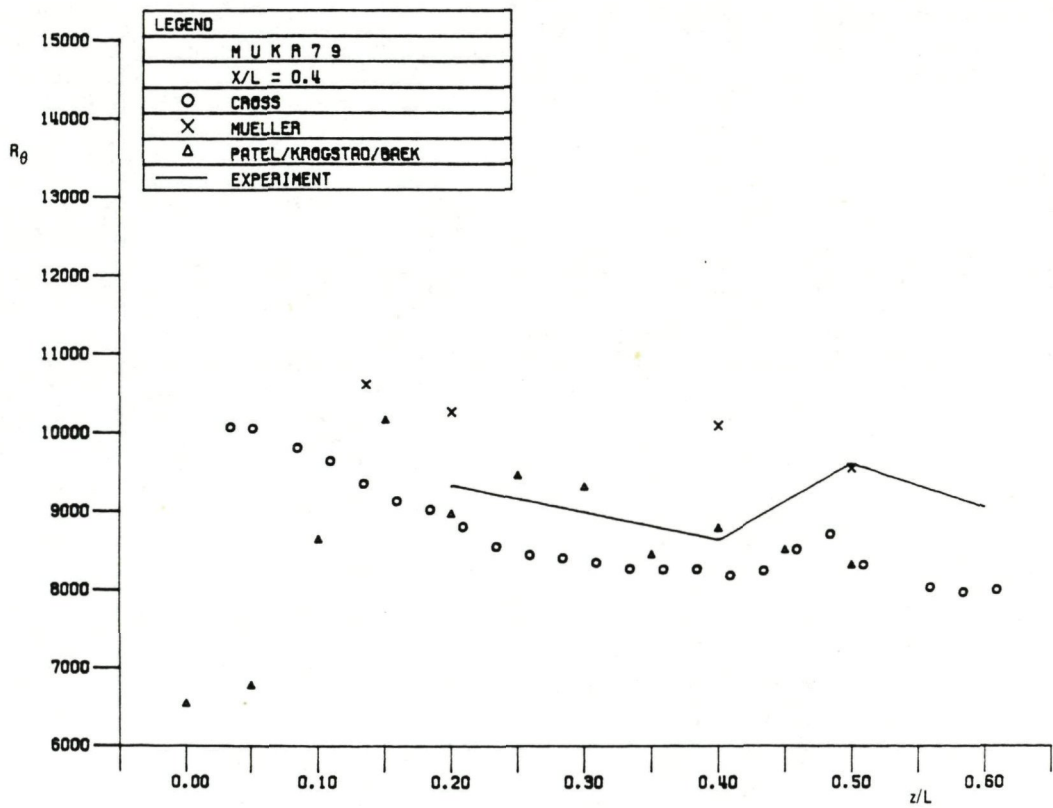
Fig. 6.4b Variation of momentum thickness Reynolds number
with z/L at x/L = 0.4
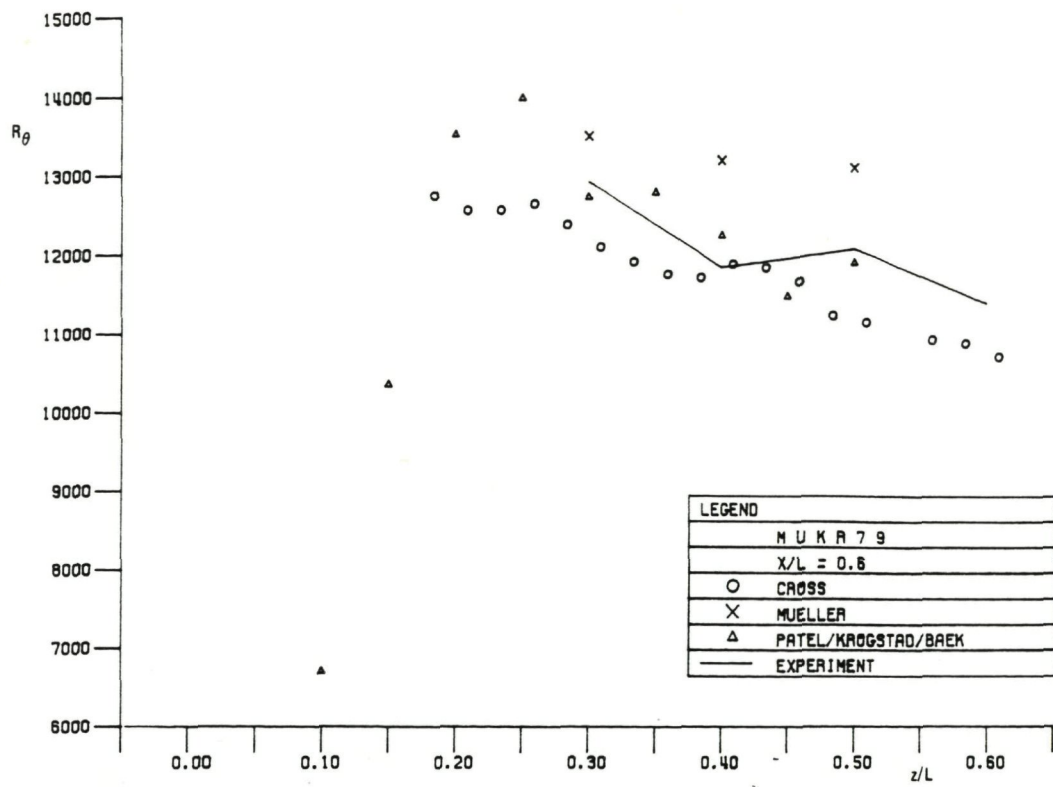
Fig. 6.4c   Variation of momentum thickness Reynolds number
            with z/L at x/L = 0.6
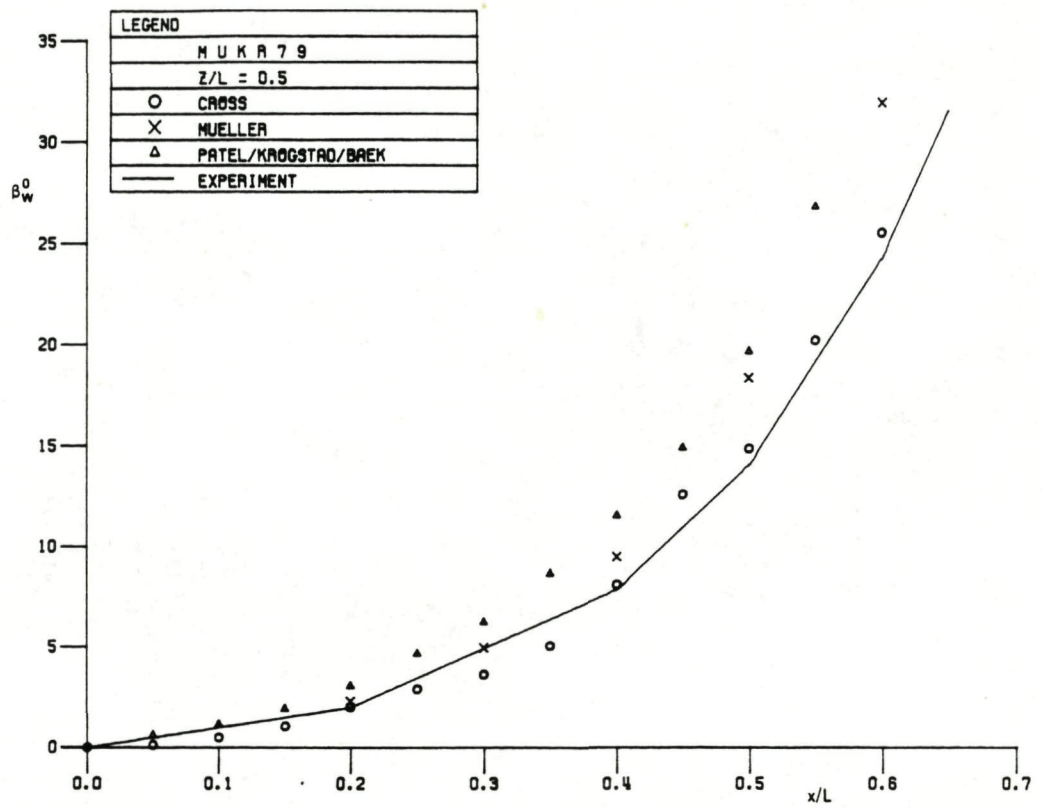
Fig. 6.5a Variation of wall flow angle with x/L at z/L = 0.5
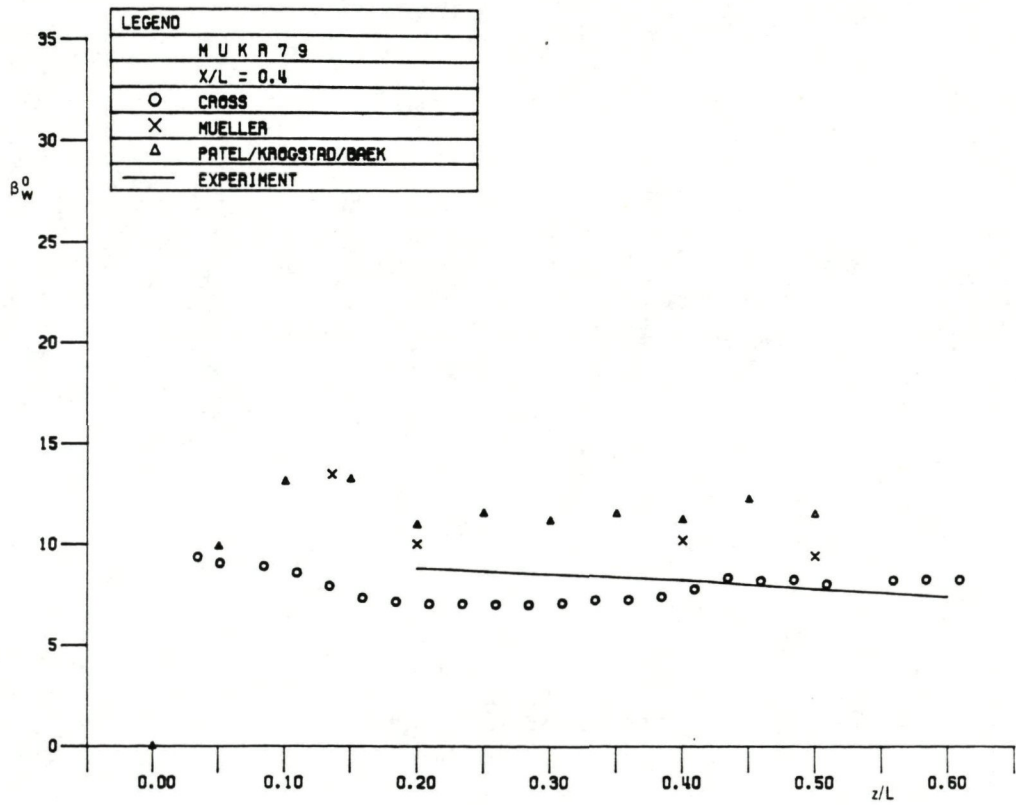
Fig. 6.5b Variation of wall flow angle with z/L at x/L = 0.4
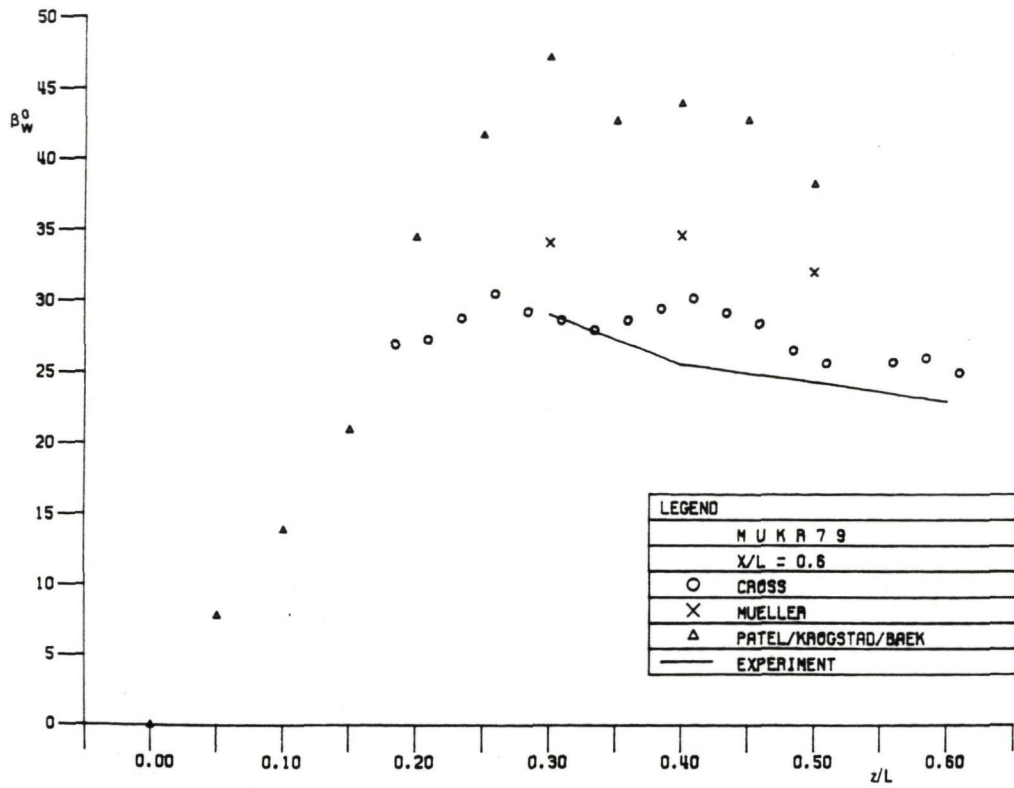
Fig. 6.5c Variation of wall flow angle with z/L at x/L = 0.6
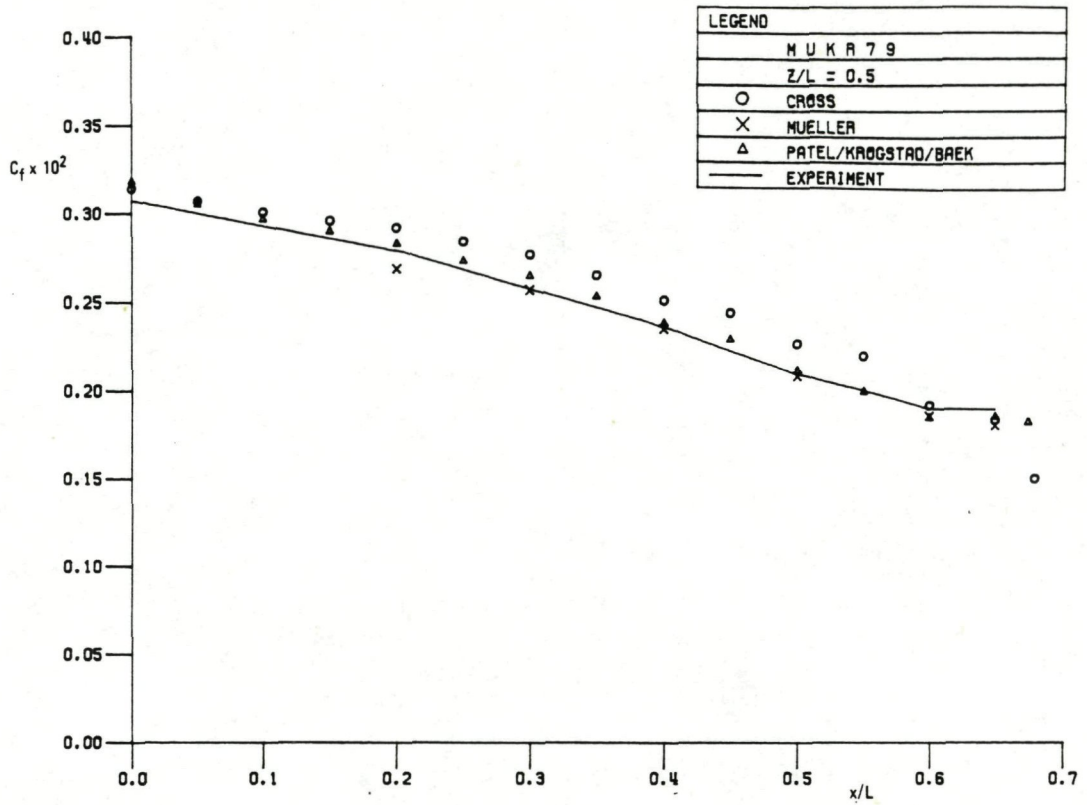
Fig. 6.6a   Variation of skin friction with x/L at z/L = 0.5
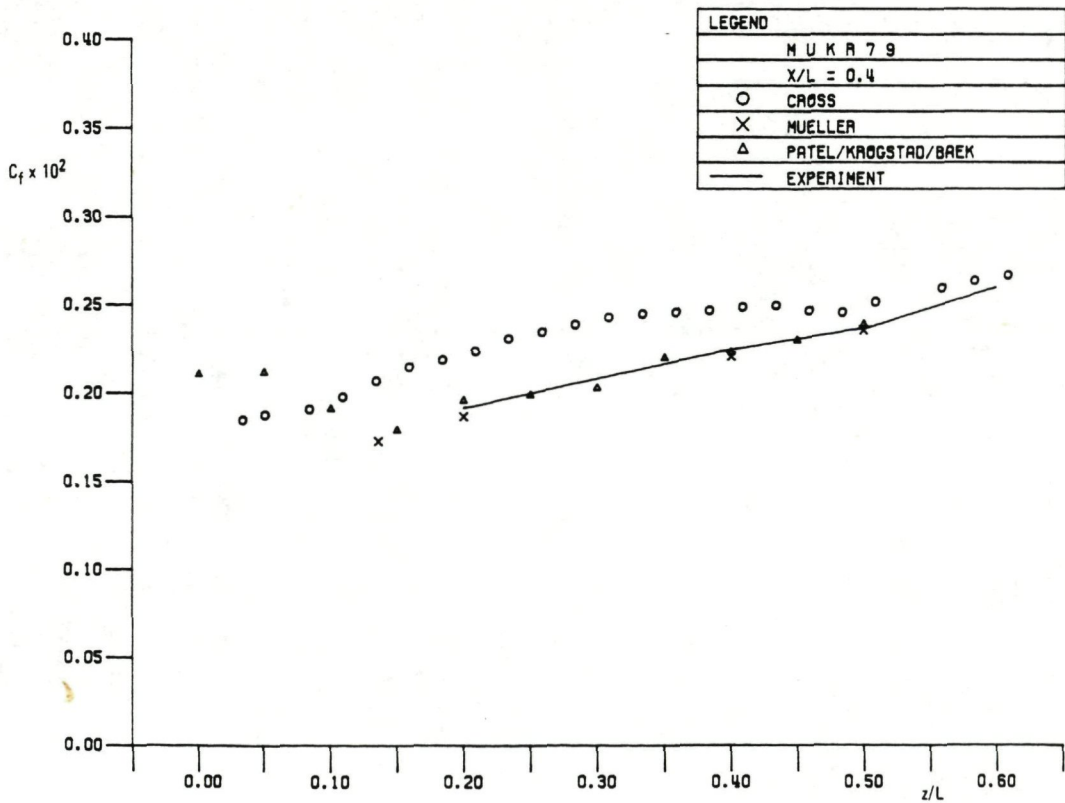
Fig. 6.6b   Variation of skin friction with z/L at x/L = 0.4
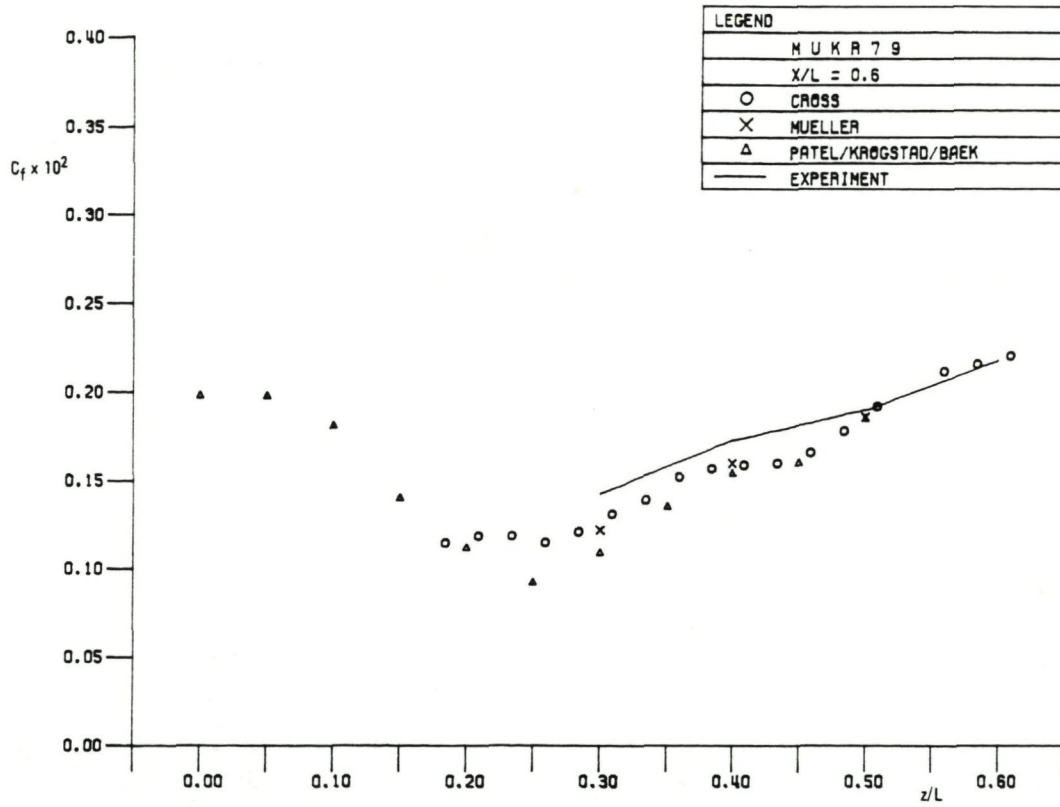
Fig. 6.6c Variation of skin friction with z/L at x/L = 0.6
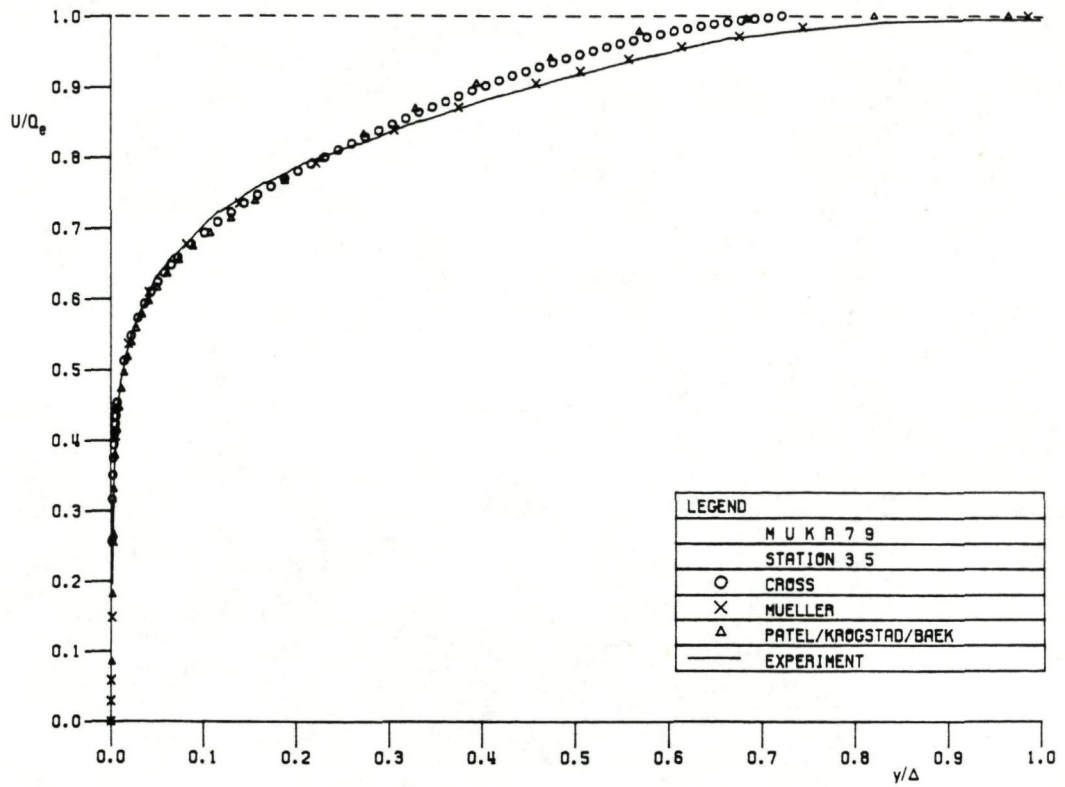
Fig. 6.7a   Streamwise velocity profiles at station 3, 5
(x/L = 0.4, z/L = 0.5)
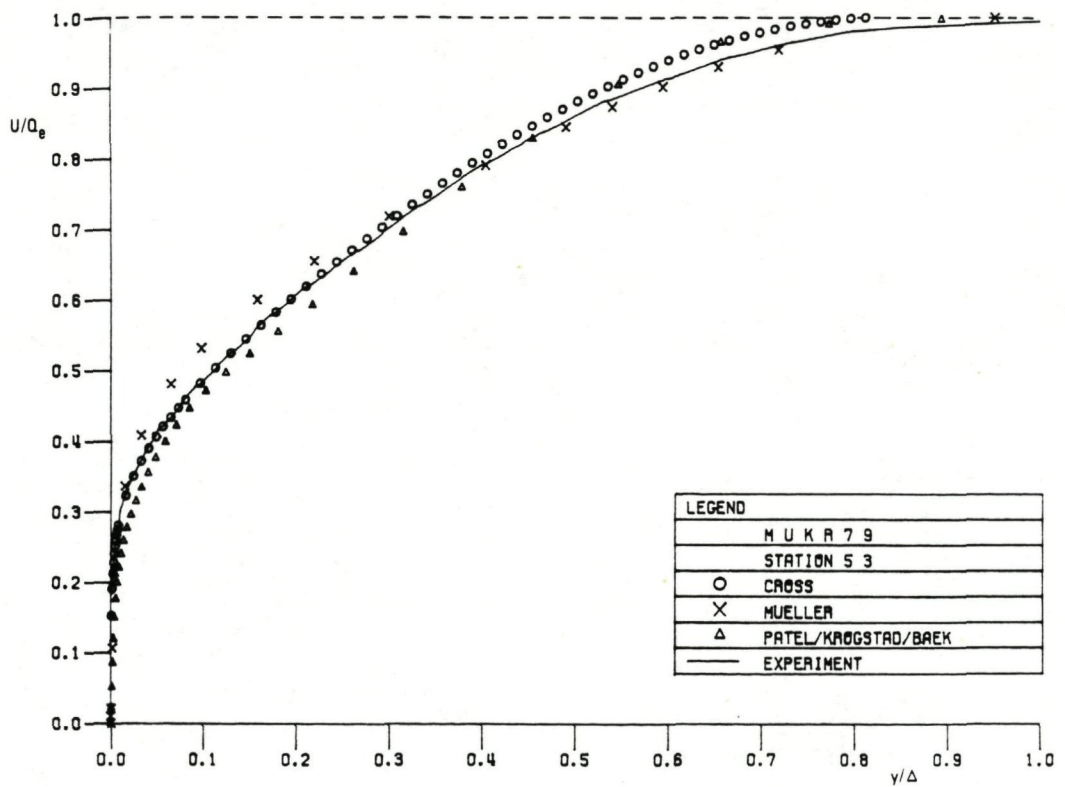
Fig. 6.7b   Streamwise velocity profiles at station 5, 3
(x/L = 0.6, z/L = 0.3)
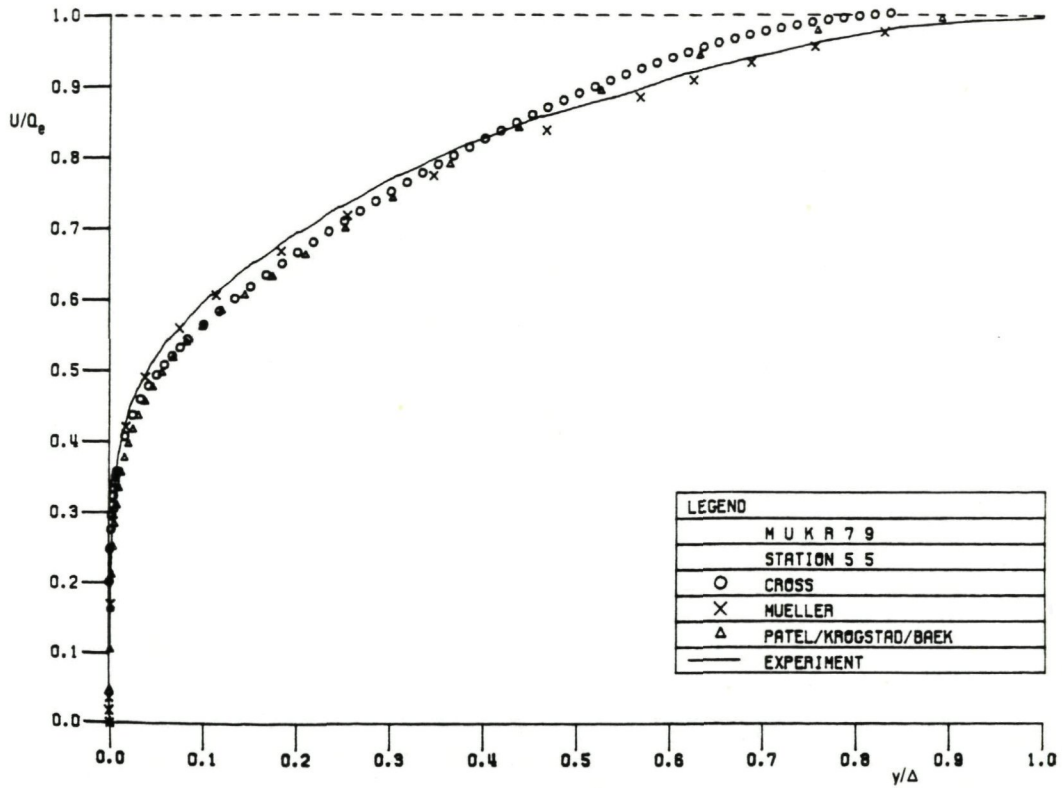
Fig. 6.7c   Streamwise velocity profiles at station 5, 5
             (x/L = 0.6, z/L = 0.5)
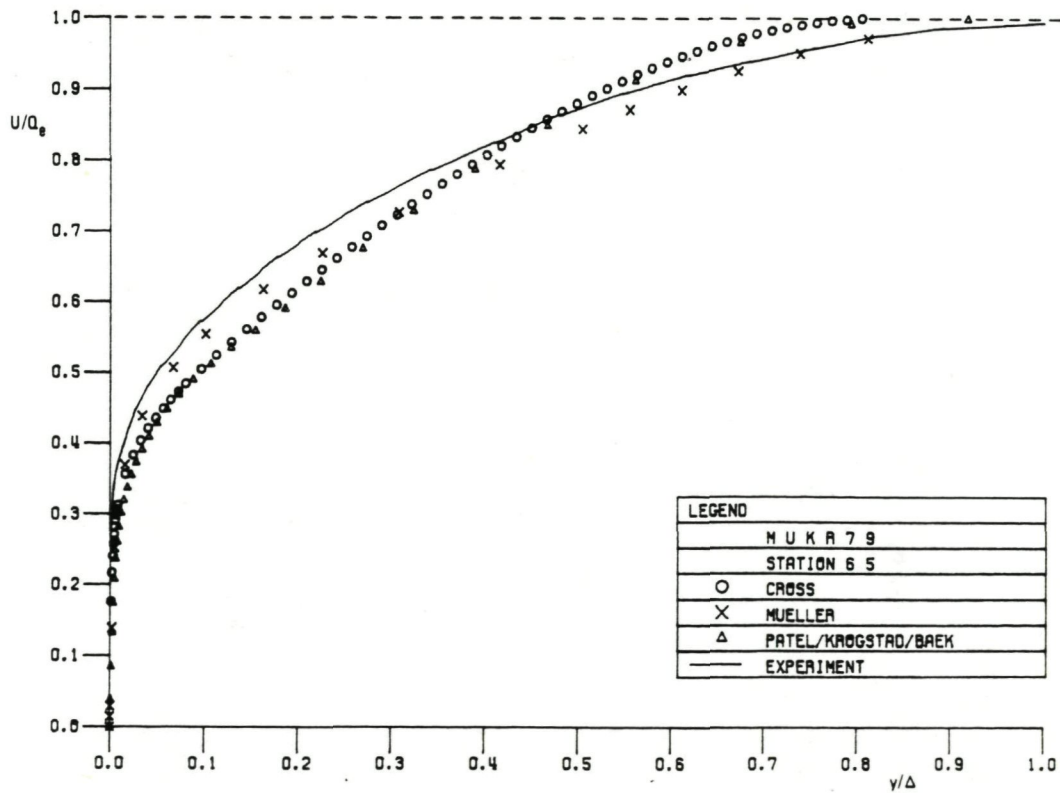
Fig. 6.7d   Streamwise velocity profiles at station 6, 5
             (x/L = 0.65, z/L = 0.5)
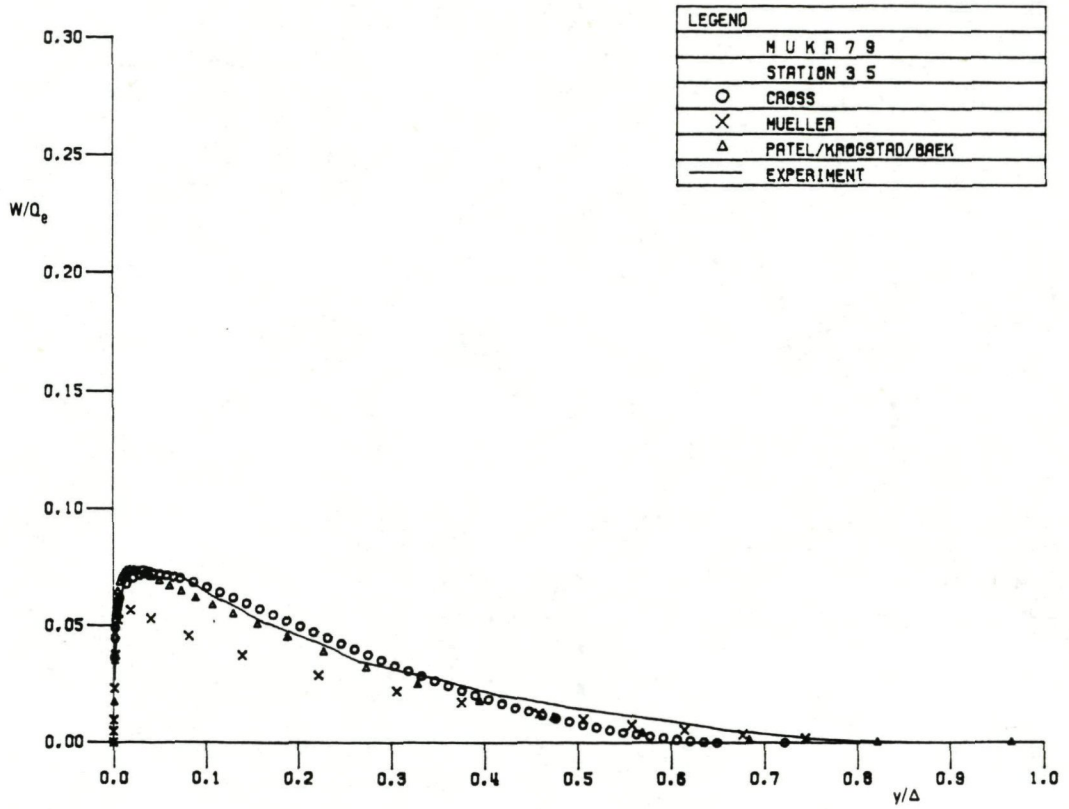
Fig. 6.8a   Crosswise velocity profiles at station 3, 5
(x/L = 0.4, z/L = 0.5)
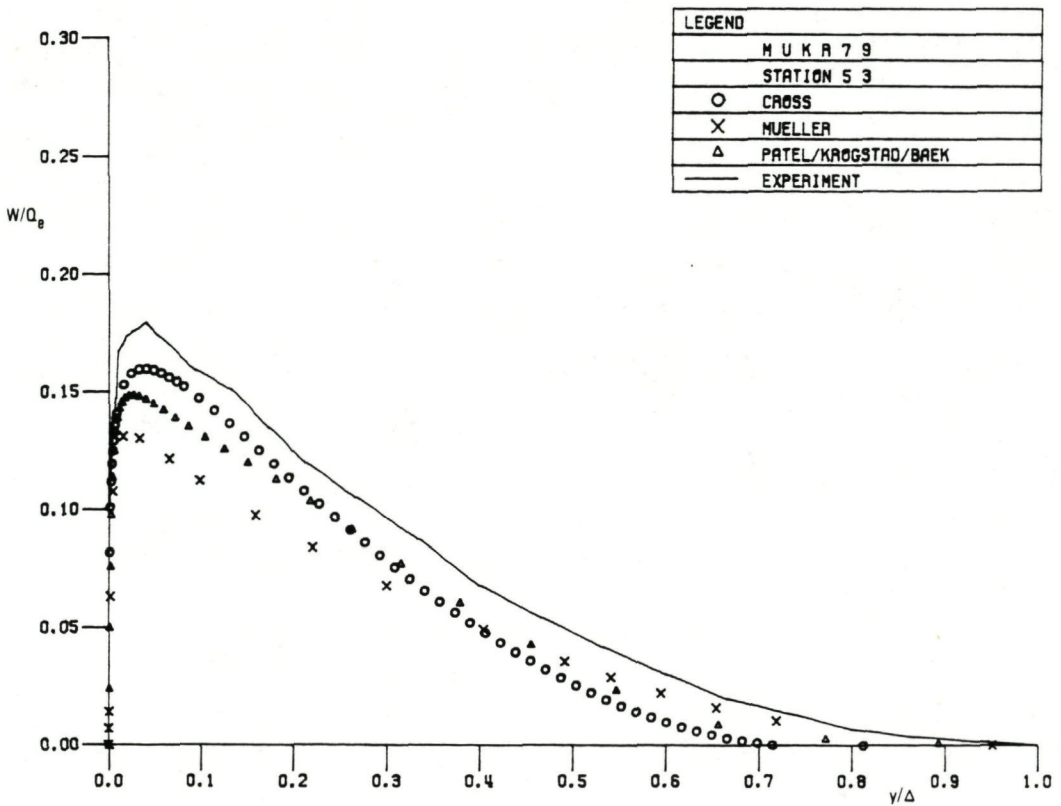
Fig. 6.8b   Crosswise velocity profiles at station 5, 3
(x/L = 0.6, z/L = 0.3)
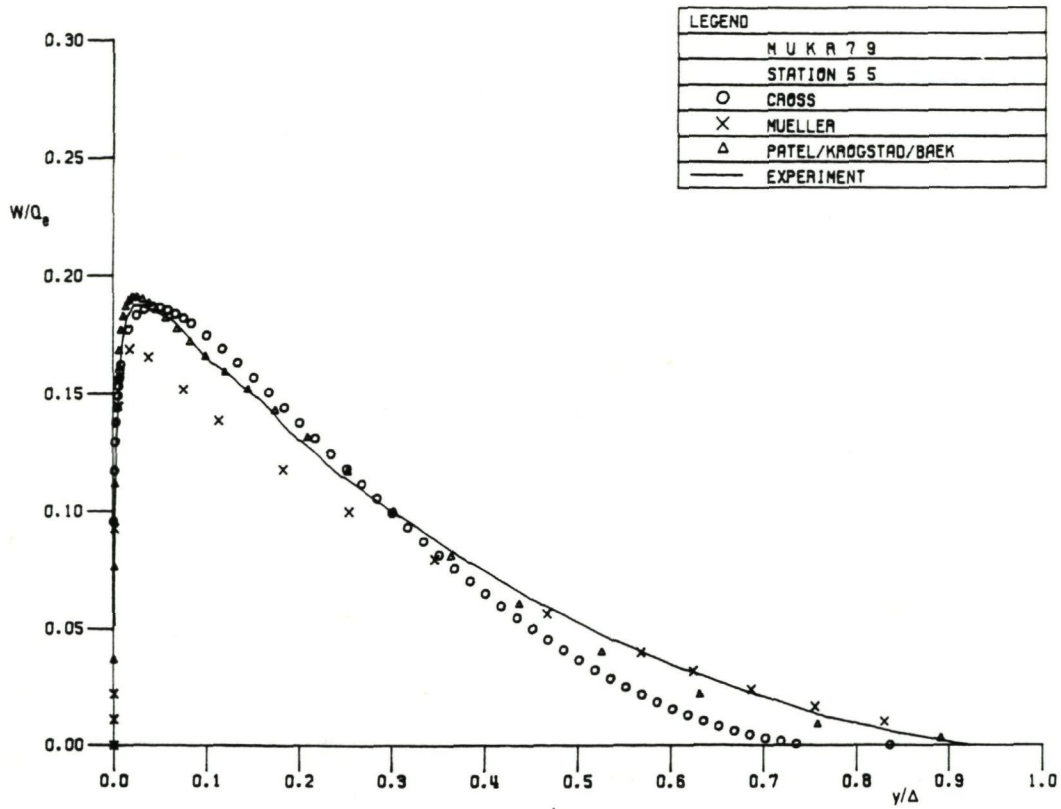
Fig. 6.8c   Crosswise velocity profiles at station 5, 5
            (x/L = 0.6, z/L = 0.5)
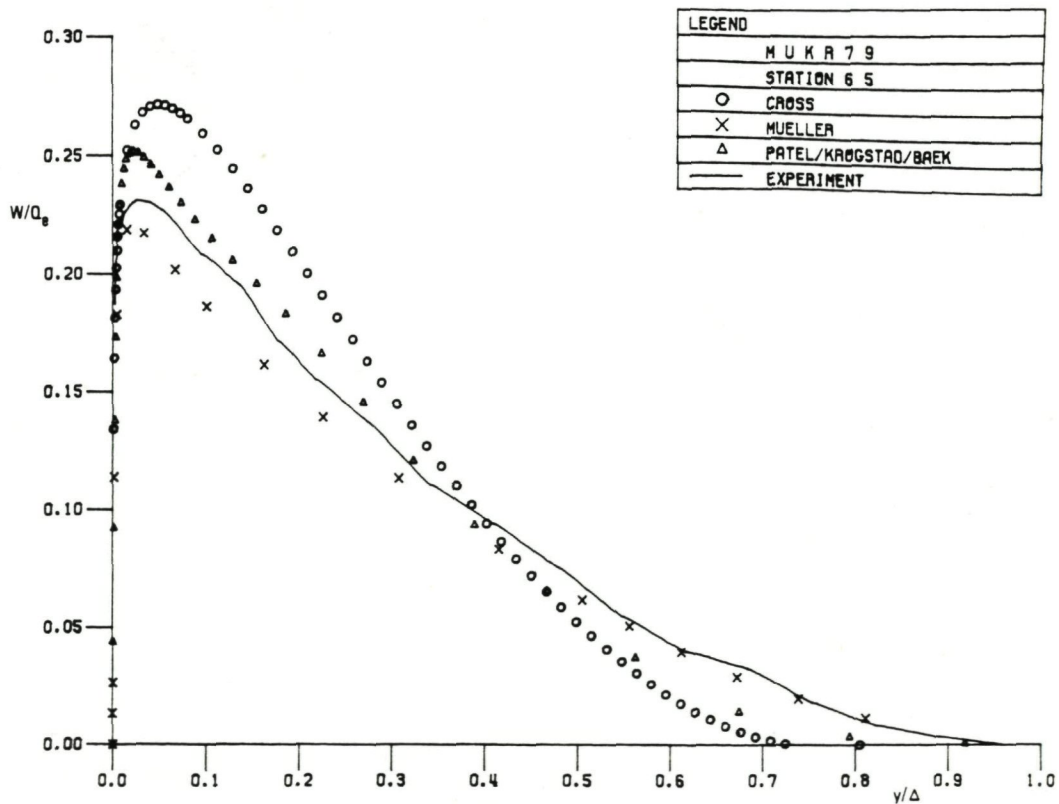
Fig. 6.8d   Crosswise velocity profiles at station 6, 5
            (x/L = 0.65, z/L = 0.5)
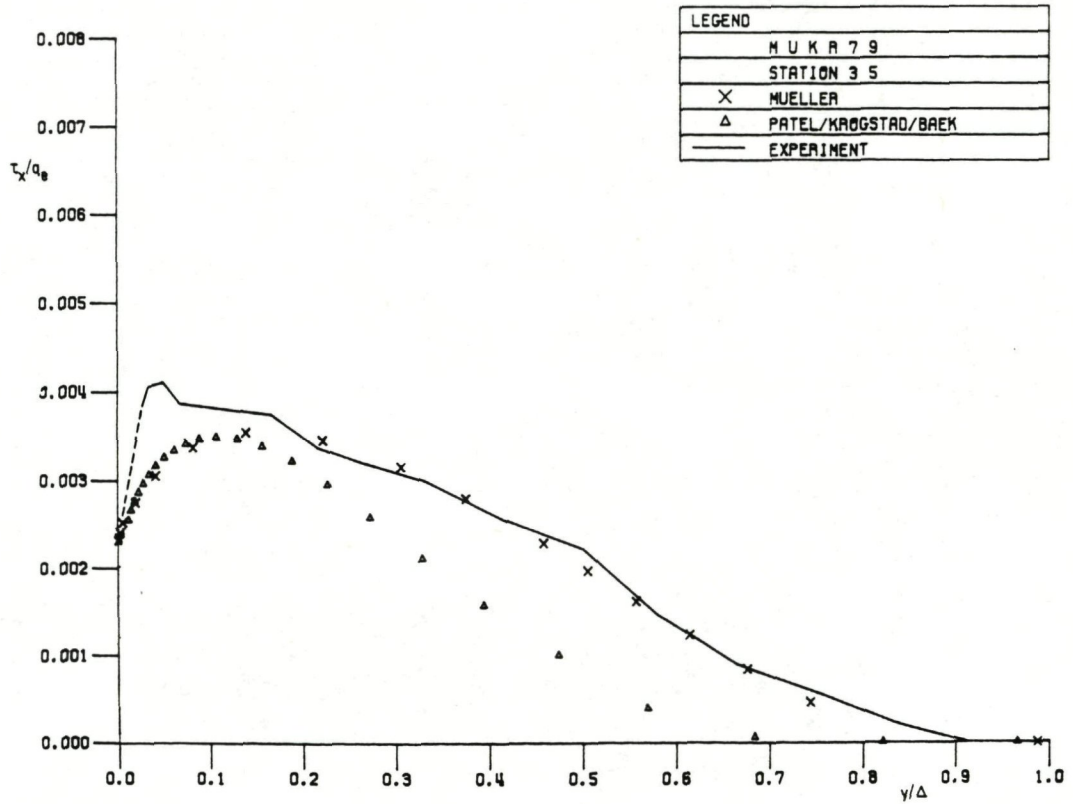
Fig. 6.9a   Streamwise shear stresses at station 3, 5
(x/L = 0.4, z/L = 0.5)
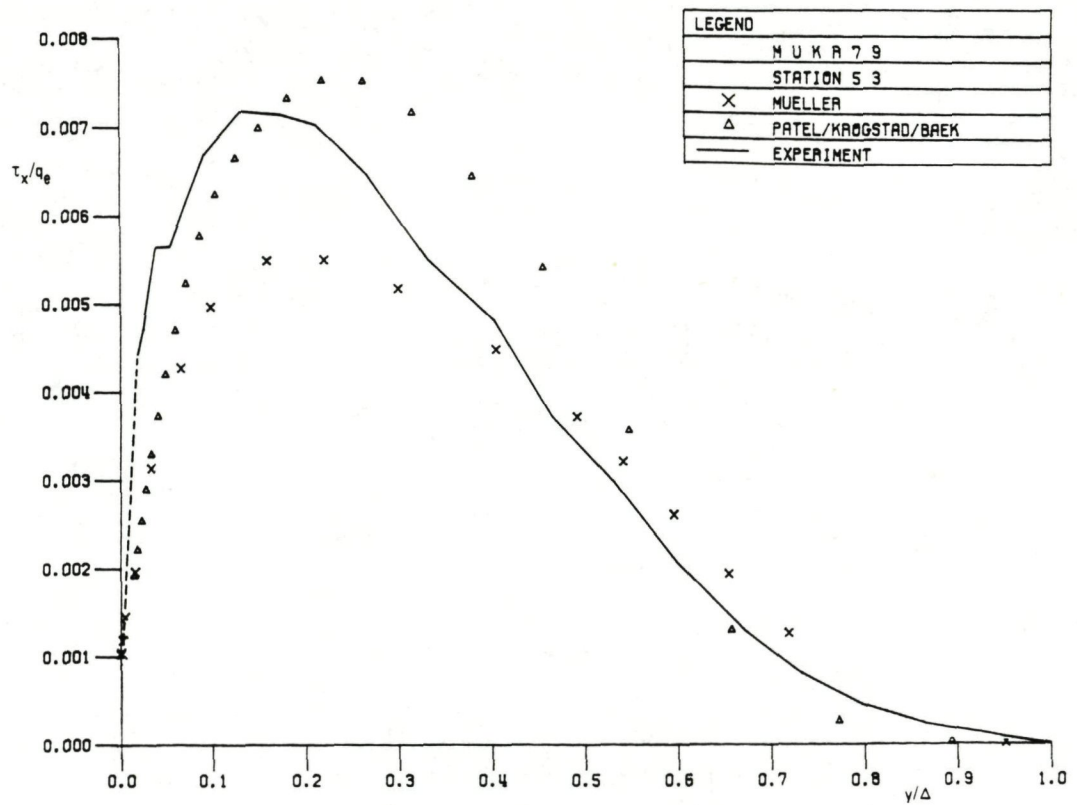
Fig. 6.9b   Streamwise shear stresses at station 5, 3
(x/L = 0.6, z/L = 0.3)
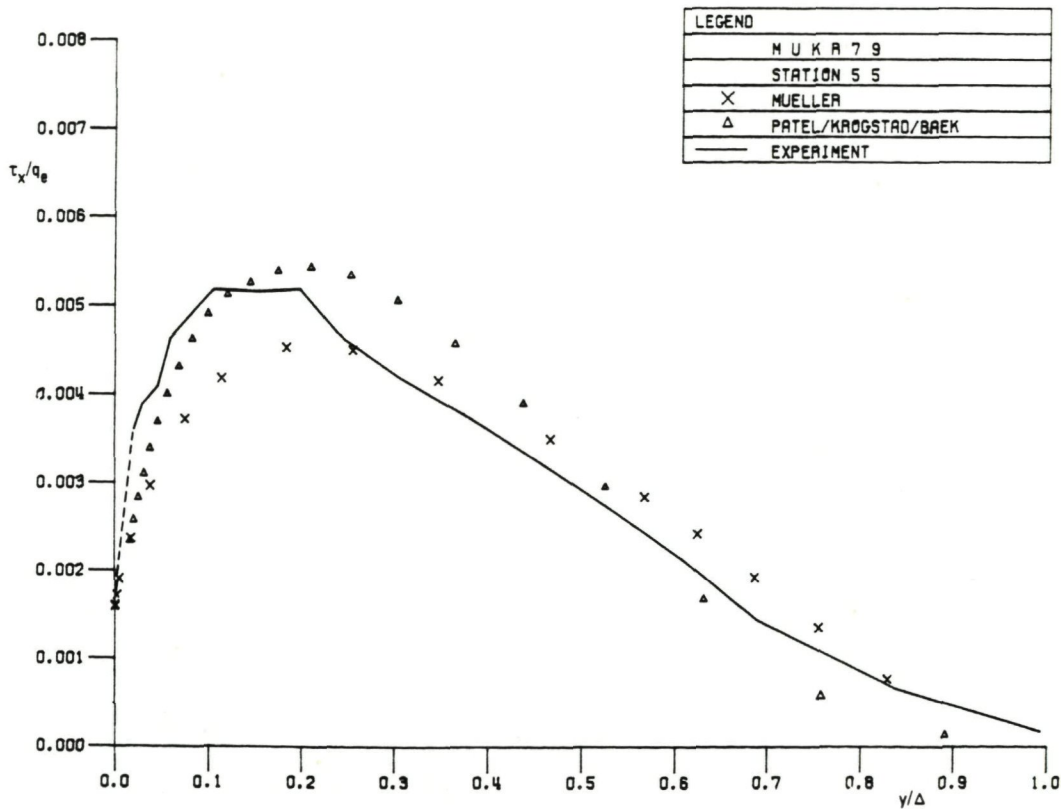
Fig. 6.9c Streamwise shear stresses at station 5, 5
(x/L = 0.6, z/L = 0.5)
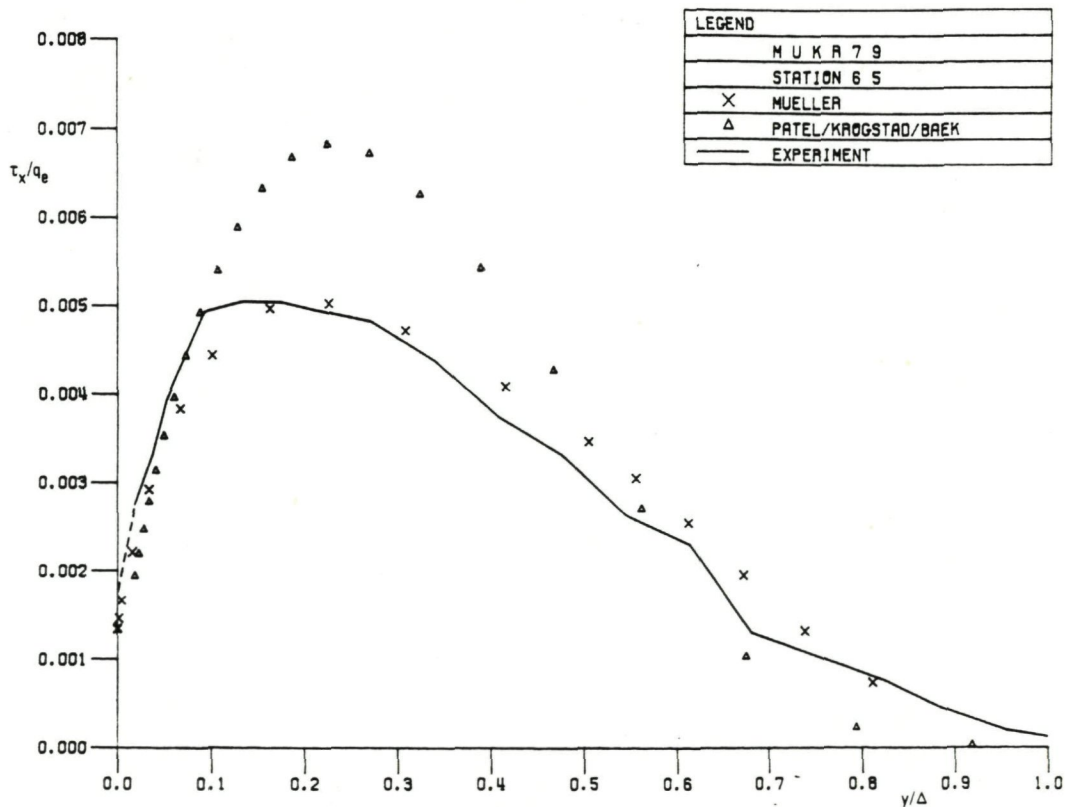
Fig. 6.9d Streamwise shear stresses at station 6, 5
(x/L = 0.65, z/L = 0.5)
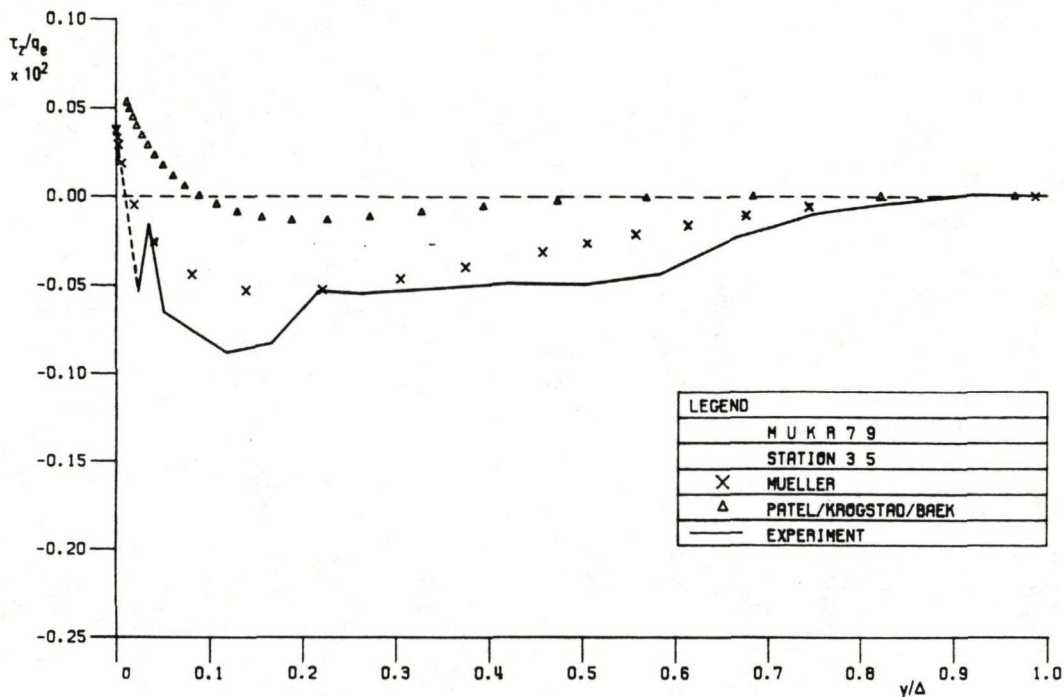
Fig. 6.10a   Crosswise shear stresses at station 3, 5
             (x/L = 0.4, z/L = 0.5)
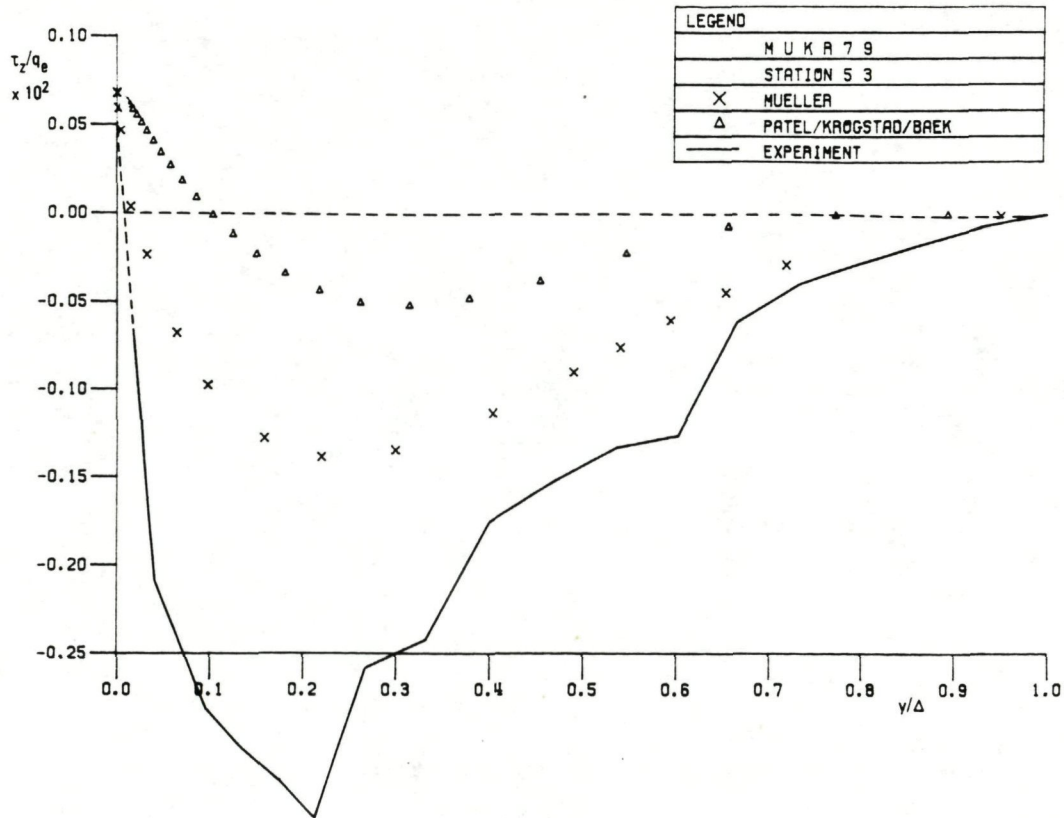
Fig. 6.10b   Crosswise shear stresses at station 5, 3
             (x/L = 0.6, z/L = 0.3)
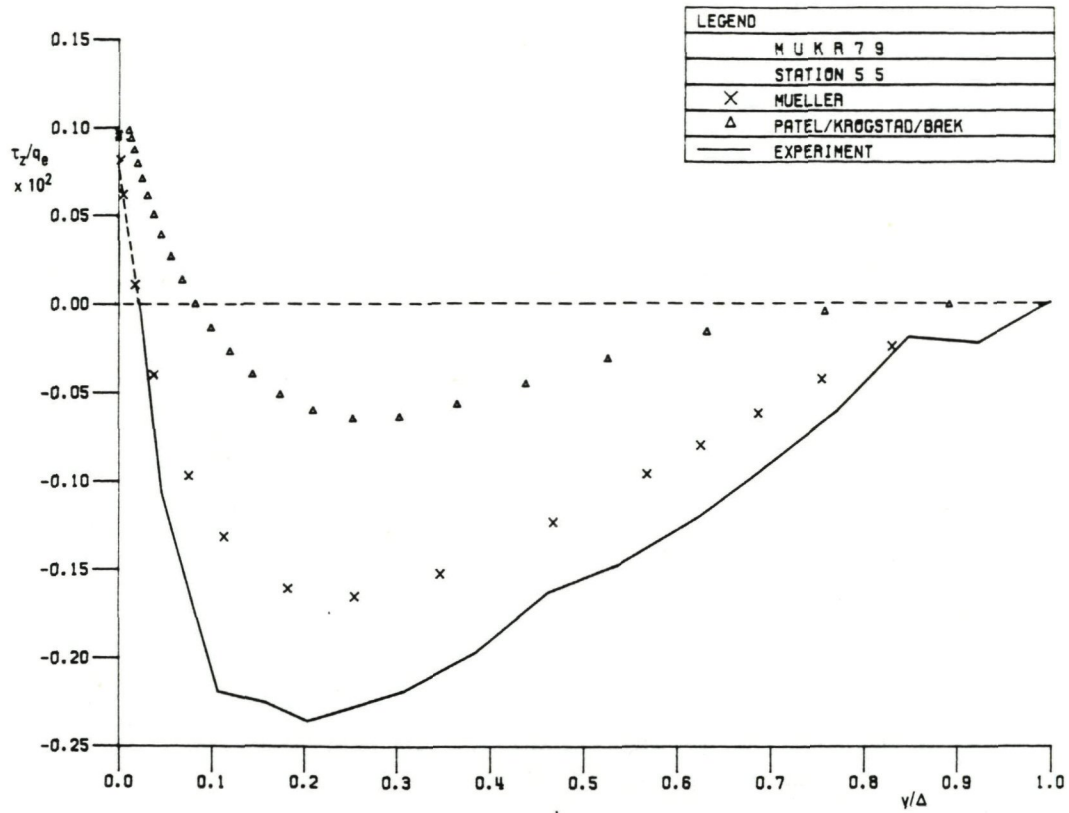
Fig. 6.10c Crosswise shear stresses at station 5, 5
            (x/L = 0.6, z/L = 0.5)
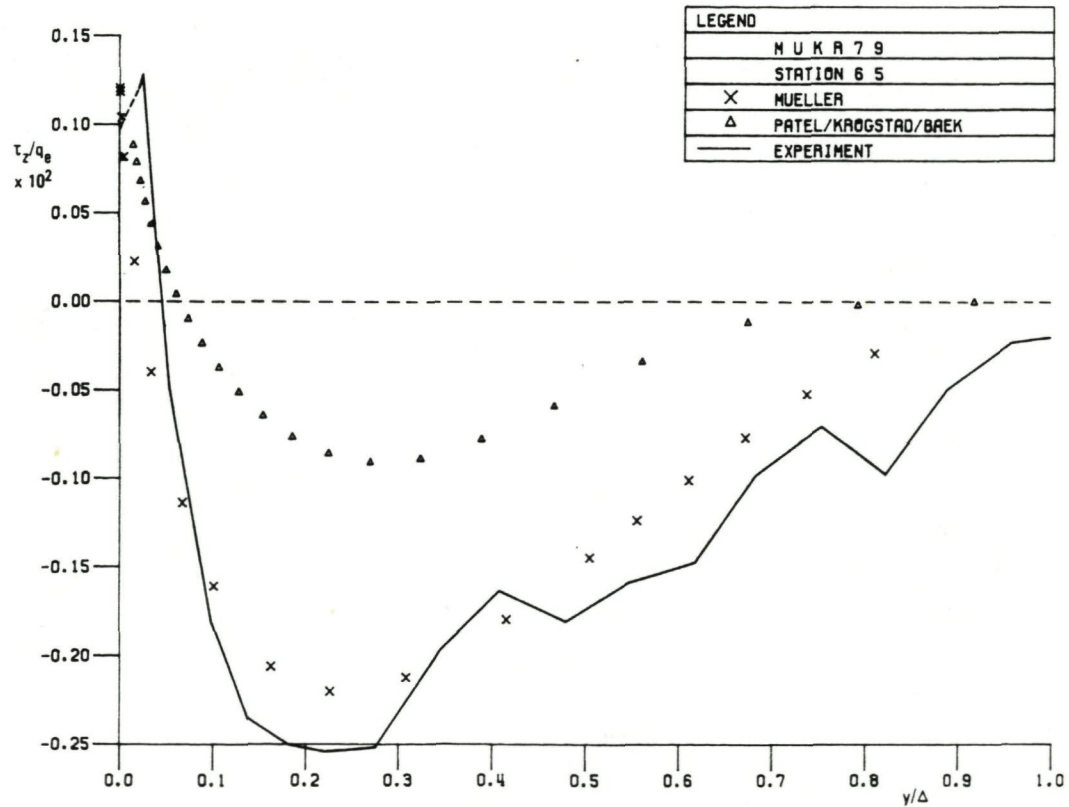
Fig. 6.10d Crosswise shear stresses at station 6, 5
            (x/L = 0.65, z/L = 0.5)

7   CONCLUSIONS

The purpose of the Workshop was to assess the accuracy of available three-dimensional turbulent boundary layer calculation methods by applying them to selected experiments. To evaluate the calculations the numerical accuracy, the empirical assumptions and the experimental uncertainty must all be taken in consideration. Experimental error estimates, so far as available, have been quoted. In this Workshop an attempt was made to assess also the numerical accuracy of the calculations. Two types of test were suggested to yield information on the numerical errors. The outcome was very useful, but still falls short of uncertainty estimation. Yet sufficient information about experimental and numerical uncertainty was obtained to allow an evaluation of the empirical assumptions in the calculations.

The participating calculation methods can be divided into integral methods and field methods. In integral methods the empiricism is contained in assumptions such as boundary layer velocity profile shapes, entrainment rate and skin friction law. Only mean flow quantities are computed by these methods. In this Workshop the integral methods were found to produce generally similar or better agreement with experiment than the field methods. The level of agreement may have benefited from the fact that the empirical assumptions in integral methods utilize available data of three-dimensional turbulent boundary layer experiments, notably on crossflow velocity profile shapes.

In field methods the empiricism is contained in the turbulence model. Most turbulence models used here are straightforward extensions of existing turbulence models for two-dimensional flow. Most of the field methods applied in this Workshop employ algebraic eddy vis-cosity models. Only a few more complex models based upon the turbu-lence transport equations were applied. No evidence was found that the latter lead to better agreement with experiment, as far as can be concluded from the few calculations with such models.

One of the experiments used as a test case here (BEEL72), was also a test case in an earlier Workshop in 1975. The conclusions reached at that time seem still to hold. When the crossflow is small the methods perform adequately but as the crossflow develops the computations fail to keep pace and as a consequence the three-dimensional separation observed in this pressure-driven flow is not computed. The cause of the difference between calculated and measured mean flow quantities becomes clear when comparing the Reynolds shear stresses. The use of standard algebraic isotropic eddy viscosity models leads to an overestimation of the shear stresses, especially the crosswise shear stresses. Improved agreement with experiment was obtained in calculations using modified algebraic eddy viscosity models, for instance by introducing an eddy viscosity anisotropy. These modified models have been applied only to the one test case, however. Consequently no general validity of the modifications can be claimed.

The pattern described above of computing high streamwise and very high crosswise shear stresses as compared with experiment is also evident in one other test case representing a three-dimensional adverse pressure gradient flow (DEFE77). In contrast the shear stresses are not overestimated in the third comparable case (MUKR 79). This may be connected with the high initial shear stress level in this experiment and the consequent high stress level downstream due to turbulence history effects, which were not taken into account in the calculation methods applied.

There was only one test case with a shear-driven three-dimensional boundary layer flow (LOHM73). The main conclusion here is that the crosswise shear stresses were computed too low in the downstream part of the flow.

It is not possible from the information to hand to draw clear-cut conclusions about the causes for the discrepancies found between the measured and calculated Reynolds shear stresses. There are indications that turbulence history effects play a role. It is well known that streamline convergence and divergence have a large influence on the turbulence properties. The same holds for the effects of streamline curvature, which can occur in different planes in three-dimensional flows. The skewed mean velocity profile will distort the structure of the large eddies, which play an important role in turbulent flows. To obtain better insight into the relative importance of these and other effects, well-designed experiments are needed, which provide detail information about the turbulence properties in three-dimensional boundary layers in various conditions.

ACKNOWLEDGEMENT

8   REFERENCES

Aquilar, F., Pierce, F.J., 1979 - "Numerical analysis of turbulent
flow along an abruptly rotated cylinder". J. Fluids Eng., Vol. 101,
p. 251.

Berg, B. van den, Elsenaar, A., 1972 - "Measurements in a three-dimen-
sional incompressible turbulent boundary layer under infinite swept
wing conditions". NLR TR 72092 U.

Berg, B. van den, 1976 - "Investigations of three-dimensional incompres-
sible turbulent boundary layers". NLR TR 76001 U.

Berg, B. van den, 1982 - "Some notes on three-dimensional turbulent
boundary layer data and turbulence modelling". IUTAM Symp., Berlin,
Eds.: H.H. Fernholz, E. Krause.

Bissonette, L.R., Mellor, G.L., 1974 - "Experiments on the behaviour
of an axisymmetric turbulent boundary layer with a sudden circumferential
strain". J. Fluid Mech., Vol. 63, p. 369.

Bradshaw, P., 1973 - "Effects of streamline curvature on turbulent flow",
AGARD-AG-169.

Bruin, A.C. de, 1983 - "Sensitivity of computational results to
modification in the pressure gradient for the Van den Berg-Elsenaar
3D boundary layer experiment". NLR Memorandum AI-83-007 U.

Cebeci, T., Smith, A.M.O., 1974 - "Analysis of turbulent boundary layers".
Academic Press.

Chang, K.C., Patel, V.C., 1975 - "Calculation of three-dimensional
boundary layers on ship forms". Iowa Inst. Hydr. Research Report 178.

Coles, D., 1956 - "The law of the wake in the turbulent boundary layer".
J. Fluid Mech., Vol. 1, p. 191.

Cousteix, J., 1974 - "Analyse théorique et moyens de prévisions de la
couche limite turbulente tridimensionelle". ONERA Publ. 157.

Cousteix, J., Houdeville, R., 1981 - "Singularities in three-dimensional
turbulent boundary layer calculations and separation phenomena".
AIAA J., Vol. 19, No. 8.

Cross, A.G.T., 1979 - "Calculation of compressible three-dimensional
turbulent boundary layers with particular reference to wings and
bodies". BAe Brough Note YAD 3379.

Cross, A.G.T., 1980 - "Two-dimensional boundary layer calculations
using a three-parameter velocity profile". BAe Brough Note YAD 3428.

Dechow, R., 1977 - "Mittlere Geschwindigkeit und Reynoldsscher Spannungs-
tensor in der dreidimensionalen turbulenten Wandgrenzschicht vor einem
stehenden Zylinder". Diss. Un. Karlsruhe, Strömungsmechanik und
Strömungsmachinen Heft 21.

Dechow, R., Felsch, K.O., 1977 - "Measurements of the mean velocity and
of the Reynolds stress tensor in a three-dimensional turbulent boundary
layer induced by a cylinder standing on a flat wall". First Symp. "Turb.
Shear Flows"; Univ. Park, Pennsylvania.

East, L.F., 1975 - "Computation of three-dimensional turbulent boundary
layers". Euromech 60, Trondheim. FFA TN AE-1211.

Elsenaar, A., Boelsma, S.H., 1974 - "Measurements of the Reynolds stress
tensor in a three-dimensional turbulent boundary layer under infinite
swept wing conditions". NLR TR 74095 U.

Elsenaar, A., Berg, B. van den, Lindhout, J.P.F., 1975 - "Three-dimensional separation of an incompressible turbulent boundary layer on an infinite swept wing". AGARD Conf. Proc. No. 168.

Fanneløp, T.K., Humphreys, D.A., 1975 - "The solution of the laminar and turbulent three-dimensional boundary layer equations with a simple finite difference technique". FFA Report 126.

Fernholz, H.H., Vagt, J.D., 1978 - "Measurements in an axisymmetric turbulent boundary layer with weak and strong three-dimensional disturbances". Structure and Mechanics of Turbulence, Ed. H. Fiedler, Springer.

Fernholz, H.H., Vagt, J.D., 1981 - "Turbulence measurements in an adverse pressure gradient three-dimensional turbulent boundary layer along a circular cylinder", J. Fluid Mech., Vol. 111, p. 233.

Fulachier, L., Arzoumanian, E., Dumas, R., 1982 - "Effect of a sudden discontinuity of the strain at the wall of a rotating cylinder; close-to-wall region of the boundary layer". IUTAM Symp., Berlin, Eds.: H.H. Fernholz, E. Krause.

Gibson, M.M., Jones, W.P., Younis, B.A., 1981 - "Calculations of turbulent boundary layers on curved surfaces". Phys. Fluids, Vol. 24, p. 386.

Green, J.E., Weeks, D.J., Brooman, J.W.F., 1973 - "Prediction of turbulent boundary layers and wakes in compressible flow by a lag-entrainment method". ARC R. & M. 3739.

Higuchi, H., Rubesin, M.W., 1979 - "Behaviour of a turbulent boundary layer subjected to sudden transverse strain". AIAA J., Vol. 17, No. 9, p. 931.

Hoekstra, M., 1981 - "Application of a high-order finite-difference method to the solution of the boundary layer equations". NSMB Report 44519 - 2 - SR.

Humphreys, D.A., 1979 - "Comparison of boundary calculations for a wing: the May 1978 Stockholm Workshop test case". FFA TN AE-1522.

Humphreys, D.A., 1982 - " A reasonable extension to three dimensions of a good two-dimensional model for boundary layer turbulence". In: "A taste of today's research aerodynamics" (in Swedish). FFA Memo 123, Eds.: I. Jonason, C. Thomson.

Humphreys, D.A., Lindhout, J.P.F., 1986 - "Calculation methods for three-dimensional turbulent boundary layers". To be published in "Progress in Aerospace Sciences".

Humphreys, D.A., Berg, B. van den, 1981 - "Evaluation of flow 0250: the three-dimensional turbulent boundary layer". AFOSR-HTTM Stanford Conf., Eds.: S.J. Kline, B.J. Cantwell, G.M. Lilley.

Jones, W.P., Launder, B.E., 1972 - "The prediction of laminarization with a two-equation model of turbulence". Int. J. Heat Mass Transfer, Vol. 15, p. 301.

Keller, H.B., 1971 - "A new difference scheme for parabolic problems". Numerical solutions of partial differential equations, II. Academic Press.

Launder, B.E., Reece, G.J., Rodi, W., 1975 - "Progress in the development of a Reynolds stress turbulence closure". J. Fluid Mech., Vol. 68, p. 537.

Lindhout, J.P.F., Berg, B. van den, Elsenaar, A., 1980 - "Comparison of boundary layer calculations for the root section of a wing. The September 1979 Amsterdam Workshop test case". NLR MP 80028 U.

Lindhout, J.P.F., Bruin, A.C. de, Gooden, J.H.M., 1982 - "A method for three-dimensional boundary layer calculations on arbitrary bodies: Some results on aircraft wings and engine cowls". IUTAM Symp., Berlin, Eds.: H.H. Fernholz, E. Krause.

Lindhout, J.P.F., Moek, G., Boer, E. de, Berg, B. van den, 1981 - "A method for the calculation of 3D boundary layers on practical wing configurations". J. Fluid Eng., Vol. 103, p. 104.

Lohmann, R.P., 1976 - "The response of a developed turbulent boundary layer to local transverse surface motion", J. Fluid Eng., Vol. 98, p. 354.

Michel, R., Quémard, C., Durant, R., 1968 - "Hypotheses on the mixing length and application to the calculation of the turbulent boundary layer". AFOSR-IFP Stanford Conf., Eds.: S.J. Kline, M.V. Morkovin, G. Sovran, D.J. Cockrell.

Müller, U.R. 1979 - "Messung von Reynoldsschen Spannungen und zeitlich gemittelten Geschwindigkeiten in einer drei-dimensionalen Grenzschicht mit nichtverschwindenden Druckgradienten". Ph.D. Thesis, University of Aachen.

Müller, U.R., Krause, E., 1979 - "Measurements of mean velocities and Reynolds-stresses in an incompressible three-dimensional turbulent boundary layer". Second Symp. "Turbulent shear flows", London.

Müller, U.R. 1982 a - "Measurements of the Reynolds stresses and the meanflow field in a three-dimensional pressure-driven boundary layer". J. Fluid Mech., Vol. 119, p. 121.

Müller, U.R. 1982 b - "Comparisons of three-dimensional turbulent boundary layer calculations with experiment". IUTAM Symp., Berlin, Eds.: H.H. Fernholz, E. Krause.

Patankar, S.V., Spalding, D.B., 1970 - "Heat and mass transfer in boundary layers, a general calculation procedure". Intertext Books, London.

Rao, G.N.V., 1967 - "The law of the wall in thick axisymmetric turbulent boundary layers". J. Appl. Mech., Vol. 89, p. 327.

Ryhming, I.L., Fanneløp, T.K., 1982 - "A three-dimensional law of the wall including skewness and roughness effects". IUTAM Symp., Berlin, Eds.: H.H. Fernholz, E. Krause.

Rotta, J.C., 1977 - "A family of turbulence models for three-dimensional thin shear layers". First Symp. "Turbulent shear flows", Pennsylvania.

Schneider, G.R., 1977 - "Calculation of the turbulent boundary layer on an infinite swept wing using a three-dimensional mixing length model". DLR FB 77-73 (also ESA-TT-534).

Smith, P.D., 1972 - "An integral prediction method for three-dimensional compressible turbulent boundary layers". ARC R. & M. 3739.

Smith, P.D., 1984 - "Direct and inverse integral calculation methods for three-dimensional turbulent boundary layers". Aeron. Journal, May 1984.

Vooren, A.I. van de, Dijkstra, D., 1970 - "The Navier-Stokes solution for laminar flow past a semi-infinite flat plate". J. Eng. Math., Vol. 4, p. 9.

APPENDIX A

DEFINITION OF TEST CASES

General

A package containing magnetic tape with a reading program and compacted initial and boundary conditions for each test case may be obtained from D.A. Humphreys, FFA, Box 11021, S-161 11 BROMMA, SWEDEN. The program reads, interprets and displays in tabular form each data set.

Test cases

Note that the station numbering used here and in the supplied data does not always agree with that appearing in the original published reports of the corresponding experiments. Station numbers consist of two integers I and K. For the quasi-two-dimensional cases, however, K (=0) is suppressed in the text but included in the data.

A distinction is made between recommended and optional test cases. The cases are listed in alphabetical order.

BEEL72 (recommended)

This three-dimensional turbulent boundary layer experiment was carried out by B. van den Berg and A. Elsenaar at NLR, Amsterdam. The flow simulates the (flat) upper surface of a swept infinite wing. The general arrangement is shown in figure A.1.
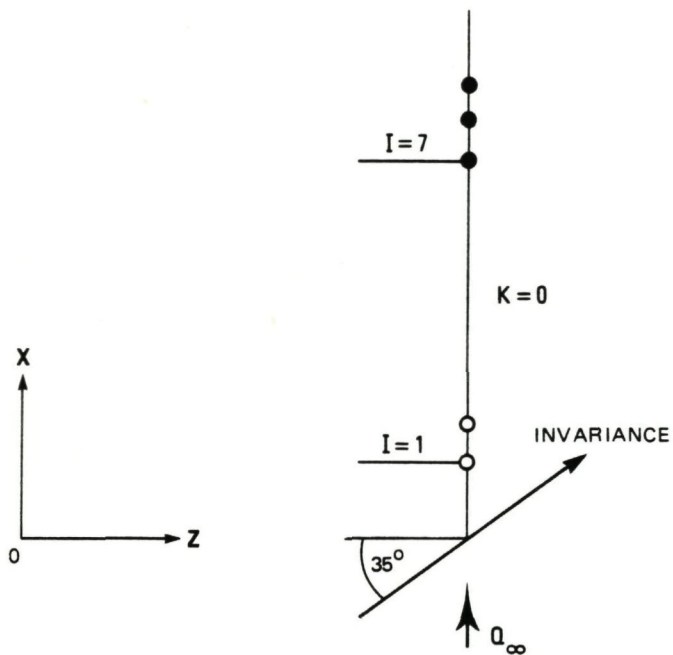
Fig. A.1 BEEL72 schematic

Treat the flow as quasi-two-dimensional, invariant along lines set at 55° to the x-axis. Start calculations at station 2 (x/L = 0.520) but take the initial turbulence data, at station 2, to be those measured actually at station 1 (x/L = 0.495). For normalizing purposes use Δ scales given in Table A.1.

Table A.1

station	7	8	9	10	11	12
x/L	0.895	0.920	0.995	1.020	1.095	1.120
Δ/L	0.0245	0.0245	0.0305	0.0305	0.0400	0.0400

DEFE77 (recommended)

This is the boundary layer on a flat plate measured by R. Dechow and K.O. Felsch at the University of Karlsruhe. Three-dimensionality was produced by mounting an obstacle on the test surface (Figure A.2).

Treat the flow as fully three-dimensional with free side boundaries. Take W=0 initially and other initial data from station (1,1) and (1,2). The precise location of (1,2) may be adjusted slightly to ensure that all output stations just lie within the domain of influence of the initial line. Use the normalizing lengths Δ given in Table A.2.
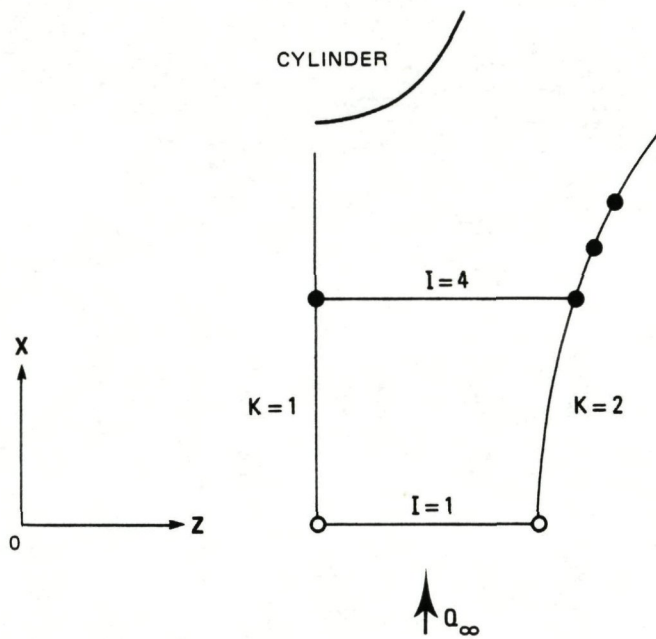
Fig. A.2   DEFE77 schematic

Table A.2

station	(4,1)	(4,2)	(5,2)	(6,2)
x/L	0.7391	0.7391	0.8261	0.8713
z/L	0.0	0.1531	0.1617	0.1687
Δ/L	0.061	0.061	0.070	0.070

Additional calculations may be made by treating z = 0 as a symmetry line and solving for it alone using the equations for quasi-two-dimensional plane of symmetry flow.

FEVA78 (optional)

This turbulent boundary layer on a circular cylinder was investigated by H.H. Fernholz and J.D. Vagt at the University of Berlin. Three-dimensionality was induced by a skew-mounted back plate (Figure A.3).

Fig. A.3   FEVA78 schematic

The boundary layer thickness reached one third of the cylinder radius R (R/L = 1/12.4). (Note, however, that curvature has been neglected in the reference coordinate system used for the supplied data; treat z as arc length on the cylinder surface).

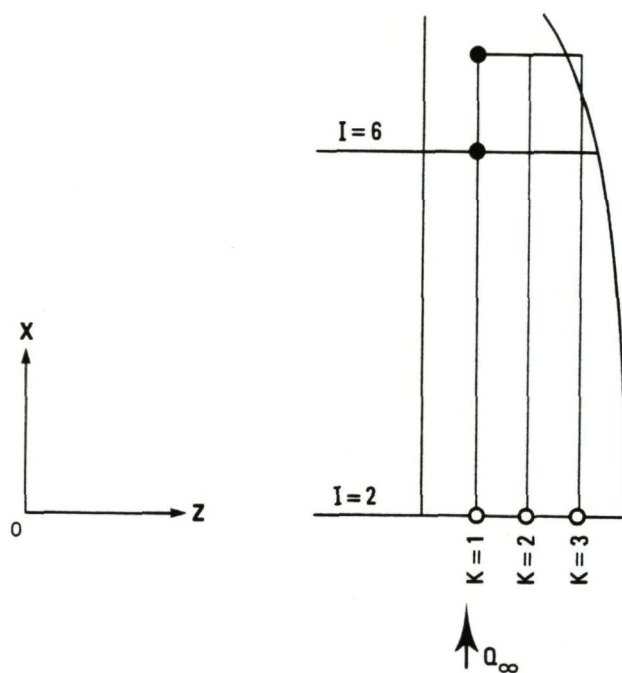Compute the flow as fully three-dimensional with free side boundaries. The initial line, $x/L = 0.5361$ spans $z/L = \pm 0.2813$. Take the measured initial conditions at stations (2,1) (2,2) and (2,3) and assume constant initial conditions in $z/L > 0.1408$ and in $z/L < -0.1408$. Use the normalizing lengths Δ shown in Table A.3.

Table A.3

station	(6,1)	(8,1)
x/L	0.6439	0.6871
z/L	-0.1408	-0.1408
Δ/L	0.021	0.026

LOHM73 (recommended)

R.P. Lohmann measured the three-dimensional turbulent boundary layer set up in axi-symmetric flow along a circular cylinder with rotating afterbody (Figure A.4). The experiment was carried out at the University of Connecticut. The measured boundary layer thickness approached 20% of the cylinder radius ($R/L = 5.277$).
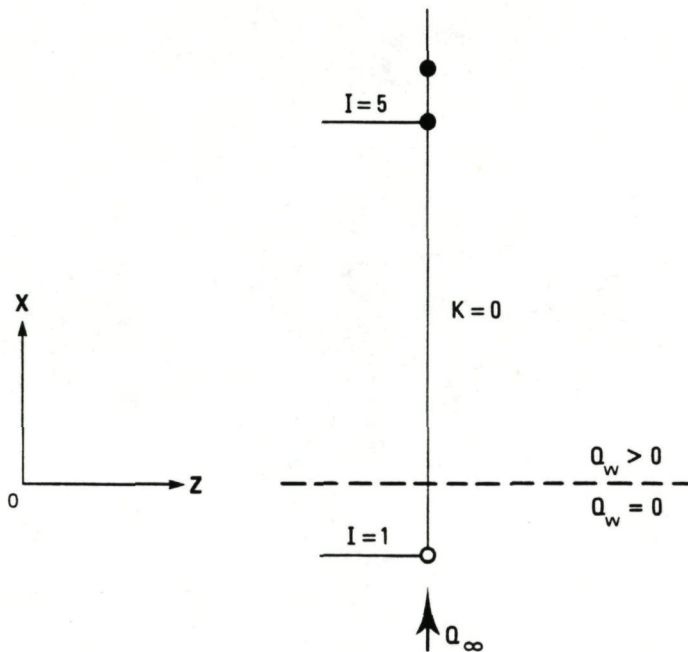
Fig. A.4 LOHM73 schematic

Assume quasi-two-dimensional axi-symmetric flow, invariant along the
z-direction, at constant free stream pressure. The wall velocity is
$Q_w/Q_\infty = 0$ for $x < 0$ and $Q_w/Q_\infty = 1.411$ for $x > 0$. Take initial profiles
as measured at station 1 and use normalizing scales as shown in Table A.4.

Table A.4

station	3	5	8
x/L	3.0	8.0	16.0
Δ/L	0.88	0.96	1.07

MUKR79 (optional)

This three-dimensional turbulent boundary layer was measured by
U. Müller and E. Krause at the University of Aachen. Three-dimensional
flow was produced by fixing deflector walls to the flat test surface
(Figure A.5).

Fig. A.5 MUKR79 schematic

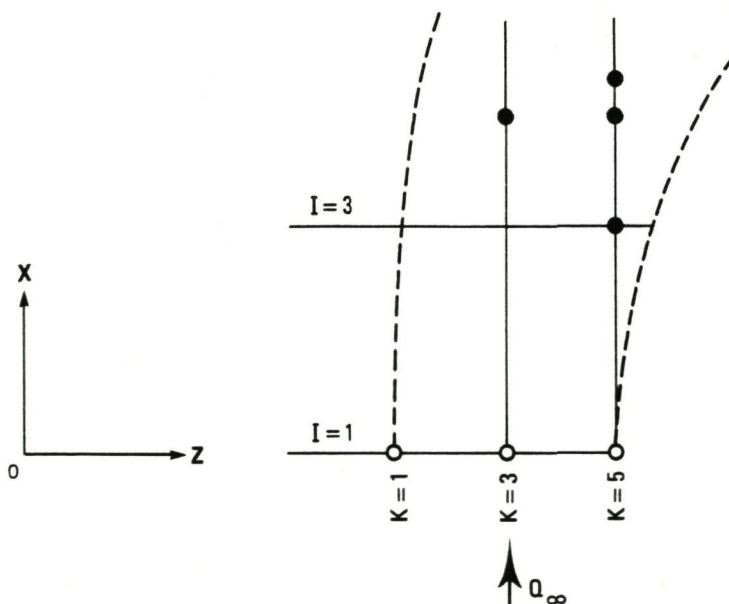The case should be computed as a fully three-dimensional flow with free side boundaries issuing from stations (1,1) and (1,5). Initial data are given at stations (1,1), (1,3) and (1,5). Wall distance normalizing lengths Δ to be used are shown in Table A.5.

Table A.5

station	(3,5)	(5,3)	(5,5)	(6,5)
x/L	0.40	0.60	0.60	0.65
z/L	0.50	0.30	0.50	0.50
Δ/L	0.060	0.075	0.065	0.073

Numerical Tests

A comparison between a given boundary layer calculation and the corresponding experiment may be deemed successful if the calculation reproduces the measurements to within experimental uncertainty starting from a minimum of assumptions. The calculation method is likely to be more generally useful if it can be shown that its success does not depend on fortuitous cancellation of errors. Therefore it is suggested to carry out some form of numerical consistency check.

The suggestion is in the first place to apply the usual test for demonstrating that the solution to the difference equations is converging to the solution to the differential equations, that is, to repeat calculations with average stepsizes reduced by a factor of two in all directions, either separately or all at once. Global differences resulting may be expressed in any natural way.

Another test suggested here is to check how well the numerical solution does satisfy the integral momentum equation. This is not a trivial question, even if the same equations are the basis of the solution procedure.

The individual terms in the equations in streamline coordinates for the three flat plate cases are designated as follows:

$$T_{s1} = \frac{\partial \Theta_{11}}{\partial s} \qquad\qquad T_{s2} = \frac{\partial \Theta_{12}}{\partial n}$$

$$T_{s3} = \frac{(2\Theta_{11}+\delta_1)}{Q_e} \frac{\partial Q_e}{\partial s} \qquad\qquad T_{s4} = \frac{(2\Theta_{12}+\delta_2)}{Q_e} \frac{\partial Q_e}{\partial n}$$

$$T_{s5} = - (\Theta_{12}+ \Theta_{21})\kappa_s \qquad\qquad T_{s6} = - (\Theta_{11}- \Theta_{22})\kappa_n$$

$$T_{s7} = - C_{fs}/2$$

The L_2 norm of these terms is T_s (> 0)

$$T_s^{\,2} = \sum_{i=1}^{7} T_{si}^{\,2}$$

and the normalized terms are therefore

$$t_{si} = T_{si}/T_s.$$

Note that $|t_{si}| < 1$. All the t_{si} are of interest but the measure of accuracy adopted here is

$$\Omega_s = \sum_i t_{si} ,$$

which should be small compared to unity.

Along the orthogonal trajectories,

$$T_{n1} = \frac{\partial \Theta_{21}}{\partial s} \qquad\qquad T_{n2} = \frac{\partial \Theta_{22}}{\partial n}$$

$$T_{n3} = \frac{2\Theta_{21}}{Q_e} \frac{\partial Q_e}{\partial s} \qquad\qquad T_{n4} = \frac{2\Theta_{22}}{Q_e} \frac{\partial Q_e}{\partial n}$$

$$T_{n5} = - (\Theta_{22}- \Theta_{11} - \delta_1)\kappa_s \qquad\qquad T_{n6} = - (\Theta_{21}+ \Theta_{12} + \delta_2)\kappa_n$$

$$T_{n7} = - C_{fn}/2$$

The L_2 norm is T_n

$$T_n^{\,2} = \sum_i T_{ni}^{\,2}$$

The normalized terms

$$t_{ni} = T_{ni}/T_n$$

and the accuracy measure

$$\Omega_n = \sum_i t_{ni}$$

APPENDIX B

EXPERIMENTAL ACCURACY ESTIMATES

	BEEL 72	DEFE 77	LOHM 73	MUKR 79
c_p	$\pm\ 2\times10^{-3}$			$\pm\ 5\times10^{-3}$
$\alpha°$	$\pm\ 0.2°$		$\pm\ 1°$	$\pm\ 0.7°$
c_f	$\pm\ 1.5\times10^{-4}$			$\pm\ 1.5\times10^{-4}$
$\beta_w°$	$\pm\ 1°$			
y/L	$\pm\ 2\times10^{-5}$	$\pm\ 4\times10^{-5}$		$\pm\ 5\times10^{-5}$
U/Q_e	$\pm\ 10^{-2}$	$\pm\ 2\times10^{-2}$	$\pm\ 10^{-2}$	
W/Q_e	$\pm\ 10^{-2}$	$\pm\ 2\times10^{-2}$	$\pm\ 3\times10^{-2}$	
τ_x/q_e	$\pm\ 10\%$ or $\pm\ 2\times10^{-4}$	10%	$\pm\ 20\%$	$\pm\ 10\%$
τ_z/q_e	$\pm\ 10\%$ or $\pm\ 2\times10^{-4}$	10%	$\pm\ 20\%$	$\pm\ 15\%$

The above table contains accuracy estimates - to 95% confidence level
or similar - for the various measurement quantities.
The numbers given are based upon information provided by the experimental
investigators themselves. Unfortunately accuracy estimates were not
given in every case for all relevant quantities.